Interreg
Danube Transnational Programme
lifelineMDD

Project co-funded by European Union funds (ERDF, IPA)
Project number: DTP3-308-2.3- lifeline MDD

Sediment balance and transport in the Five-Country Biosphere Reserve Mura-Drava-Danube

DTP3-308-2.3 lifelineMDD

D.T1.2.3 Sediment balance and transport study

University of Natural Resources and Life Sciences, Vienna

Institute of Hydraulic Engineering and River Research

September, 2022

IMPRESSUM

Authors:

Mario Klösch, Roman Dunst, Helmut Habersack

University of Natural Resources and Life Sciences, Vienna, Department of Water, Atmosphere and Environment, Institute of Hydraulic Engineering and River Research

Suggested citation:

Klösch, M., Dunst, R., Habersack, H. (2022). Sediment balance and transport in the Five-country Biosphere Reserve Mura-Drava-Danube, deliverable D.T1.2.3 for the EU-Interreg DTP project 'lifelineMDD'.

Date:

September 2022

Project Manager:

Kerstin Böck

World Wide Fund for Nature Austria - WWF Austria

Many thanks to:

Marina Babić-Mladenović, Hannes Badura, Sándor Baranya, Danko Biondić, Kerstin Böck, Duška Divović, Sándorné Fekete, Peter Frantar, Keve Gábor, Philipp Gmeiner, Jochen Göglburger, Tamás Gruber, Emöke Györfi, Marlene Haimann, Severin Hohensinner, Katarína Holubová, Aljaž Lesjak, Katarína Mravcová, Sašo Petan, Monika Podgorelec, Szilvia Rádi, Robert Schatzl, Ulrich Schwarz, Tomislav Šletah, Saša Sobočan, Branka Španiček, Robert Stöffler, Tadej Törnar, Igor Tošić

Contents

1 Introduction 10
1.1 General introduction 10
1.2 Problem statement 11
1.3 Study aims 11
1.4 State of general knowledge 12
1.4.1 Sediment transport processes 12
1.4.2 Morphodynamics 15
1.4.3 Sediment budget 19
1.4.4 Morphology of natural rivers with balanced sediment budget 20
1.4.5 Morphology of rivers at budget imbalance 26
2 Methodology 29
2.1 Analysis of planform change 29
2.1.1 Width analysis 31
2.1.2 Sinuosity and slope 31
2.1.3 Analyses of river bend radii 32
2.2 Analyses of bed level change 32
2.3 Analysis of cross-sectional channel evolution 33
2.4 Sediment transport 34
2.5 Sediment budgeting 34
2.6 Analyses of implications of morphodynamics for riverine habitats 35
3 Results 36
3.1 Planform change 36
3.1.1 Changes in discharging channel width and total width 36
3.1.2 Changes in channel length 42
3.1.3 Changes in sinuosity and slope 44
3.1.4 Changes in the radii of river bends 48
3.2 Morphological change 51
3.2.1 Mura 51
3.2.2 Drava 53
3.2.3 Danube 66
3.3 Analyses of bank obstruction 68
3.4 Dredging activities 69

3.5 Sediment balance 71
3.5.1 Mura 72
3.5.2 Drava 74
3.5.3 Danube 82
3.6 Effects on riverbed levels 87
3.6.1 Incision based on annual minimum river stage 87
3.6.2 Incision based on river stage-discharge relation 96
3.7 Relevance of lateral dynamics in habitat provision 103
4 Conclusions 105
5 Annex 108
6 References 115

List of Figures

Figure 1. Map of the 5-country Biosphere Reserve Mura-Drava-Danube according to UNESCO designation in September 2021 (WWF Austria). ---------- 10
Figure 2. Component of weight of a water volume in the direction of the channel slope.---------- 13
Figure 3. Shields diagram showing the threshold of dimensionless shear stress to motion of particles (Shields, 1936). ---------- 14
Figure 4. Resisting and driving forces F_R and F_D, counteracting in the slip surface and determining the bank stability with respect to mass failure. The unit weight γ, cohesion c' and friction angle ϕ' as the geotechnical properties and the bank inclination i determine both F_D and F_R. The angle β is the angle producing the smallest factor of safety $FS=F_R/F_D$. ---------- 17
Figure 5. Sequence of the emergence of a mid-channel bar (Hooke, 1986). ---------- 18
Figure 6. Conceptual model of bar- bank interactions, explaining the excessive widenings occurring at mid-channel bar sections (Klösch et al., 2015). ---------- 19
Figure 7 Sediment budget components (modified by Klösch and Habersack, 2017 from Frings et al., 2014). ---------- 20
Figure 8. Values of channel slope and bankfull discharge for different natural rivers and an identified threshold function separating meandering and braiding rivers (Leopold and Wolman, 1957).--------- 21
Figure 9. The Da Silva (1991) plan (displayed here in its revised form based on Ahmari and Da Silva (2011)) provides an understanding of thresholds in river morphology useful in planning bed widenings. B: flow width, h: flow depth, and D: grain size. ---------- 22
Figure 10. Left: Regime equations derived from natural rivers (British and US-American), calculating from the bankfull discharge Q_{bf} and the median sediment grain size of the bed surface D_{s50} the depth and width of bankfull discharge (H_{bf} and B_{bf}) and the channel slope S. Right: British rivers tended to be narrower than American Rivers, probably due to the effect of increased presence of riparian vegetation in the more humid climate. ---------- 22
Figure 11. Morphological river type, characterised by the bank mode (number of bars in a cross section) as calculated with the analytical model from Crosato and Mosselman (2009).---------- 23
Figure 12. Dependency of the river morphology on sediment characteristics, including sediment yield (Schumm, 1985). ---------- 24
Figure 13. Dependence of morphology and stability on the amount of sediment input and grain size (Church, 2006**).** ---------- 25
Figure 14. Dependence of morphology on bedload concentration according to Mueller and Pitlick (2014). Q_{bf} is the bankfull discharge, Q* is a dimensionless flow, s = the specific density of the sediment (ρ_s/ρ) and D_{50} the median grain diameter. The bedload concentration C is calculated from the relation between the volumetric bedload transport at bankfull discharge and the bankfull discharge. C_t is the bedload concentration at the transition between single-thread and braided channels. ---------- 26
Figure 15. Dependency of the channel slope on the sediment supply. ---------- 26
Figure 16. Effects of uniform aggradation/degradation on the sediment discharge.---------- 27
Figure 17. Trajectory of a river as a reaction to a) decrease, b) increase of sediment supply. Qs,in: Sediment discharge supplied into a reach, Qs,out: Sediment supply transported out of a reach (Klösch et al., 2019a). ---------- 27
Figure 18. Development from a braided channel to a narrow, single-thread channel after reduction of sediment input (Marti and Bezzola, 2009).---------- 28
Figure 19. Division of the Mura, Drava and Danube into sections as proposed by Schwarz (2022).--- 30

Figure 20. Historic main and side channels of the Mura, Drava and Danube (black) with the overlaying valley axis (red). ---------- 30
Figure 21. Methodology of the width analysis: Along the valley axis (red, dotted), perpendicular cross sections (red) were placed at a distance of 500 m. Along these valley cross sections, again cross sections (blue) were placed at each intersection of the valley cross section with the centre lines of the individual channels. The sum of the individual blue cross sections along a valley cross section results in the discharged width of the respective valley cross section. ---------- 31
Figure 22. Considered gauging stations. ---------- 32
Figure 23. Stations with both discharge and river stage data.---------- 33
Figure 24. Most upstream section of the Drava River in the TBR MDD. ---------- 33
Figure 25. Stations with available data on suspended sediment transport. The recorded periods at Mursko Sredisce, Batina, Dalj and Ilok however proved to be too short to provide significant conclusion on the average annual suspended sediment transport. ---------- 34
Figure 26. Discharging width of the Mura River from Spielberg to the confluence with the Drava River. The average wetted width decreased by 58% from the historic state (grey) to the present state (black). ---------- 36
Figure 27. Total width between the left water's edge of the most left-discharging channel and the right water's edge of the most right-discharging channel along the Mura River in the historic and present state. ---------- 37
Figure 28. Wetted width of the Drava River from Ormož to the Danube confluence in the historic state (grey) and in the present state (black).---------- 38
Figure 29. Total width between the left water's edge of the most left-discharging channel and the right water's edge of the most right-discharging channel along the Drava River in the historic and present state. ---------- 39
Figure 30. Wetted width of the Danube from the Drava confluence to Backa Palanka in the historic state (grey) and in the present state (black). ---------- 40
Figure 31. Total width between the left water's edge of the most left-discharging channel and the right water's edge of the most right-discharging channel along the Danube River in the historic and present state. ---------- 41
Figure 32. Relative changes in width along the MDD rivers. ---------- 41
Figure 33. Relative change in the standard deviation of the width within the individual segments. -- 42
Figure 34. Length of the main channel of the Mura, Drava and Danube as during the second military mapping survey (1810s-1850s, grey) and in 2012 (black).---------- 43
Figure 35. Length of Mura, Drava and Danube within the predefined sections in the reference state (grey) and the actual state (black). ---------- 44
Figure 36. The sinuosity of the rivers within the individual sections in the reference state (grey) and the present state (black). ---------- 45
Figure 37. Relative changes in sinuosity and corresponding relative changes in slope ---------- 45
Figure 38. Relative change in sinuosity along the TBR. ---------- 46
Figure 39. Relative change in the channel number of formerly braided sections and relative change in the sinuosity of former meandering sections---------- 47
Figure 40. Relative change in slope along the TBR ---------- 47
Figure 41. Relative changes in the median radius of the Mura, Drava and Danube.---------- 48
Figure 42. Proportion of different radius classes of the total length of TBR rivers. ---------- 49
Figure 43. Arc radius as function of the arc length in the historic state (blue) and in the present state (orange) for Mura section M3. ---------- 49

Figure 44. Arc radius as function of the arc length in the historic state (blue) and in the present state (orange) for Drava section Dr3 ---------- 50
Figure 45. Arc radius as function of the arc length in the historic state (blue) and in the present state (orange) for Danube section D1. ---------- 50
Figure 46. Arc radius as function of the arc length in the historic state (blue) and in the present state (orange) for Danube section D2. ---------- 51
Figure 47. Mura section M1 in the present and historic state. ---------- 51
Figure 48. Mura section M1 along the Austrian-Slovenian border. ---------- 52
Figure 49. Along the Mura sections M2 and M3, the river length stayed almost the same, yet the narrowing is clearly apparent---------- 52
Figure 50. Number of channels along the valley axis of the Mura river in the TBR MDD. The once braided river system has been heavily altered, changing the Mura to a single channel stream in the present state. ---------- 53
Figure 51. Relative occurrence of number of channels along the Mura. ---------- 53
Figure 52. Detail of the Drava section Dr1: Here, three hydropower dams were built in the end of the 20th century (in the picture: Varaždin and Dubrava). ---------- 54
Figure 53. Drava section Dr2 downstream of the Mura confluence ---------- 54
Figure 54. In the Drava section Dr3, meander cut-offs led to significant shorter length of the Drava compared to the historic state ---------- 55
Figure 55. Number of channels along the valley axis of the Drava River from to the Danube confluence. ---------- 55
Figure 56. D50 (a) and slope (b) along the course of the Drava river (Pirkhoffer et al., 2021) ---------- 56
Figure 57. Relative occurrence of channel numbers along the Drava. ---------- 56
Figure 58. Residual flow stretch near Varaždin between 2003 and 2021 (source: Google Earth). ----- 58
Figure 59. Repeated cross-sectional surveys at the residual flow stretch at Varaždin between 2007 and 2020. ---------- 59
Figure 60. Cross sections along the old Drava downstream HPP Varaždin 2007-2020. ---------- 60
Figure 61. The Drava river below the Dubrava reservoir in 2003 and 2021---------- 61
Figure 62 Residual flow stretch at HPP Dubrava with repeated cross-sectional surveys available starting with 2009 (red) and 2012 (black). ---------- 62
Figure 63. Morphological changes in the residual flow stretch downstream HPP Donja Dubrava between 2009 and 2018. Only cross sections directly below the dam and upstream of the confluence of head race channel and residual flow channel were available for the year 2009. ---------- 62
Figure 64. Morphological changes in the residual flow stretch downstream HPP Donja Dubrava between 2012 and 2018. For this time period, 49 cross sections along the residual flow stretch were considered. ---------- 63
Figure 65. Morphological change in the cross section P 41 downstream HPP Donja Dubrava from 2009 (dashed) to 2018. ---------- 64
Figure 66. Changes in cross section P41 downstream of the HPP Donja Dubrava from 2009-2018.--- 64
Figure 67. Morphological change in the cross section P54 downstream HPP Donja Dubrava from 2009 (dashed) to 2018. ---------- 65
Figure 68. Channel evolution diagram of cross section P54 below the Dubrava reservoir. ---------- 65
Figure 69. a) upstream part of the Danube section D1 and b) section D1 upstream of the Drava confluence. ---------- 66
Figure 70. Danube section D2 downstream of the Drava confluence. ---------- 67
Figure 71. Number of channels of the Danube in the historic (grey) and present state (black).-------- 67
Figure 72. Relative occurrence of channel numbers along the Danube.---------- 68

Figure 73. Training structure density along the TBR rivers (Data source: Schwarz, 2022). ---------- 69
Figure 74. Annually dredged bed material in the Drava River (Baranya et al., 2020). ---------- 70
Figure 75. Bed degradation due to dredging in the Drava River (Baranya et al., 2020). ---------- 70
Figure 76. Annual bedload transport at Letenye (data source: Rákóczi and Szekeres, 2004) ---------- 72
Figure 77. Cumulative discharge of sediment volume from the Grenzmur over the period 1974 to 2006. ---------- 73
Figure 78. Annual suspended sediment transport at Mureck (data source: ehyd). ---------- 74
Figure 79. Annual suspended sediment transport at Gorican (data source: Croatian Waters). --------- 74
Figure 80. Measured bedload transport along the Drava (data source: Rákóczi and Szekeres, 2004). 75
Figure 81. Grain size distribution along the Drava between rkm 236 and rkm 75, named after the rkm of the sampling site (Terra-Graph Kft., 2020). ---------- 76
Figure 82. Annual suspended sediment transport at Varaždin (data source: Croatian Waters). ------- 77
Figure 83. Annual suspended sediment load as measured at Botovo divided into periods: before the construction of the HEPP Varaždin 1975, HEPP Čakovec 1981 and after operation start of HEPP Dubrava in 1989. (Bonacci and Oskorus, 2009). ---------- 77
Figure 84. Total suspended sediment transport per year from 1967 - 2019 at Botovo (data source: Croatian Waters)---------- 78
Figure 85. Annual suspended sediment load at Terezino Polje (data source: Croatian Waters)-------- 78
Figure 86. Annual suspended sediment load as measured at Donji Miholjac. (Bonacci and Oskorus, 2009). ---------- 79
Figure 87. Suspended sediment transport at Donji Miholjac since 1989 (data source: Croatian Waters) ---------- 80
Figure 88. Mean bed level change in the Lake Ormož from 2006-2015 (data source: Croatian Waters). ---------- 81
Figure 89. Differences in bed elevation at Lake Ormož between 2006 and 2015 (data source: Croatian Waters). ---------- 81
Figure 90. Mean bed level change at Lake Varaždin from 2006-2015 (data source: Croatian Waters). ---------- 82
Figure 91. Differences in bed elevation at Lake Varaždin between 2006 and 2015 (data source: Croatian Waters). ---------- 82
Figure 92 Annual suspended sediment transport at Dombori (data source: Croatian Waters). -------- 83
Figure 93 Annual suspended sediment transport at Mohács (data source: Croatian Waters) ---------- 83
Figure 94 Suspended sediment balance of the Danube river and its tributaries before (left) and after the construction of hydropower plants (right) (Habersack et al., 2019). ---------- 84
Figure 95 Aggradation/Degradation (blue) and Dredging (red) per kilometre along the Danube within the TBR between 1971 and 1990(Source: DanubeSediment).---------- 85
Figure 96. Aggradation/Degradation (blue) and Dredging (red) along the Danube within the TBR between 1991 - 2017 (Source: DanubeSediment). ---------- 85
Figure 97. Cumulative annual erosion/sedimentation 1991-2017 (Source: DanubeSediment) --------- 86
Figure 98. Danube-Thalweg in the periods 1920-1970 (blue) and 1991-2017 (black) (data source: DanubeSediment) ---------- 86
Figure 99. Variation in the D50 grain size over the three periods 1920-1970 (green), 1971-1990 (blue), 1991-2017 (red) with the TBR section marked in red. Within the upper TBR section, the bed material changes from coarse sand to fine sand (Zone 2, source: DanubeSediment). ---------- 87
Figure 100. Annual minimum, maximum and mean river stage at Mureck ---------- 88
Figure 101. Riverbed incision of the Mura River downstream of Misselsdorf along the border between Austria and Slovenia.---------- 89

Figure 102. Annual minimum, maximum and mean river stage at Murakeresztúr. ---- 89
Figure 103. Annual minimum, maximum and mean river stage at Botovo. ---- 91
Figure 104. Annual minimum, maximum and mean river stage at Terezino Polje. ---- 91
Figure 105. Annual mimimum, maximum and mean river stage at Osijek. ---- 92
Figure 106. Annual minimum, maximum and mean river stage at Bijelo Brdo; here Data is only available until 2013. ---- 92
Figure 107 Change of the annual maximum, mean and minimum river stage at gauging station Paks upstream of the TBR MDD ---- 93
Figure 108 Change of the annual maximum, mean and minimum river stage at gauging station Ilok 94
Figure 109. Total incision at gauging station cross sections based on minimum river stage analyses. 94
Figure 110. Mean annual riverbed incision rates at gauging stations along the TBR rivers. The incision rates are based on the annual minimum river stage analysis. ---- 95
Figure 111. Mean annual riverbed incision rates between 1993 and 2019 based on annual minimum river stages. ---- 95
Figure 112. River stages at Qmean at Petanjci. ---- 96
Figure 113. Abrupt changes in the riverstage within one year indicates a change to a differnt rating curve. ---- 97
Figure 114. River stage at Q_{mean} at Donji Miholjac. ---- 98
Figure 115. River stage at Q_{mean} at Terezino Polje. Since 2011 the riverbed seems to be relative stable. ---- 98
Figure 116. Gauging station cross section at Terezino Polje between 1962 and 2014. ---- 99
Figure 117. Riverbed incision at gauging stations from 2010-2019. ---- 100
Figure 118. Riverbed incision at gauging stations from 1993-2019. ---- 100
Figure 119. Annual miminum (blue), maximum (red) and mean (green) discharges at the Hungarian gauging stations along the Danube. ---- 102
Figure 120. Annual minimum, maximum and mean discharge at Mureck. ---- 103
Figure 121. Annual minimum, maximum and mean discharge at Letenye. ---- 103
Figure 122. a) Restored site at Sicheldorf with the analysed cross section and b) cross-sectional change in the period between 2012 and 2018, analysed with the HyMoLink tool (Klösch et al., 2019b) for potential habitat provision. ---- 104

List of Tables

Table 1. Sections of the Mura, Drava and Danube as proposed by Shwarz et al. (in prep.). ---- 29
Table 2. Average discharging widths of the Mura River, relative change and standard deviation in the historic and present state. ---- 36
Table 3. Average total widths of the Mura River, relative change and standard deviation in the historic and present state. ---- 37
Table 4. Average discharging widths of the Drava River, relative change and standard deviation in the historic and present state. ---- 38
Table 5. Average total widths of the Drava River, relative change and standard deviation in the historic and present state. ---- 39
Table 6. Average discharging widths of the Danube river, relative change and standard deviation in the historic and present state ---- 39
Table 7. Average total widths of the Danube River, relative change and standard deviation in the historic and present state. ---- 40

Table 8. Historic and present widths and relative changes in width of the entire Mura, Drava and Danube and overall change in the TBR MDD.---------- 42
Table 9. Length of the MDD rivers in the historic and present state.---------- 42
Table 10. Historic and present length of the TBR rivers.---------- 43
Table 11. Sinuosity of the MDD rivers in the historic and present state. ---------- 44
Table 12. Relative changes in slope based on changes in sinuosity (%). ---------- 45
Table 13. Relative change in the median radius (%).---------- 48
Table 14. Mean annual bedload transport along the Drava River between 1986 and 2003. ---------- 75
Table 15 total suspended sediment transport in 2019. ---------- 83
Table 16. Changes in the annual minimum river stage at gauging stations along the Mura River.----- 88
Table 17. Change in annual minimum river stage at gauging stations along the Drava with rates per year and number of years recorded.---------- 90
Table 18. Change in the annual minimum river stage at gauging stations along the Danube with derived incision rate and number of years recorded. ---------- 93
Table 19. Average annual bed incision rate at the Mura.---------- 96
Table 20. Average annual bed incision rate at the Drava. ---------- 97
Table 21. Average annual bed incision rate at the Danube.---------- 99

1 Introduction

1.1 General introduction

The present report is the result of a study conducted within the DTP3-308-2.3 lifeline MDD, financed by the European Union´s Interreg Danube Transnational Programme. The area analysed and targeted by the present study (hereinafter called "target area") comprises river sections in the 5-country Biosphere Reserve Mura-Drava-Danube (TBR MDD, Figure 1), shared between Austria, Slovenia, Hungary, Croatia and Serbia. Spanning Austria, Slovenia, Hungary, Croatia and Serbia, the lower courses of the Drava and Mura Rivers and related sections of the Danube are among Europe's most ecologically important riverine areas. The three rivers form a "green belt" 700 kilometres long, connecting almost 1.000,000 hectares of highly valuable natural and cultural landscapes, including a chain of 13 individual protected areas and 3.000 km2 of Natura 2000 sites. This is the reason why, in 2009, the Prime Ministers of Croatia and Hungary signed a joint agreement to establish the Mura-Drava-Danube Transboundary Biosphere Reserve across both countries. Two years later, in 2011, Austria, Serbia and Slovenia joined this initiative. Together with Croatia and Hungary, the five respective ministers of environment agreed to establish the world´s first five-country Biosphere reserve and Europe´s largest river protected area. Step by step the TBR MDD was realized: Hungary and Croatia (in 2012), Serbia (in 2017), Slovenia (in 2018) and Austria (2019) achieved UNESCO designation. The pentalateral designation was submitted in 2020 and designation finally achieved in September 2021.

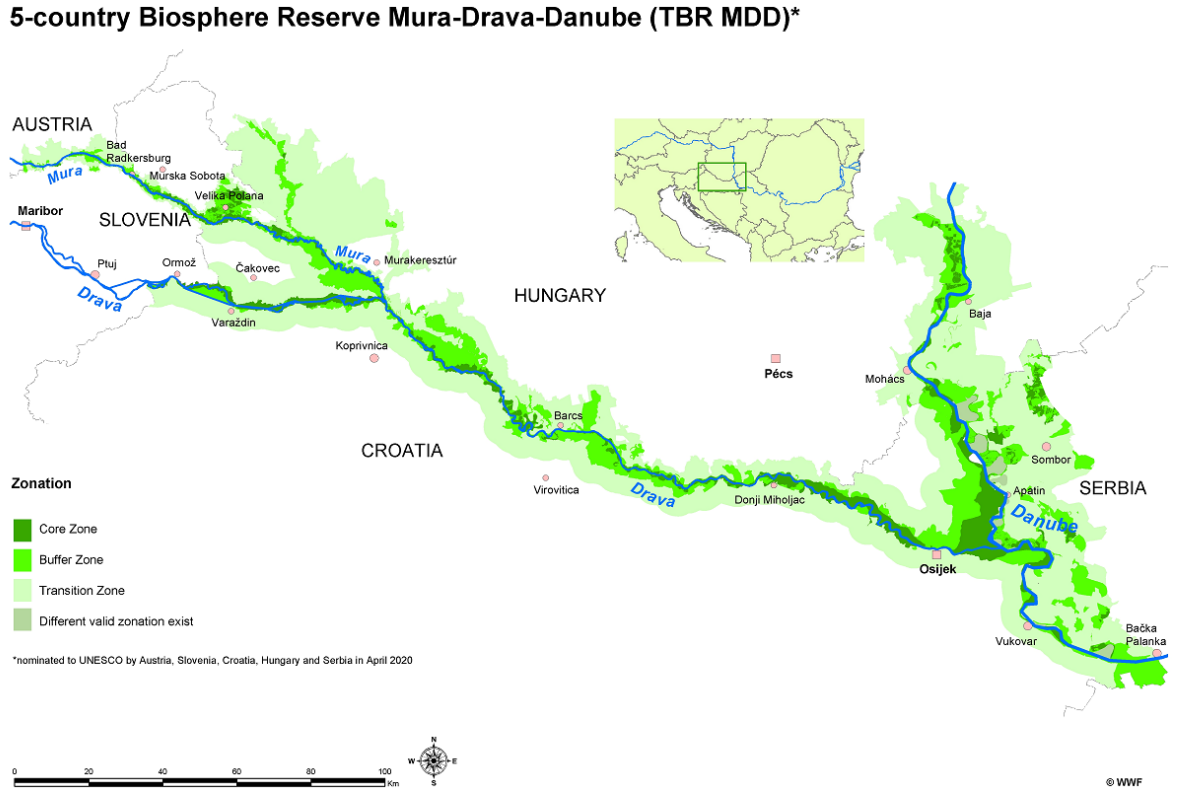

Figure 1. Map of the 5-country Biosphere Reserve Mura-Drava-Danube according to UNESCO designation in September 2021 (WWF Austria).

The project´s work package for Establishing the scientific knowledge base (Work Package T1) has proposed as its aim to establish, as a first, a scientific knowledge base regarding vertical, lateral and longitudinal connectivity within the Mura-Drava-Danube bio-corridor. All studies' results and the overlaid GIS data collected therefore build the basis for a synthesis report on biotic indicators and abiotic framework conditions. This builds the basis for long-term conservation and restoration goals within the 5-country Biosphere Reserve Mura-Drava-Danube (TBR MDD) as well as for formulation of a TBR MDD River Restoration Strategy, elaborated in the framework of the same project (Output OT2.4). The facts and results presented in this project therefore come from a first ever such scientific assessment, which was done between July 2020 and (Month) (year), harmonized on 5-country scale, setting the ground for future decision-making on 5-country level on river management and restoration. Whereas such activities and knowledge in each of the countries involved in the TBR MDD partly exist, this was the first time methods and area were harmonized for monitoring and studies of the biotic elements and the abiotic framework conditions for the Mura-Drava-Danube river corridor.

1.2 Problem statement

Rivers combine the transport zones of both the water and sediment cycle. The interaction of both forms a landscape which is unique, as it frequently changes with river stage and morphodynamics. The life cycle of many riverine species adapted to the dynamics of a frequently changing river landscape. In the 19th century, many rivers were systematically channelized to gain agricultural land, to protect from the floods and from the lateral dynamics of the river, or to improve or enable ship navigation. The rivers, now steeper and deeper in the straightened and narrowed channel, became able to transport more sediment than supplied from upstream, while the sediment supply from upstream decreased: the construction of hydropower plants and check dams retained sediment and mining removed sediment in the river sections and in its upstream river network. The channelization immediately reduced the habitat variability, but the situation aggravated as the riverbed incised and as the rivers increasingly decoupled from their floodplain.

Similarly, the Mura, Drava and Danube Rivers were impacted by human alterations. While still forming a long free-flowing section embedded in wide floodplain forests, the Mura, Drava and Danube in the target area were subject to channelization, reduction of sediment supply and sediment mining. Still, the riverine landscape provides habitats to a variety of riverine species, but abiotic river elements created from morphodynamic processes were reduced in quantity so that they now constitute bottleneck habitats, determining the abundance for their populations.

An assessment of the sediment conditions throughout the entire target area is missing. An improved understanding of the effects of human impacts would provide a basis for implementing effective counter measures for preservation and for restoration actions.

1.3 Study aims

The aim is to provide basic knowledge useful for future restoration actions in the TBR MDD. The preparation of the results as maps and the insights on process understanding

from all applied methods finally should serve to identify priority reaches from morphological and sediment transport point of view. An overlay of the results of this study with the results from the other studies should allow a holistic assessment for preparing the River Restoration Strategy for the TBR MDD.

1.4 State of general knowledge

First, we give an overview on the processes involved in sediment transport and on the mechanisms leading to erosion and deposition. Then, based on collected literature, we describe the resulting morphodynamics, the sediment budgeting in rivers, and the role of human alterations for sediment budgets and the consequences for river morphology.

1.4.1 Sediment transport processes

Rivers like the Mura, Drava and Danube Rivers in the TBR MDD flow in their own alluvium, and the riverbed is formed by the sediment transported by the rivers. Accordingly, the morphology, including river bed elevations, depends on the sediment regime of the rivers, which is determined by the size, quantity and sorting of the sediment. Repeated transport, and varying transport capacities in the channel, constitute the preconditions for morphologies to develop and to sustain.

The following introduction serves as the basis for an understanding of sediment transport processes and their linkage to external boundary conditions, such as exerted by river channelization, damming and dredging.

Two main sediment transport processes may be distinguished:

- Bedload, where grains move in vicinity of and in repeated contact with the river bed via rolling, saltating and sliding with intermediate rests (Einstein, 1936)
- Suspended load, where turbulence allows smaller particles to distribute in the entire water column, which are transported solely by convective fluxes (ASCE, 2008)

The transition from transport as bedload and transport in suspension is smooth, but can be estimated via Kresser (1964) to occur around:

$$\frac{\bar{u}^2}{gd} = 360 \qquad (1)$$

where $\bar{u}$ = mean flow velocity (m s^{-1}), g = gravitational acceleration (m s^{-2}), and d = grain size (m).

1.4.1.1 Bedload transport

The driving factor for bedload transport showed to be well described by the bed shear stress, so that it is often used as the determining variable in bedload formulas (e.g., Wong and Parker, 2006). Bed shear stress along the boundary of the wetted perimeter counteracts the component of the weight in the direction of the channel slope (Figure 2).

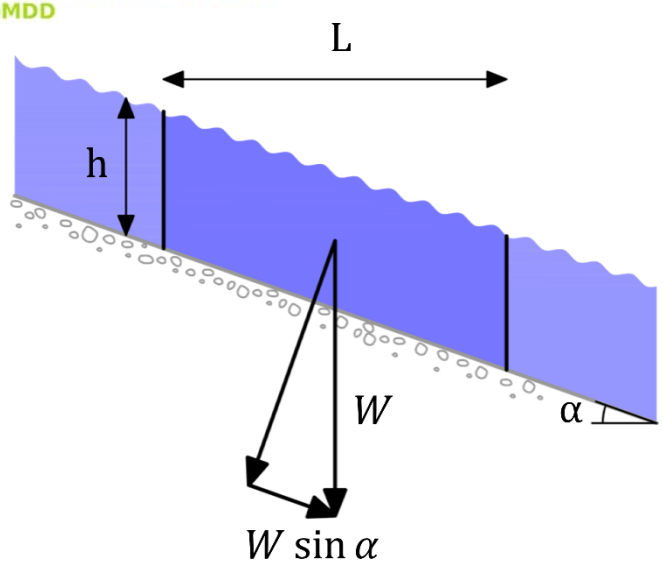

Figure 2. Component of weight of a water volume in the direction of the channel slope.

For the small slopes of larger rivers sin α can be replaced by the channel gradient S, measured as vertical difference per horizontal distance. In steady and uniform conditions, the bed shear stress τ (N m^{-2}) acting on the bed of a river to counteract the driving weight component of the water can be calculated as follows:

$$\tau = \rho g R S \tag{2}$$

where ρ = density of water (kg m^{-3}), R = hydraulic radius (m), and S = channel slope (m m^{-1}. The hydraulic radius R is calculated via:

$$R = \frac{A}{U} \tag{3}$$

where A = cross-sectional wetted area (m^2), and U = the wetted perimeter (m). In wide channels as the Mura, Drava and Danube, R approaches the values of the water depth h (m).

Accordingly, the bed shear stress increases with water depth h and channel slope S, hence it is directly affected by river channelization, which increases water depth in the narrowed width and which increases slope in the straightened river course.

Shields (1936) investigated the role of the bed shear stress for sediment transport in a dimensional analysis, and calculated a dimensionless shear stress τ* (-) via

$$\tau^* = \frac{\tau}{(\rho_s - \rho) g d} \tag{4}$$

where ρ_s = sediment density (kg m^{-3}). Shields (1936) related τ* to the Reynolds number of the grain Re* (-), which is calculated via:

$$Re^* = \frac{u^* d}{\nu} \tag{5}$$

where u* (m s^{-1}) = the shear velocity (calculated via $u^* = \sqrt{\tau/\rho}$), and ν = kinematic viscosity of water (m^2 s^{-1}). Based on the relationship found in Figure 3, Shields (1936) suggested that the critical dimensionless shear stress to motion τ^*_c (-) becomes a constant value in the higher range of Re*, which applies to the conditions of common natural rivers.

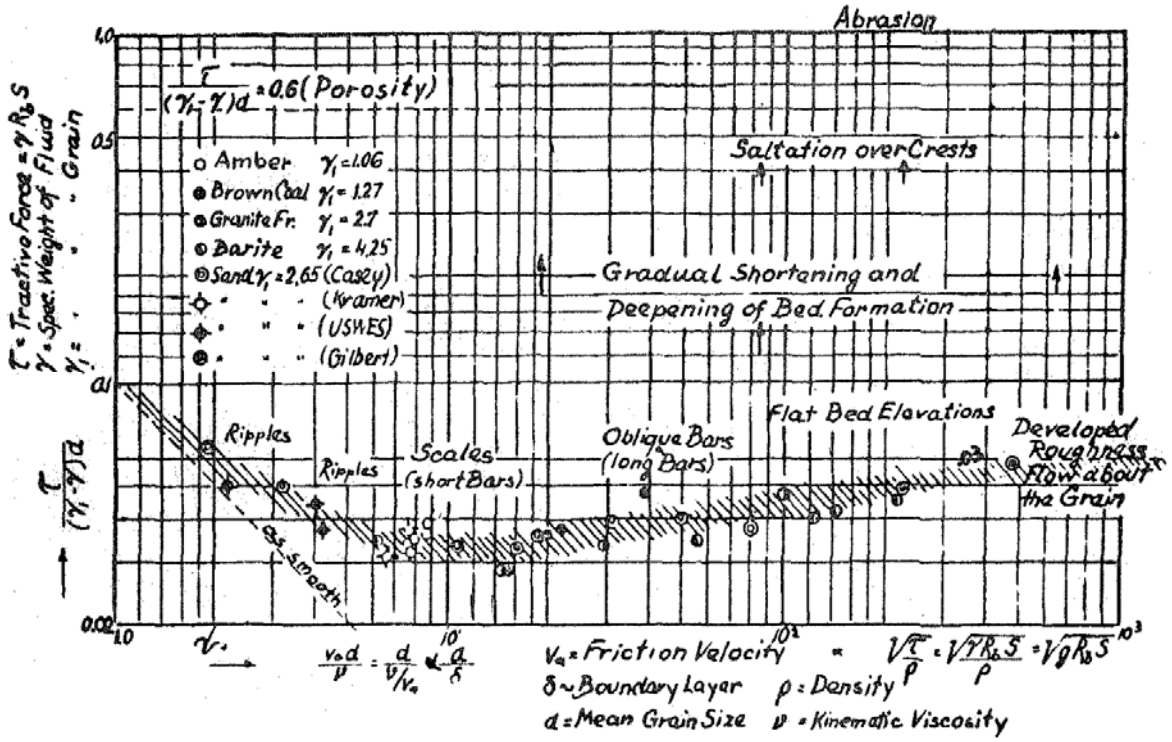

Figure 3. Shields diagram showing the threshold of dimensionless shear stress to motion of particles (Shields, 1936).

A constant value of τ^*_c = 0.047 was identified in the experiments of Meyer-Peter and Müller (1948) in this higher range of Re*, which was then used as the threshold of motion in their widely applied bedload formula. In its version revised by Wong and Parker (2006), motion starts at a value of τ^*_c = 0,0495:

$$q_b = 3.97\sqrt{\frac{\rho_s - \rho}{\rho} g d^3}\left[\frac{\tau}{(\rho_s - \rho)gd} - 0.0495\right]^{\frac{3}{2}} \quad (6)$$

Where q_b is the volumetric bedload transport per m of river width (m^3 s^{-1} m^{-1}). Note that the exponent increases bedload transport with increasing bed shear stress according to a concave-up power function.

At the same discharge, bedload decreases with increasing grain size, as a larger bed shear stress τ is needed to exceed the critical dimensionless shear stress τ^*_c.

Due to the dependence of the bed shear stress on the water depth and the gradient shown here, these two variables are decisive for bedload transport and must be taken into account accordingly in analysing the effects of channelization on sediment transport.

1.4.1.2 Transport of suspended sediment

With decreasing grain size the settling velocity in water decreases. Below a threshold, as delineated in Eq. 1, the turbulence maintains the grains in suspension. Then, the grains are transported at about the same speed as the flowing water, and they only deposit on the bed when the flow velocities strongly reduce (Knighton, 1998).

1.4.2 Morphodynamics

1.4.2.1 Bed level change

Morphodynamics result from changes of sediment transport in space. In one-dimensional view, if sediment transport increases in downstream direction, the bed is eroded, whereas deposition of sediment causes a decrease of sediment transport. This relationship between bed level change and sediment transport is expressed by the Exner equation:

$$\frac{\delta \eta}{\delta t} = \frac{1}{n-1}\frac{\delta q_s}{\delta x} \tag{7}$$

where η = bed elevation (m), q_s = sediment transport ($m^3\ s^{-1}\ m^{-1}$), n = porosity, t = time, and x = distance in downstream direction (m).

1.4.2.2 Riverbank erosion

River bank erosion is an integral element of rivers, as lateral dynamics are essential for natural morphologies to develop. Riverbank erosion causes a shift of the bank lines as a reaction to the flow of water and sediment in the channel, in turn changing the boundary conditions for hydrodynamics and sediment transport in the channel. Bank erosion widens the channel and reduces the shear stresses in other parts of the channel, there allowing the deposition and eventually the emergence of bars above the water surface. Due to the lateral dynamics caused by bank erosion, and due to the bank-derived sediment delivered into the channel, a large amount of sediment participates in sediment transport. The repeated reworking of the river bed reduces armouring of the riverbed surface and clogging with interstitial fines.

At the Mura, Drava and Danube, the floodplains consist at least to a part of fine sediment with cohesive properties. These fines deposited during overbank flow or on bars, so that the fine sediment layers are usually located in higher elevations of the bank. Given the cohesion between the particles, the bank faces may reach inclinations which are higher than the friction angle of the sediment.

Riverbank erosion mainly is the result of two processes, fluvial erosion and mass failure (e.g. Thorne, 1982; Rinaldi and Darby, 2008):

Fluvial erosion: Fluvial erosion is caused by the shear stresses of the flow at the surface of the bank, where it entrains single particles or particle aggregates. Fluvial erosion concentrates on the lower part of the bank, where the shear stresses more likely and more often exceed critical thresholds, eventually scouring more erodible layers. This causes the bank to steepen and to decrease the stability with respect to mass failure.

While formulas to consider the transport of loose gravel on inclined surfaces exist (e.g. Lane. 1955), fluvial erosion is more complex when the river bank consists of fine sediment

with cohesive properties. Given the variety of factors involved, the erosion rate of cohesive sediment is usually described based on empirically measured erodibility parameters with an excess shear stress formula (e.g., Partheniades, 1965):

$$\varepsilon = k_d(\tau - \tau_c)^a \quad (8)$$

where ε = erosion rate (m s^{-1}), k_d = erodibility coefficient (m^2 s kg^{-1}), and a = empirically fitted exponent (-).

Mass failure: In contrast to the more continuous process of fluvial erosion, mass failures are spontaneous collapses of blocks, eventually ranging over the entire bank height. Mass failures are caused by gravitation when destabilising forces exceed stabilising forces. The stabilising resisting force F_R and the destabilising driving force F_D counteract in a failure plane within the bank, which is illustrated for a simple geometrical scenario based on a simple analysis method in Figure 4.

The driving force is calculated via:

$$F_D = sin\beta\, W \quad (9)$$

where W = the weight of the potential failure block (N), and β = the inclination of the slip surface (°). For the geometry in Figure 4, W is calculated via:

$$W = \frac{H^2}{2}\gamma\left(\frac{1}{\tan\beta} - \frac{1}{\tan i}\right) \quad (10)$$

Where i = the inclination of the bank surface (°), γ = the unit weight of the bank sediment (N m^{-3}), and H = bank height (m).

The resisting force is given by:

$$F_R = W\cos\beta\tan\varphi' + L\,c' \quad (11)$$

Where φ' = the friction angle (°), c' = cohesion of the bank sediment (N m^{-2}), and L = the length of the slip surface (m).

$$L = \frac{H}{\sin\beta} \quad (12)$$

The bank collapses, when the factor of safety $FS=F_R/F_D$ falls below the value of one.

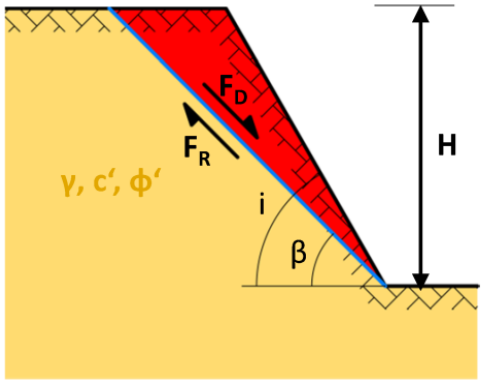

Figure 4. Resisting and driving forces F_R and F_D, counteracting in the slip surface and determining the bank stability with respect to mass failure. The unit weight γ, cohesion c' and friction angle φ' as the geotechnical properties and the bank inclination i determine both F_D and F_R. The angle β is the angle producing the smallest factor of safety $FS=F_R/F_D$.

Depending on the bank characteristics, but also on the elevation of fluvial erosion along the bank, different geometries of the bank face develop. In non-cohesive banks, the banks have a small inclination and bank failures are shallow. With increasing cohesion, banks may become steeper and tension cracks may leave behind vertical bank faces after failure. In addition, the inclination depends on the water surface elevation with respect to the bank height during erosive flows. The flow condition is strongly related to the bed morphodynamics. While along the outer banks of a river bend the strength of the flow usually increases with discharge, the timing of bank erosion – and hence the elevation of bank scouring – is different in interaction with bars, as described in the following chapter.

1.4.2.3 Bar-bank interactions

Mid-channel bars are observed in straight and meandering rivers (Hooke, 1995). In braided rivers mid-channel bars cause flow divergence (Leopold and Wolman, 1957), while in meandering rivers mid-channel bars may facilitate the formation of meander loops, after one of the two surrounding branches fills up with sediment and becomes attached to the bank (Knighton, 1972). Mid-channel bars may develop quickly and may be associated with excessive widening of the channel (Knighton, 1972; Hooke and Yorke, 2011). Based on repeated field mapping, Hooke (1986) derived the sequence of possible mid-channel bar growth shown in Figure 5.

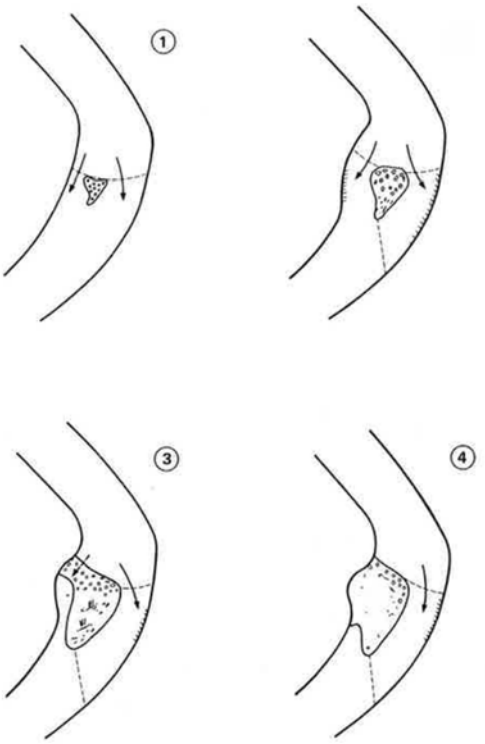

Figure 5. Sequence of the emergence of a mid-channel bar (Hooke, 1986).

Mid-channel bars grow during the higher discharges of flow events, when the bar becomes submerged. The lower flows, which follow the event find a strongly altered geometry of the branches, which causes increased flow velocities and discharges at low water levels and massive scouring along the bank toe and transport of failed material. The occurrence of several events then may cause excessive widening. Klösch et al. (2015) conceptualized the interaction between bar accretion and bank erosion in Figure 6. The bank erosion processes related to this bar-bank interaction produce steep bank faces, given the concentration of scour along the bank toe and the development of vertical tension cracks prior to failure. Supply of sediment from upstream is required to cause bar aggradation and to initiate the described process and bank formation.

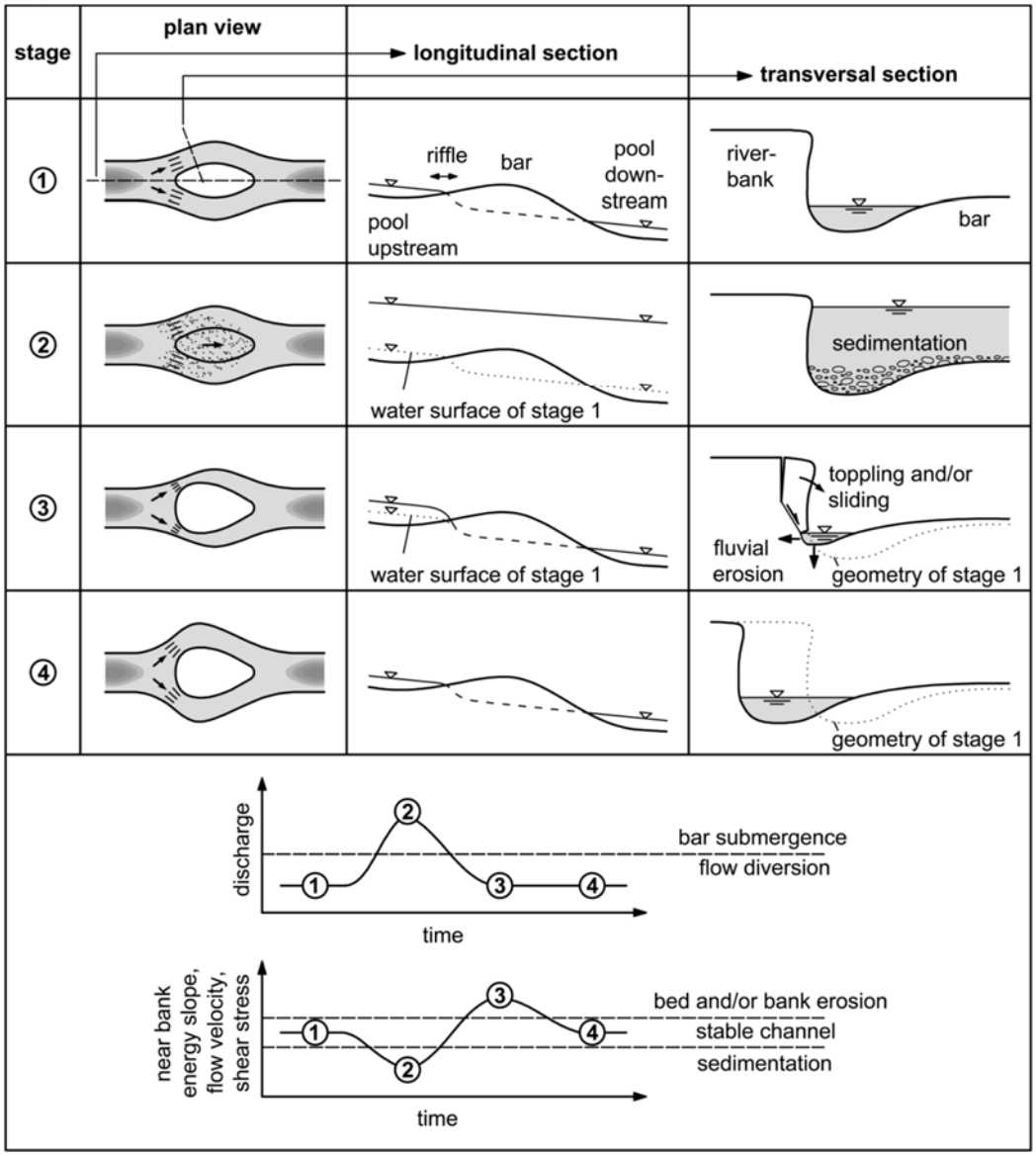

Figure 6. Conceptual model of bar- bank interactions, explaining the excessive widenings occurring at mid-channel bar sections (Klösch et al., 2015).

1.4.2.4 Ecological relevance of morphodynamics

Riverbank erosion repeatedly creates steep bank faces used as habitats by bank-nesting birds, which without continued erosion would flatten, become vegetated and stabilise over time. Similarly, bars provide bare surfaces for pioneer vegetation and for bar breeding birds, but become fully vegetated once they reach higher elevations, eventually becoming a new floodplain and providing other services to the ecosystem. However, the habitats required for rejuvenation often are bottlenecks for populations of riverine species (Cantin and Post, 2018) given the multiple human impacts. Accordingly, repeated morphodynamics are required for a sustaining provision of habitats.

1.4.3 Sediment budget

The sediment budget of natural rivers usually develops towards a state of dynamic equilibrium, where the amount of sediment supplied from upstream into a reach equals the sediment transported out of this reach. The sediment budget in this reach can be

dynamic as the volumes naturally fluctuate around mean values. The dynamics of the budget result from sediment moving as pulses through the system and from discontinuous processes such as bank failures. Figure 7 displays the different components of the sediment budget.

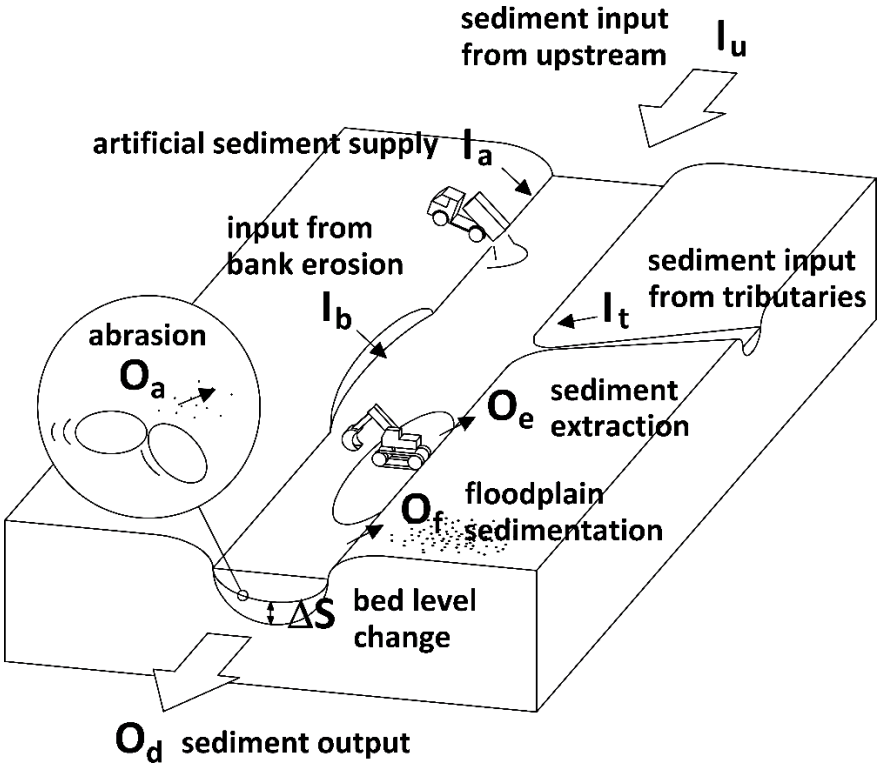

Figure 7 Sediment budget components (modified by Klösch and Habersack, 2017 from Frings et al., 2014).

1.4.4 Morphology of natural rivers with balanced sediment budget

Natural rivers adjust their morphology to their boundary conditions. Altered boundary conditions hence force the rivers to form a new bed. Given the limited sediment discharge, and depending on the size of the catchment, these changes may take decades or centuries, and problems related to the change usually already occur before the river attained its new dynamic equilibrium.

Attempts were made to delineate morphologies based on channel parameters. Leopold and Wolman (1957) related the channel slope to the bankfull discharge and determined a threshold between meandering and braiding, suggesting that rivers with a lower gradient tend to form single-thread rivers (Figure 8). The threshold found between braided and meandering rivers is given by:

$$I = 0.06Q^{-0.44} \quad (13)$$

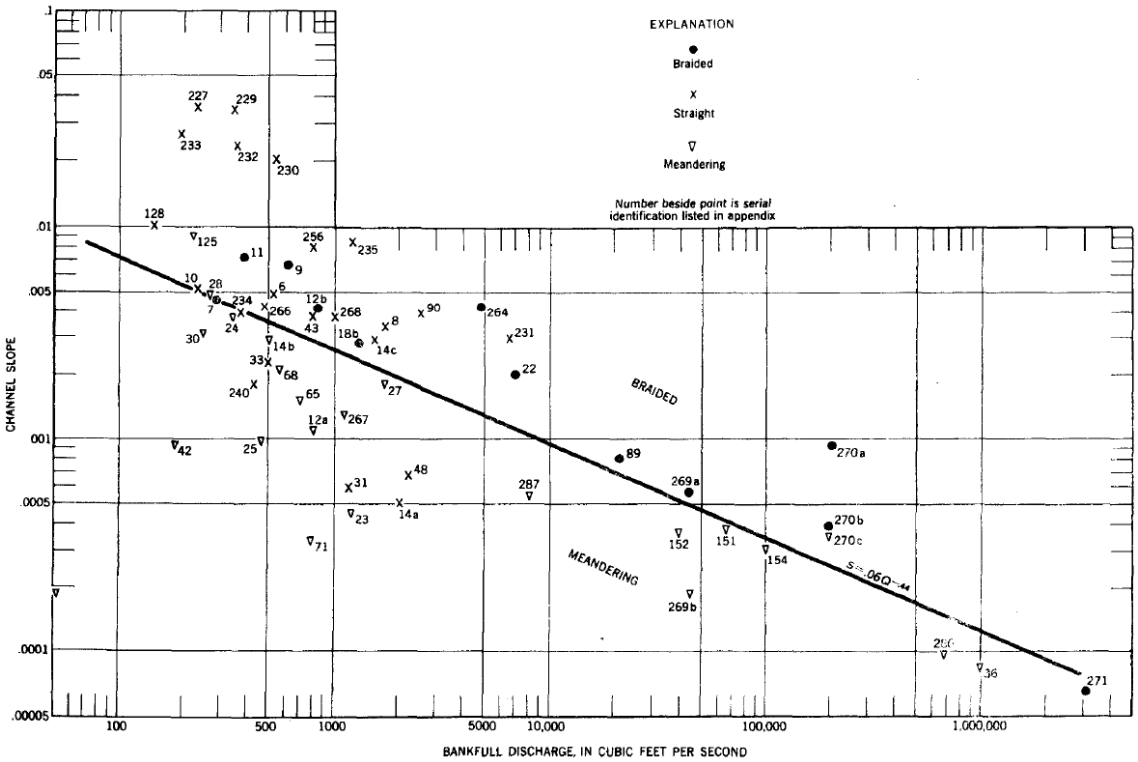

Figure 8. Values of channel slope and bankfull discharge for different natural rivers and an identified threshold function separating meandering and braiding rivers (Leopold and Wolman, 1957).

The (B/h;h/D) diagram of Da Silva (1991) relates the width/depth ratio to the ratio between water depth and grain size, allowing different morphological types to be delineated (Figure 9). This diagram can be used to estimate the channel width required to restore a particular morphology. The formulas delineating different morphologies were derived from natural rivers and from laboratory rivers in dynamic equilibrium, hence they are applicable to disturbed rivers only with limitations.

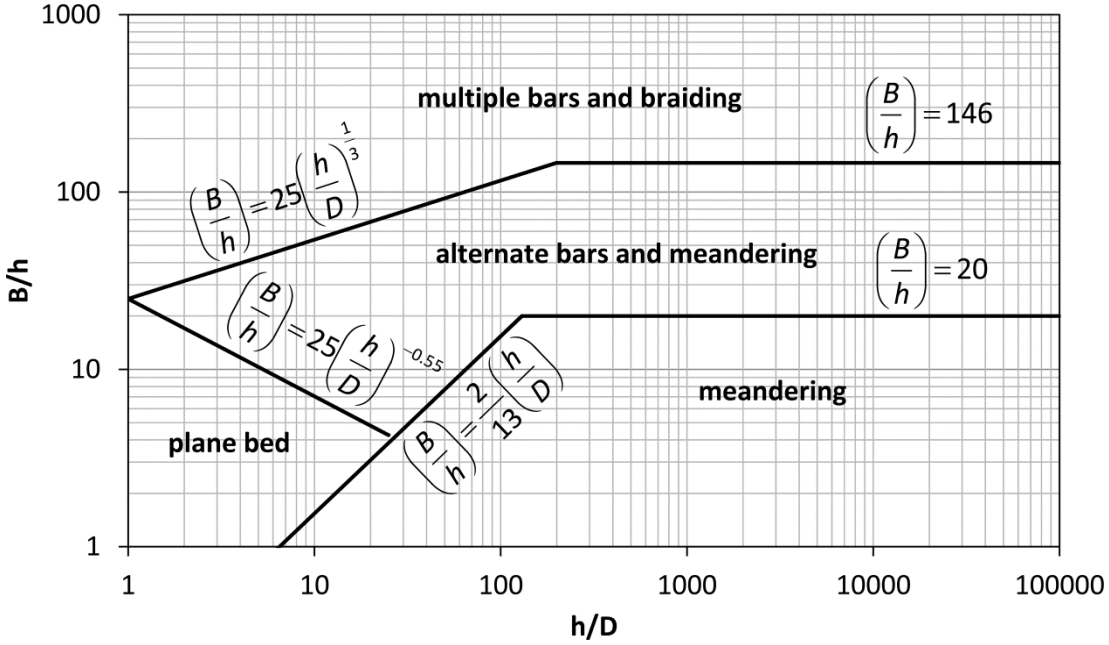

Figure 9. The Da Silva (1991) plan (displayed here in its revised form based on Ahmari and Da Silva (2011)) provides an understanding of thresholds in river morphology useful in planning bed widenings. B: flow width, h: flow depth, and D: grain size.

Parker et al. (2007) could well derive morphological parameters (depth, width and slope) based only on water discharge and median grain size (Figure 10). As these regime equations were derived on data from natural rivers only, it is not accounting for alterations such as reduced sediment supply. Also, these equations were derived from single-thread channels only. However, the relationships reflect the dependency of the morphology on larger scale boundary conditions.

$$H_{bf} = \frac{0.382}{g^{1/5}} Q_{bf}^{2/5}$$

$$B_{bf} = \frac{4.63}{g^{1/5}} Q_{bf}^{0.4} \left(\frac{Q_{bf}}{\sqrt{g D_{s50}}\, D_{s50}^2} \right)^{0.0667}$$

$$S = 0.101 \left(\frac{Q_{bf}}{\sqrt{g D_{s50}}\, D_{s50}^2} \right)^{-0.344}$$

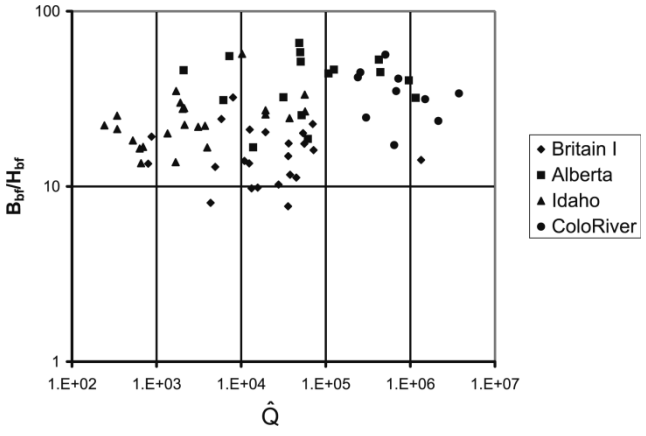

Figure 10. Left: Regime equations derived from natural rivers (British and US-American), calculating from the bankfull discharge Q_{bf} and the median sediment grain size of the bed surface D_{s50} the depth and width of bankfull discharge (H_{bf} and B_{bf}) and the channel slope S. Right: British rivers tended to be narrower than American Rivers, probably due to the effect of increased presence of riparian vegetation in the more humid climate.

Crosato and Mosselman (2009) developed a simple model to predict the number of river bars that occur within a cross-section for a given channel width (Figure 11). It can be used

to determine the effects of width changes on morphological appearance. It should be noted that this tool was derived for channels with a sediment budget in equilibrium. Moreover, the channel width used for the calculations should not exceed the natural channel width under unconstrained conditions.

Table 1. Observed Bar Mode and Number of Bars or Channels per River Cross Section

Number of Bars/Channels	Observed Bar Mode
1	1
1–2	2
2	3
2–3	4
3	5
3–4	6
4	7
4–5	8
5	9
5–6	10
6	11
6–7	12
7	13
7–8	14
8	15
8–9	16
9	17

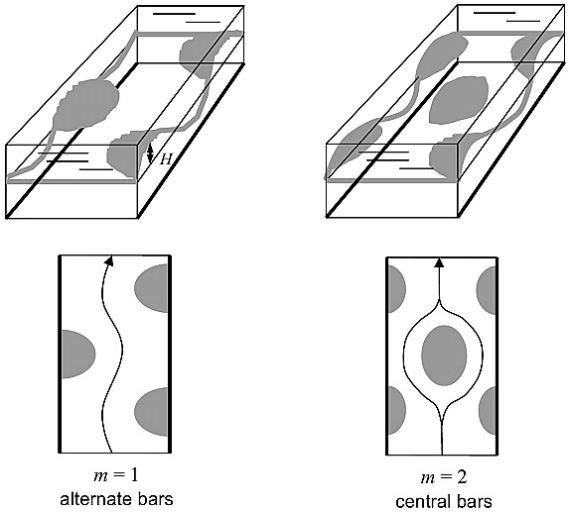

Figure 11. Morphological river type, characterised by the bank mode (number of bars in a cross section) as calculated with the analytical model from Crosato and Mosselman (2009).

The role of sediment supply for the river morphology was mostly investigated for natural rivers in dynamic equilibrium. At dynamic equilibrium, the average sediment discharge in a reach corresponds to the sediment discharge supplied from upstream. We describe insights from natural rivers first, before we illustrate the effects of alterations in sediment supply.

Rivers have often been classified according to their morphological patterns (e.g. Mollard, 1973; Schumm, 1981), based on the appearance of natural rivers which form their bed in their own alluvium. However, only few related the morphologies to the conditions of sediment and sediment supply. Schumm (1985) was the first in relating patterns to conditions of sediment transport. From observations, he derived that higher sediment loads produced wider and less stable morphologies (Figure 12).

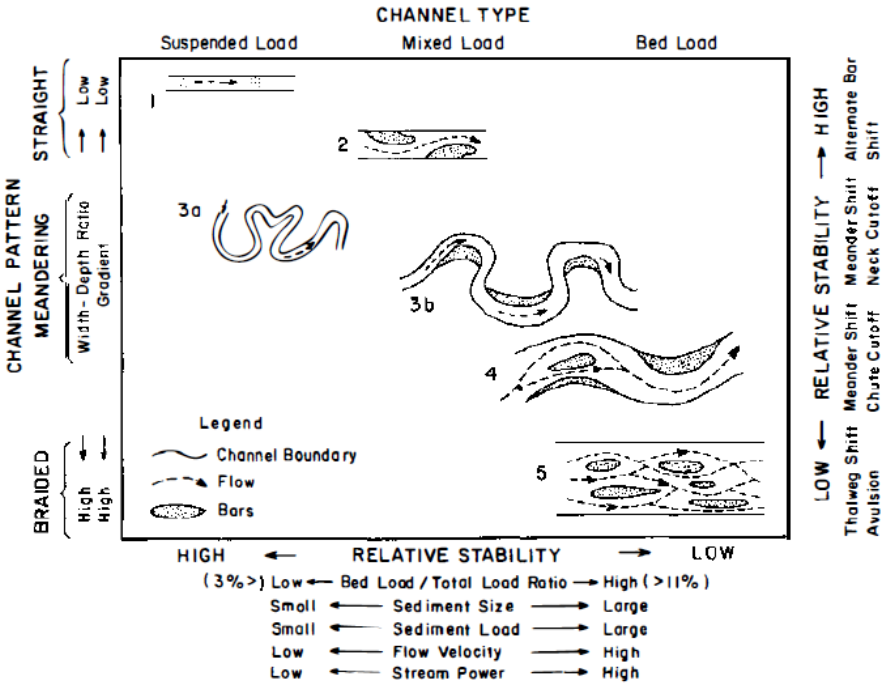

Figure 12. Dependency of the river morphology on sediment characteristics, including sediment yield (Schumm, 1985).

Church (2006) described a similar relationship, in which rivers gain greater widths and/or a more pronounced curvature at larger sediment supplies (Figure 13).

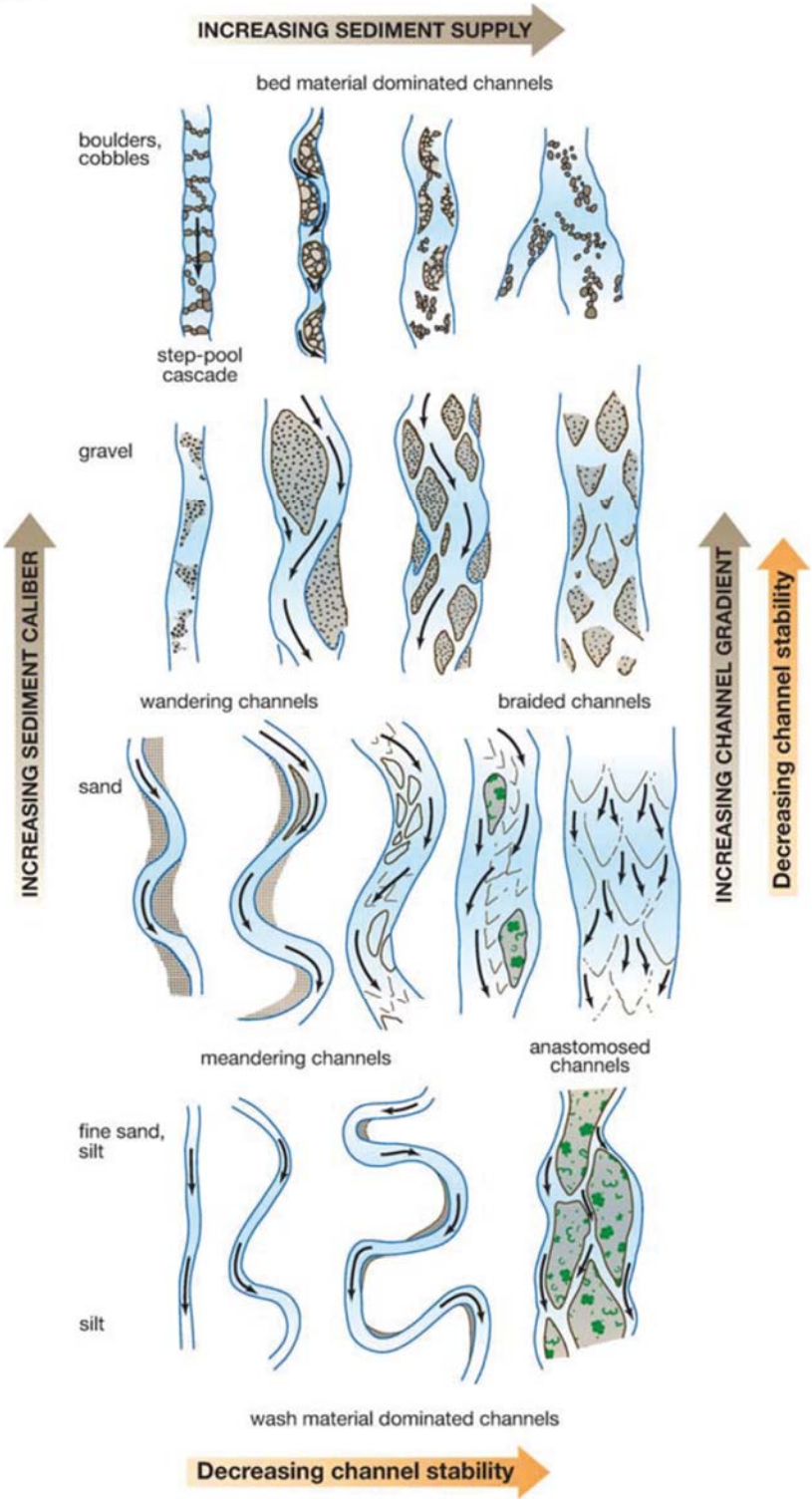

Figure 13. Dependence of morphology and stability on the amount of sediment input and grain size (Church, 2006).

A direct link between sediment discharge and forming morphologies, which is based on measured parameters, could be established by Mueller and Pitlick (2014). In relating the bedload concentration (bedload discharge divided by the water discharge) at bankfull discharge, Mueller and Pitlick (2014) identified a threshold between a single thread morphology and a braided morphology (Figure 14).

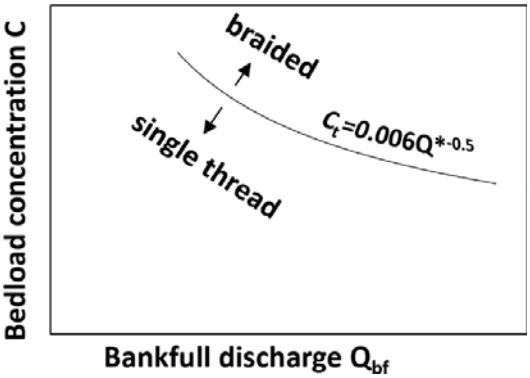

$$Q^* = \frac{Q_{bf}}{\sqrt{(s-1)gD_{50}}D_{50}^2}$$

Figure 14. Dependence of morphology on bedload concentration according to Mueller and Pitlick (2014). Q_{bf} is the bankfull discharge, Q is a dimensionless flow, s = the specific density of the sediment (ρ_s/ρ) and D_{50} the median grain diameter. The bedload concentration C is calculated from the relation between the volumetric bedload transport at bankfull discharge and the bankfull discharge. C_t is the bedload concentration at the transition between single-thread and braided channels.*

1.4.5 Morphology of rivers at budget imbalance

The relationships described above are based on observations at natural rivers, the sediment budget of which at the time of observation was in a state more or less in a dynamic equilibrium. At rivers, which are in disequilibrium as a result of human impacts, the river adjusts to changes in sediment supply by aiming for an adjusted slope. In the case of a sediment deficit, the decrease of slope reduces the sediment transport capacity, until it corresponds to the reduced sediment supply. A river, which suffers a sediment deficit, decreases its slope via bed degradation (Figure 15).

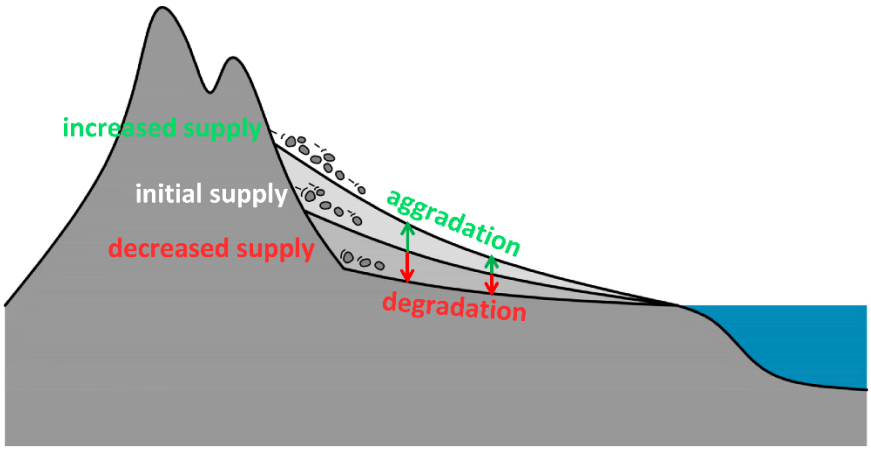

Figure 15. Dependency of the channel slope on the sediment supply.

A deficit of especially bedload is most remarkable directly downstream of sediment barriers, where the bedload discharge is lowest. With increasing distance from the barrier, the bedload discharge increases as the degrading bed cumulatively provides sediment for transport, while in aggrading rivers the bedload discharge would decrease (Figure 16).

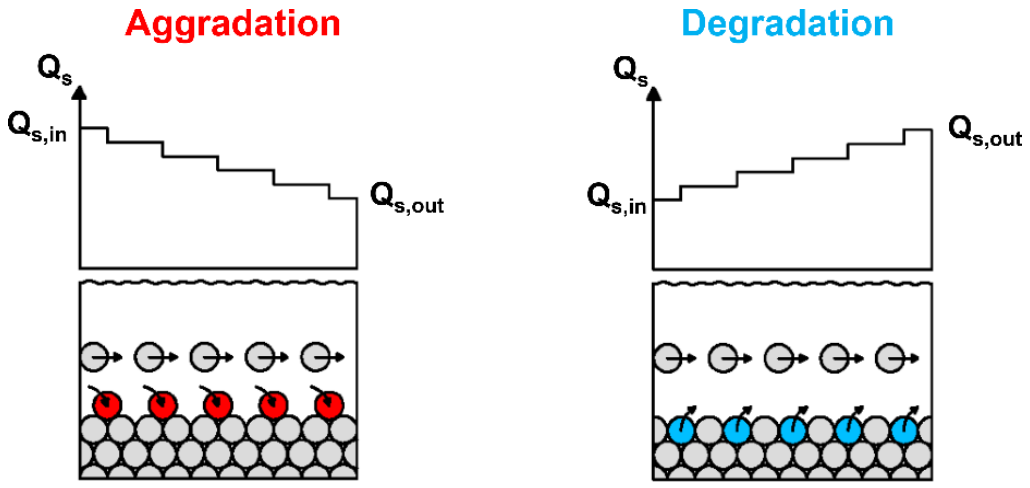

Figure 16. Effects of uniform aggradation/degradation on the sediment discharge.

As depicted in Figure 12 and Figure 13, the sediment discharge does not only affect the channel slope (named channel gradient in Figure 13), but the entire morphological pattern, which includes parameters such as width and depth. Klösch et al. (2019a) related the sediment discharge to the water discharge, and explained trajectories of channel change when either water discharge or sediment supply, or both, are changed (Figure 17).

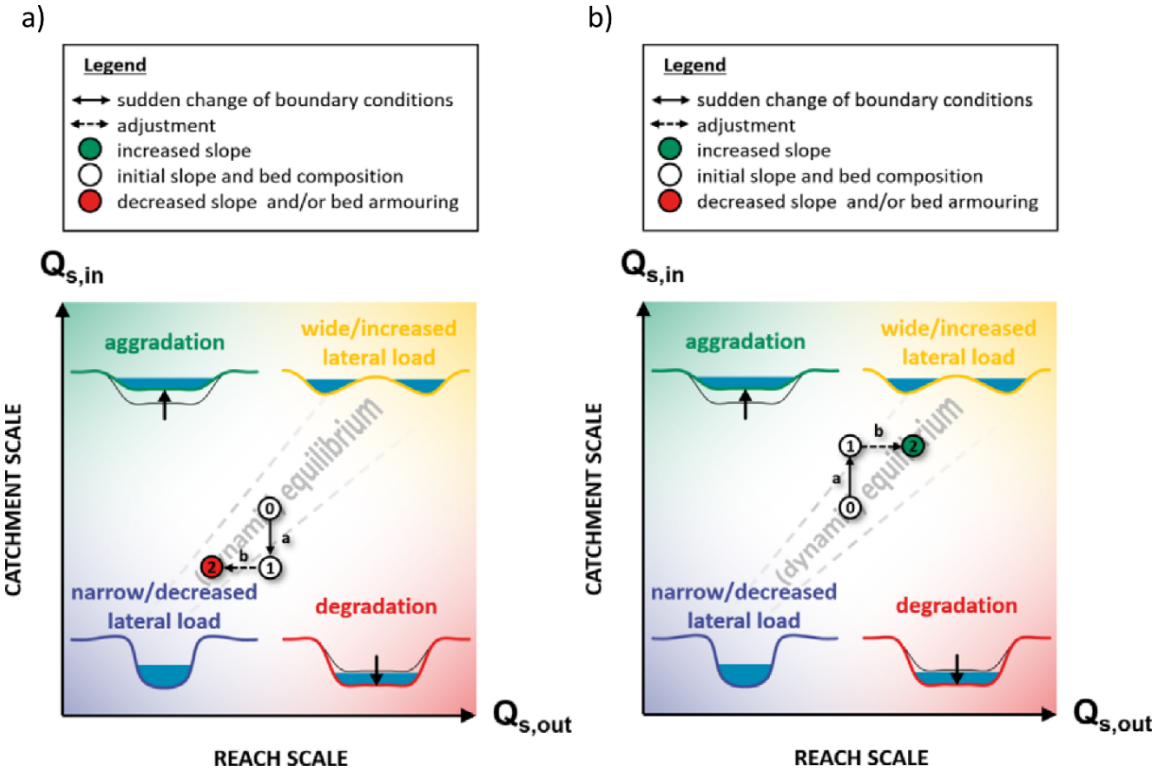

Figure 17. Trajectory of a river as a reaction to a) decrease, b) increase of sediment supply. Qs,in: Sediment discharge supplied into a reach, Qs,out: Sediment supply transported out of a reach (Klösch et al., 2019a).

Accordingly, a decrease of sediment supply would cause degradation (trajectory a in left diagram of Figure 17), until a morphology and slope develop which adjusts the sediment transport capacity to the supply (trajectory b in left diagram of Figure 17). In the end, the morphology is narrower with decreased lateral dynamics given a decreased hydraulic

load acting onto the banks. Conversely, when sediment supply increases, a river would aggrade (trajectory a in right diagram of Figure 17) and in the end form a wider morphology with increased lateral dynamics after adjusting the sediment transport in the reach to the increased supply (trajectory b in right diagram of Figure 17).

The relationships between the sediment supply and channel width are confirmed by investigations of Marti and Bezzola (2009). In their laboratory experiment, channel width and lateral dynamics decreased strongly when the sediment input was reduced (Figure 18).

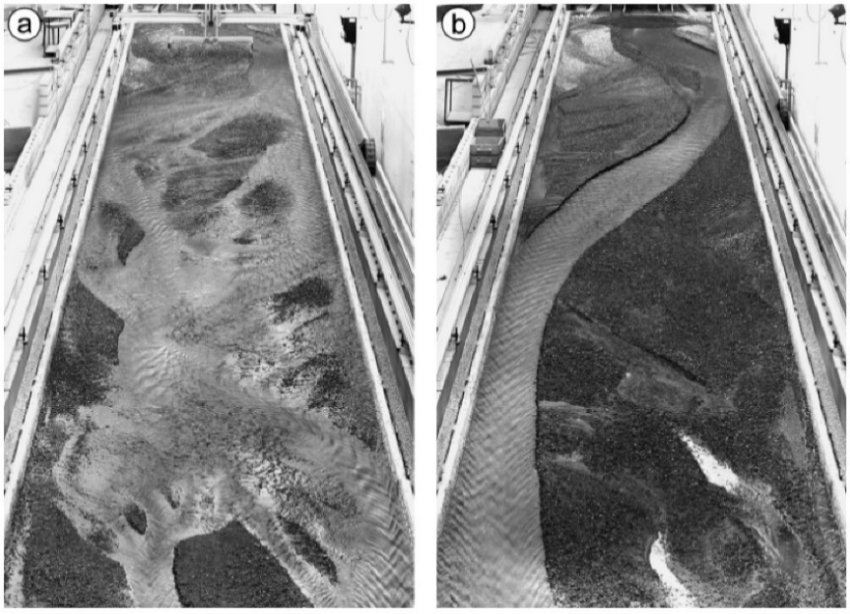

Figure 18. Development from a braided channel to a narrow, single-thread channel after reduction of sediment input (Marti and Bezzola, 2009).

2 Methodology

This chapter shows the methods applied in this study. First, the methods are introduced which were used to characterise the historic and present morphology and the methods used to quantify the differences caused by human alterations. Then, methods are described which allowed an estimation of bed level changes in the TBR MDD. The lateral changes were additionally considered in another method, which addressed the entire cross-sectional changes. Methods are described which delivered sediment budgets, as well as one method to link the morphodynamic changes to the provision of habitats for rejuvenation of key riverine species. For some of the methods data was available for the entire project reach. In that case, results were prepared for the overlay map of the synthesis report D.T1.3.1.

2.1 Analysis of planform change

The basis of these analyses are historical maps from the Second Military Survey of the Austrian Empire (started in 1815, source: Austrian State Archive) which were mapped by Schwarz (2022) in deliverable D.T1.2.1 of the present project. The maps from the Second Military Survey were partly complemented with sections from the Josephinian Land Survey (First Military Survey; source: Austrian State Archive), which was conducted from 1763 to 1787. The use of the less detailed Josephinian Land Survey was necessary to reconstruct the historic meanders in the lower Drava and at some parts of the Danube, which were already heavily altered in the Second Military Survey (Schwarz, 2022). The analyses of the present condition of river training is based on a previous mapping, also conducted by Schwarz (2013).

Some results are presented for individual sections of the Mura, Drava and Danube respectively, as suggested for preparation of the synthesis report on science-based needs for action (D.T1.3.1), which are listed in Table 1.

Table 1. Sections of the Mura, Drava and Danube as proposed by Shwarz et al. (in prep.).

River	Section		Rkm from	Rkm to
Mura	M1	Spielfeld – Croatian border	143	85
	M2	Croatian border – Hungarian border	85	45
	M3	Hungarian border - Drava confluence	45	0
Drava	Dr1	Ormož – Mura confluence	310	235
	Dr2	Mura confluence – Heresznye	235	185
	Dr3	Heresznye – Danube confluence	185	0
Danube	D1	Sio confluence – Drava confluence	1510	1382
	D2	Drava confluence – Backa Palanka	1382	1295

These sections are depicted below in Figure 19.

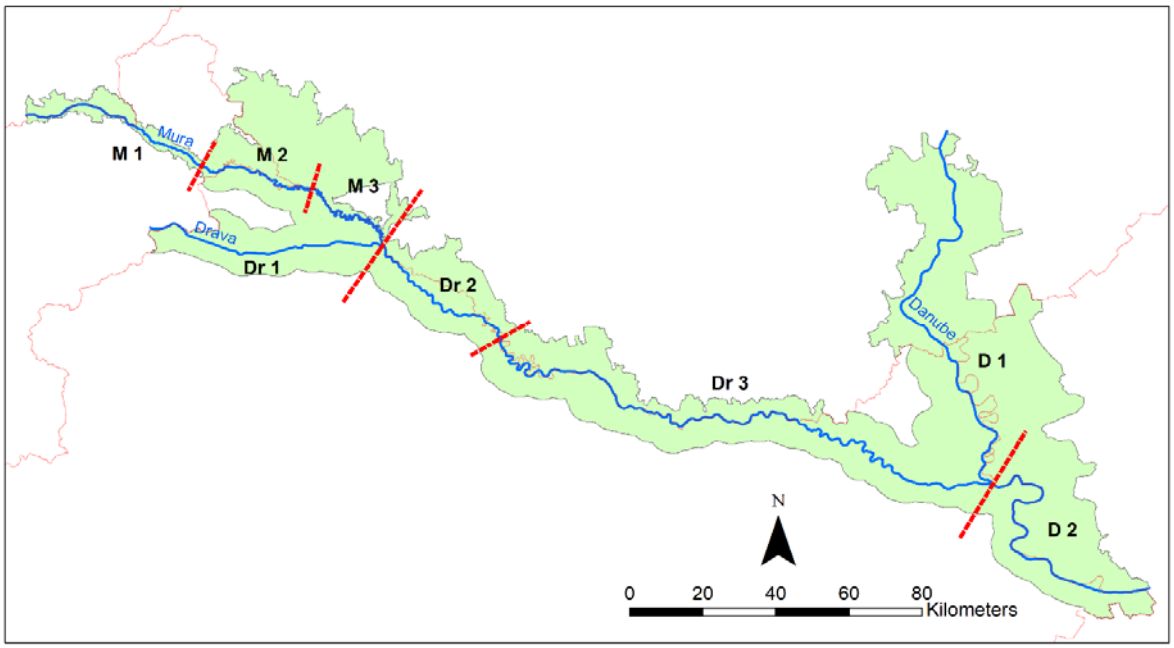

Figure 19. Division of the Mura, Drava and Danube into sections as proposed by Schwarz (2022).

The historic and present planform was analysed along the river network of the TBR MDD. The course of the rivers in their historical and the present condition exhibited to deviate strongly. Accordingly, to compare present and historic planform properties, both states needed to be projected onto a common line. For this purpose, Schwarz (2022) used elevation maps to establish valley axes (Figure 20) of the three TBR rivers that meet this criterion of consistency over time. These valley axes were provided to the partnership as a basis for visualisation of the results of the scientific studies.

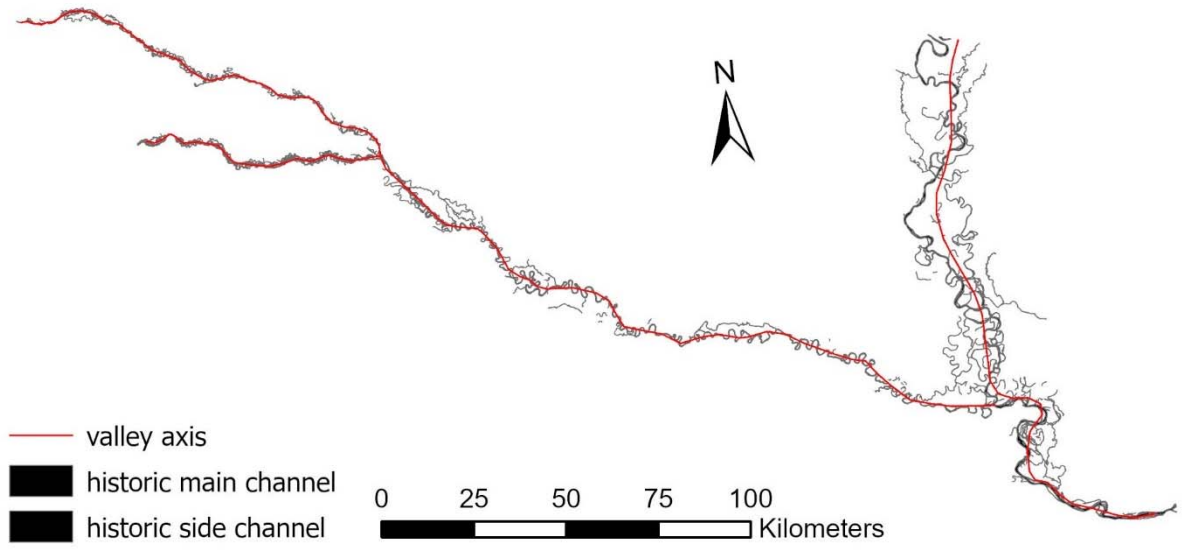

Figure 20. Historic main and side channels of the Mura, Drava and Danube (black) with the overlaying valley axis (red).

Hence, when the results of these analyses are shown, it is often referred to as “valley km” when indicating a position along the rivers.

2.1.1 Width analysis

Perpendicular cross sections were placed along these valley axes at 500 m intervals, which were used to examine the widths of discharging channels. This was achieved by intersecting every valley cross section with the centre lines of all crossing channels, and by measuring the width at every intersection. The channel width was measured perpendicular to the assumed flow direction (Figure 21). Here, the main channels are considered as well as the side channels, as long as they were connected to the flow on both ends. The total discharging width in one valley cross section was then given by the sum of the widths in the individual cross sections.

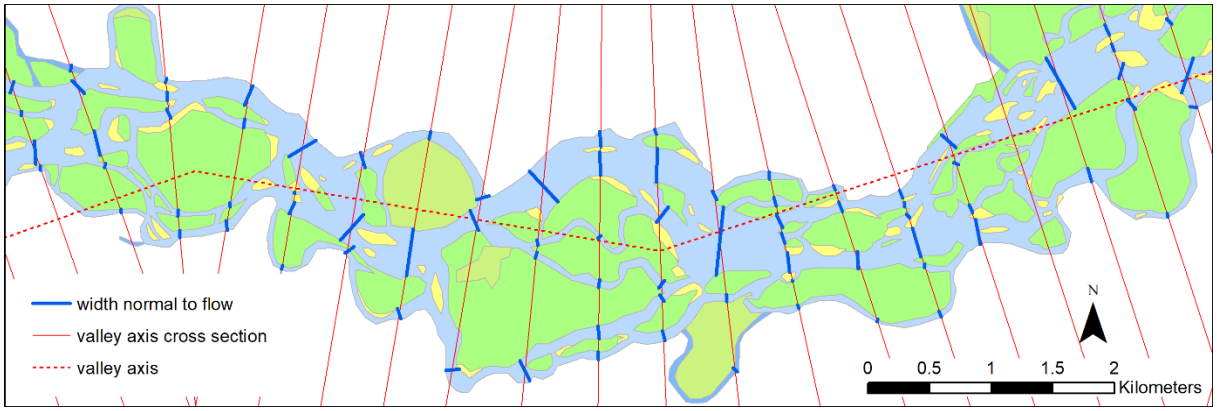

Figure 21. Methodology of the width analysis: Along the valley axis (red, dotted), perpendicular cross sections (red) were placed at a distance of 500 m. Along these valley cross sections, again cross sections (blue) were placed at each intersection of the valley cross section with the centre lines of the individual channels. The sum of the individual blue cross sections along a valley cross section results in the discharged width of the respective valley cross section.

The main criterion here was to capture the entire discharge of the river in the respective valley axis, so whenever the same channel is intersected more than one time by the same valley axis, instead of adding up all cross sections, the arithmetic mean was calculated when calculating the total width. Disconnected side channels which were not connected to the main stream on both ends were neglected, as it was done with tributaries. Note that the obtained width depends on the discharge at the time of mapping, which can only be conjectured.

In addition to assessing the discharging width, the total width between the left water's edge of the most left-discharging channel and the right water's edge of the most right-discharging channel was determined as a measure of the overall width of the river morphology.

In the course of the width assessment, the number of channels in each valley cross section was assessed too, where again multiple intersections of one channel with the same valley axis were counted as one.

2.1.2 Sinuosity and slope

The sinuosity of the TBR rivers was assessed by the quotient of the length of river centreline and the length of the respective valley axis. Since sinuosity is inversely related to slope, the relative change in slope could be derived once the sinuosity was known.

2.1.3 Analyses of river bend radii

For the assessment of the river bend radii once again the river centre lines were considered. Since manual measurement of the numerous bends would have been too time consuming and hence not feasible, a workaround in AutoCAD was used. By fitting a curve to the polyline of the river centrelines and disassembling it into its component parts, the individual radii of the arcs could be exported. This method has the consequence however, that one bend is not described by one single arc with a specific radius, but by multiple individual arcs. The lengths of the arcs however depended on the amount of feature points used to create the polyline, so in bends with small radii, arcs tend to be shorter than in straighter segments.

2.2 Analyses of bed level change

To assess trends in the evolution of the river bed elevations, it is crucial to have long term data at the same locations. Since repeated cross section surveys are rare and/or don't go back far enough in time, gauging stations provide an alternative way of evaluating bed level changes by inferences from water level. Many gauging stations within the TBR MDD were established early in the 20th century and hence allowed a long-term analysis.

Due to different data providers and different recording intervals, it was sometimes necessary to convert the data; for example, existing quarter-hourly values were converted to daily values. In addition to the adjustment of the intervals, changes in the zero level of some stations had to be considered and corrected in the data as well, if possible.

First, river stage data was used to assess the annual values for the maximum, minimum and mean discharge over the entire available period. Here, the river stage at low flow allows to draw conclusions about riverbed elevation changes. Results of this analysis form the first subchapter in the results-chapter.

The station considered within this analysis are depicted below (Figure 22).

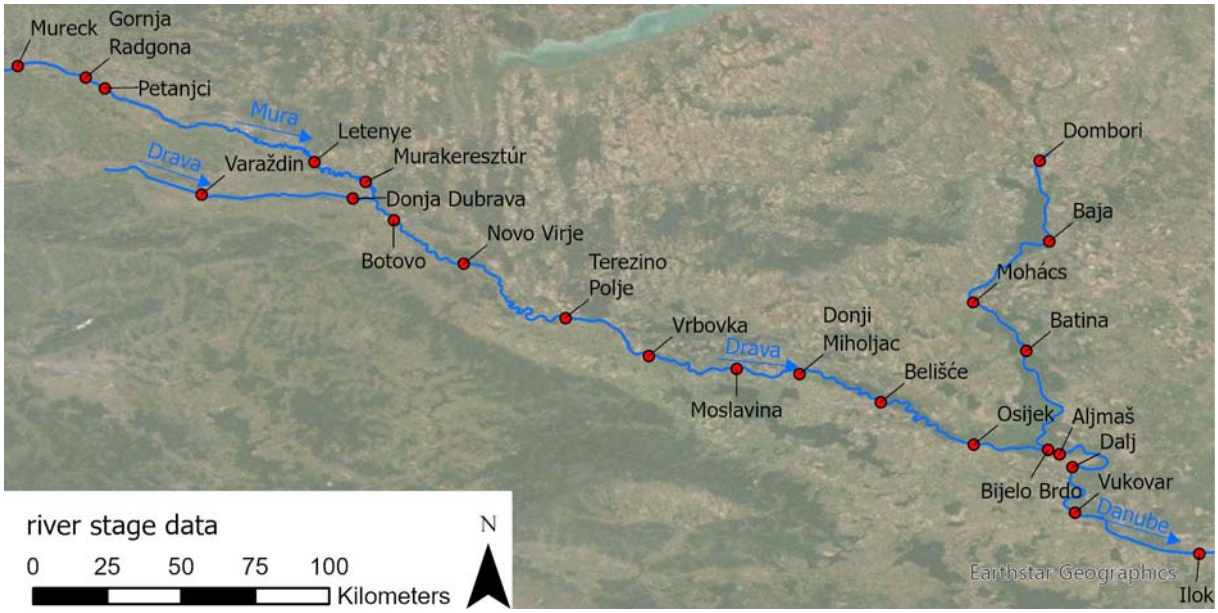

Figure 22. Considered gauging stations.

However, periods with either high or low precipitation may affect the suitability of the water level as a proxy for the bed elevation. Therefore, in combination with discharge data, the average annual mean flow of a given period was calculated and the respective river stage plotted over time, which allowed for an estimation of riverbed incision, which is less dependent on the hydrological variations. The periods analysed are 1993-2019 and 2010-2019, as data is available at many of the gauging stations during these periods.

Stations with both discharge and river stage data are shown in Figure 23.

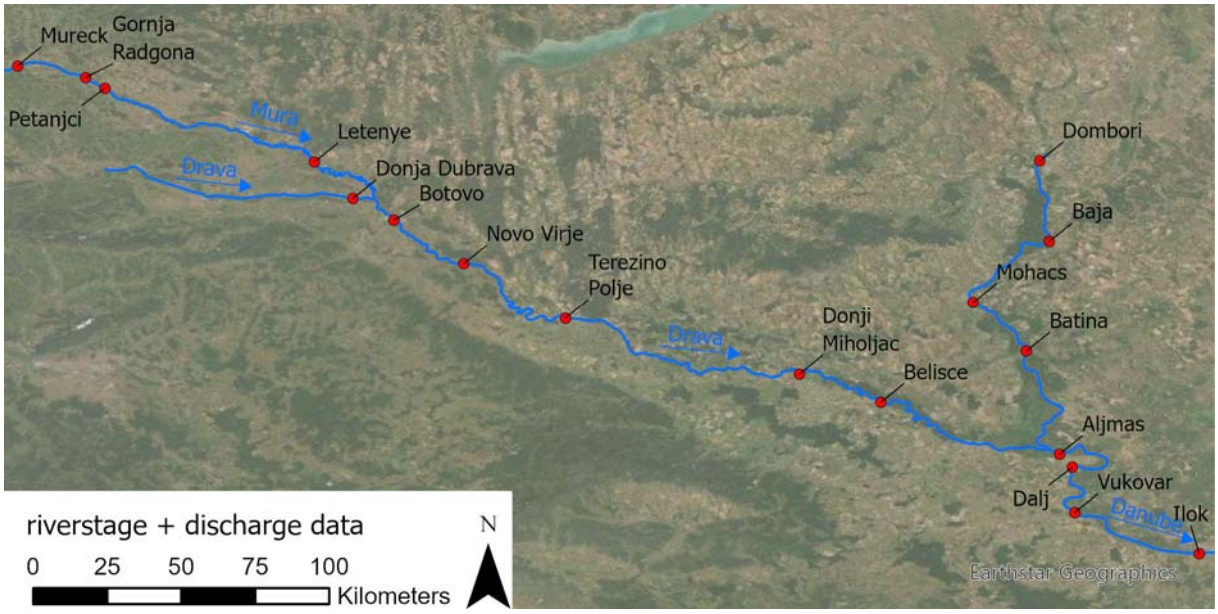

Figure 23. Stations with both discharge and river stage data.

Consequently, the results were plotted in a map showing the mean annual incision rates at those gauging stations.

2.3 Analysis of cross-sectional channel evolution

Along the Drava river, in the most upstream section Dr1 (Figure 24), repeated cross-sectional surveys of the residual flow stretches at the hydropower plants Varaždin, Čakovec and Dubrava were provided for this study.

Figure 24. Most upstream section of the Drava River in the TBR MDD.

The tool CHEVO (Tool for standardised assessment of channel evolution; Klösch et al., 2019a) was used to assess morphological changes in terms of riverbed incision/aggradation, migration of the channel and widening/narrowing. Next to cross

section geometries from repeated surveys, the required input is the channel forming discharge, the manning value and the slope. The manning value was derived by the use of the median diameter d_{50}. Since the only grain size distribution available for the old Drava is at Šemovec at the residual flow of the Čakovec dam, the parameter set for CHEVO was assessed for this reach and used for the Varaždin and Dubrava section as well.

2.4 Sediment transport

Recordings of suspended sediment transport were provided for 12 locations (Figure 25) at varying periods of time. Along the Mura, there are three stations with continuous recordings of suspended sediment transport, the recording period at Mursko Sredisce however proved to be too short to allow for a significant conclusion on the mean annual sediment transport. The same applies to the Danube stations at Batina, Dalj and Ilok, for which only the time series of 2019 was available, which leaves two stations at the Danube River, Dombori and Mohacs. Along the Drava, there are three stations at Botovo, Terezino Polje and Donji Miholjac.

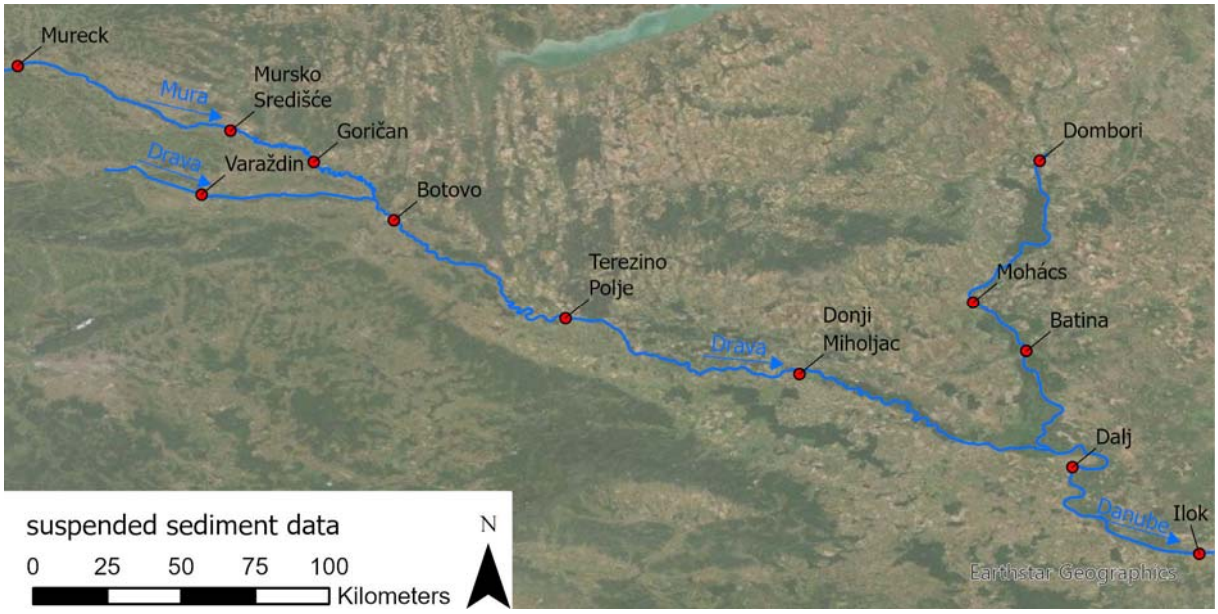

Figure 25. Stations with available data on suspended sediment transport. The recorded periods at Mursko Sredisce, Batina, Dalj and Ilok however proved to be too short to provide significant conclusion on the average annual suspended sediment transport.

The time series of daily suspended sediment transport were used to calculate the annual transport, which was further used to calculate the average transport over longer periods, depending on the data availability.

Data on bedload transport data was available at Letenye (Mura) Botovo, Bélavár, Barcs and Drávaszabolcs (Drava) between 1986 and 2003.

2.5 Sediment budgeting

Sediment budgets could be derived via analysing cross-sectional changes and by calculating sediment yields from recorded bedload and suspended sediment data. Repeated cross section surveys were available from the Mura section along the border between Austria and Slovenia for more than the last 40 years.

2.6 Analyses of implications of morphodynamics for riverine habitats

By using the tool HyMoLink (Klösch et al., 2019b) created in the EU Alpine Space Interreg project HyMoCARES repeated cross section surveys were used to evaluate the relevance of occurring morphodynamics for habitats.

The tool provides data especially on habitats for rejuvenation, which are bottleneck habitats for riverine species in degraded rivers (Cantin and Post, 2018) and must therefore be given top priority in river restoration.

3 Results

The following chapter reports the outcomes of the sediment balance and transport study.

3.1 Planform change

This chapter deals with the flow parameters that can be measured in the planform and that influence sediment transport. Other planform parameters that affect morphological features, such as the number of channels, are described in the following chapter 3.2.

3.1.1 Changes in discharging channel width and total width

Here we distinguish the wetted width of the flowing water and the total width of the morphology, which lies between the outer water edges of the outermost channels. The results are given individually for the Mura, the Drava and the Danube.

3.1.1.1 Mura

The analysis of the widths of the discharging channels of the Mura River are listed below (Table 2).

Table 2. Average discharging widths of the Mura River, relative change and standard deviation in the historic and present state.

	average discharging width (m)		rel. change	standard deviation (m)	
	historic	present	(%)	historic	present
M1	175.43	68.13	-61.16	60.78	13.62
M2	171.95	75.86	-55.89	45.75	18.52
M3	179.96	78.95	-56.13	64.48	20.04

Figure 26 shows the discharging widths of the Mura River in the historic (grey) and present state (black).

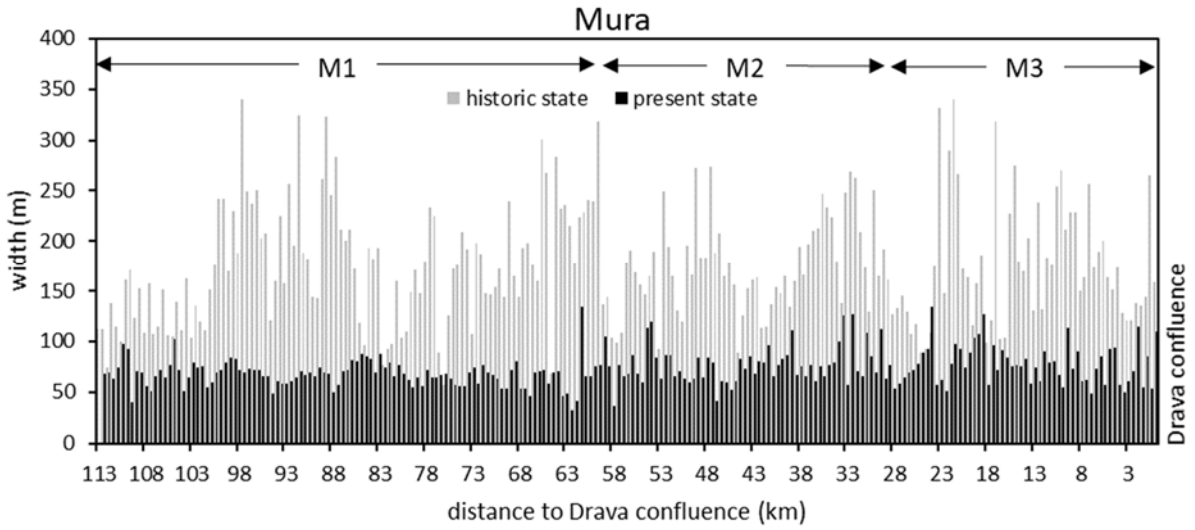

Figure 26. Discharging width of the Mura River from Spielberg to the confluence with the Drava River. The average wetted width decreased by 58% from the historic state (grey) to the present state (black).

The analysis of the Mura River shows discharging wetted widths of up to 350 m in the historic state, with a high diversity of widths along its course. In the present state, the average channel width of the TBR-Mura has been decreased by 58 %, from initially 176 m in 1815 to merely 74 m in 2013. Especially along section M1 from Spielfeld to the Hungarian border, the Mura shows a uniform channel in its present state. All three sections however show a similar decrease in mean wetted width ranging from 39 % to 44 % of the widths in the reference state. The standard deviation along the Mura, ranging from 45 m to 61 m in the historic state, dropped to 13 m to 20 m in the present state, which shows the loss of variety in width.

Table 3 contains the total widths measured between the left water's edge of the most left-discharging channel and the right water's edge of the most right-discharging channel along the Mura River in the historic and present state. The relative reduction in total width is even greater than the reduction in discharging width, reaching an average value of minus 89.17 % for the Mura River.

Table 3. Average total widths of the Mura River, relative change and standard deviation in the historic and present state.

	average total width (m)		rel. change
	historic	present	(%)
M1	1139.44	72.86	-93.61
M2	784.86	110.31	-85.94
M3	527.18	129.07	-75.52

Figure 27 displays the most apparent reduction in total width between Bad Radkersburg (valley km ~83) and Mureck (valley km ~102) in the Mura section M1. The systematic channelization disconnected the Mura from the floodplains of its former river morphology.

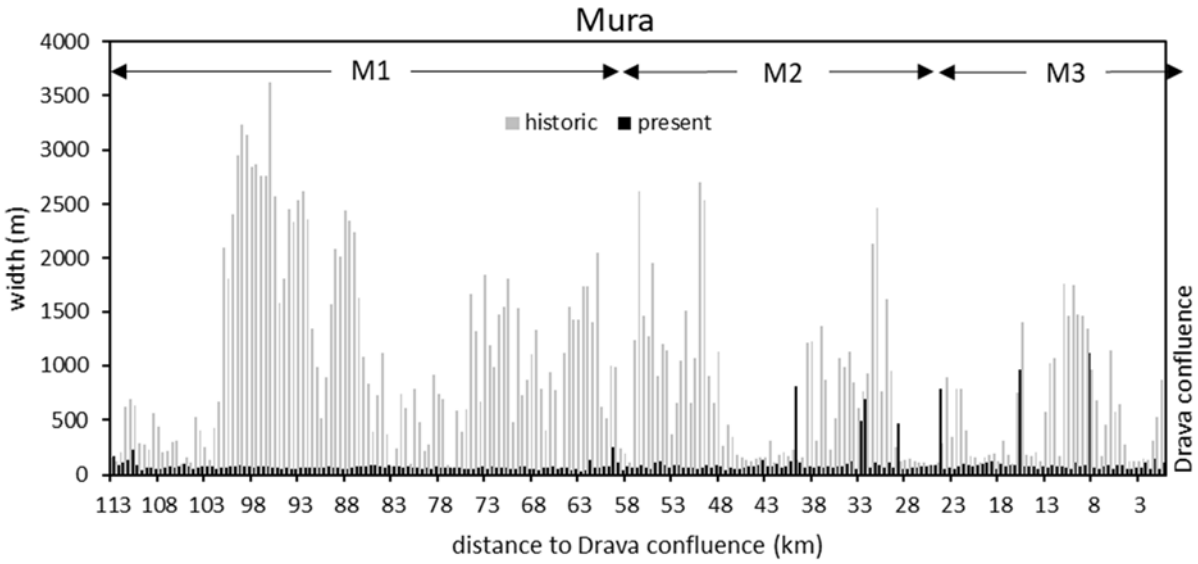

Figure 27. Total width between the left water's edge of the most left-discharging channel and the right water's edge of the most right-discharging channel along the Mura River in the historic and present state.

3.1.1.2 Drava

The analysis of the widths of the discharging channels of the Drava River are listed below (Table 4).

Table 4. Average discharging widths of the Drava River, relative change and standard deviation in the historic and present state.

	average discharging width (m)		rel. change	standard deviation (m)	
	historic	present	(%)	historic	present
Dr1	374.25	81.04	-78.34	129.89	31.97
Dr2	382.46	194.99	-49.02	182.61	51.65
Dr3	230.36	198.43	-13.86	64.95	45.06

The sections Dr1, Dr2 and Dr3 of the Drava River differ significantly from each other, as illustrated in Figure 28.

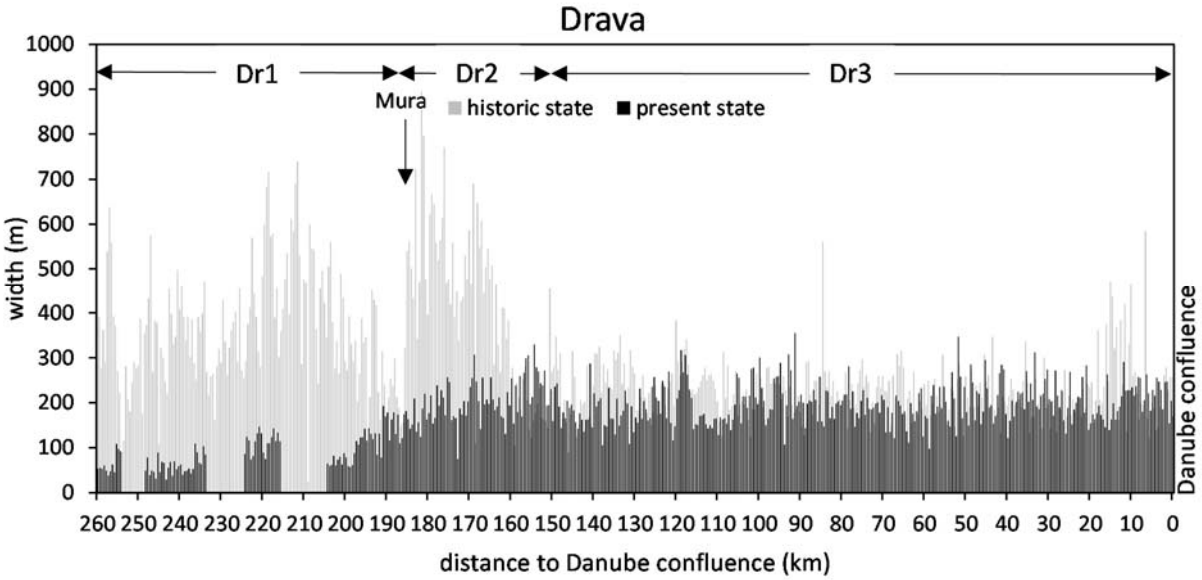

Figure 28. Wetted width of the Drava River from Ormož to the Danube confluence in the historic state (grey) and in the present state (black).

In section Dr1, upstream of the Mura confluence, the differences between the reference state and the present state are most apparent. With the three large reservoirs Varaždin, Čakovec und Donja Dubrava and their headrace channels excluded, the mean wetted width in this section drops by 78%, from initially 374 m to 81 m in 2013. In section Dr2 (between the Mura confluence and Hereszney), the average wetted width of 195m is only about half of the original width of 383 m. In section Dr3 upstream of the Danube confluence, the width reduction is relatively low; by reaching an average width of 198m, the Drava still has 86 % of its original width of 230 m. However, this is due to the transition of the river system from an anabranching to a meandering morphological type, the artificial constraints are particularly noticeable here in the river length, as will be shown further below.

Table 5 compiles the total widths measured between the left water's edge of the most left-discharging channel and the right water's edge of the most right-discharging channel along the Drava River in its historic and present state. On average, the total width of the entire Drava in the TBR MDD is reduced by 82.05 %.

Table 5. Average total widths of the Drava River, relative change and standard deviation in the historic and present state.

	average total width (m)		rel. change
	historic	present	(%)
Dr1	1156.35	150.81	-86.96
Dr2	3552.45	469.39	-86.79
Dr3	1212.51	274.44	-77.37

The reduction of the overall width is most obvious downstream of the confluence of the Mur with Dr2 (Figure 29). There, the river morphology still retains some of its width, mainly because of the small but discharging side channels.

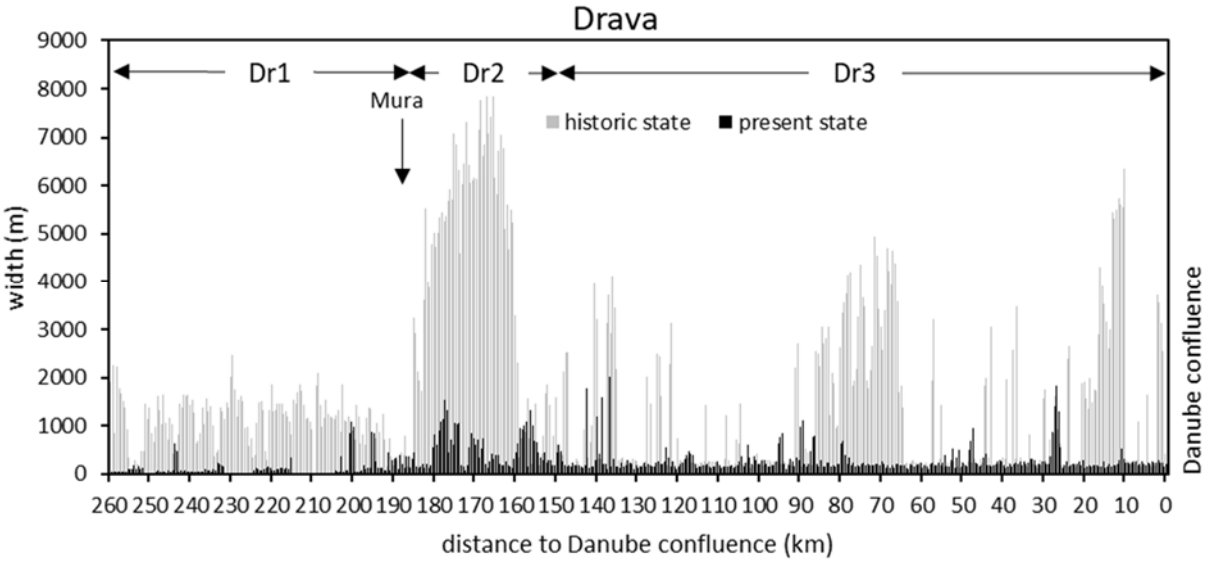

Figure 29. Total width between the left water's edge of the most left-discharging channel and the right water's edge of the most right-discharging channel along the Drava River in the historic and present state.

3.1.1.3 Danube

Table 6 lists the average widths of the discharging channels and standard deviation in the present and the historic state as well as the relative changes.

Table 6. Average discharging widths of the Danube river, relative change and standard deviation in the historic and present state

	average discharging width (m)		rel. change	standard deviation (m)	
	historic	present	(%)	historic	present
D1	567.01	485.39	-14.40	190.05	85.09
D2	660.63	512.88	-22.36	161.30	123.71

Figure 30 shows the wetted widths along the Danube within the TBR.

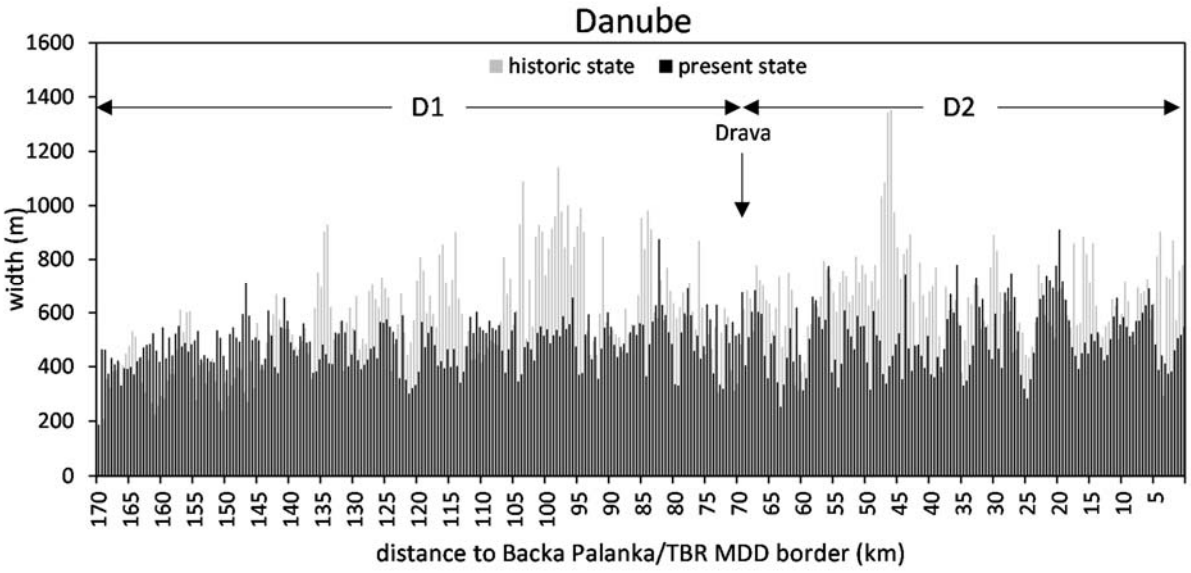

Figure 30. Wetted width of the Danube from the Drava confluence to Backa Palanka in the historic state (grey) and in the present state (black).

While in the upper part of D1 the change in width is less distinct, it changes with distance downstream, mainly given due to an increase of historic width. On average, the wetted width of the historically meandering river in D1 was 17 % wider than it is in the present state, which means a reduction from initially 567 m to 485 m. Downstream of the Drava confluence, the mean wetted width decreases by 22 % from 661 m to 513 m.

Table 7 contains the total widths measured between the left water's edge of the most left-discharging channel and the right water's edge of the most right-discharging channel along the Danube River in the historic and present state. Also at the Danube, the relative reduction in total width is even greater than the reduction in discharging width, reaching an average reduction by minus 76.56 %.

Table 7. Average total widths of the Danube River, relative change and standard deviation in the historic and present state.

	average total width (m)		rel. change
	historic	present	(%)
D1	6133.19	1318.38	-78.50
D2	2522.37	775.49	-69.26

Figure 31 displays the total width along the sections D1 and D2 of the Danube. Upstream of the confluence with the Drava River, side channels at far distance from the main channel yielded total widths of up to 18 km. Large parts of a wide floodplain remained at the confluence with the Drava in the nature park Kopački rit.

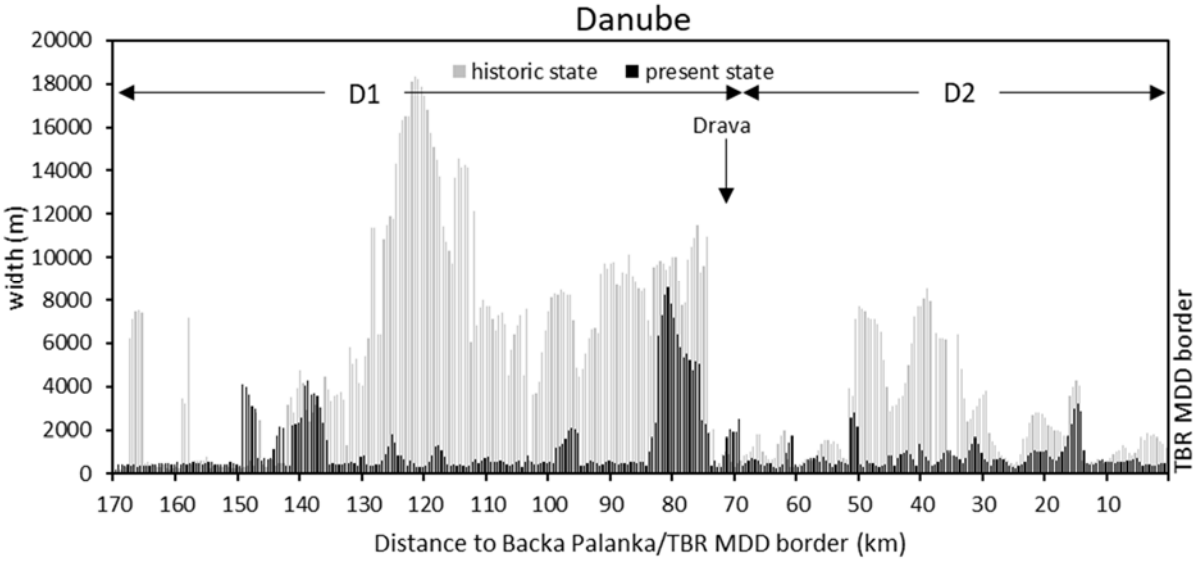

Figure 31. Total width between the left water's edge of the most left-discharging channel and the right water's edge of the most right-discharging channel along the Danube River in the historic and present state.

3.1.1.4 Joint analyses

Figure 32 shows the average reductions of discharging width in segments that were defined by Schwarz (2022) to overlay results of all studies for the project's synthesis, each 5 km in length along the Mura and Drava, and 10 km in length along the Danube.

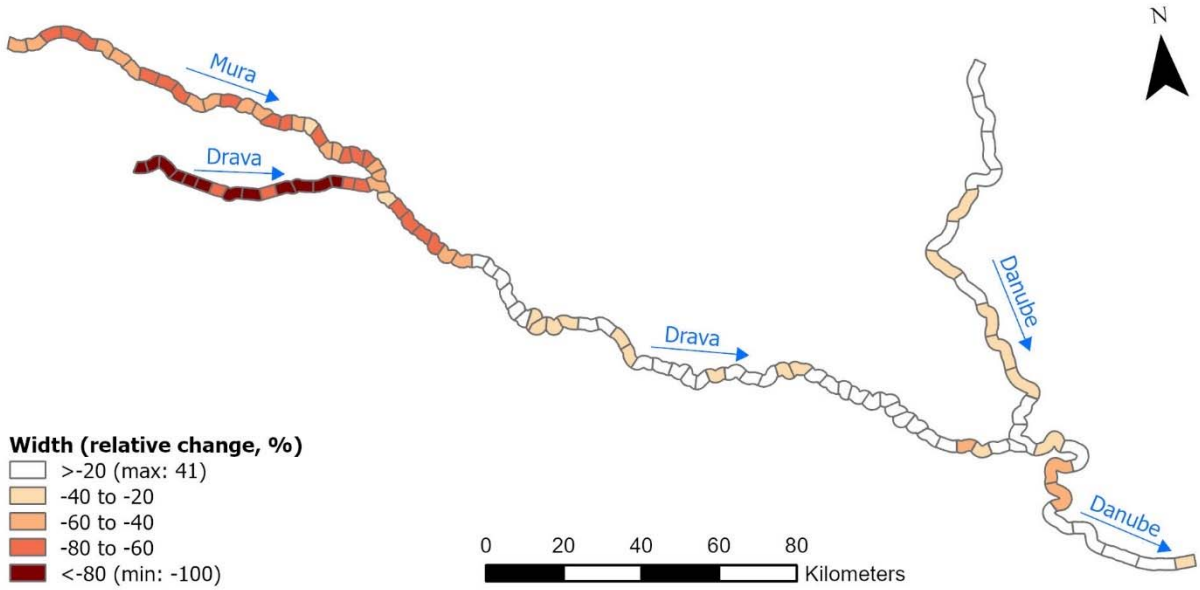

Figure 32. Relative changes in width along the MDD rivers.

Drastic changes are immediately noticeable: Both, the Mura and the upper segments of the Drava experience a strong decrease in river width (Mura -59%; entire Drava -40%). While the entire Mura River is affected by narrowing, the Drava has gained width in some sections, especially downstream. However, this is due to the fact that the river has been channelized to a greater width than the width measured from the historical maps. An increase in width there may be related to the more plane bed in the straightened course,

while, historically, natural bars exerted more constriction of the flow into a narrower channel at the discharge present during the generation of the maps. The changes of the entire Mura, Drava and Danube are listed in Table 8.

Table 8. Historic and present widths and relative changes in width of the entire Mura, Drava and Danube and overall change in the TBR MDD.

	historic width (m)	present width (m)	relative change (%)
Mura	175.49	72.89	-58.47
Drava	292.89	177.18	-39.51
Danube	605.24	496.55	-17.96
overall	**365.63**	**259.24**	**-29.10**

The loss of variability in channel width is shown in Figure 31.

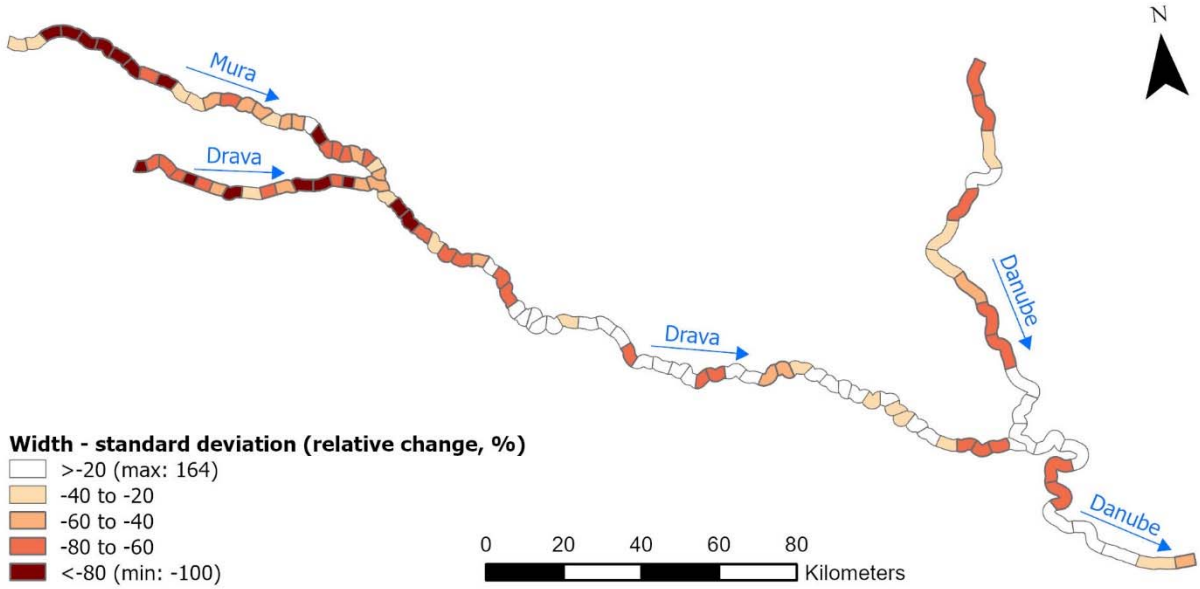

Figure 33. Relative change in the standard deviation of the width within the individual segments.

The loss in width variability is most prominent in the strongly altered upper Mura, as well as in Drava section Dr1 and Dr2.

3.1.2 Changes in channel length

The length of the Mura, the Drava and the Danube was determined along the main channels of their historical and current state (Table 5). The strong reduction in length results from the straightening of the river, which was most effective in the downstream section of the Drau due to the cutting off of the highly sinuous meanders.

Table 9. Length of the MDD rivers in the historic and present state.

	historic length (km)	present length (km)	relative change (%)
Mura	158	143	-9
Drava	472	306	-35
Danube	282	216	-23

Figure 34 shows the same information in graphical form and illustrates the severe shortening of the Drava.

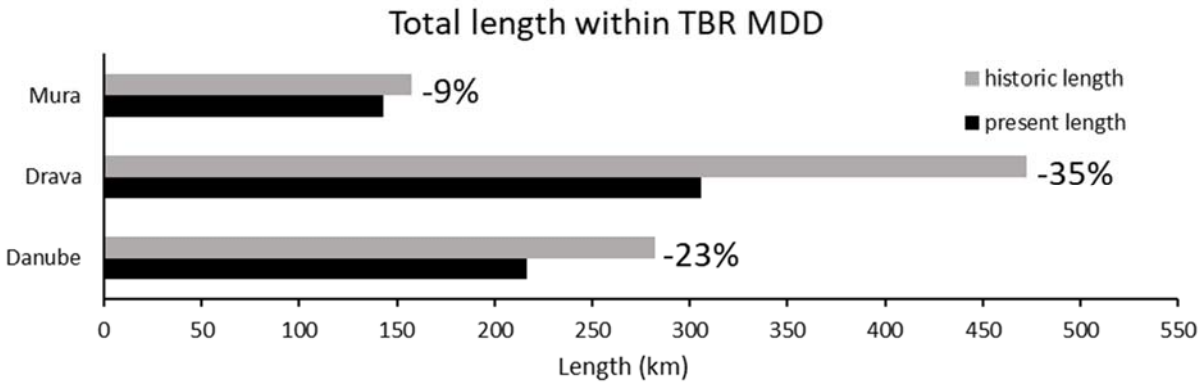

Figure 34. Length of the main channel of the Mura, Drava and Danube as during the second military mapping survey (1810s-1850s, grey) and in 2012 (black).

In the reference state, the main channel length of the Mura within the TBR MDD was 158 km, which decreased by 9 %to 143 km. The main channel length of the Drava, being 472 in the historic state, was reduced by 35 % to 306 km and the Danube by 23 % from 282 km in the reference state to 216 km in 2012.

Figure 35 and Table 10 show the reduction in length for each of the 8 river sections, which were defined for the scientific studies in the project. The numbers reflect very different degrees of shortening, which depend on the historical sinuosity (and hence the possibility for straightening) and on the straightening that was finally implemented.

Table 10. Historic and present length of the TBR rivers.

	Mura			Drava			Danube	
length (km)	**M1**	**M2**	**M3**	**Dr1**	**Dr2**	**Dr3**	**D1**	**D2**
historic	68.023	43.385	46.225	87.341	68.806	316.119	191.317	90.534
present	56.223	41.740	45.113	68.550	49.233	187.985	127.947	88.218

Along the Mura, the reduction in length is largest within the first section M1 from Spielfeld to the Hungarian Border (km 143 – 85). The river length in the section M2 and M3, from kilometer 85 down to the Drava confluence at kilometer 0, remained fairly similar.

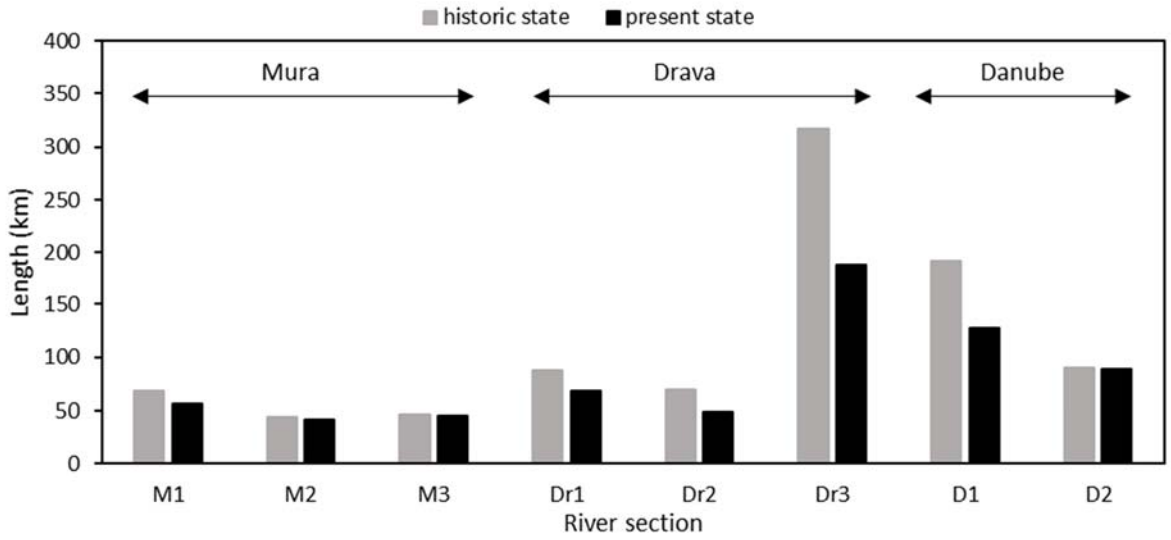

Figure 35. Length of Mura, Drava and Danube within the predefined sections in the reference state (grey) and the actual state (black).

The Drava experienced a decrease in length along its entire course, with the most significant reduction in the third section from Hereszny to the Danube confluence (rkm 185-0), where the length decreased by 40 percent. In this section, due to a drop in the gradient, the historic river morphology changed into a meandering system, so that channelization and meander cutoffs have a particular effect on the length of the course. The Danube has undergone the greatest reduction in length in the section D1 upstream of the Drava confluence (rkm 1433-1382). Downstream of the Drava confluence the river length has remained almost the same.

3.1.3 Changes in sinuosity and slope

The trend of flow length reduction can also be shown by the sinuosity, as the quotient of valley axis and river length, which is listed in Table 11.

Table 11. Sinuosity of the MDD rivers in the historic and present state.

	Mura			Drava			Danube	
sinuosity	**M1**	**M2**	**M3**	**Dr1**	**Dr2**	**Dr3**	**D1**	**D2**
historic	1.26	1.34	1.71	1.28	1.58	2.11	1.91	1.30
present	1.04	1.29	1.67	1.01	1.13	1.25	1.28	1.26

The sinuosity of the individual sectors is also depicted in Figure 36.

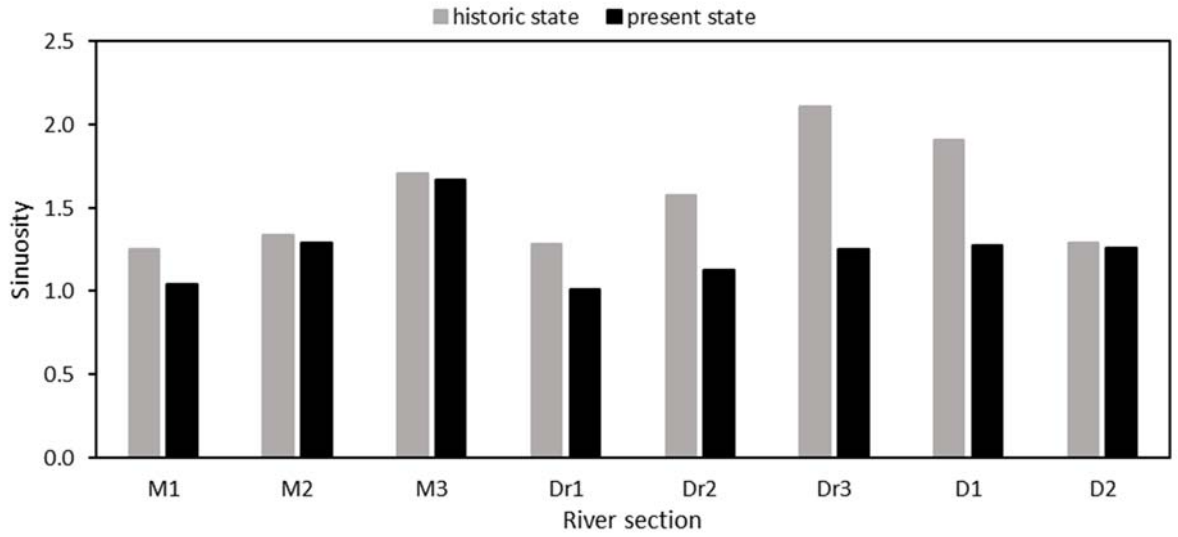

Figure 36. The sinuosity of the rivers within the individual sections in the reference state (grey) and the present state (black).

For the evaluation of the sinuosity values, the respective river centre lines were considered. While in the formerly meandering sections (lower Mur M3, lower Drava Dr3 and Danube D1 and D2) they represent the main course of the flow, the more relevant parameter for the morphological change in the formerly anabranching/braided sections M1, M2, Dr1 and Dr2 is the reduction in the number of channels, as shown in the next subchapter.

Since the sinuosity of a river is inversely proportional to its slope, the changes in Figure 36 can be transformed into relative slope changes (Table 12). In total, the sinuosity of the MDD rivers decreased by 27% while the slope increased by 37%.

Table 12. Relative changes in slope based on changes in sinuosity (%).

	Mura			Drava			Danube		Total
change	**M1**	**M2**	**M3**	**Dr1**	**Dr2**	**Dr3**	**D1**	**D2**	
sinuosity	-17.36	-3.81	-2.41	-21.51	-28.48	-40.53	-33.13	-2.57	-27.07
slope	+21.00	+3.96	+2.47	+27.41	+39.82	+68.15	+49.54	+2.63	+37.11

Figure 37 gives the same information in graphical form.

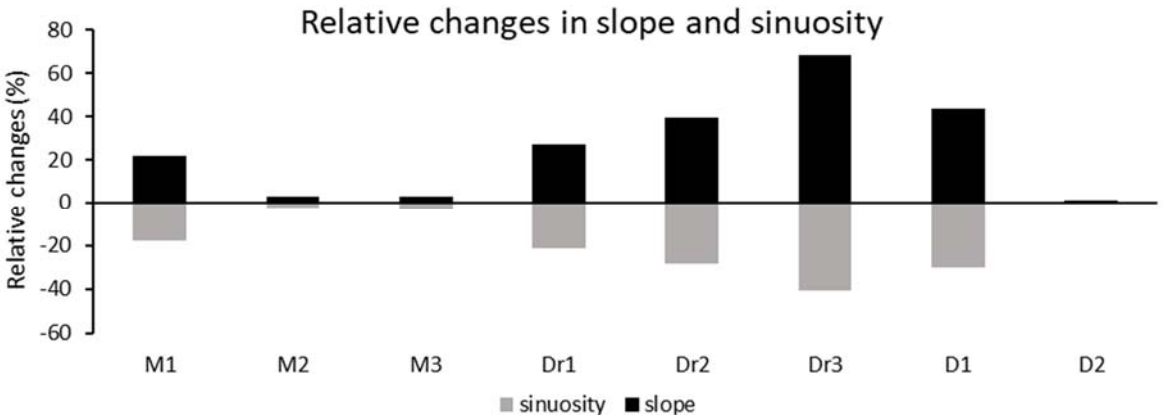

Figure 37. Relative changes in sinuosity and corresponding relative changes in slope

The decrease in sinuosity leads to an increase in slope in the entire TBR MDD. While these changes remain relatively small in the sections M2, M3 and D2, the straightening of the channels has a drastic impact in the upper Mura, where the slope increased by 22 %. Along the entire Drava, the increase in slope ranges from 27 % upstream of the Mura confluence to 68 % in section Dr3 upstream of the confluence with the Danube. In Danube section D1, the slope increased by 50 %, while D2 remained relatively unchanged.

The changes in sinuosity shown in Figure 36 and Figure 37 were also calculated for the individual segments of equal length, which are depicted in Figure 38 below.

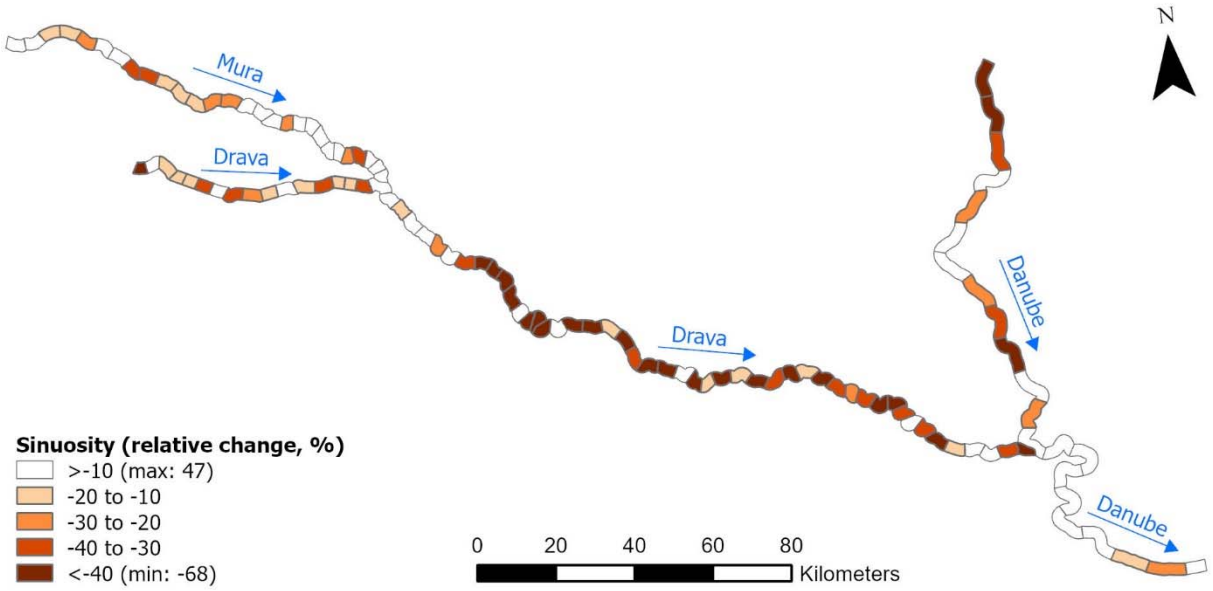

Figure 38. Relative change in sinuosity along the TBR.

Due to the inherent differences between the historical section types, the significance of parameter changes for the appearance of the river and for sediment transport is different. For the formerly anabranching and braided sections with multiple channels, the reduction in channel number is more relevant than the change in sinuosity, while the formerly meandering sections did not divide into many channels, but showed large sinuosity. Therefore, Figure 39 shows the change in sinuosity along the formerly meandering stretches M3, Dr3, D1 and D2 and the change in the channel number as relevant parameter for the formerly braided and anabranching sections M1, M2, Dr1 and Dr2 in one map.

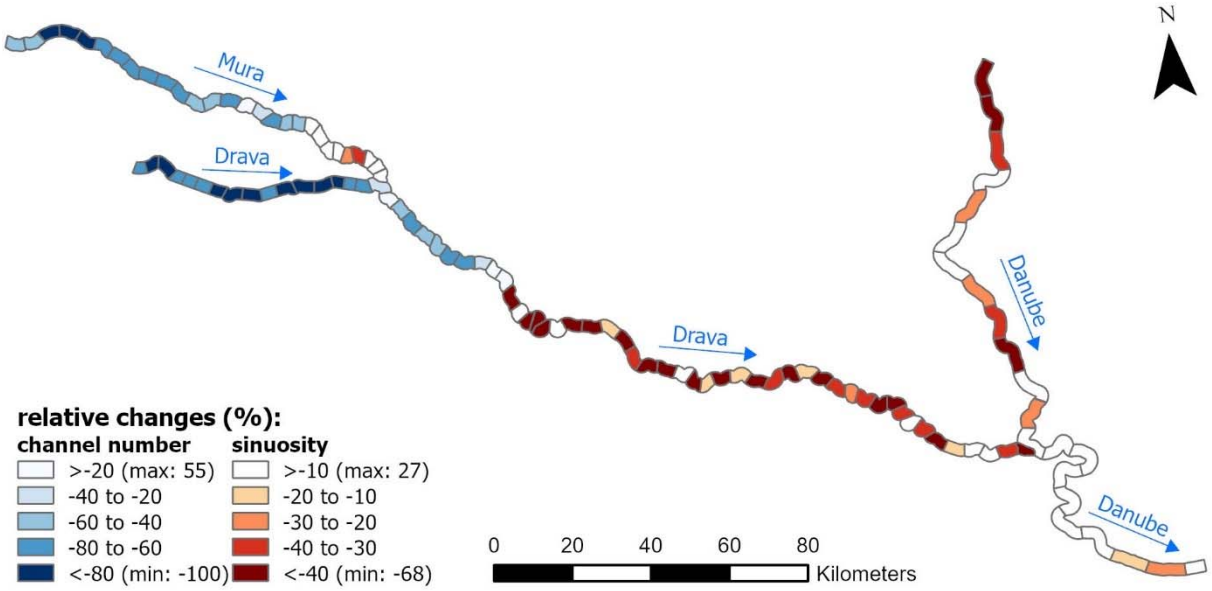

Figure 39. Relative change in the channel number of formerly braided sections and relative change in the sinuosity of former meandering sections

The relative change in slope of the riverbed, based on the sinuosity, is depicted in Figure 40.

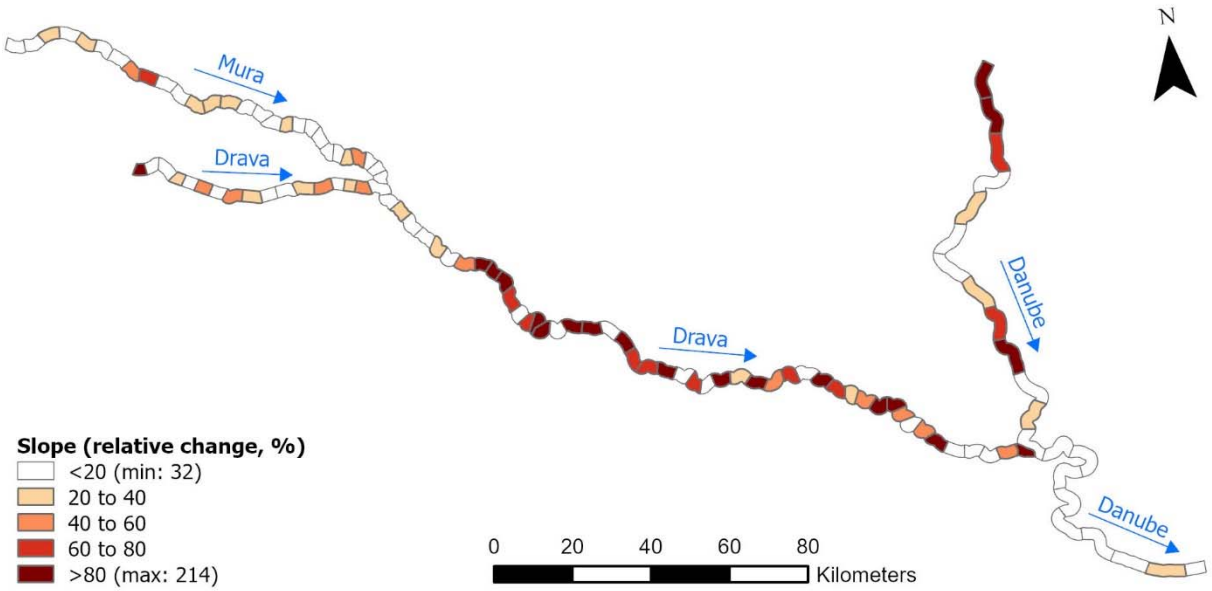

Figure 40. Relative change in slope along the TBR

The Mura exhibits the largest increase in slope in section M1. Along section M2 and M3 changes in sinuosity and slope vary between an increase and a decrease from segment to segment, resulting in relatively little overall change. However, while Drava section Dr3 along some segments experienced even an artificial increase in river width (Figure 32), Figure *38* and Figure 40 clearly show the impacts of straightening also at this section, where the decrease in sinuosity led to drastic changes in the slope of the riverbed. The

Danube is heavily affected along its upstream part within the TBR. Section D2, downstream of the Drava confluence, experiences both elongation and shortening, on average producing little change.

3.1.4 Changes in the radii of river bends

Table 13 reports the relative changes in the median radius of the river bends in the individual sections of the Mura, Drava and Danube.

Table 13. Relative change in the median radius (%).

river section	M1	M2	M3	Dr1	Dr2	Dr3	D1	D2
relative change in the median radius (%)	+158	+18	+12	+238	+43	+69	+104	+17

Figure 40 illustrates the information listed in Table 13 in graphical form.

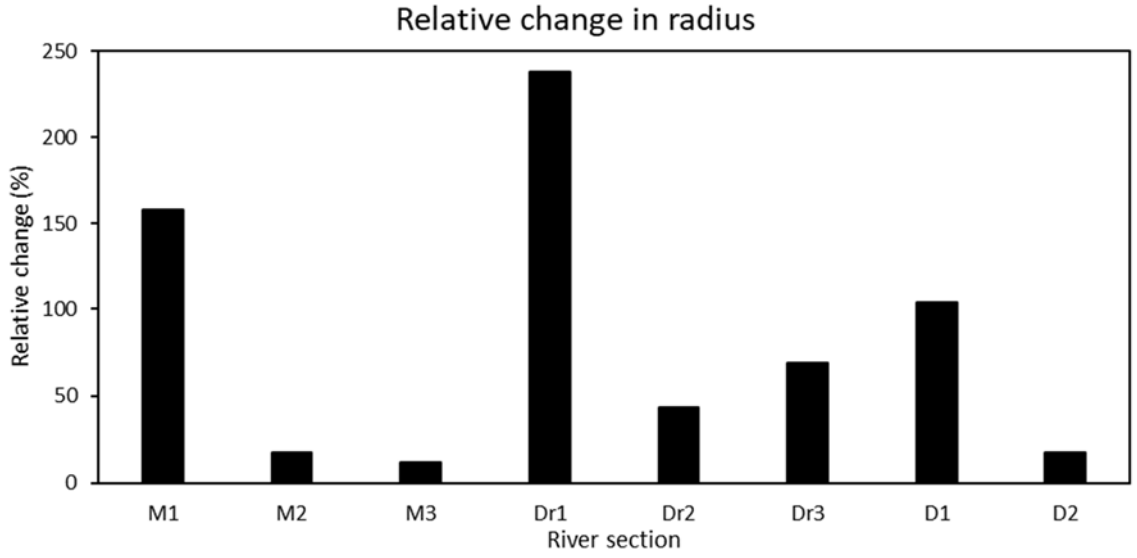

Figure 41. Relative changes in the median radius of the Mura, Drava and Danube.

In the Mura section M1, the median increased by nearly 158%. M2 and M3 show smaller increases of 18 % and 12 % respectively. In the once braided section Dr1, the radius increased by 238%, which is to be expected considering the three major reservoirs and the respective headrace channels (The headrace channel was used to determine the radius, not the residual flow sections of the Drava). In sections Dr2 and Dr3, the median river bend radius is 43% and 69% respectively larger than in the reference state.

Figure 42 illustrates the proportion of the total length of different radius classes for the historic and for the present state for the main channels of the TBR MDD.

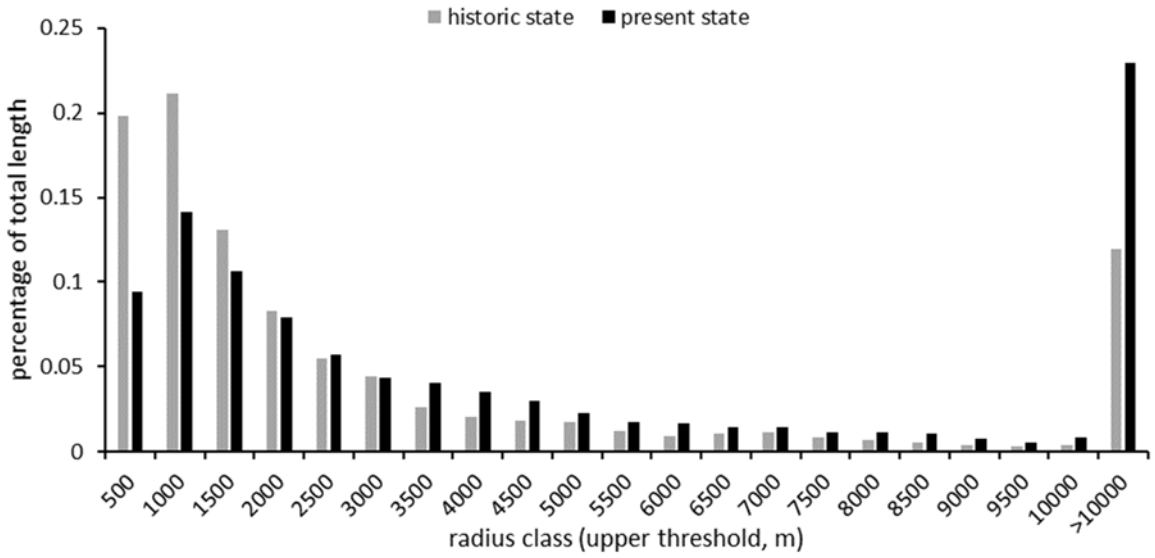

Figure 42. Proportion of different radius classes of the total length of TBR rivers.

Compared to the historic state, the share of radii under 500 m of the total river length are reduced by half in the present state. All classes under 2500 experience a decrease, while the shares of radii above 2500 increased.

For demonstration purposes, the present state (orange) and the historic state (blue) are presented as point clouds for historically meandering/sinuous/transition types. (Figure 43) displays the changes in arc radius versus arc length for the most downstream section of the Mura, where a significant sinuosity remained, but where deviations from the historic state are evident in the radii analyses.

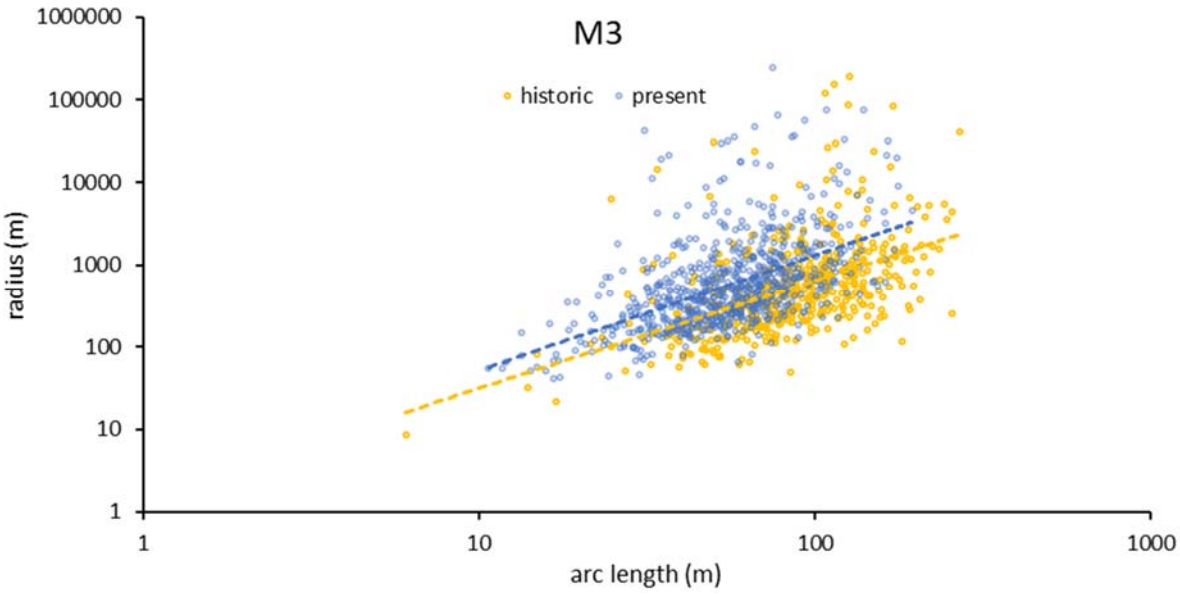

Figure 43. Arc radius as function of the arc length in the historic state (blue) and in the present state (orange) for Mura section M3.

Similar changes are evident in the most downstream section of the Drava (Figure 44).

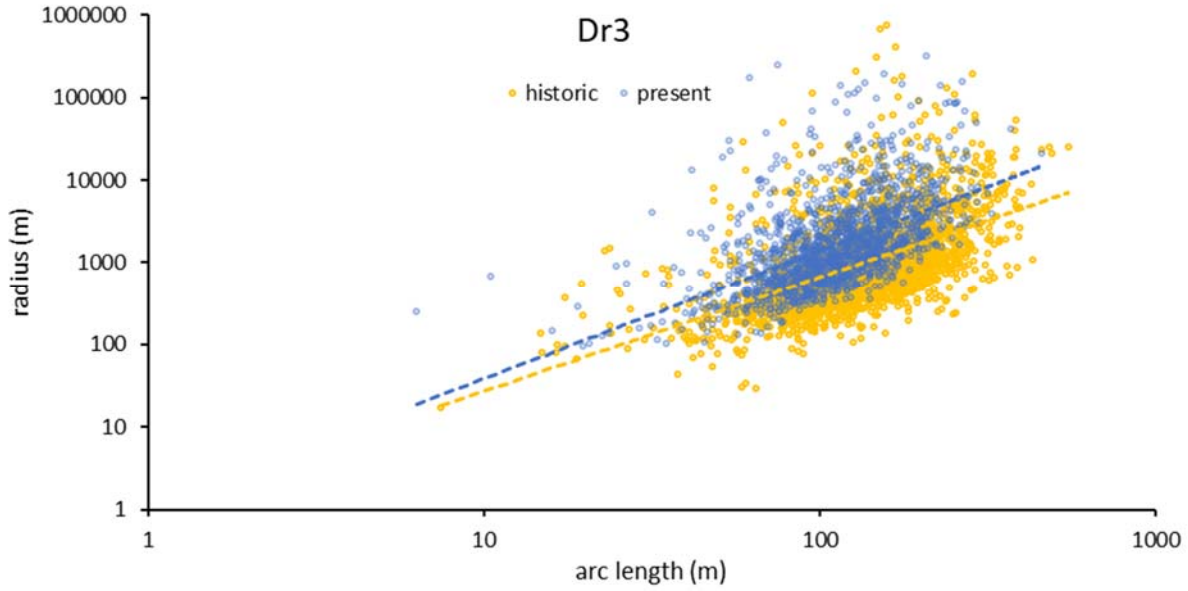

Figure 44. Arc radius as function of the arc length in the historic state (blue) and in the present state (orange) for Drava section Dr3

The Danube sections upstream and downstream of the Drava confluence also show an increase in radii. In the Danube upstream of the confluence with the Drava, especially the longer bends have strongly increased in radius (Figure 45).

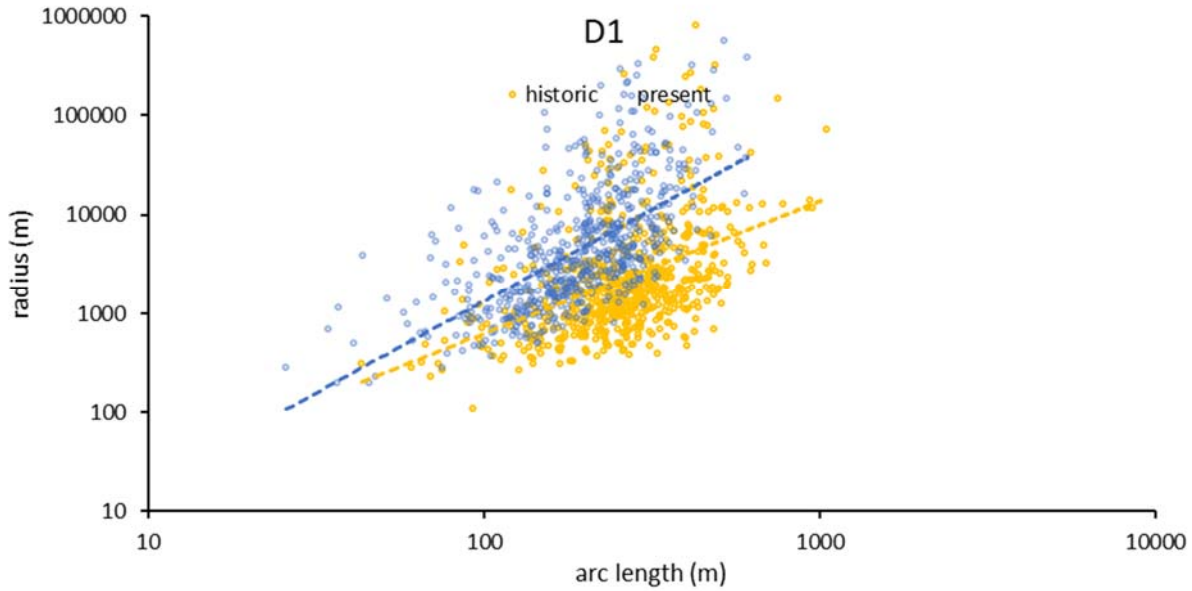

Figure 45. Arc radius as function of the arc length in the historic state (blue) and in the present state (orange) for Danube section D1.

Even downstream of the confluence with the Drava, where the sinuosity analysis exhibited little change, the river radii increased (Figure 46).

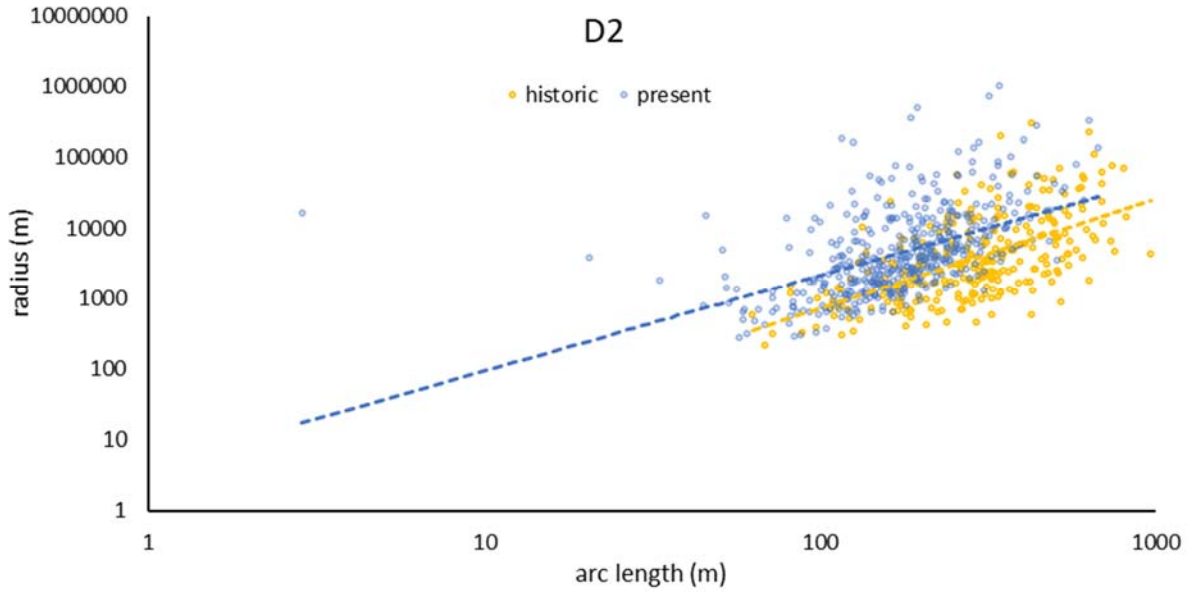

Figure 46. Arc radius as function of the arc length in the historic state (blue) and in the present state (orange) for Danube section D2.

There is a clear shift towards a larger radius in the current state. At the Danube, in section D1, the median radius nearly doubled, while D2 in comparison experienced a relatively minor change of only 17% compared to the historic state.

3.2 Morphological change

In this chapter, the changes in the channel morphology are analyzed and the deviations from the historical state are pointed out.

3.2.1 Mura

The decrease in sinuosity and therefore channel length of the upper Mura section M1, as shown in the previous chapter, is depicted in planform for an exemplified river section in Figure 47.

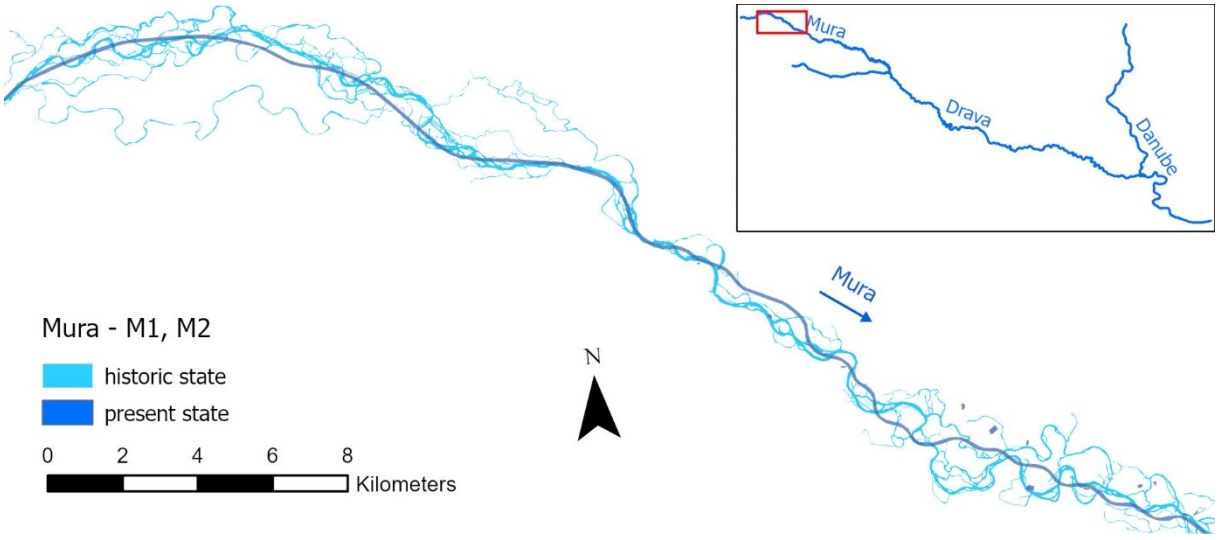

Figure 47. Mura section M1 in the present and historic state.

The artificial confinement is most obvious in the section along the border between Austria and Slovenia (Figure 48). Historically, the Mura in section M1 along the Austrian-Slovenian border was an anabranching and braided river, with several bars and islands of different sizes diverting the flow.

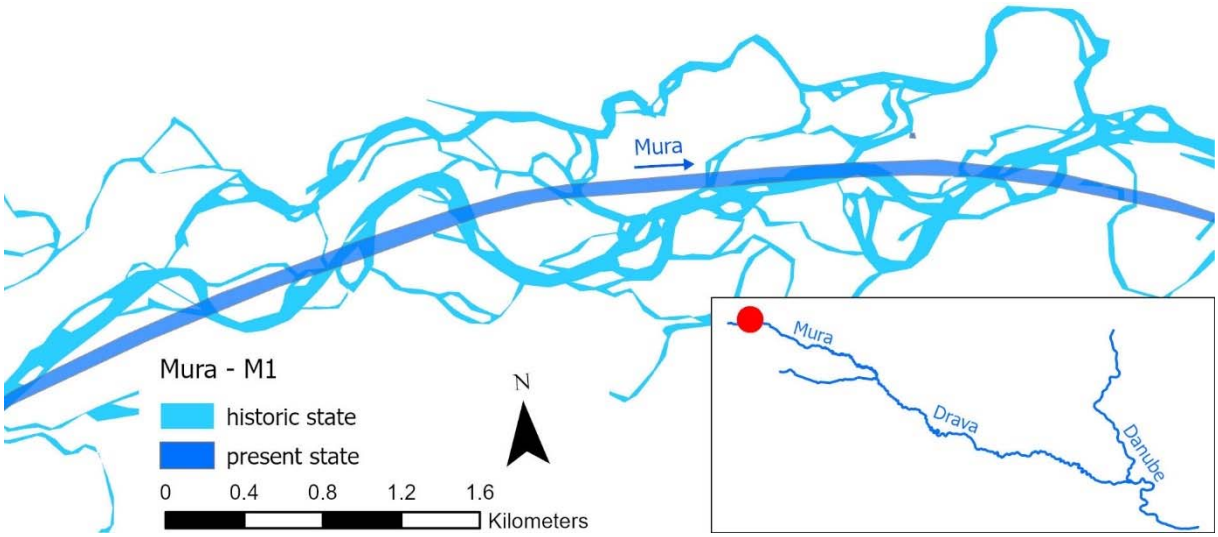

Figure 48. Mura section M1 along the Austrian-Slovenian border.

The Mura River can be described as a medium-large lowland gravel bed river. Historically, section M2 was a transition type from anabranching/braiding in section M1 to a sinuous and meandering type with moderate anabranching and small side channels in M3 (Schwarz, 2007).

The channel length in M3 has undergone relatively little change, compared to other sections, yet the narrowing of the riverscape is evident (Figure 49).

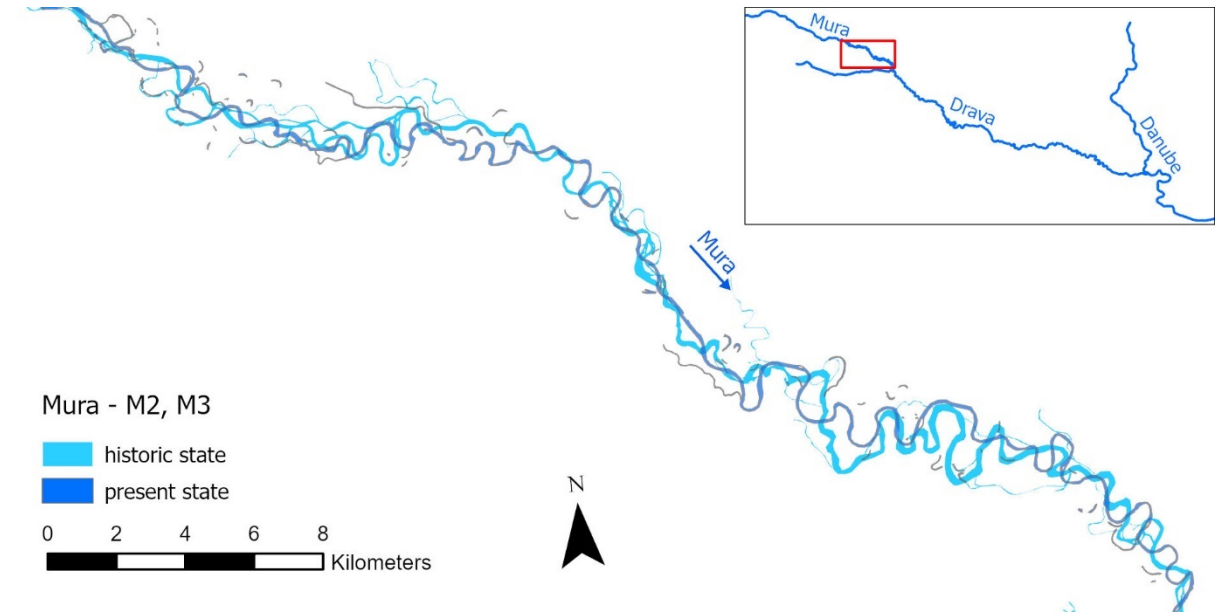

Figure 49. Along the Mura sections M2 and M3, the river length stayed almost the same, yet the narrowing is clearly apparent

Figure 50 compares the cross-sectional number of channels of the Mura within the TBR MDD in the historic and present state.

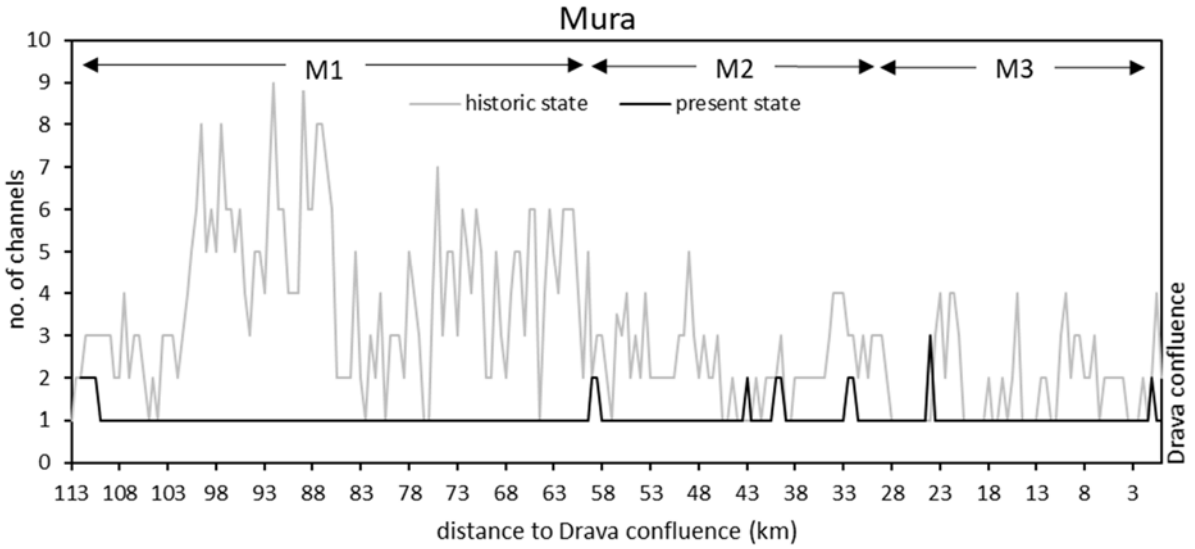

Figure 50. Number of channels along the valley axis of the Mura river in the TBR MDD. The once braided river system has been heavily altered, changing the Mura to a single channel stream in the present state.

After several channelization works, along 94 % of its course the Mura was restricted to one channel in the present state, whereas in the reference state, this number was as small as 20 %. In section M1, a single-thread channel formed in the historic state almost only when the channel was in contact with the right valley margin. Along 28 % of its course, the Mura previously consisted of two channels, along 20 % of three channels. 31 % of the total length featured four or more channels, with up to nine channels in the formerly braided section M1 (Figure 51).

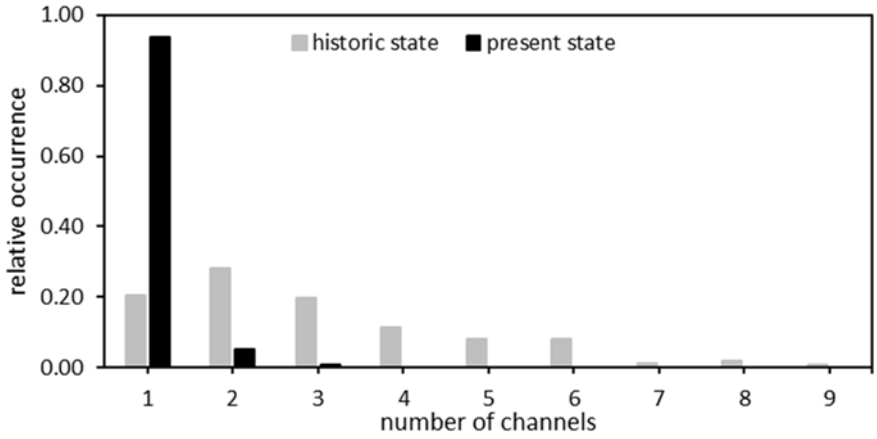

Figure 51. Relative occurrence of number of channels along the Mura.

3.2.2 Drava

Schwarz (2007) classifies the historic Drava in section D1 as a braided river system, anabranching with many small side-channels. With decreasing slope, the sinuosity

increases and the number of side channels decreases. In this section, the Drava is considered a large lowland river with gravel prevailing.

Presently the three dams that supply the hydropower plants dominate the appearance of the Drava (Figure 52). Here, the main discharge is carried by the headrace channels, with the old Drava only carrying the residual flow.

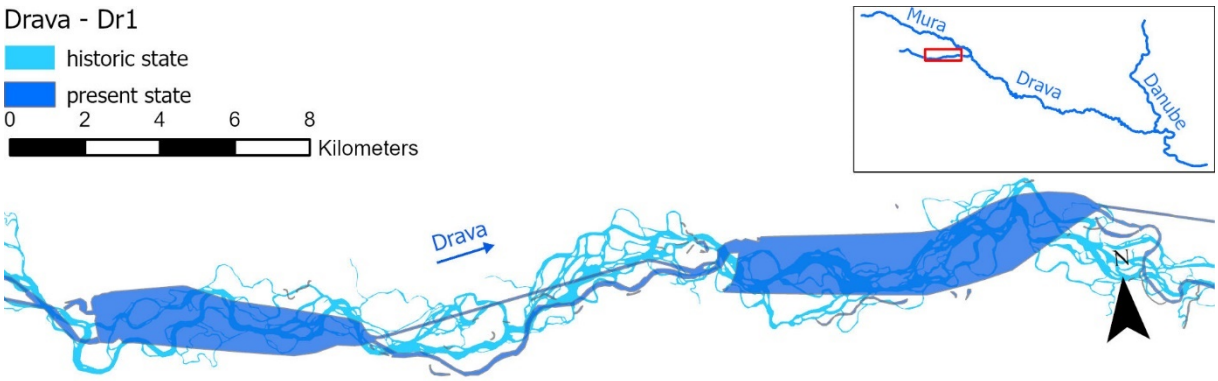

Figure 52. Detail of the Drava section Dr1: Here, three hydropower dams were built in the end of the 20th century (in the picture: Varaždin and Dubrava).

Drava section Dr2 is historically a transition type from a predominantly braided type (Dr1) to a sinuous and meandering river type with only partial anabranching (Dr3). Bedload is dominated by gravel and coarse sand (Schwarz, 2007). The number of channels has been greatly decreased in the present state, as has the sinuosity due to meander cut-offs (Figure 53).

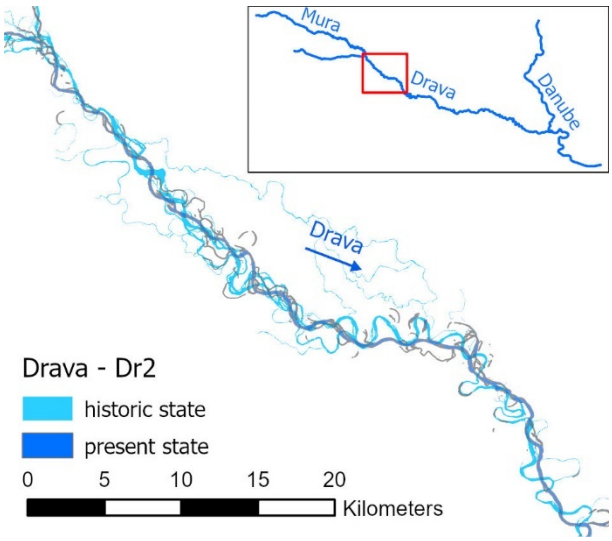

Figure 53. Drava section Dr2 downstream of the Mura confluence

In its historic state, the Drava in Dr3 can be classified as a meandering single-channel river system with several small side channels and typical floodplain waters. Here, the dominant sediment is sand (Schwarz, 2007).

Figure 54 shows the section Dr3, in which the loss of sinuosity is most apparent. Multiple meander cut-offs in the past led to a drastic reduction in length.

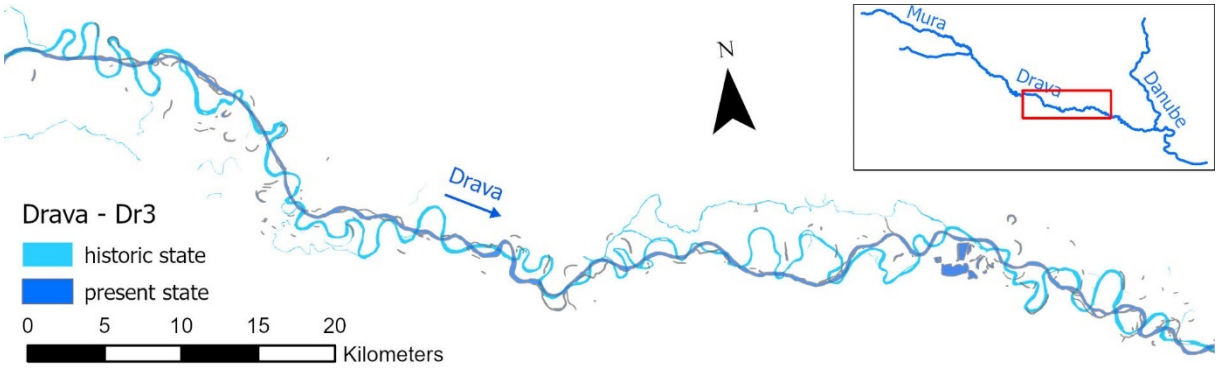

Figure 54. In the Drava section Dr3, meander cut-offs led to significant shorter length of the Drava compared to the historic state

Looking at the number of channels, a dramatic decrease in the number of channels can be observed in the upper section, similar to the situation in the Mur along the border between Austria and Slovenia (Figure 55).

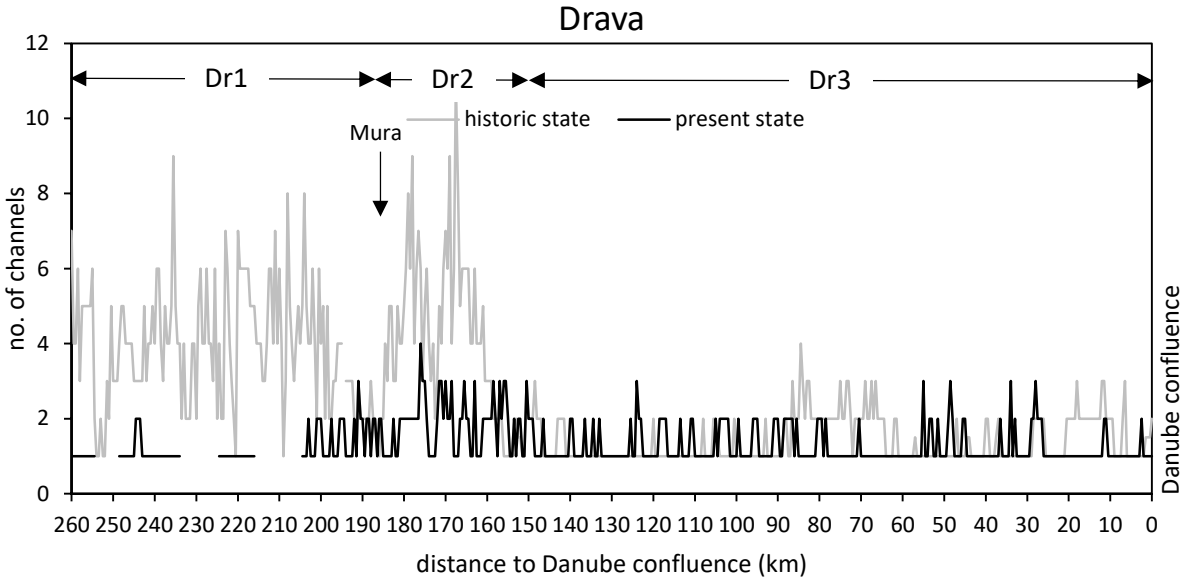

Figure 55. Number of channels along the valley axis of the Drava River from to the Danube confluence.

Hydropower dams strongly altered the river morphology in in section Dr1. Here, only the residual flow stretch of the Drava is considered, leaving out the headrace channels and the reservoir, which were neglected in this analysis given their irrelevant morphological value. Despite few lateral constraints, the residual sections experienced a drastic decrease in the number of channels, changing the once braided systems with up to nine channels in one cross section to mainly a single-thread residual flow channel, where the flow is divided only occasionally near the confluence with the Mura River. Directly downstream of the confluence, at section Dr2, the Drava presently shows up to four channels, which still is a strong alteration compared to the historic state. At axis-km 150 (~rkm 170), a drastic drop in channel number, historic as well as present, is visible, which elongates

downstream to the drop in slope upstream of Barcs, where the river naturally changes to meandering. Here, the texture of the riverbed changes from mainly coarse gravel upstream of rkm 190 and coarse and medium gravel between rkm 190 and 172 to fine gravel and predominantly sand downstream of rkm 170 (Pirkhoffer et al., 2021; Figure 56). Rivers naturally exhibit such an abrupt transition in bed grain size from gravel to sand over a short distance (e.g. Shaw and Kellerhals, 1982; Ferguson et al., 1996), which is referred to as the gravel-sand transition. The location of the gravel-sand transition can also be recognised by a knickpoint in bed slope (Figure 56b).

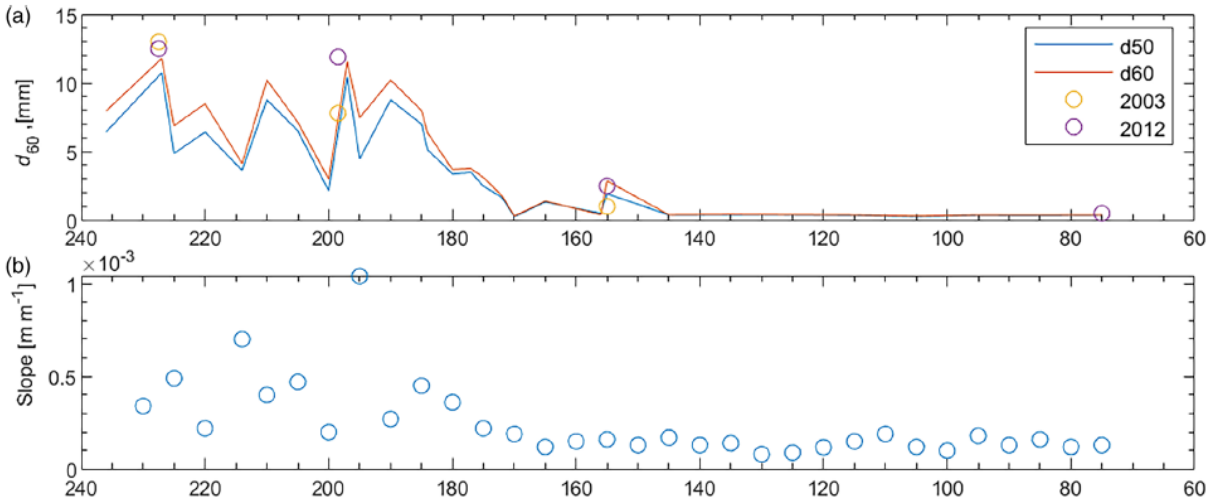

Figure 56. D50 (a) and slope (b) along the course of the Drava river (Pirkhoffer et al., 2021)

The number of channels in the historic and present states are compared in Figure 57.

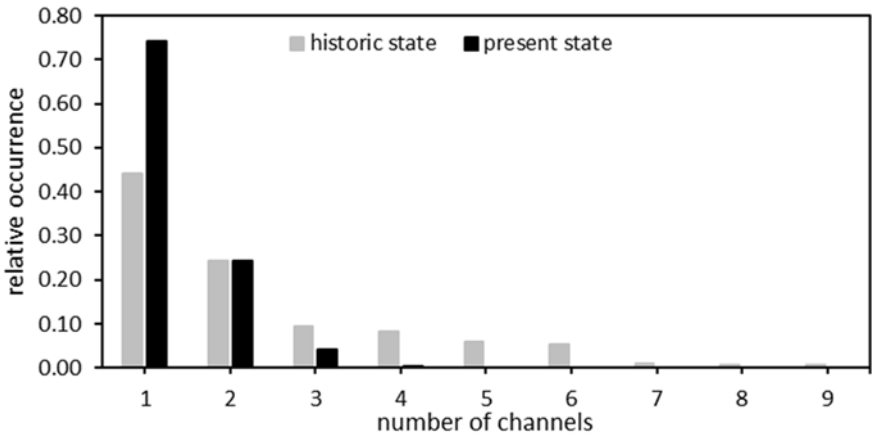

Figure 57. Relative occurrence of channel numbers along the Drava.

Currently, the Drava is restricted to only one channel along 74% of its length (compared to 45% in the past), while multi-channel systems of 4-9 channels, that were present upstream in Dr1 and Dr2 in the historic state, nearly completely disappeared. In section Dr3 however, the main anthropogenic drivers of morphological change were the cut-offs of the meanders.

3.2.2.1 Residual flow stretches along the Drava in section Dr1

In section Dr1, three major power plants interrupt the continuum of the Drava and only the residual water stretches, with respect to bank protections, are in a relatively natural state (regarding the intensity of lateral constraints). At the Croatian-Slovenian border, downstream of the Ormož dam, the residual flow (10 m^3/s) runs alongside the headrace channel of HPP Varaždin in the riverbed of the old Drava. The next dam in the chain is the Varaždin dam, which powers HPP Čakovec and has a residual flow of again 10 m^3/s. The residual flow of the last hydropower plant, HPP Dubrava, is 20 m^3/s.

In the following, morphological changes between 2009 and 2018 are shown for the available cross sections of the residual flow stretches Varaždin, Čakovec and Dubrava. For the stretch near Varaždin, annual surveys between 2007 and 2020 were available (Figure 59). Furthermore, the annual changes over the entire period are shown for specific cross sections.

Figure 58 shows the residual flow reach near Varaždin in 2003 (Figure 58a) and in 2021 (Figure 58b), exhibiting significant lateral dynamics.

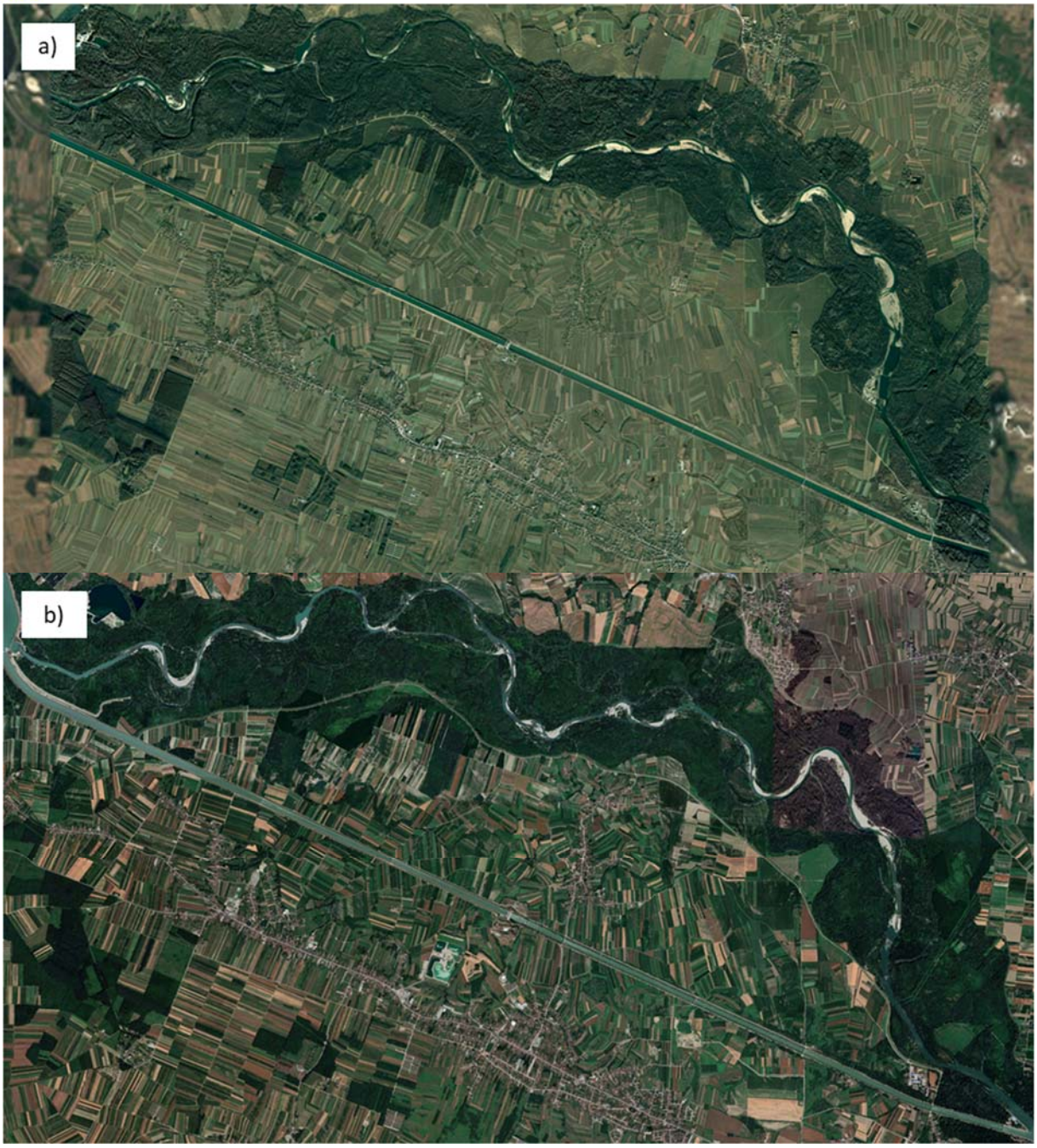

Figure 58. Residual flow stretch near Varaždin between 2003 and 2021 (source: Google Earth).

Within this reach, 59 cross sections were analysed in the period from 2007 to 2020. The locations of the analysed cross sections are displayed in Figure 59.

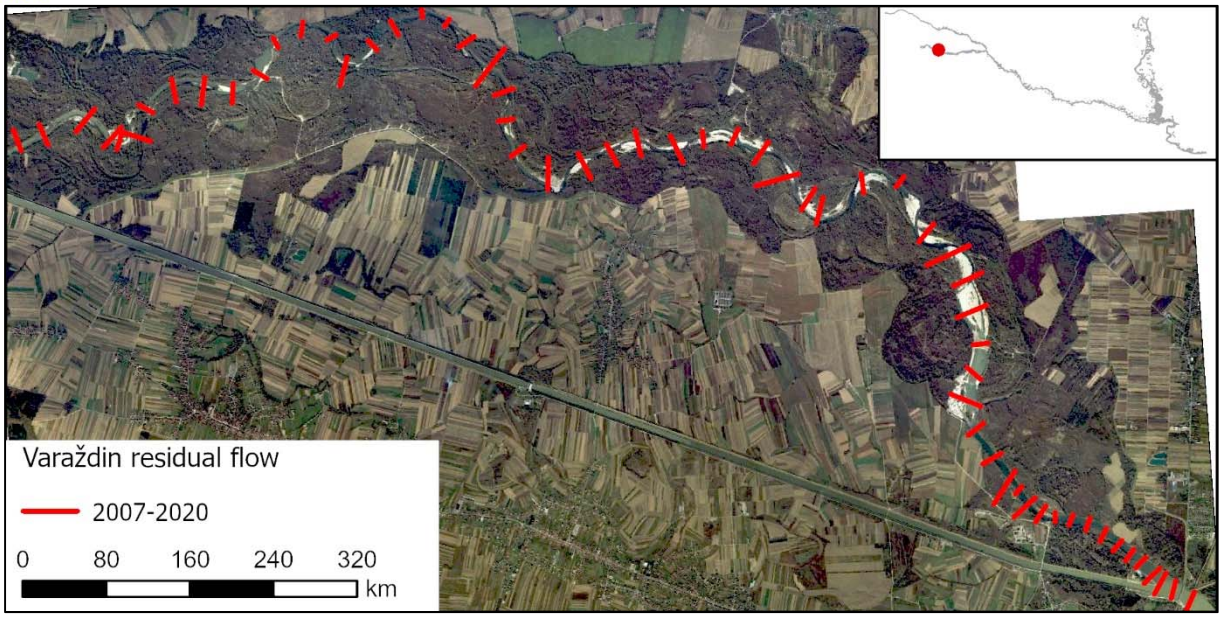

Figure 59. Repeated cross-sectional surveys at the residual flow stretch at Varaždin between 2007 and 2020.

The morphological development of these cross sections is depicted in the channel evolution diagram below (Figure 60). In this analysis, the width was measured between the outer water edges of the channel system. Narrowing of this width shows to go along with a deepening of the bed, while widening shows an increase of bed levels. The mean bed elevation was assessed for the wetted bed surface.

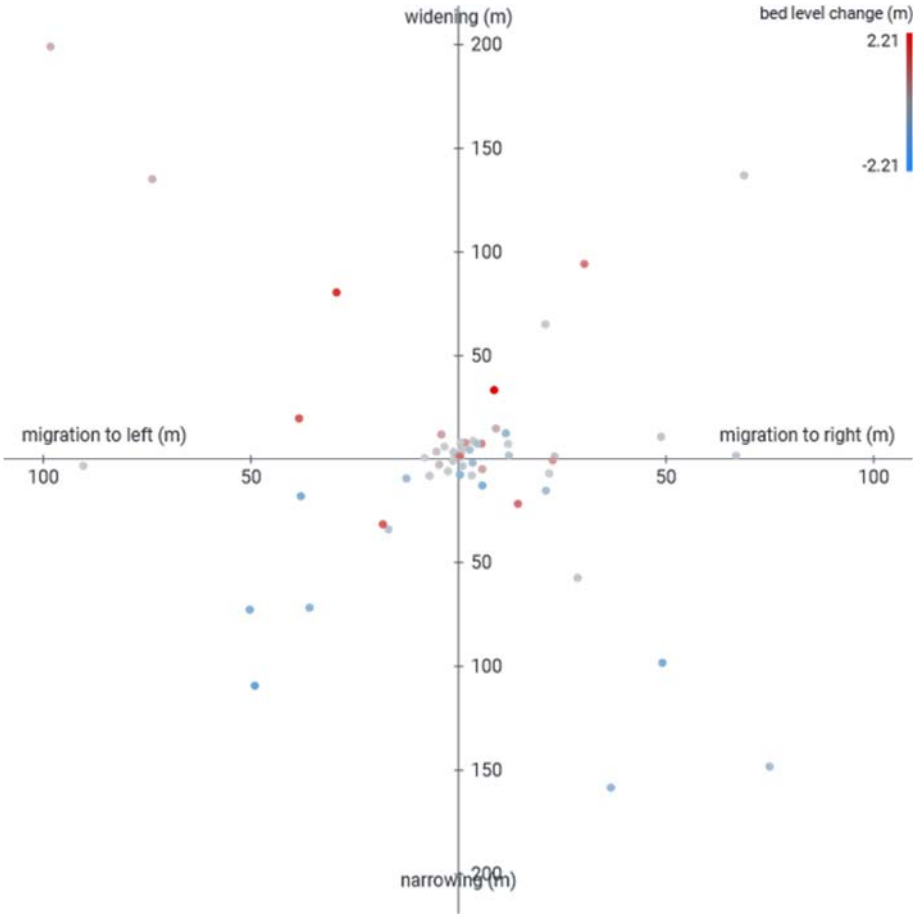

Figure 60. Cross sections along the old Drava downstream HPP Varaždin 2007-2020.

In Figure 61, orthophotos of the residual flow stretch below the Dubrava dam are depicted. Figure 61a shows the old Drava as in the state of 2003, Figure 61b shows the situation in 2021. Again, significant lateral dynamics can be observed.

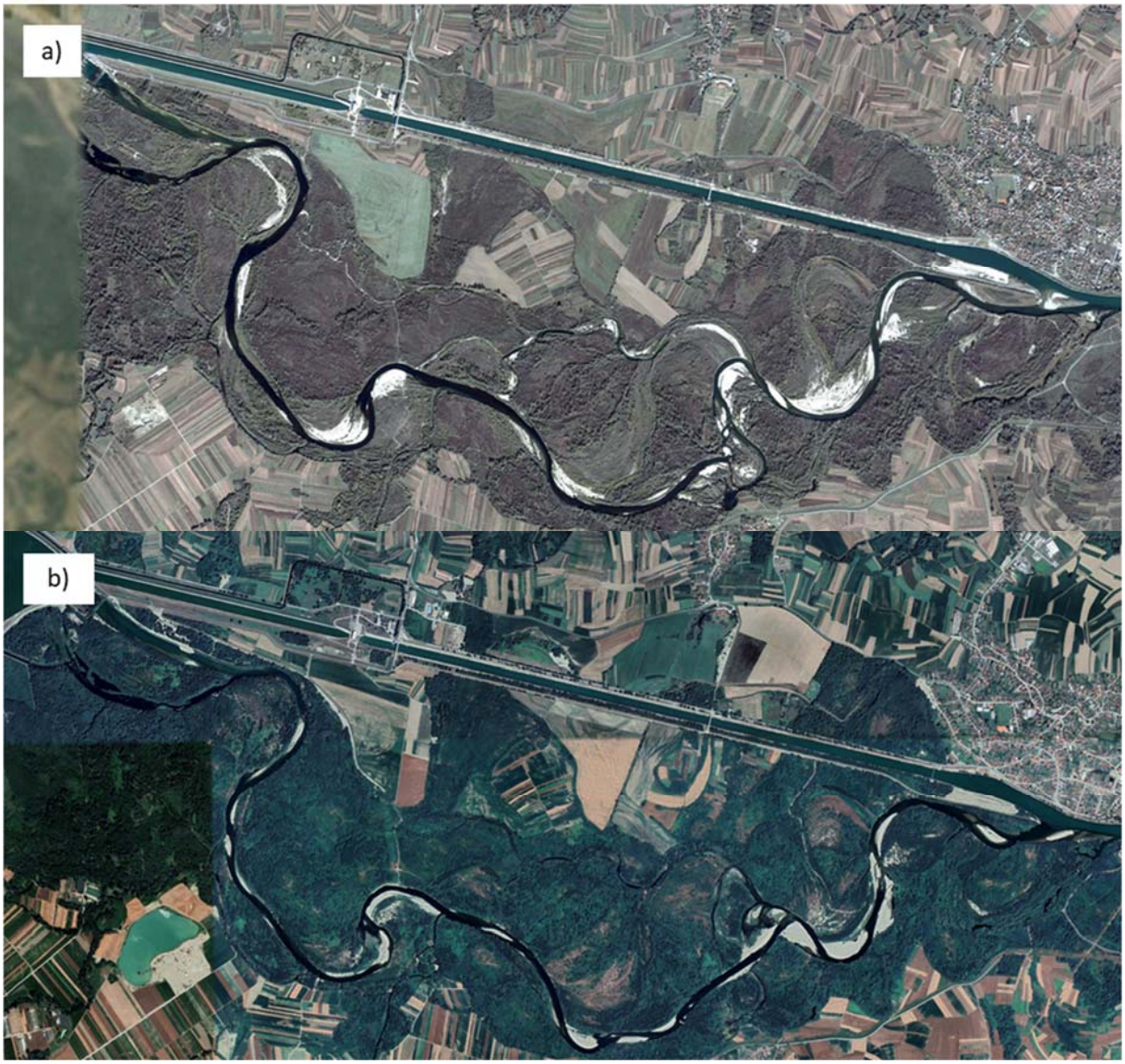

Figure 61. The Drava river below the Dubrava reservoir in 2003 and 2021

Between 2003 and 2021, near natural morphodynamics were able to form along the residual flow stretch, where the river's outer banks were not protected. In the section marked red, a natural meander cut-off occurred, leading to a shift of the river's course at the location of cross section P54.

Repeated cross sectional surveys of the residual flow stretch started in 2009, however, before 2012 the survey was restricted to only 24 cross sections downstream of the dam and upstream of the confluence. Starting in 2012, the whole stretch was covered by the surveys (Figure 62).

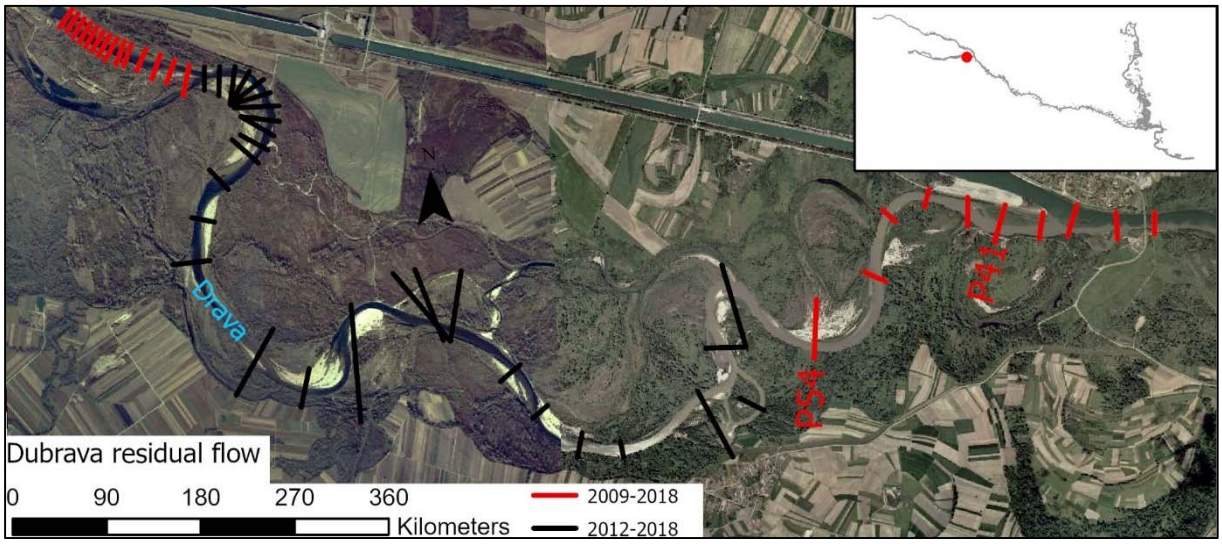

Figure 62 Residual flow stretch at HPP Dubrava with repeated cross-sectional surveys available starting with 2009 (red) and 2012 (black).

Morphological changes between 2009 and 2018 in the 24 cross sections marked red in Figure 62, are presented in Figure 63.

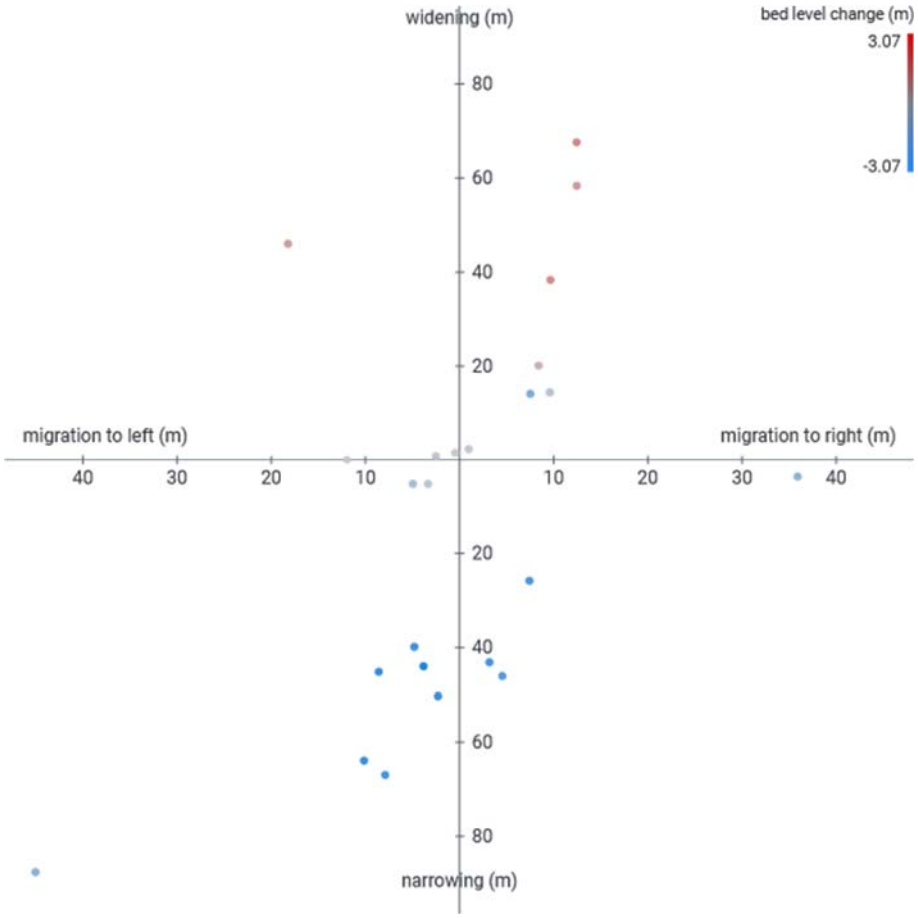

Figure 63. Morphological changes in the residual flow stretch downstream HPP Donja Dubrava between 2009 and 2018. Only cross sections directly below the dam and upstream of the confluence of head race channel and residual flow channel were available for the year 2009.

The points in Figure 63 which show narrowing are from cross sections located downstream of the dam. Here, an incision of up to 2.9 m occurred. Cross sections near the confluence of headrace channel and residual flow channel plot in the upper half of the diagram of Figure 63, hence experiencing widening as well as, for the largest part, aggradation of the riverbed.

When assessing the changes between 2012 and 2018, it shows a similar picture for the upstream and downstream sections (Figure 64). In the middle section, which wasn't considered in Figure 63, the channel also migrated, the mean bed elevation however stayed relatively constant.

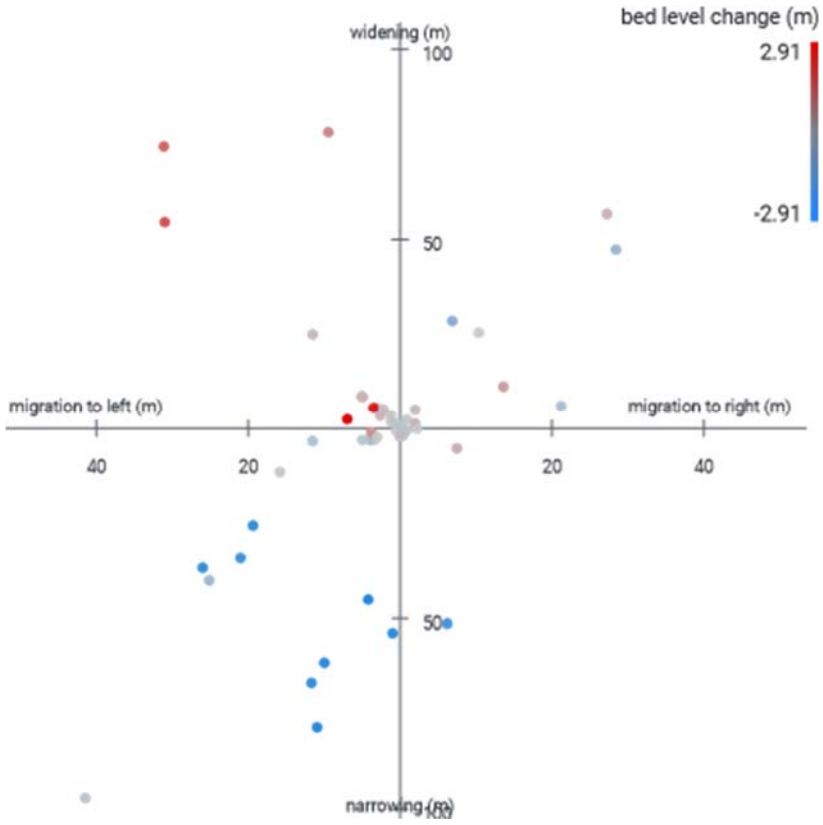

Figure 64. Morphological changes in the residual flow stretch downstream HPP Donja Dubrava between 2012 and 2018. For this time period, 49 cross sections along the residual flow stretch were considered.

Figure 64 shows the connection between widening and aggradation: While the majority of the cross sections, that widened, also experienced a rise in the mean bed elevation, it decreased where cross sections narrowed in comparison to the pre-state.

In Figure 65 cross section P41 is shown in the state of 2009 (dashed) and 2018 (solid). The change exemplifies the bed-lifting effect of widening.

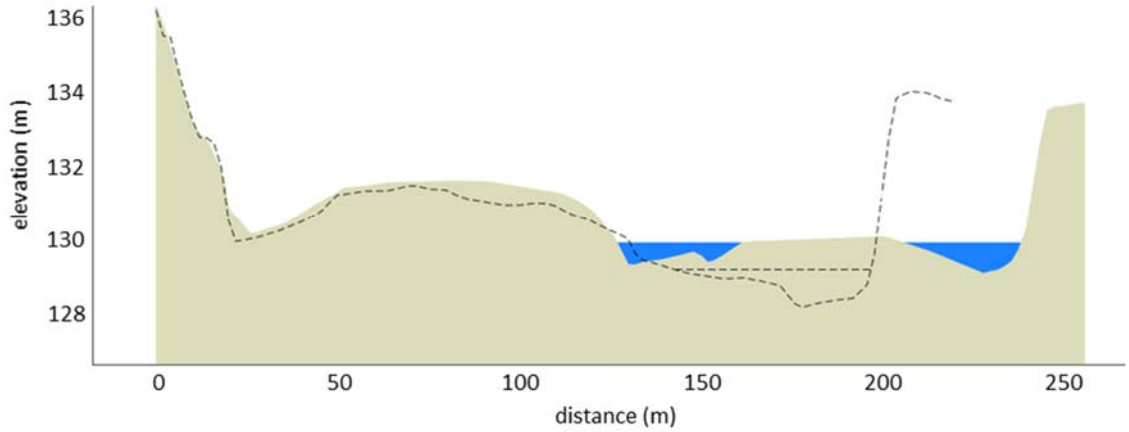

Figure 65. Morphological change in the cross section P 41 downstream HPP Donja Dubrava from 2009 (dashed) to 2018.

Repeated analyses between the individual time steps allow determination of the entire intermediate trajectory of the channel Figure 66 in the same cross section (P41).

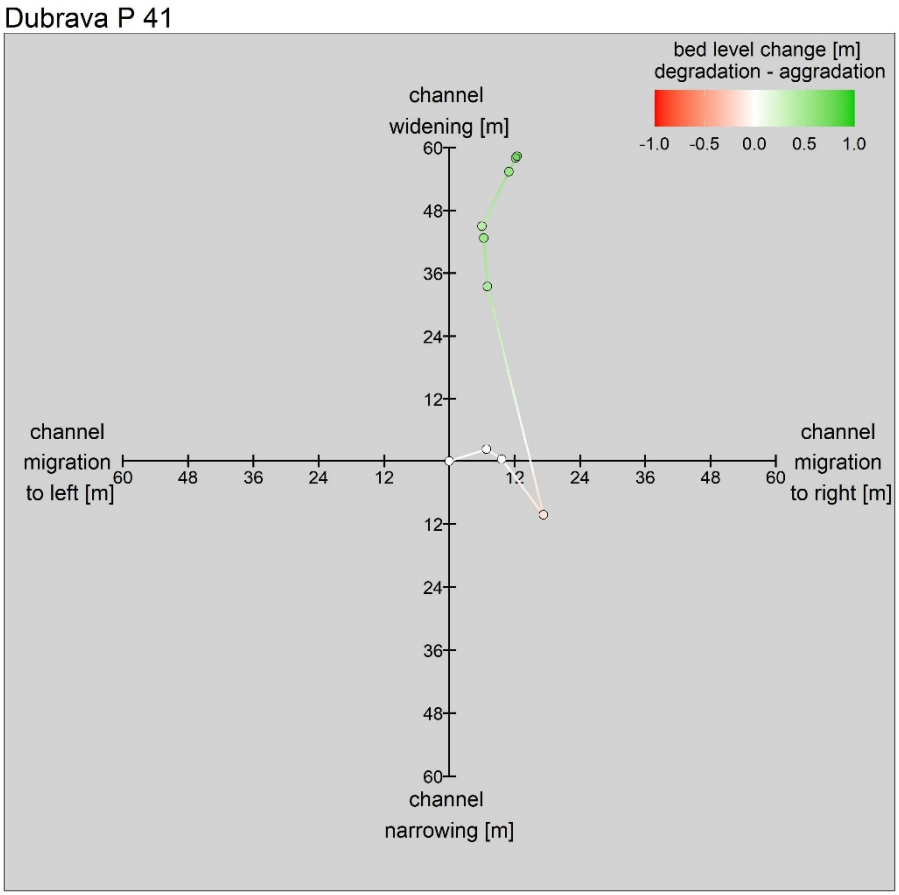

Figure 66. Changes in cross section P41 downstream of the HPP Donja Dubrava from 2009-2018.

While the river bed in this section was clearly widening, the majority of the extent resulted from division of the flow into two channels.

Figure 67 shows the shift of cross section P54, which is situated in a bend in the residual flow of HPP Dubrava, where the river is able to move freely, hence erosion of the outer bank occurred.

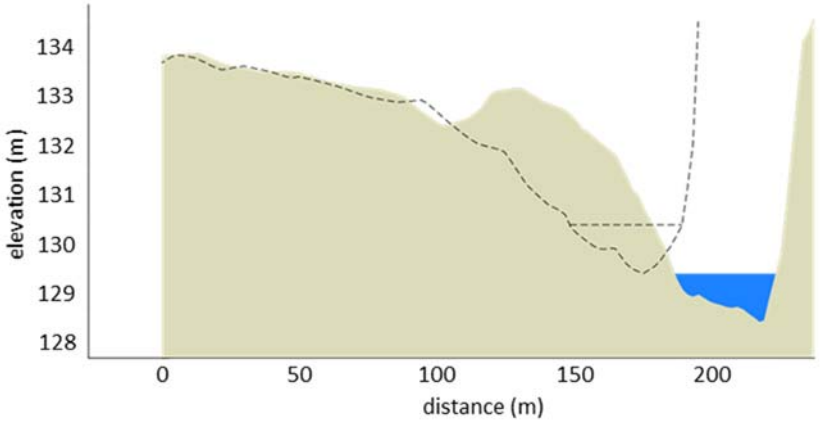

Figure 67. Morphological change in the cross section P54 downstream HPP Donja Dubrava from 2009 (dashed) to 2018.

The evolution of this cross section between 2009 and 2018 is depicted in the channel-evolution-diagram in Figure 68. The results demonstrate the important role of river curvature for triggering lateral dynamics.

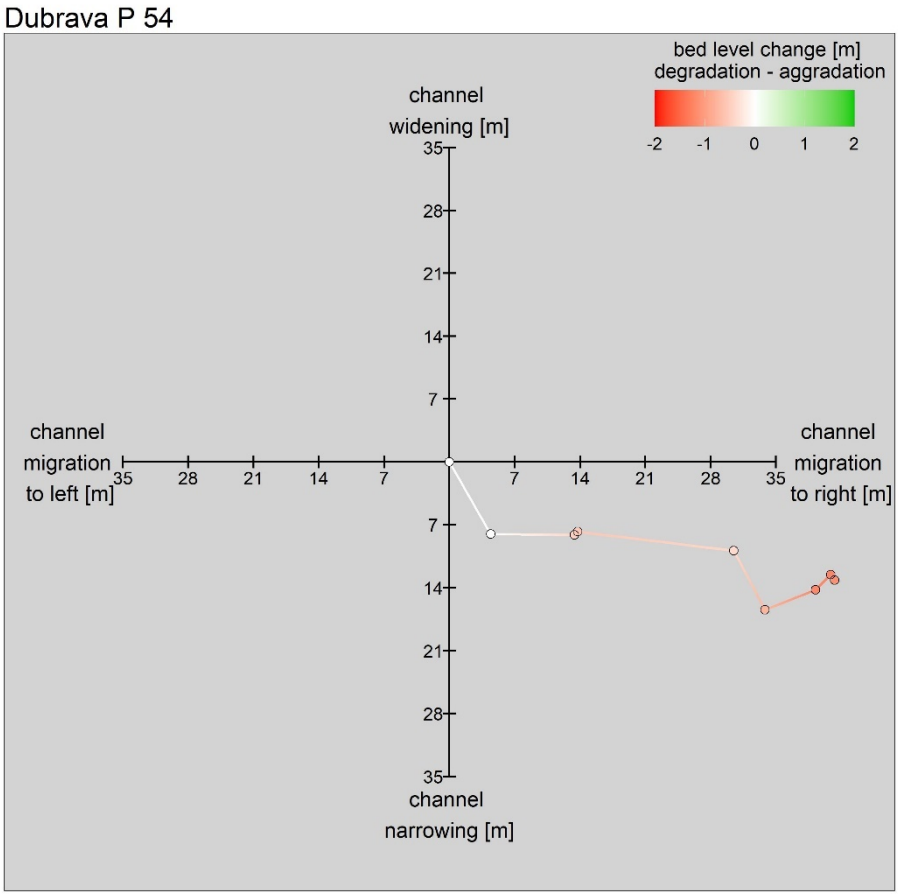

Figure 68. Channel evolution diagram of cross section P54 below the Dubrava reservoir.

3.2.3 Danube

In section D1, the Danube historically is strongly meandering and predominantly a single channel river with anastomosing side channels. The dominant sediment fraction is sand. Historically, the reach D2 is partially anabranching and has lots of side channels as well as meanders (Schwarz, 2007).

In the present state however, meander cut-offs had a heavy impact on the length of the Danube in this part (Figure 69).

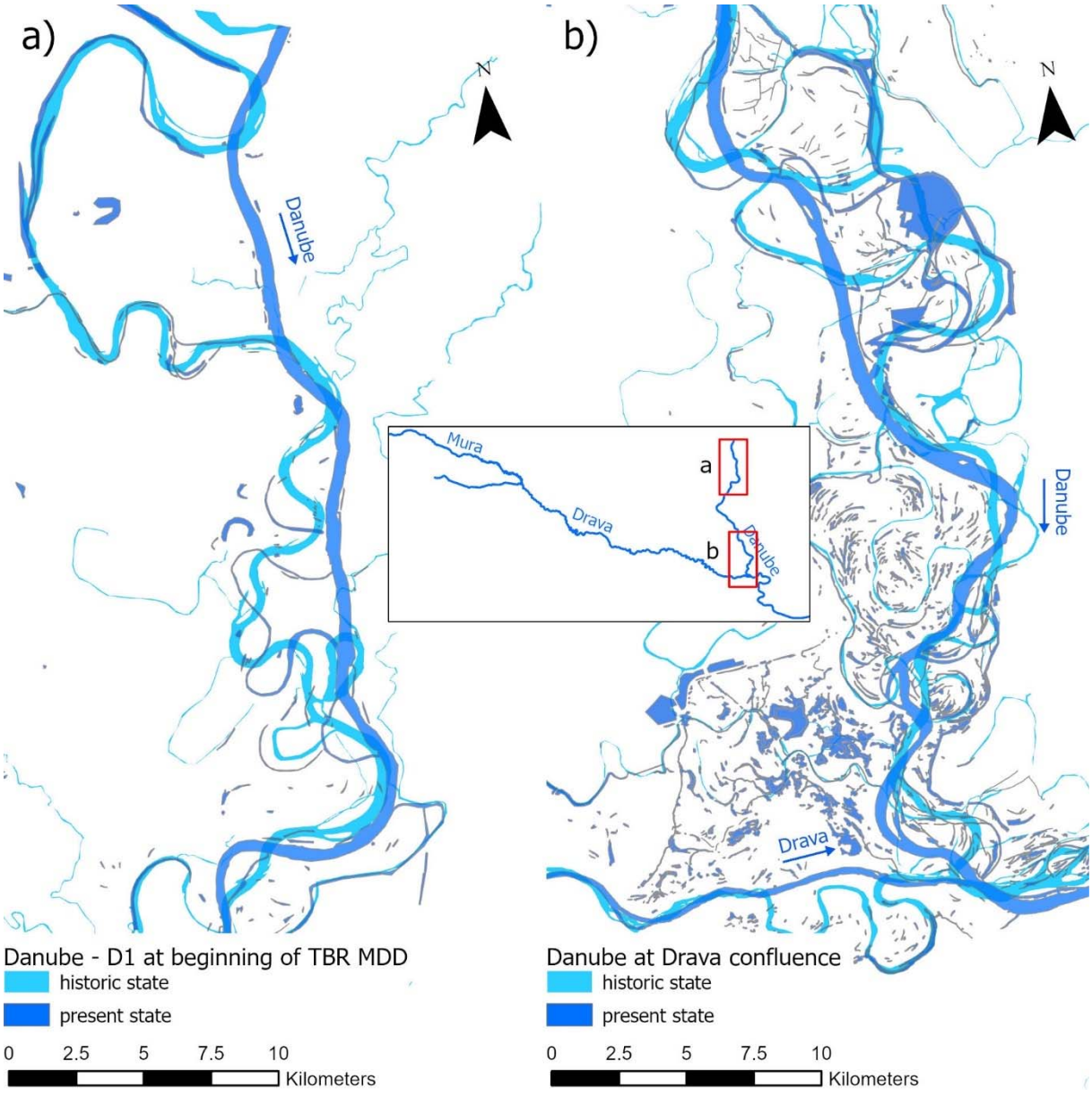

Figure 69. a) upstream part of the Danube section D1 and b) section D1 upstream of the Drava confluence.

The main course of the Danube in section D2 has experienced little change, except for one meander cut-off in the downstream region. However, the loss of the multiple side channels in the present state is apparent (Figure 70).

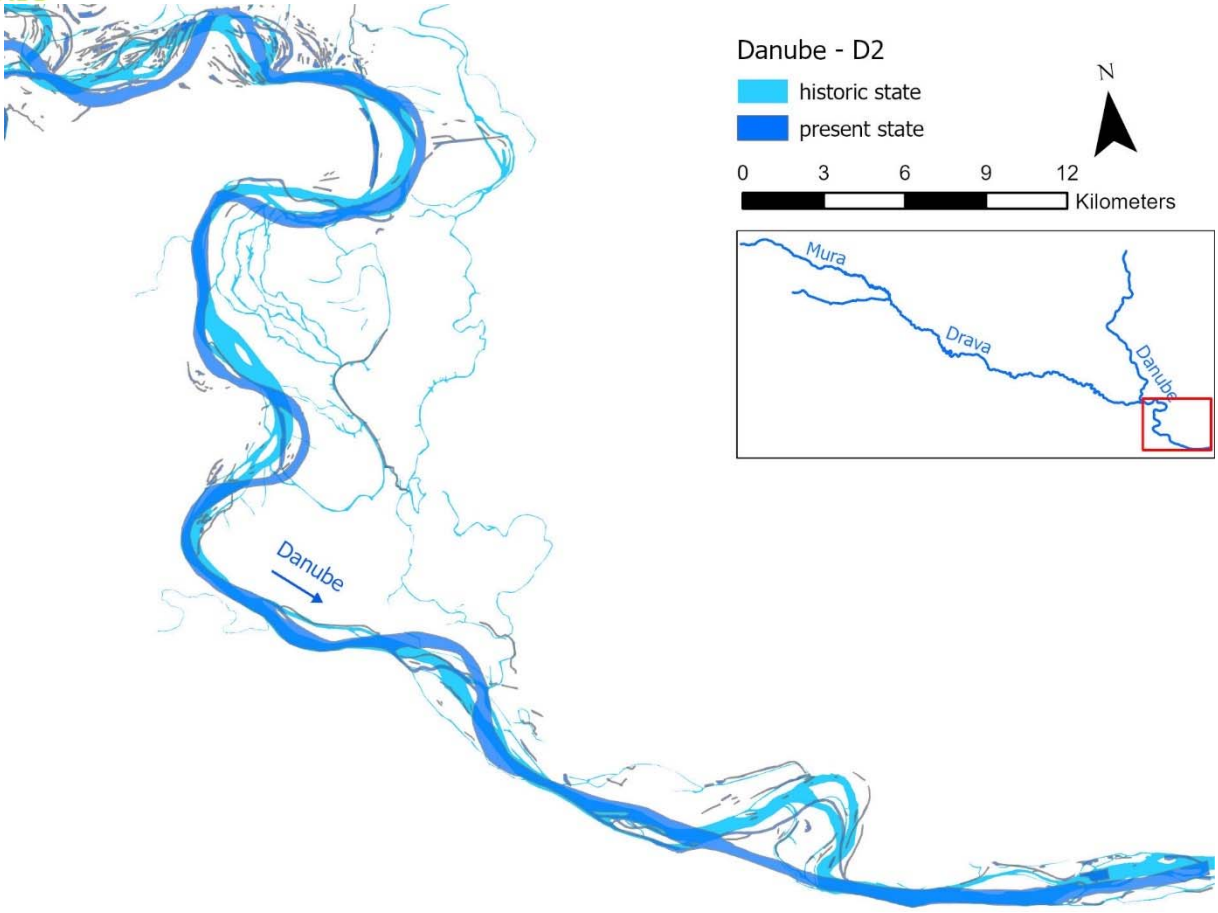

Figure 70. Danube section D2 downstream of the Drava confluence.

Within the TBR, the channel numbers of the Danube historically used to range from one to nine (Figure 71).

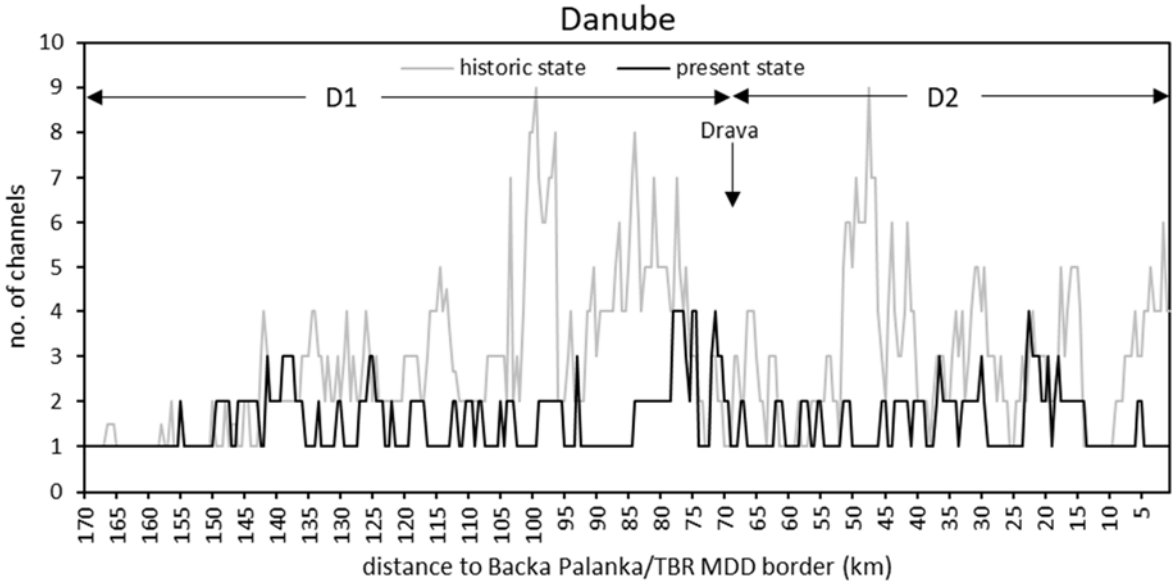

Figure 71. Number of channels of the Danube in the historic (grey) and present state (black).

Historically, along 21% of its course the Danube consisted of three channels and along 27% of two. It was a single thread channel only along 21% and along 30% it consisted of four or more channels. In the present state, the Danube also mostly consists of only one (58%) or two channels (36%). Occasionally, the channel number goes up to three or four, but only at 8% of its length within the TBR (Figure *72*).

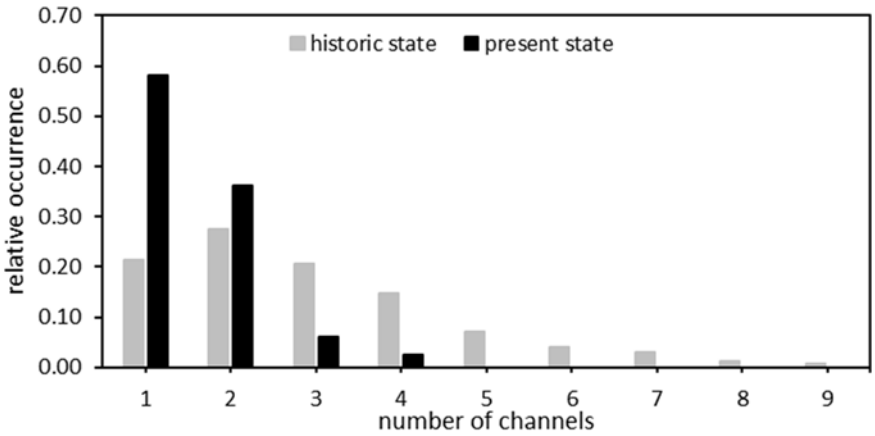

Figure 72. Relative occurrence of channel numbers along the Danube.

3.3 Analyses of bank obstruction

Of the approximately 1350 km bank length (Mura, Drava and Danube plus permanent side channels), 538 km are constrained by rip-rap (Schwarz, 2022). Schwarz (2022) considered a groyne's morphological impact of 300 m in length, which increases the length of constrained banks by another 200 km, which means that in total 55% of all banks are constrained. Since often partial obstructions (i.e. outer banks in bends) are sufficient to fix the river course, nearly the entire rivers can be considered constrained, with a few meanders, that can still migrate freely, as exception (Schwarz, 2022).

Looking at the individual sections (Figure 73), the Mura section M1 is highly modified over most of its length. This also applies to the upstream part of M2; further downstream, however, the density of the training structures decreases. Throughout its length, the training structures density in section M3 is 8-12 km/segment. Along the majority of the Dr1 reach, the density is >16 km/segment, which is to be expected, considering the three hydropower plants. The density in Dr2 below the Mura-Drava confluence considerably lower, with artificial structures implemented mainly only along the outer banks at bends. The upstream part of Dr3 is quite diverse, with alternating sections of either one or both banks constrained. Between Donji Miholjac and Belišće, there is a section of about 13 km with no artificial constraints, where the Drava can flow freely; same goes for a short section downstream of Belišće. Between Osijek and the confluence with the Danube river however, the Drava is constrained along both banks by rip-rap and settlement walls over the majority of its length. Along the whole section D1, the Danube river is constrained at least along one bank, with completely channelized sections at the upstream end of the TBR-Danube and at Batina. The complete section D2 again is modified at least along one bank, with channelized stretches and settlement walls in city sections.

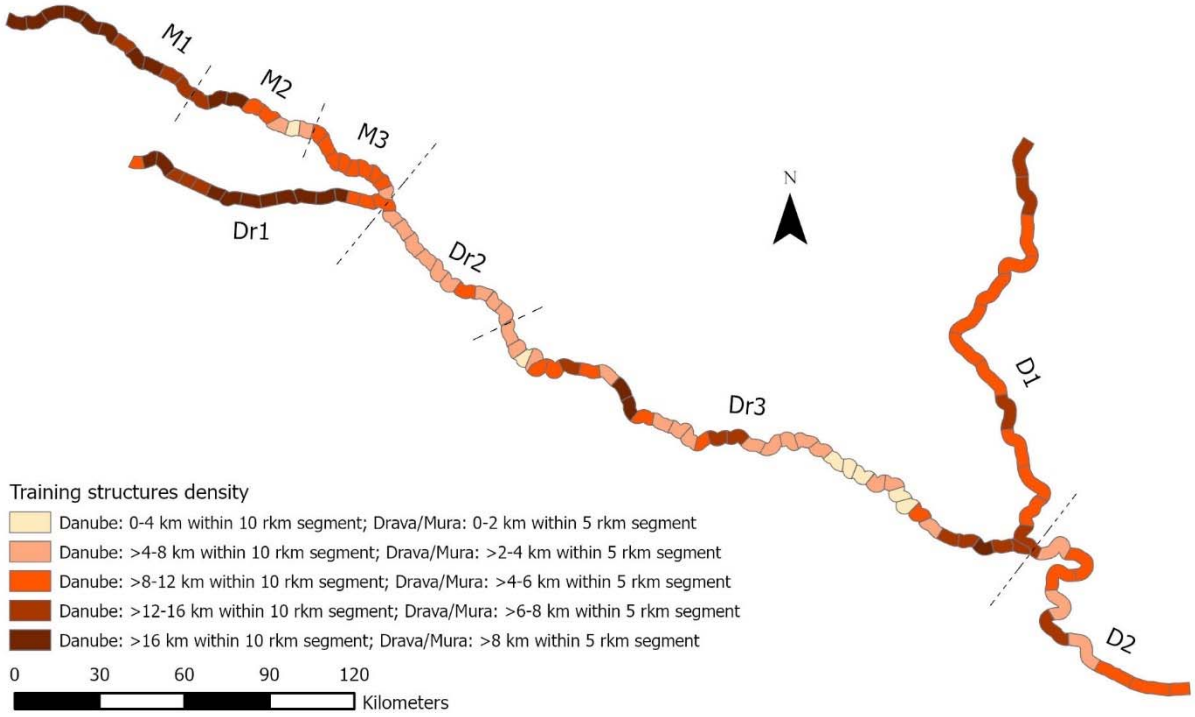

Figure 73. Training structure density along the TBR rivers (Data source: Schwarz, 2022).

Overall, near natural sectors along the TBR rivers are rare and mainly limited to the lower Drava river. In many sectors, which show relatively little training structure densities, the constraints at outer banks along bends are sufficient to significantly inhibit lateral erosion and therefore limit potential sediment input.

3.4 Dredging activities

The analyses on dredging activities reported here are extracted from Baranya et al. (2020).

Data on dredging activities along the Drava river were collected by VITUKI (2003) and EJF (2012) between Botovo to Drávaszabolcs and further assessed by Baranya et al. (2020). Between a total of 3,5mio m^3 of sediment were excavated, the majority of which was gravel (2.77 million m^3 in the section between Botovo and Barcs, hereafter referred to as “above Barcs”). In the section from Barcs to Drávaszabolcs (“below Barcs”), 0.74 million m^3 of sand were excavated. Figure 74 shows the annually dredged volumes for the two sections:

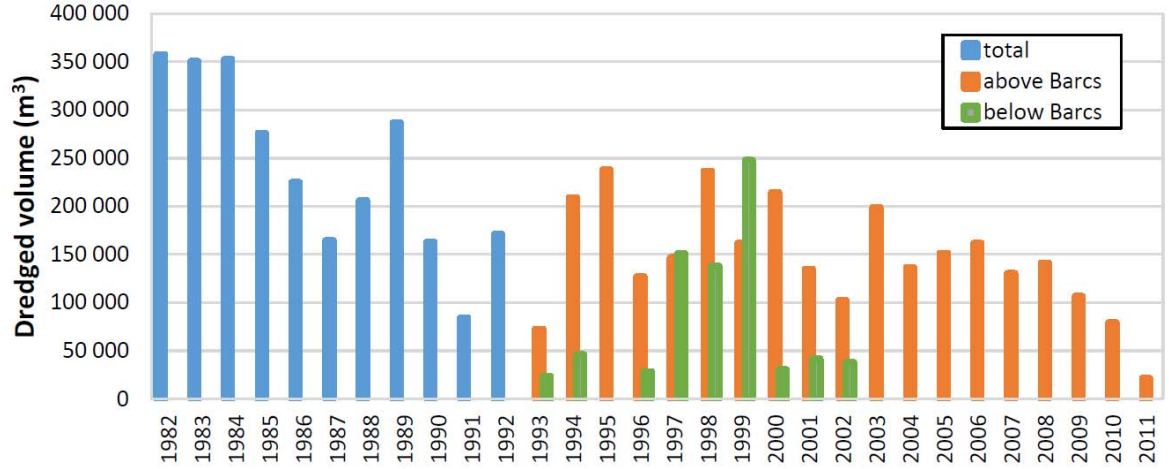

Figure 74. Annually dredged bed material in the Drava River (Baranya et al., 2020).

Assuming a uniform distribution of the excavated sediment, bed changes due to dredging were estimated by Baranya et al. (2020) based on the assumption of uniform channel widths for the individual sections (Figure 75).

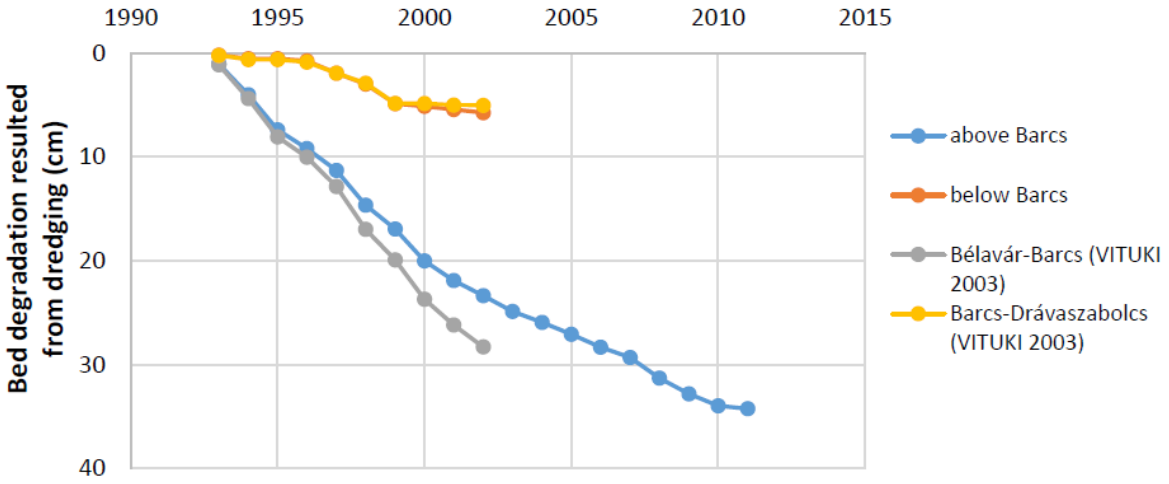

Figure 75. Bed degradation due to dredging in the Drava River (Baranya et al., 2020).

Figure 75 shows the estimated lowering of the bed level due to dredging above and below Barcs. Excavation of sand stopped below Barcs in 2003, whereas gravel mining above Barcs was undertaken until 2001. Based on the dredging data, the respective lowering of the bed level upstream of Barcs between 1993 and 2002 is estimated to be 2.34 cm/year, whereas it decreased to 1.21 cm/y between 2003 and 2011 due to less gravel excavation during this period. Downstream of Barcs, the dredging-induced lowering rate of the bed level is estimated to be 0.57 cm/year. From 1993 to 2001, the lowering of the bed due to dredging is 1.80 cm/year, resulting in a total of 34 cm.

Downstream of Barcs, the total riverbed incision is estimated to be 5.73 cm, which translates to 0.57 cm/year. Dredging-induced lowering of the bed level over the entire period from 1982 to 2011 could only be roughly estimated, since until 1993 only total volumes were known. For this entire period Baranya et al. (2020) estimated a lowering

rate of 1.67 cm/year upstream of Barcs (50cm in total) and 0.48 cm/year downstream of Barcs (10 cm in total).

While the dredging caused a bed level change, the bed elevation was additionally affected by sediment transport. Differences between in- and output into river sections due to fluvial deposition or erosion cause a change of bed levels, which, added to the rates due to dredging, either increase or decrease the lowering rates. Accordingly, Baranya et al. (2020) complemented the incision analysis with bedload transport data between cross-sections in the same period. By comparing the bedload entering the section to the bedload leaving the section, corrections in the abovementioned values were made due to the assumption that missing bedload volume was trapped in the scours caused by dredging. In the section Botovo-Bélavár, the combination of these data resulted in an estimated lowering rate of 0.21 cm/year. In the next section between Bélavár and Barcs, more bedload left the section than entering it due to fluvial erosion of the bed. The resulting lowering of the riverbed is estimated to be 2.28 cm/year. This results for the entire section in 1.11 cm/year (1.25 cm/year due to dredging minus 0.14 cm due to deposited bedload).

Between Barcs and Drávaszabolcs, sand excavation lead to an incision of 0.57 cm/year, the difference in bedload in this section adds 0.46 cm/year, resulting in a total rate of 1.03 cm/year.

Considering the data from 1982 to 1993, the total rate of bed lowering from 1982-2001 upstream of Barcs was 1.53 cm/year (1.67 cm/year due to dredging, minus 0.14 cm/year refilling with bedload) and 0.94 cm/year downstream of Barcs (0.48 cm/year due to dredging plus 0.46 cm/year fluvial erosion).

The Water Research Institute et al. (2019) reported the following dredging activities in the residual water stretches next to the headwater channels of the hydropower plants on the Drava within the DanubeSediment project: After the construction of a motorway (1993-2003) dredging stopped in the Drava or in the floodplain. Prior to the construction of the motorway, the concession holder carried out dredging activities for gaining material for the motorway from the old riverbed of the Drava along the Čakovec and Varaždin hydropower plants. In addition, sills were constructed to maintain the low water level.

According to the Water Research Institute et al. (2019), dredging served to ensure flood protection or to reduce the negative impact of the HPPs (cross-section reduction for a higher water level). The dredging was limited to places where the flood protection structures of the river were negatively affected, as well as in old riverbeds at the Varaždin and Čakovec power plants. In the Drava, no sediment dredging has been carried out since 2003 in the section between km 176.4 and km 322.8 (which is maintained by the Croatian Water Management Department for the Mura and the upper Drava).

3.5 Sediment balance

In the following chapter, available data relevant for the sediment balance were analysed and human interventions on the sediment balance assessed.

3.5.1 Mura

3.5.1.1 Bedload

The bedload of the Mura mainly consists of gravel: Bed samples excavated at Mursko Sredisce showed gravel as the dominant fraction (>85%) with addition of sand and a mean grain size d_m ranging from 15.89 mm to 21.55 mm (DHMZ, 2021). Further downstream at Gorican, the riverbed mainly consists of gravel with only a small addition of sand (<5%) and the d_m ranges from 12.54 mm to 28.37 mm (DHMZ, 2021).

Rákóczi and Szekeres (2004) gathered data on bedload transport at Letenye over the period from 1986 to 2003 (Figure 76).

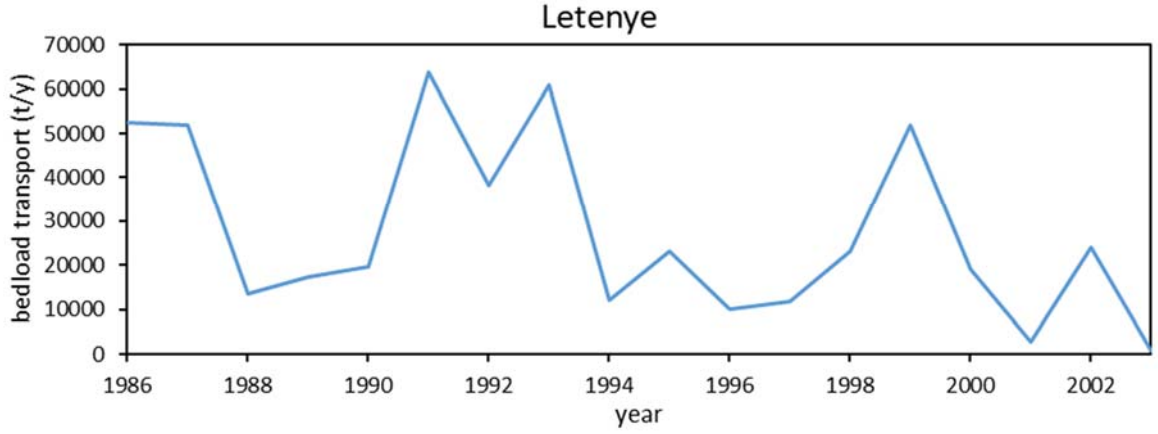

Figure 76. Annual bedload transport at Letenye (data source: Rákóczi and Szekeres, 2004)

According to this data, the average annual bedload transport in this period was 27 588 t/year.

A bedload transport capacity of approximately 45000 m3 per year (which at an estimated porosity of 30 % would convert to approximately 83000 t per year) was assessed for the Mura along the border between Austria and Slovenia (Klösch et al., 2021), which was subject to the systematic channelization of the 19th century. In contrast, the bedload entering the Mura downstream of the last large hydropower plant in Spielfeld in Austria was assumed negligible (Hengl et al., 2001). The Austrian power plant operator Verbund is striving to improve sediment permeablity and adapted the operation of the power plants from Mellach to Spielfeld, also in order to react to changed flood discharge values and increased sediment transport from the upstream section (Verbund, 2015). Effects of the adapted operation are still to be evaluated.

If the Mur along the border between Austria and Slovenia is made wider and more sinuous, taking into account the spatial constraints, the bedload demand for achieving a dynamic equilibrium could be reduced to about 20000 m3 per year (Klösch et al., 2021).

In addition, cross sections between 1974 and 2006 were also used for a calculation of the sediment balance for the Mura along the border between Austria and Slovenia. For this purpose, differences in the cross-sectional areas were multiplied by an influence width (half the distance to neighbouring profiles). Sediment supplies that already took place

before 2006 were taken into account (Table 2). In total, 860,000 m³ of bedload were discharged from the Grenzmur section in the period from 1974 to 2006 (Figure 77). Bedload supply from upstream would be added to this transport, but can be estimated as negligible or very low during this period.

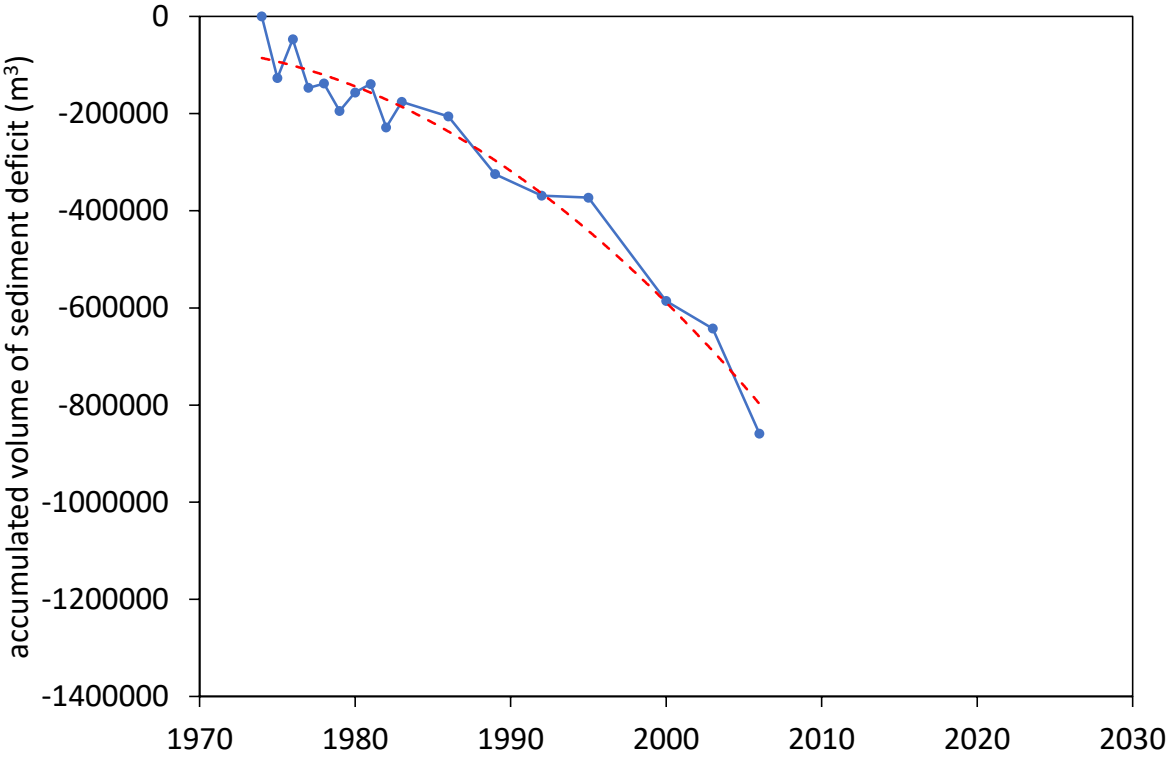

Figure 77. Cumulative discharge of sediment volume from the Grenzmur over the period 1974 to 2006.

3.5.1.2 Suspended sediment

The first location continuously recording suspended sediment transport along the Mura within the TBR is at Mureck, where since 2008 an average of 385 178 t is transported per year (Figure 78). It can be assumed that in the natural state of sediment attachment to the catchment, suspended sediments were more evenly distributed over a high discharge range. Today the runoff river plants cause an increased load when the weirs are opened, whereas otherwise especially the coarser particles are retained.

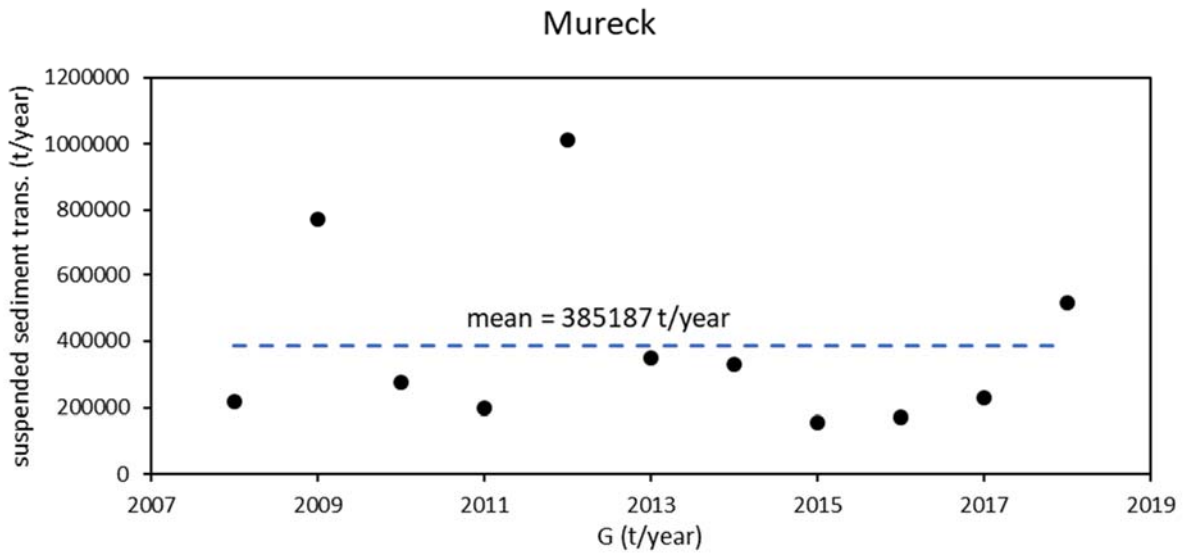

Figure 78. Annual suspended sediment transport at Mureck (data source: ehyd).

At Gorican, started in the year 1990; the recorded mean annual suspended sediment load is 256 915 t/year (Figure 79).

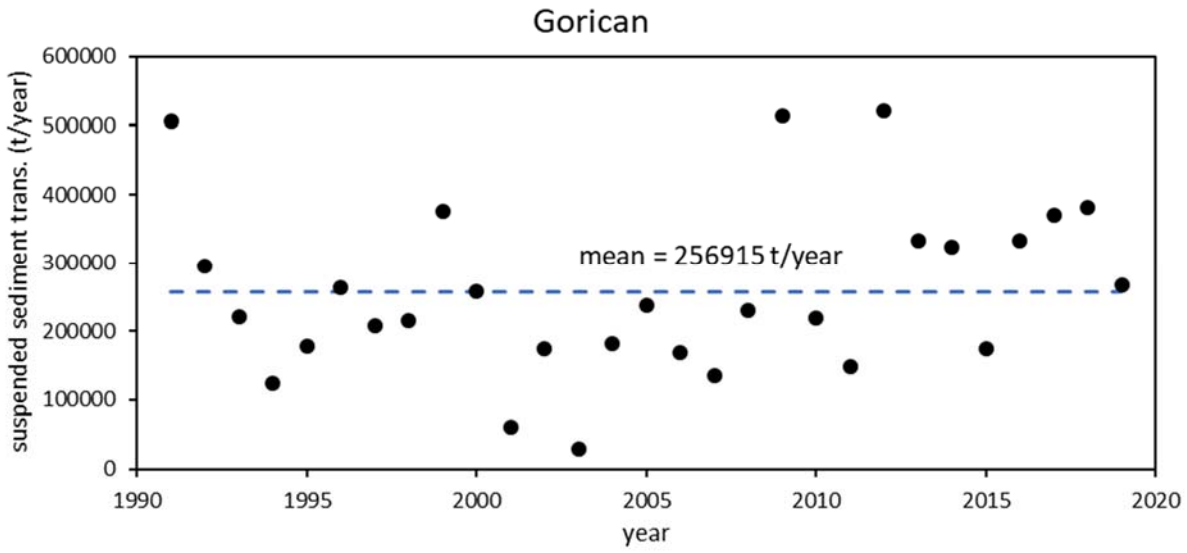

Figure 79. Annual suspended sediment transport at Gorican (data source: Croatian Waters).

3.5.2 Drava

In this chapter, the annual transport of bedload, suspended sediments and the impact of hydropower plants on sediment transport of the Drava River are discussed.

3.5.2.1 Bedload

The only found record of bedload transport over a longer period along the Drava was published by Rákóczi and Szekeres (2004), but their monitoring covers the entire period between 1986 and 2003 (Figure 79).

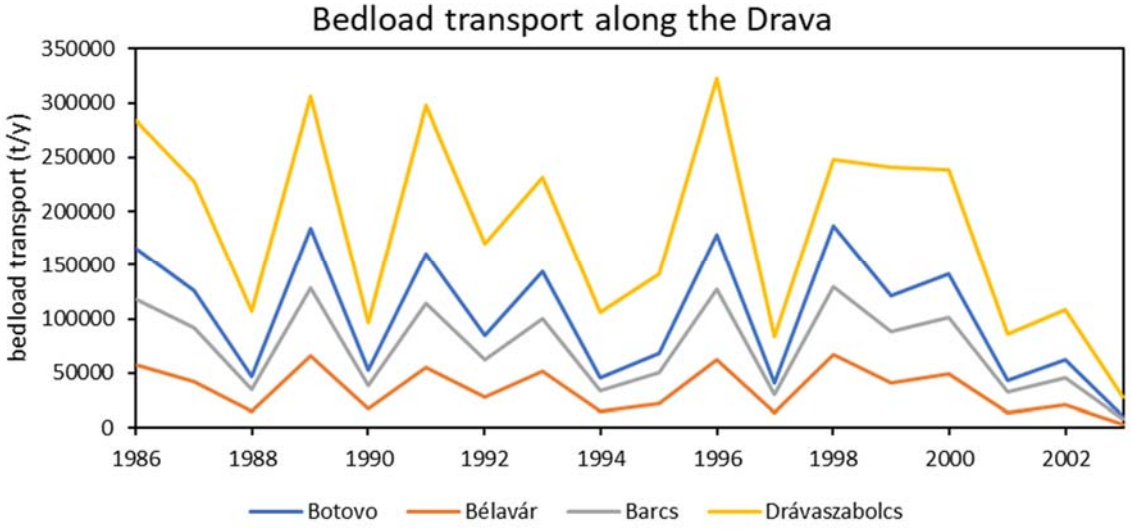

Figure 80. Measured bedload transport along the Drava (data source: Rákóczi and Szekeres, 2004).

The presumed decrease in bedload transport from 1998 to 2002 is affected by the hydrological conditions during this period, as shown by the mean annual river level and discharge data. The average annual bedload yields are listed in Table 14 below:

Table 14. Mean annual bedload transport along the Drava River between 1986 and 2003.

	Botovo	Bélavár	Barcs	Drávaszabolcs
average annual bedload transport (t/year)	103556	35364	74098	184769

The grain size distribution of the river bed was sampled by Terra-Graph Kft.. (2020) between rkm 236 and rkm 75 (Figure 81).

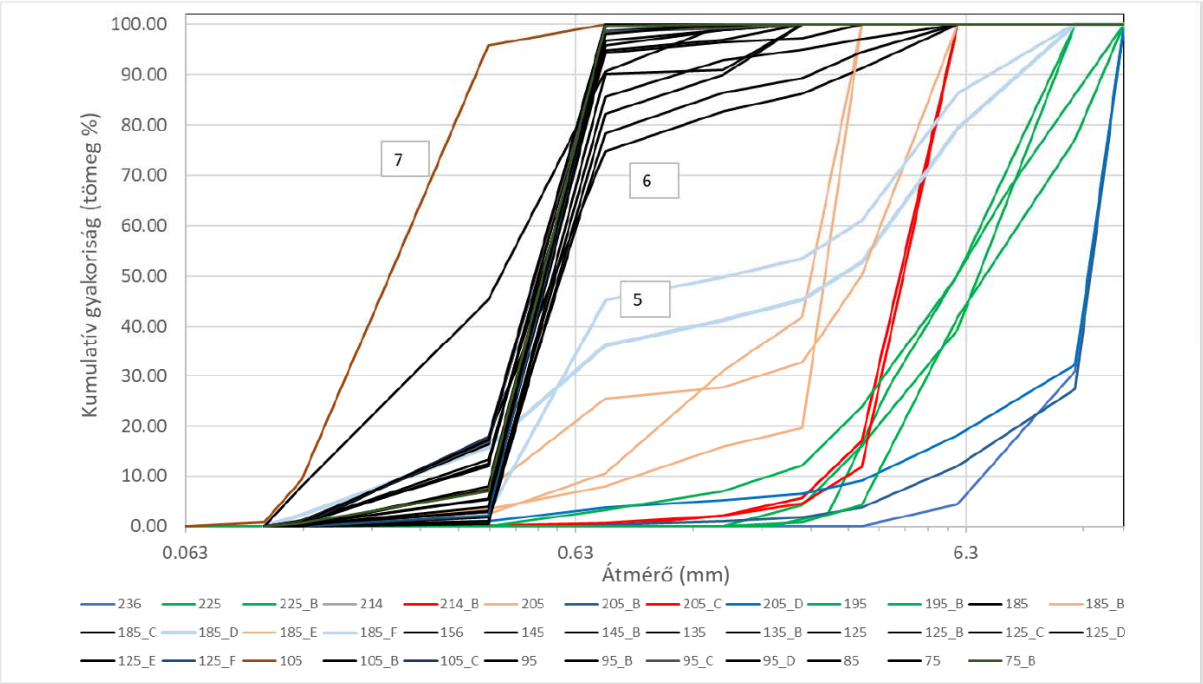

Figure 81. Grain size distribution along the Drava between rkm 236 and rkm 75, named after the rkm of the sampling site (Terra-Graph Kft., 2020).

Kovačićek et al. (2020) conducted excavations of bed material at gauging stations along the Drava in 2020. Near Botovo, the riverbed mainly consists of gravel (>76%), with 10% sand and 13% cobbles, with the d_m ranging from 11.22 mm to 29.55 mm (29.55). At Semovec between the Varaždin and Dubrava reservoirs, the grain size distribution is almost identical but the d_m ranges from 22.47 to 48.66 mm. At Terezino Polje, the dominant fractions are much finer. Here, fine gravel and sand are the dominant fractions (dm 0.16 – 4.8 (4.54,4.8)), further downstream at Donji Miholjac, the riverbed consist of 99% sand (dm 0.35 – 0.65 (0.35-0.37) (Kovačićek et al, 2020).

3.5.2.2 Suspended sediment

Bonacci and Oskorus (2009) examined the impact of three Croatian hydropower plants on the water level, discharge and suspended sediment transport. The HPP Varaždin started operation in 1975, followed by Čakovec in 1982 and Dubrava in 1989.

The station at Varaždin is situated just upstream of the Varaždin dam and recording of continuous suspended sediment data stopped in 1981, just before the construction of HPP Čakovec. Therefore, the time series is divided in a period before 1975 and the construction of the hydropower plant Varaždin and in a period afterwards. The construction of the first dam reduced the transport of fine sediments by 62% from initially 453 655 t/year to 173 227 t/year, as shown in Figure 82.

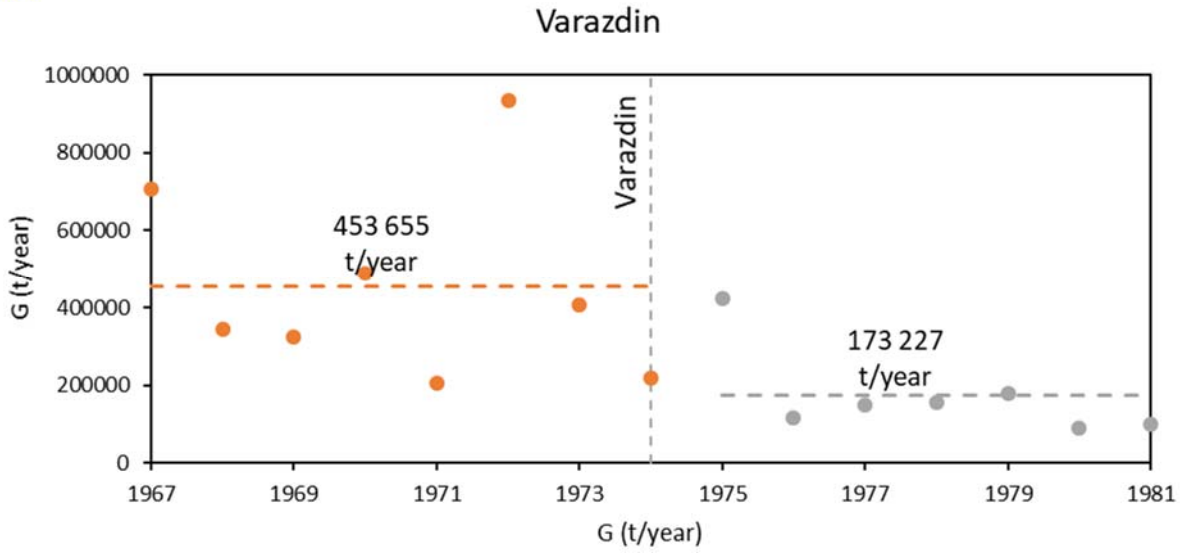

Figure 82. Annual suspended sediment transport at Varaždin (data source: Croatian Waters).

Figure 83 shows the annual suspended sediment load as monitored at Botovo. Due to the construction of the HPP Varaždin, suspended sediment transport decreased by 17%, the implementation of HPP Čakovec reduced the annual load further by 55%. After the construction of HPP Dubrava, the average annual load was further decreased by 26% to 280.862t/year. Compared to the state before 1974 with initially 1001.186t/year, this means a total decrease of 72% at Botovo.

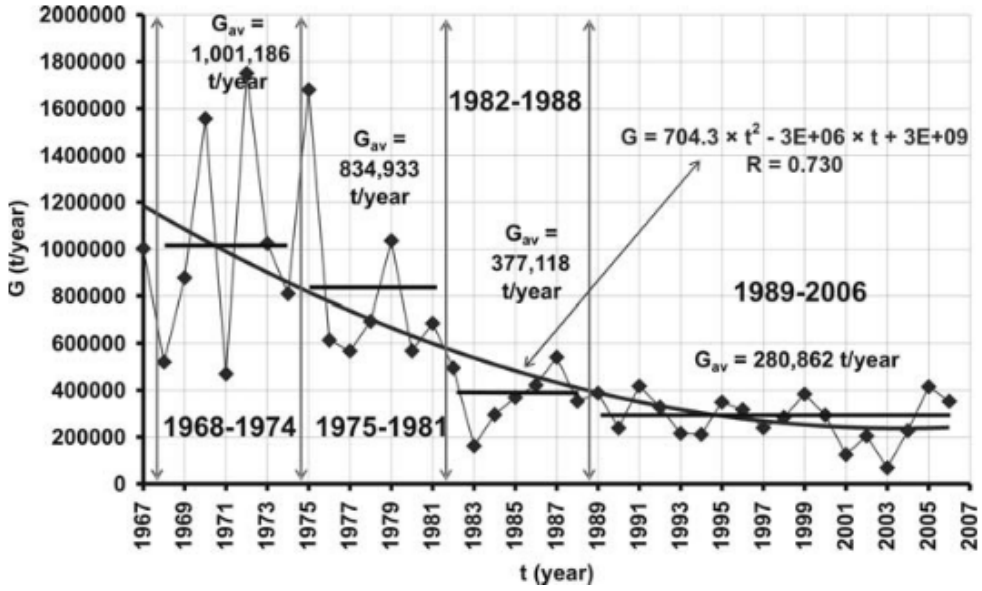

Figure 83. Annual suspended sediment load as measured at Botovo divided into periods: before the construction of the HEPP Varaždin 1975, HEPP Čakovec 1981 and after operation start of HEPP Dubrava in 1989. (Bonacci and Oskorus, 2009).

Continuation of the time series until 2019 exhibits a continuation of decreased suspended sediment loads (Figure 84). The extended series after the implementation of the Dubrava dam results in a higher mean annual suspended sediment load than in the time span from 1989-2006, as presented by Bonacci and Oskorus (2009). The average load since the last hydropower plant is impacting the Drava is only 305 287 t/year.

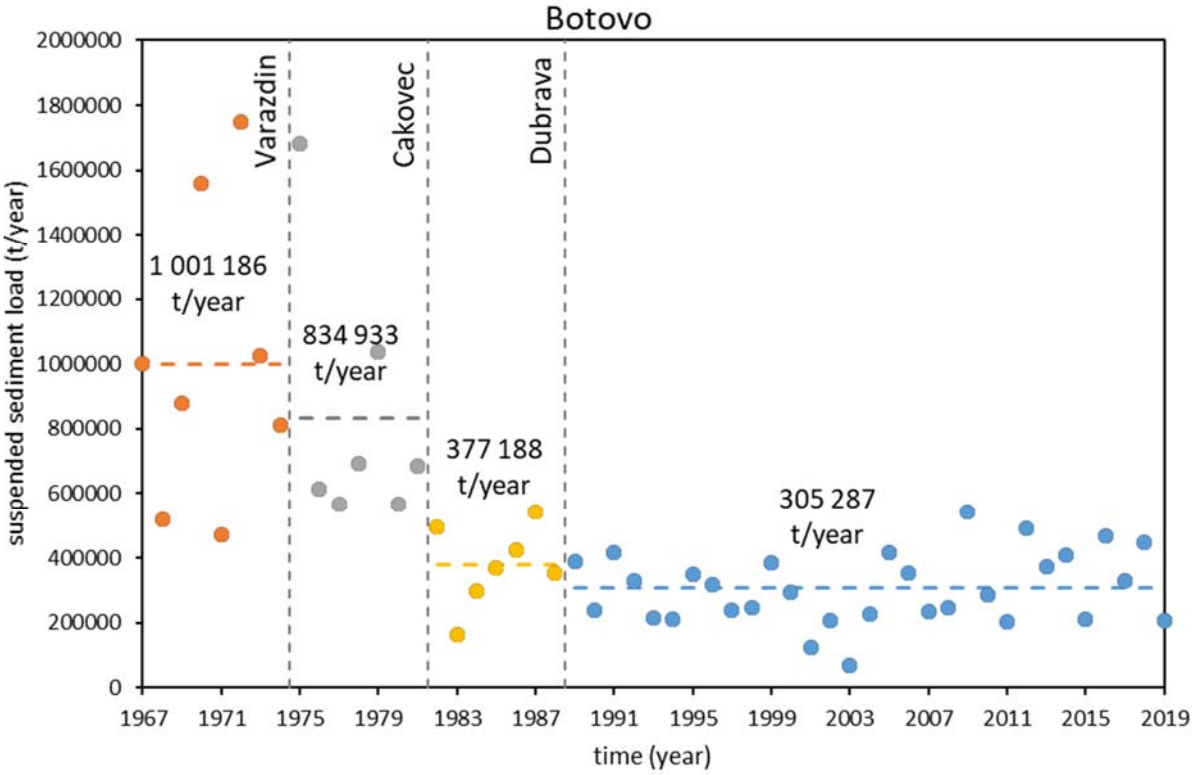

Figure 84. Total suspended sediment transport per year from 1967 - 2019 at Botovo (data source: Croatian Waters)

Approximately 175 km further downstream, data on suspended sediment is available for Terezino Polje (Figure 85). Here, 1991 is the first year in which sediment transport was consistently recorded; data on the situation before the construction of the hydropower dams is not available. The mean annual suspended sediment load for the period 1991 – 2019 is 335935 t/year.

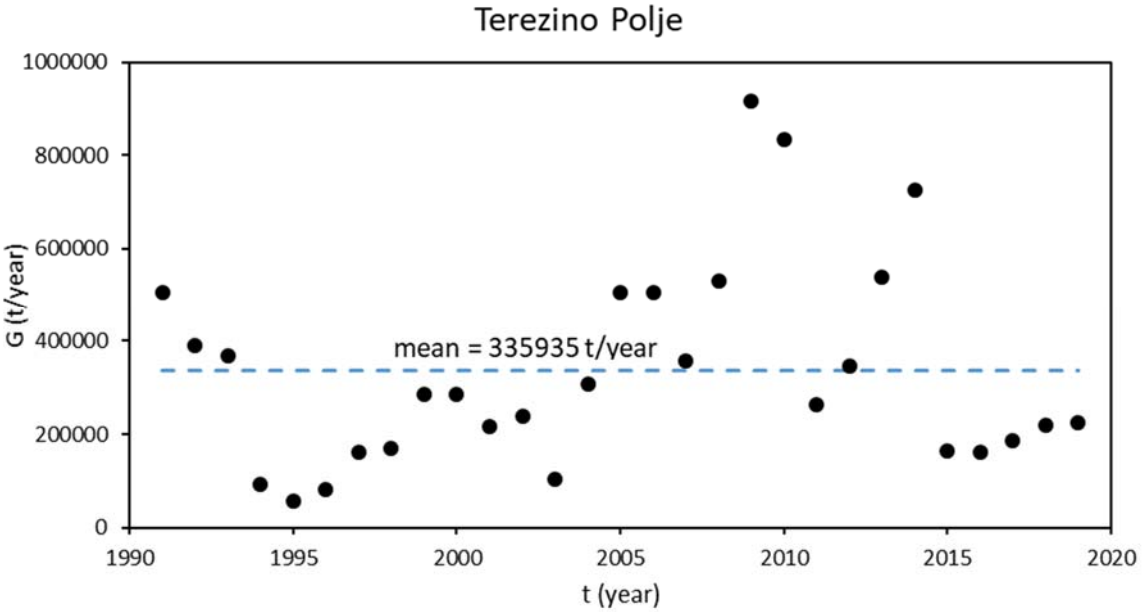

Figure 85. Annual suspended sediment load at Terezino Polje (data source: Croatian Waters)

70 km further downstream at Donji Miholjac, the effects of the HPPs are still apparent in the suspended sediment transport data (Figure 86).

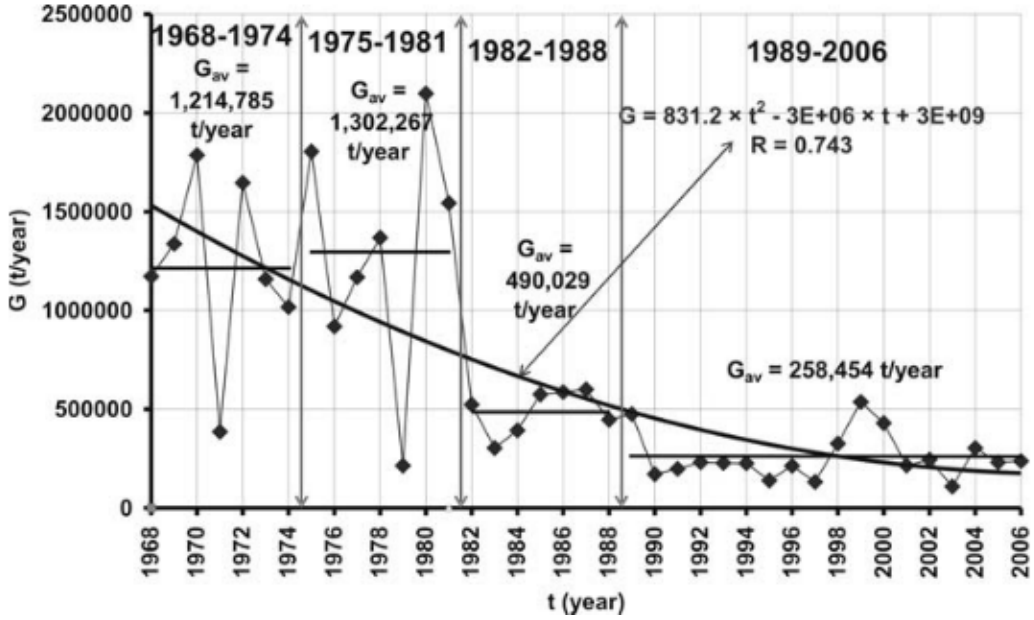

Figure 86. Annual suspended sediment load as measured at Donji Miholjac. (Bonacci and Oskorus, 2009).

At Donji Miholjac, the construction of the Varaždin dam (start of operation in 1975) did not show the same immediate effect on the suspended sediment load as in the upstream measurement stations, but the suspended load in the end dropped by a similar extent. After the construction of HPP Čakovec, annual suspended sediment load dropped by 62 %, which was further decreased by 47 % after the construction of HPP Dubrava in 1989. In total, the annual suspended sediment load at Donji Miholjac dropped from 1302.267 t/year in the pre HPP Čakovec period to 258,454 t/year after 1989.

Including the years 2007-2016 in the analysis, the mean annual suspended sediment load since 1989 is 250623 t/year (Figure 87).

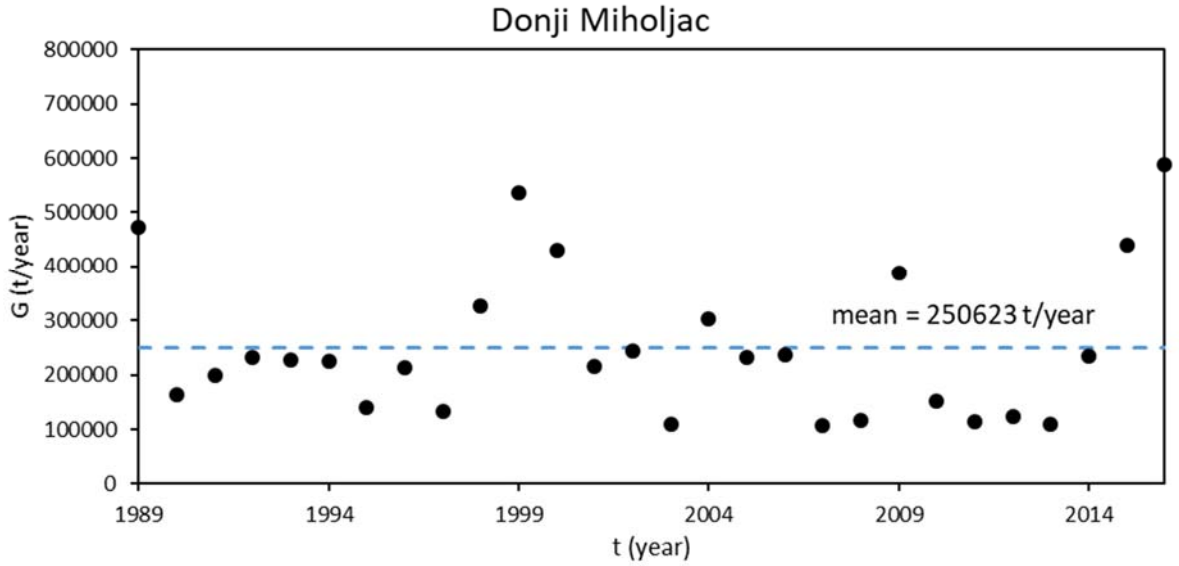

Figure 87. Suspended sediment transport at Donji Miholjac since 1989 (data source: Croatian Waters)

Tamas (2019) attributed the increase in mean annual suspended sediment load from Botovo to Terezino Polje to the hydropower dams and the change in the riverbed composition: The reservoirs, trapping the sediment, leaving a relatively sediment-free flow. Due to the riverbed consisting of mainly gravel upstream of Terezino Polje, only a limited amount of fine sediments can be entrained, which changes however downstream of Terezino Polje, hence increasing suspended sediment transport. Further downstream, the increasing width of the riverbed reduces the transport capacity and therefore leads to sedimentation, hence sediment transport at Donji Miholjac is reduced (Tamas, 2019).

Overall, the implementation of the three Croatian hydropower plants heavily altered the suspended sediment balance along the entire Drava by trapping the sediments in their reservoirs and reducing the supply to the downstream reaches.

3.5.2.3 Sediments in the HPPs

Figure 82 shows the development of the mean bed elevation along Lake Ormož, the most upstream of the three Croatian dams along the Drava River. While the bed levels remained relatively constant until 2013, a massive increase in the mean bed elevation is apparent in 2014 and 2015.

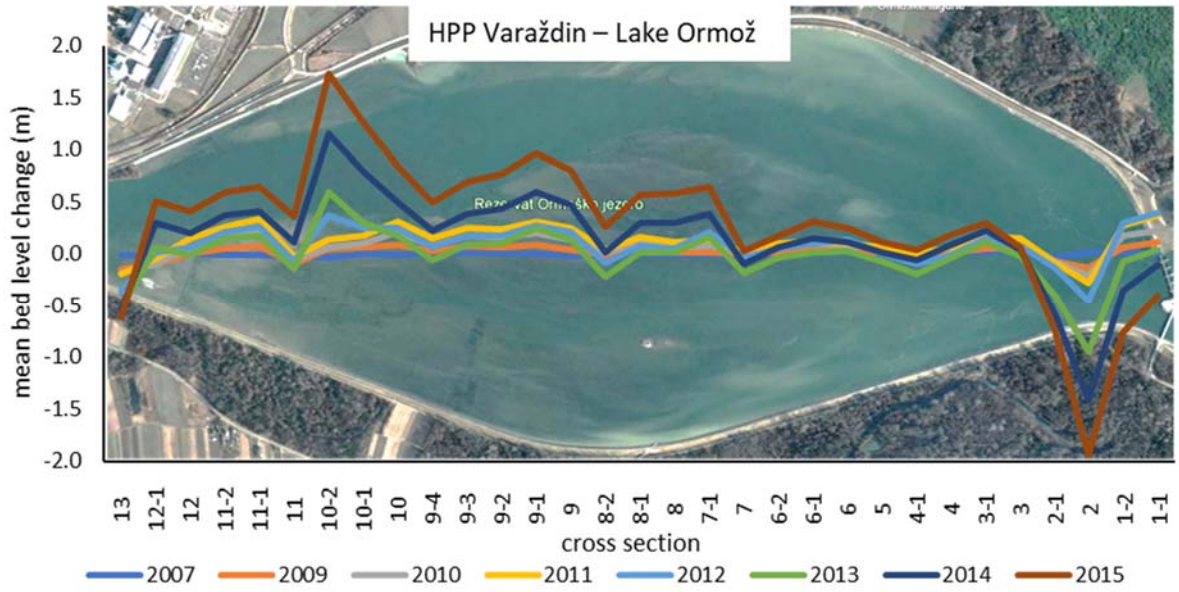

Figure 88. Mean bed level change in the Lake Ormož from 2006-2015 (data source: Croatian Waters).

Overall, in the year 2015 the Lake Ormož contained approximately 535 000 m^3 more sediment than in the year 2006 in the section depicted in Figure 82. Figure 93 shows the bed level changes in the reservoir.

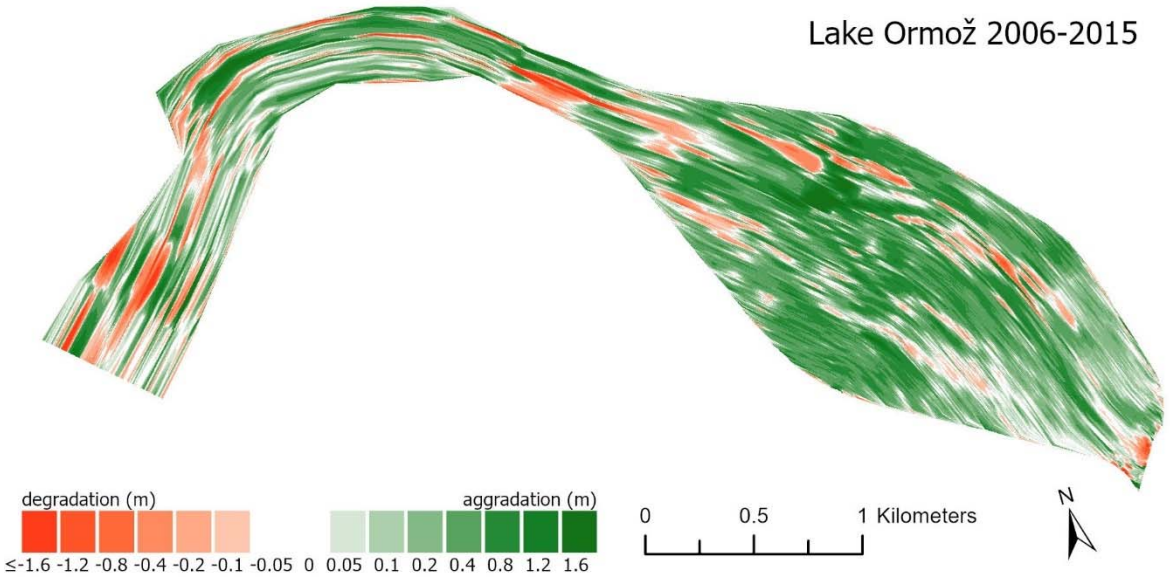

Figure 89. Differences in bed elevation at Lake Ormož between 2006 and 2015 (data source: Croatian Waters).

At the next dam downstream of Lake Ormož, at Lake Varaždin, the same pattern can be observed as in the upstream reservoir.

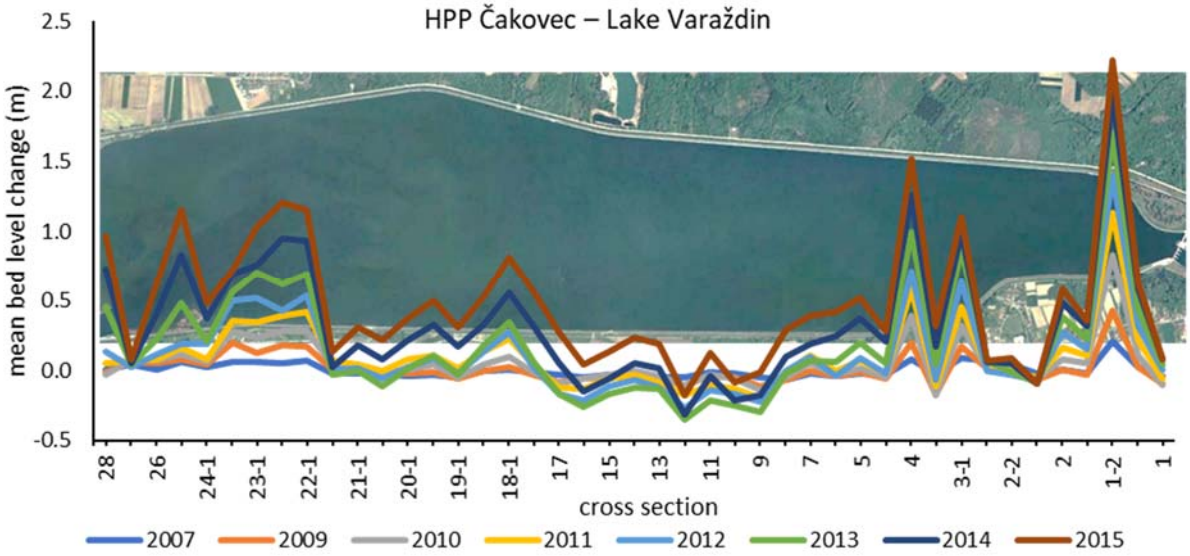

Figure 90. Mean bed level change at Lake Varaždin from 2006-2015 (data source: Croatian Waters).

At Lake Varaždin the difference between the DEMs of 2006 and 2015 is 1 840 260 m^3. This however does not necessarily equal the total amount of sediment trapped in the reservoir, since outgoing sediment (due to flushing or dredging) is not considered.

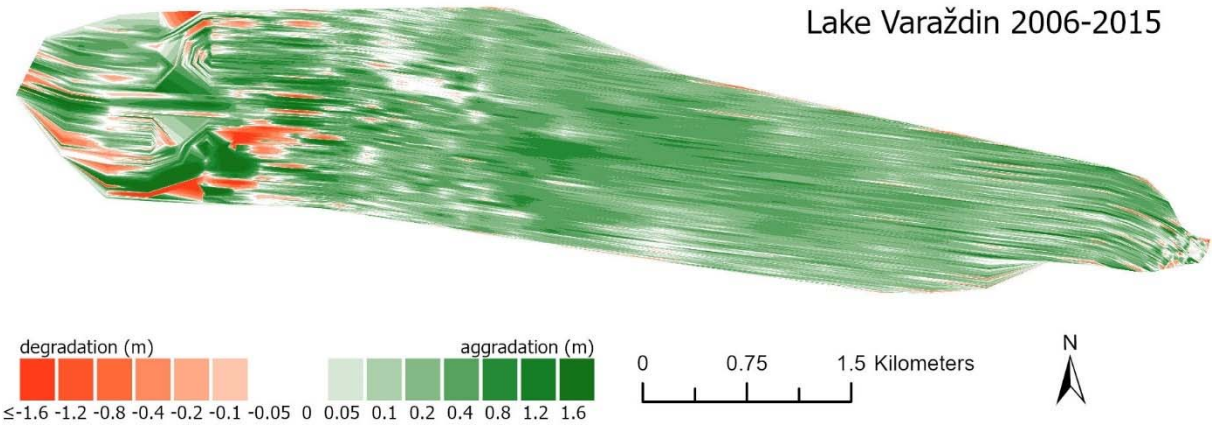

Figure 91. Differences in bed elevation at Lake Varaždin between 2006 and 2015 (data source: Croatian Waters).

No data were provided for Lake Dubrava, the largest of the three Croatian reservoirs.

Overall, while the impact on the sediment balance due to retention is evident, the exact extent remained unclear.

3.5.3 Danube

For this study, data on suspended sediment along the Danube River was available over an extended period of time at Dombori (rkm 1507) and Mohacs (rkm 1447).

The mean annual suspended sediment transport at Dombori is depicted in Figure 92.

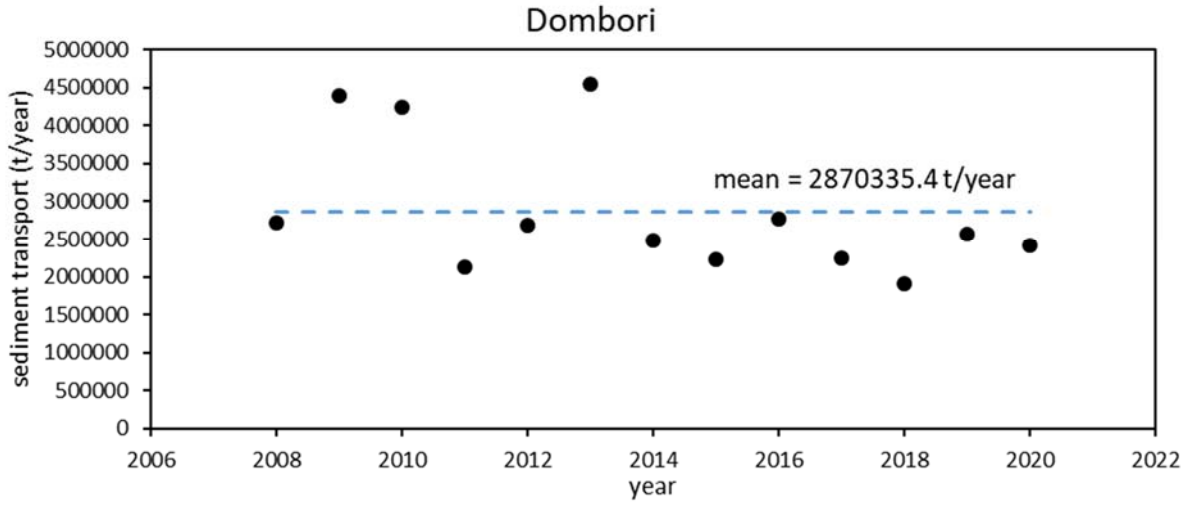

Figure 92 Annual suspended sediment transport at Dombori (data source: Croatian Waters).

In the period between 2008 and 2020, the mean annual suspended sediment transport measured at Dombori was 2 870 335 t/year.

At Mohács, a quite similar average annual yield of 2 855 003 t of suspended sediment was measured (Figure 93).

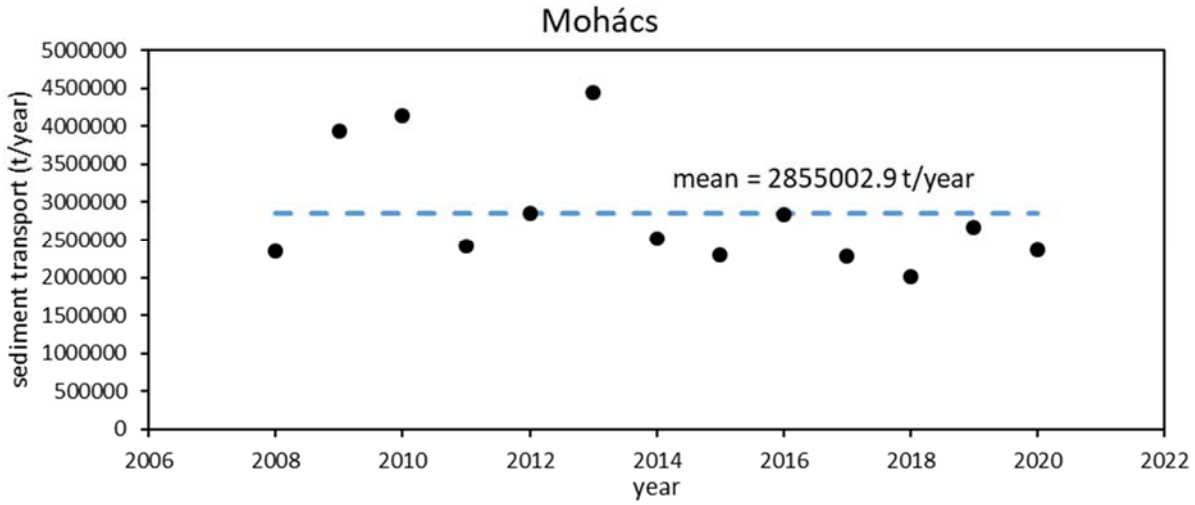

Figure 93 Annual suspended sediment transport at Mohács (data source: Croatian Waters)

Further downstream, only data for the year 2019 was available at the stations Batina (rkm 1425), Dalj (rkm 1356) and Ilok (rkm 1300):

Table 15 total suspended sediment transport in 2019.

Station (rkm)	Batina (1425)	Dalj (1356)	Ilok (1300)
total suspended sediment load 2019 (t)	2 593 275	2 217 070	1 663 109

Overall, the amount of sediment transported in suspension by the Danube River is drastically reduced in the present state (Figure 94). Analyses of suspended sediment load

along the entire Danube river network, including the contributions of tributaries at their confluences, revealed a strong reduction of suspended load compared to the historic state, causing a reduction of suspended load into the Black Sea from ca. 60 and 40 Mt/year historically to ca. 20 and 15 Mt/year. Sediment data of the Drava River however was already influenced by early hydropower dams along its course - the first hydropower plant in the Drava was already constructed in 1913-1918 near Fala in Slovenia, the first hydropower plant in the tributaring Mura was constructed even before in 1899-1903 near Lebring in Austria.

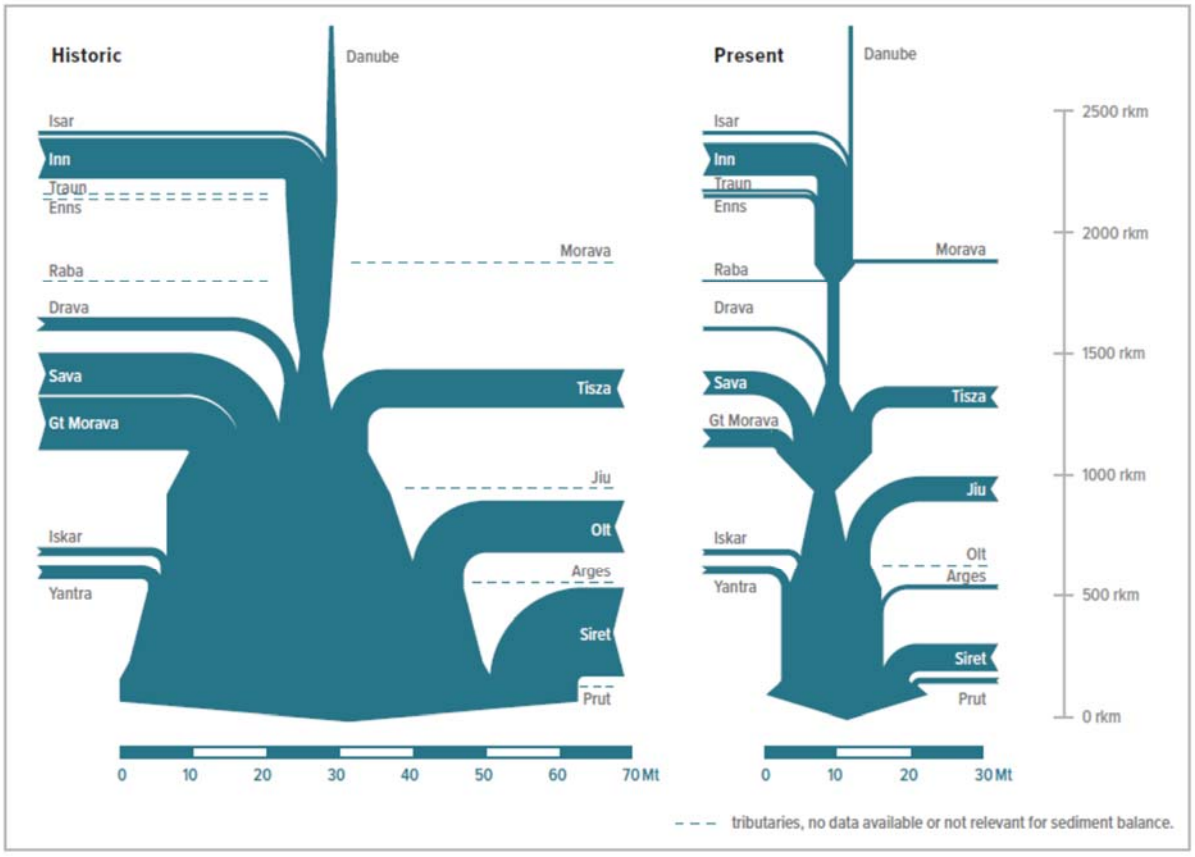

Figure 94 Suspended sediment balance of the Danube river and its tributaries before (left) and after the construction of hydropower plants (right) (Habersack et al., 2019).

Based on cross-sectional analysis, an estimation of the erosion and sedimentation and therefore the river bed change was made in the course of the DanubeSediment project. Figure 95 shows aggradation and degradation as well as dredged amounts along the Danube within the TBR in the period between 1971 to 1990. In sections 1 km in length, the annual deficits and surpluses of sediment volume range between -710000 m^3/year and +570000 m^3/year. Dredging, when distributed evenly across the length where dredging occurred in the vicinity of the Drava confluence, amounted to +22500 m^3/year. In the last three kilometres 230000 m^3 were dredged on average in each kilometre every year.

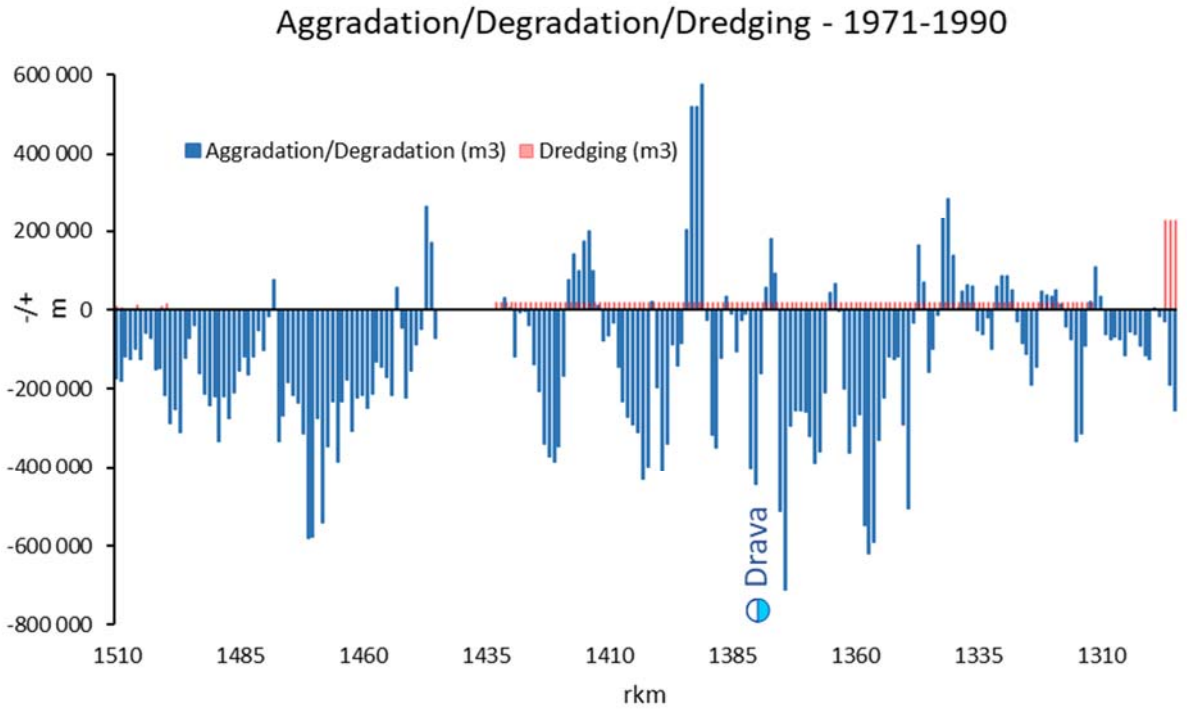

Figure 95 Aggradation/Degradation (blue) and Dredging (red) per kilometre along the Danube within the TBR between 1971 and 1990(Source: DanubeSediment).

In the time period between 1991 and 2017 bed level changes appear to be more evenly distributed near the Drava confluence, showing mainly deficits from degradation which average to 11000 m3/year in the section between rkm 1347 and rkm 1435 (Figure 96). Downstream of rkm 1345, the deficits are larger, reaching up to 193453 m3/year per kilometre. Upstream of rkm 1435, sequences of degradation, aggradation and dredging occurred, with most volumetric changes resulting from degradation.

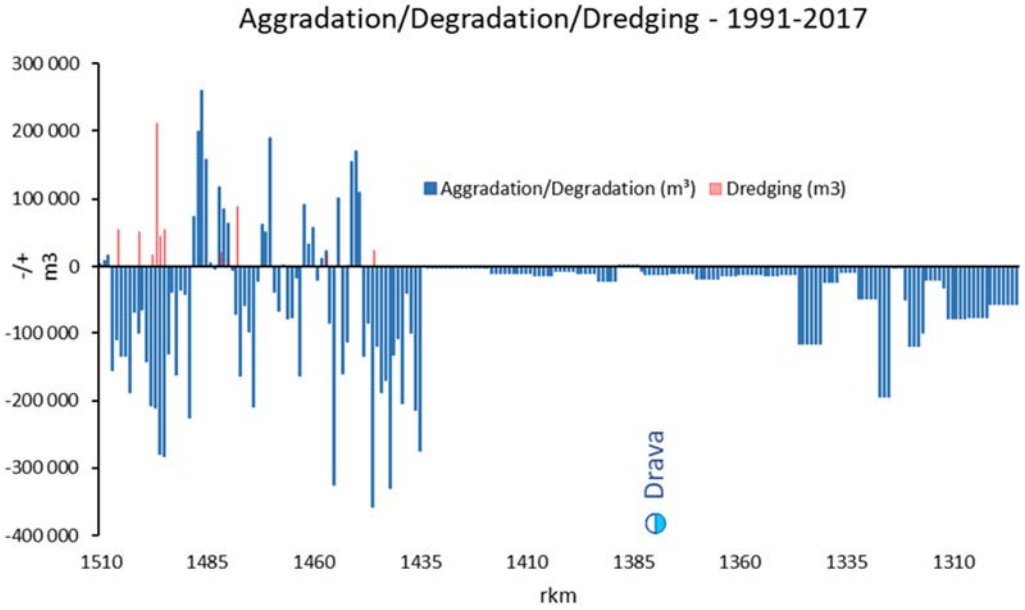

Figure 96. Aggradation/Degradation (blue) and Dredging (red) along the Danube within the TBR between 1991 - 2017 (Source: DanubeSediment).

Erosion nearly along the entire stretch resulted in an annual output of sediment volume of 800000 m³/year in the time period between 1991 and 2017. The deficit which cumulated at the upstream end of the TBR MDD to 1400000 m3/year hence increases to 2200000 m3/year at the downstream end of the TBR MDD.

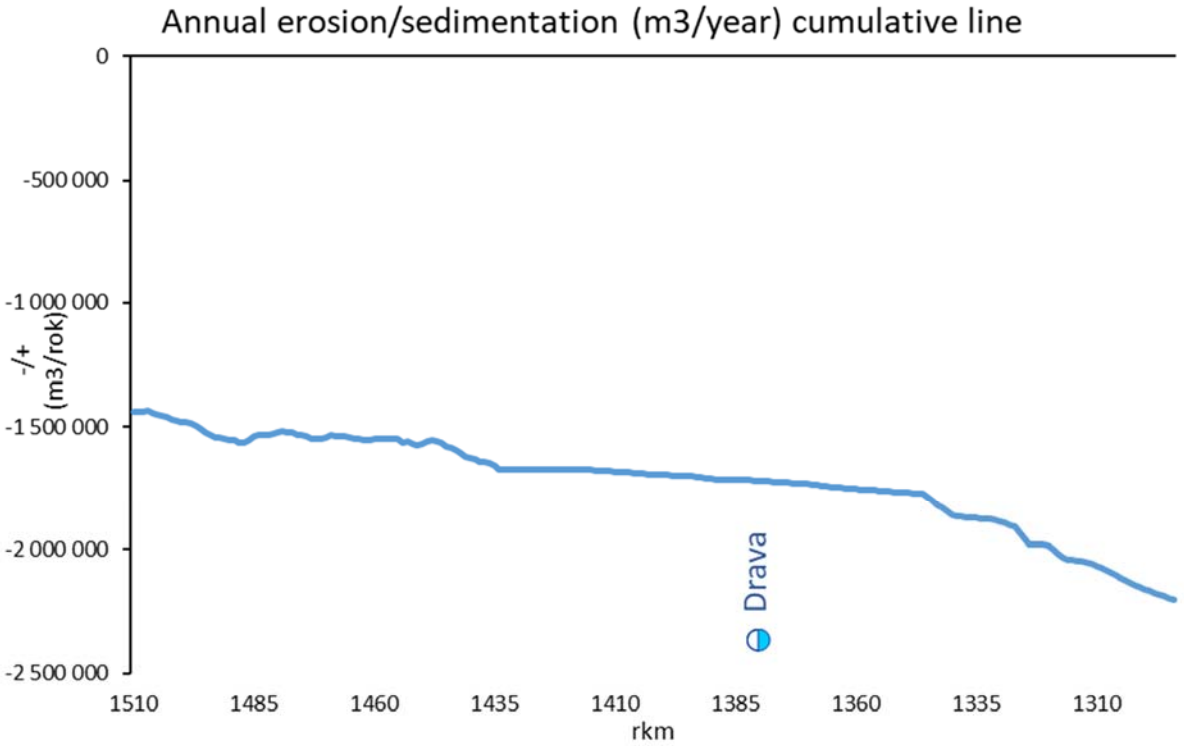

Figure 97. Cumulative annual erosion/sedimentation 1991-2017 (Source: DanubeSediment)

The channel thalweg also shows changes between the periods PI (1920-1970) and PIII (1991-2017) (Figure 98).

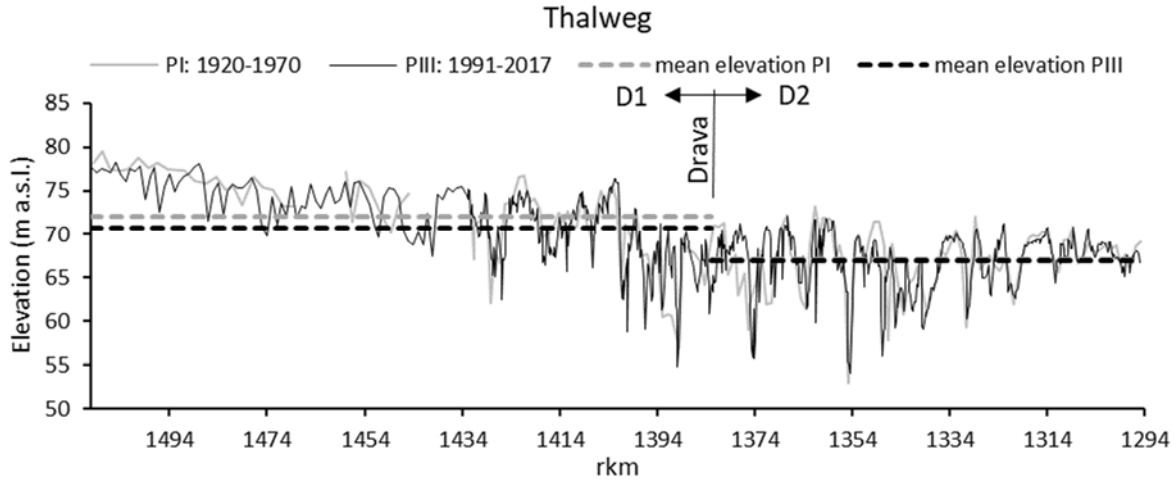

Figure 98. Danube-Thalweg in the periods 1920-1970 (blue) and 1991-2017 (black) (data source: DanubeSediment)

In D1, the mean thalweg elevation decreased by 1.35 m, whereas in section D2 the mean thalweg is only 15 cm lower than in the historic state. This reflects the change in sinuosity,

which is also greatly reduced in section D1, while in D2 the course of the Danube was altered only slightly.

The change in the median grain size D_{50} along the Danube is depicted in Figure 99.

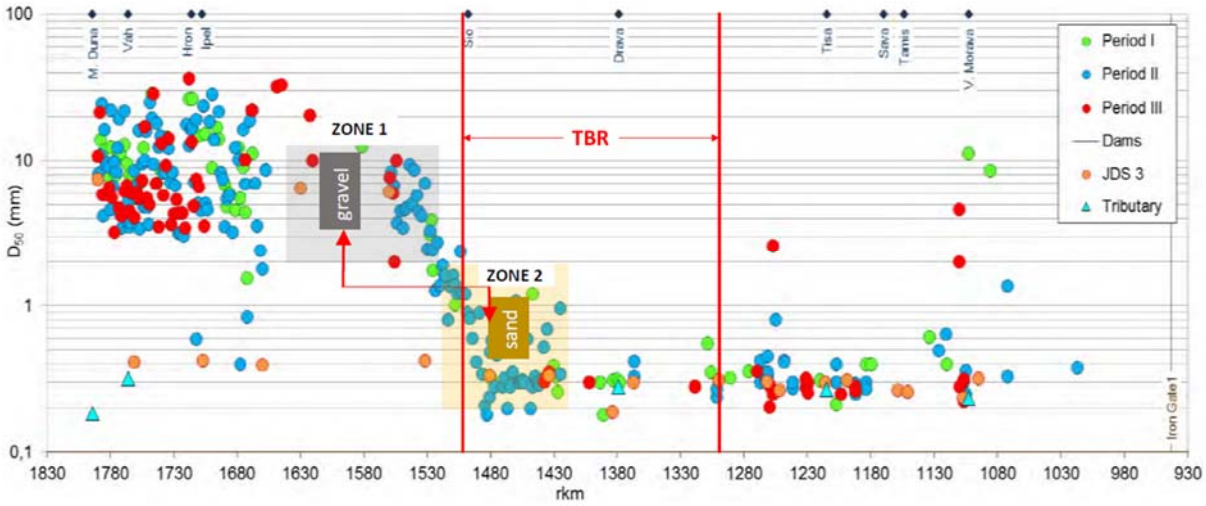

Figure 99. Variation in the D50 grain size over the three periods 1920-1970 (green), 1971-1990 (blue), 1991-2017 (red) with the TBR section marked in red. Within the upper TBR section, the bed material changes from coarse sand to fine sand (Zone 2, source: DanubeSediment).

In the upper section of the Danube within the TBR, between rkm 1520 and 1420, the bed material changes from coarse sand to fine sand.

In the first period, the grain size distribution along the Danube was already influenced by upstream weirs disrupting the continuity. In Period II, while tendencies towards fining can be observed along the gravel bed section and the transitional zones as well as in the lower reach due to the Iron Gate 1, only slight changes can be seen within the TBR reach.

The cascade of HPPs upstream, trapping coarse grain sizes as well as the impoundment from the Iron Gate1, which led to deposition of fine sediment in the lower section, both heavily affect the sediment composition in the entire Middle Danube in the recent period.

3.6 Effects on riverbed levels

The following chapter deals with the impacts of the abovementioned boundary conditions for sediment transport on the bed levels.

First, conclusions on the bed level changes are derived from the water surface elevations of every year's lowest flows. Then, to reduce the effect of hydrology in the analyses (e.g., years with droughts may produce lower water surface elevations than usual), the second analyses uses the stage-discharge relationships to analyse the water surface elevations at a certain discharge (the mean discharge was selected).

3.6.1 Incision based on annual minimum river stage

For the Mura within the TBR MDD, river stage data is available at Mureck, Gornja Radgona, Petanjci, Letenye and Murakeresztur. The gauges provide continuous data for up to 46 years (Letenye).

Table 16. Changes in the annual minimum river stage at gauging stations along the Mura River.

	total change	average change per year	years	Average change 1993-2019	Average change 2010-2019
	cm	cm/year		cm/year	cm/year
Mureck	-17.7	-0.4	45	-0.6	-1.3
Gorna Radgona	-1	0	28	-0.1	1.2
Petanjci	-29.9	-0.9	32	-1.0	-2.8
Letenye	-42.6	-0.9	48	0.1	1.9
Murakeresztur*	-49.4*	-1.1*	47*	-0.8	-0.1*

* only recording above a certain threshold

At gauging station Mureck, which is the station furthest upstream along the Mura River, river stage data is continuously being recorded since 1976 (Figure 100). The total riverbed incision based on the annual minimum river stage is estimated to be nearly -17.7 cm, resulting in an incision rate of -0.4 cm per year. Trends of the mean and maximum water levels are of comparable size. This is probably related to the fact that even the highest discharges remained in-bank, and that erosion causes a parallel shift of the plane bed.

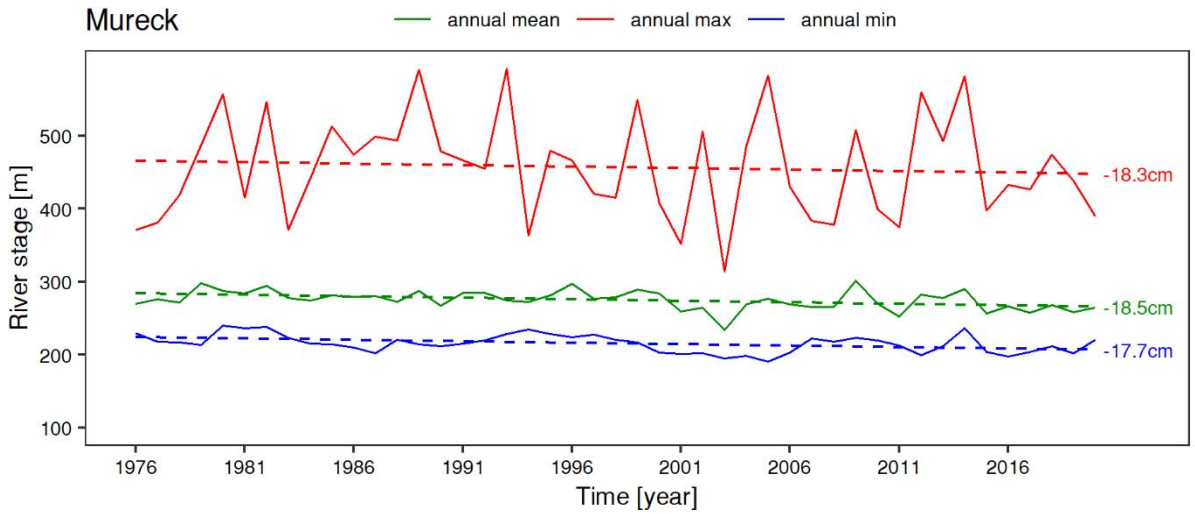

Figure 100. Annual minimum, maximum and mean river stage at Mureck

Noteworthy, this gauging station is upstream of a section showing natural bedrock outcrops acting as sills to the channel and the gauging station at Mureck is not representative for the entire river section. Three kilometres downstream (downstream of the last natural sill), cross section surveys showed higher incision rates (Figure 101). There, the riverbed threatens to break through into Tertiary fines, which may be much more erodible, eventually causing a massive drop of the river bed within one flow event.

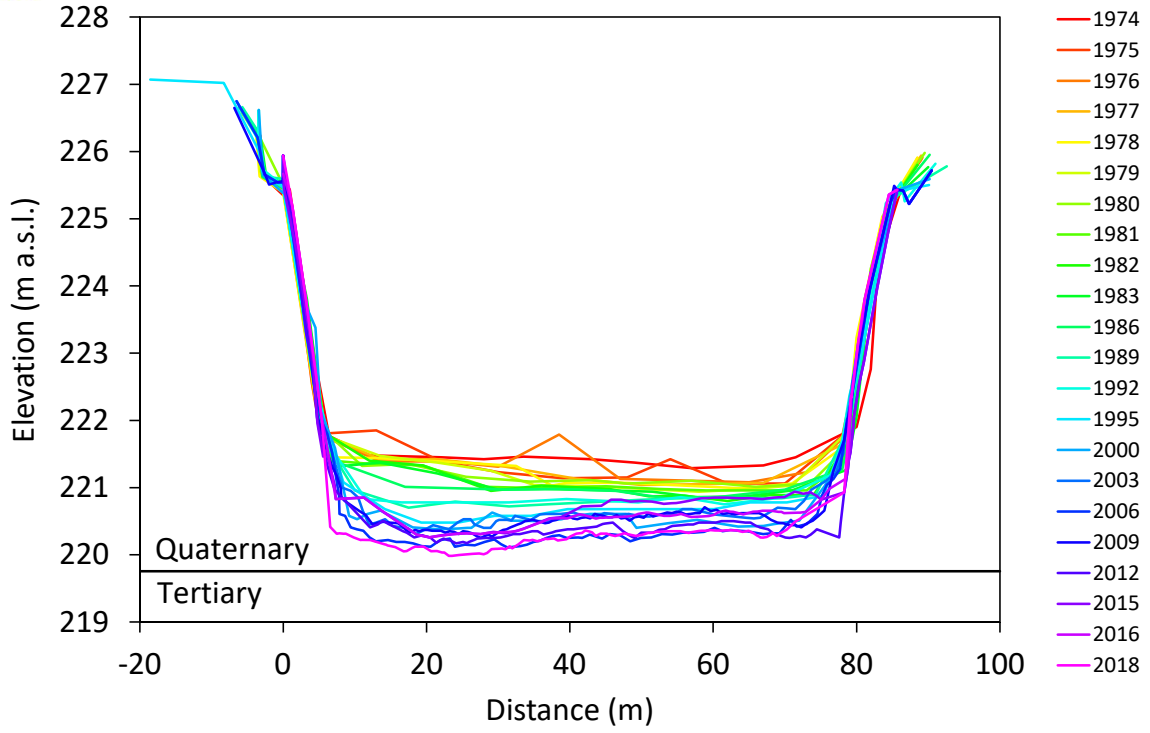

Figure 101. Riverbed incision of the Mura River downstream of Misselsdorf along the border between Austria and Slovenia.

The gauging station closest to the confluence with the Drava is situated at Murakeresztúr. Here, the incision amounts to -49.4 cm in the time period between 1972 and 2018. The respective annual rate is -1.1 cm/per year.

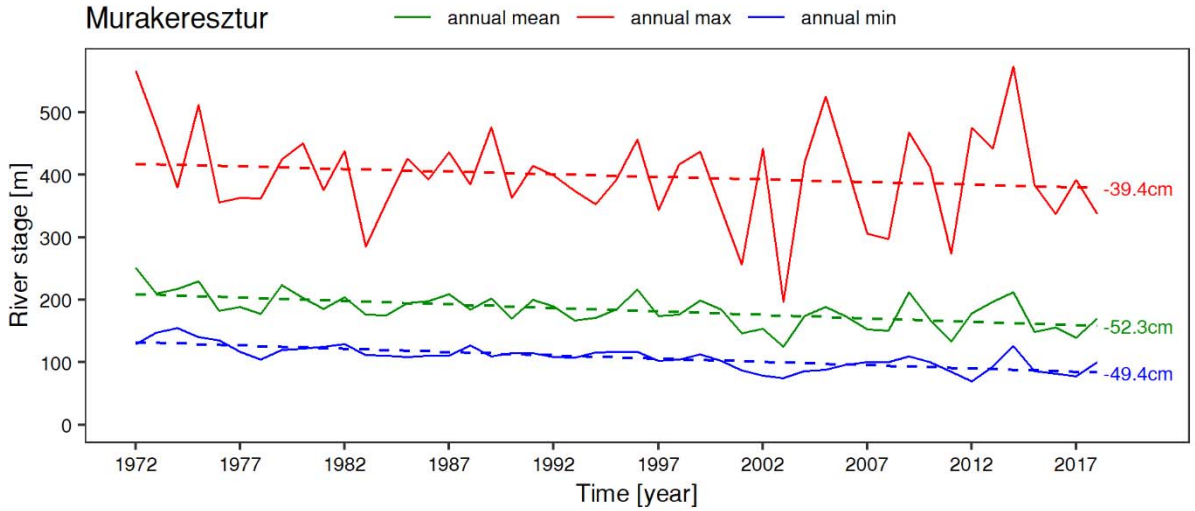

Figure 102. Annual minimum, maximum and mean river stage at Murakeresztúr.

This gauging station however only records data above a certain river stage threshold, therefore analyses of the minimum river stage would be misleading. Considering that also at the other gauging stations of the Mura River the trends of the mean river stage and the minimum river stage are nearly parallel, the minimum river stage analysis at Murakeresztúr also provides a valid result, despite missing the lowest values in the river stage time series.

Along the Drava, 12 river stage gauging stations were analysed, one of which, Šemovec, is situated along the residual flow stretch after the hydropower dam Varaždin. Table 17 shows the changes in the annual minimum river stage at those stations as well as the annual rate and the number of years recorded.

Table 17. Change in annual minimum river stage at gauging stations along the Drava with rates per year and number of years recorded.

	total change	average change per year	years	Average change 1993-2019	Average change 2010-2019
	cm	**cm/year**		**cm/year**	**cm/year**
Šemovec (residual flow)	-62.7	-1.4	44	0.3	-0.9
Varaždin	-11.1	-0.1	120	-0.8	-0.7
Donja Dubrava	-211.2	-5	42	-1.4	-1.2
Botovo	-130.2	-1.4	95	-0.9	-2.7
Novo Virje	-21.6	-0.5	43	0.3	-1.3
Terezino Polje	-268.7	-2.8	96	-2.0	-2.3
Vrbovka	27.6	1.2	23	1.2*	-3.3
Podravska Moslavina	-119.8	-2.3	52	-0.6	-3.3
Donji Miholjac	-119.8	-1	117	-0.1**	-3.1
Belišće	-38.7	-0.7	59	-0.8	-5.4
Osijek	-190	-1.6	120	-1.9	-5.9
Bijelo Brdo	-67	-1.3	50	0.3***	-

*data since 1997

**data until 2016

***data between 2001 and 2013

The first gauging station downstream of the Mura-Drava confluence is located at Botovo (Figure 103), which started recording already in 1926. In 95 years, the minimum annual water levels decreased by 130.2 cm, yielding an annual incision rate of -1.37 cm/year. The annual flood peak levels show a smaller decline, probably due to inundated areas not taking part at the incision.

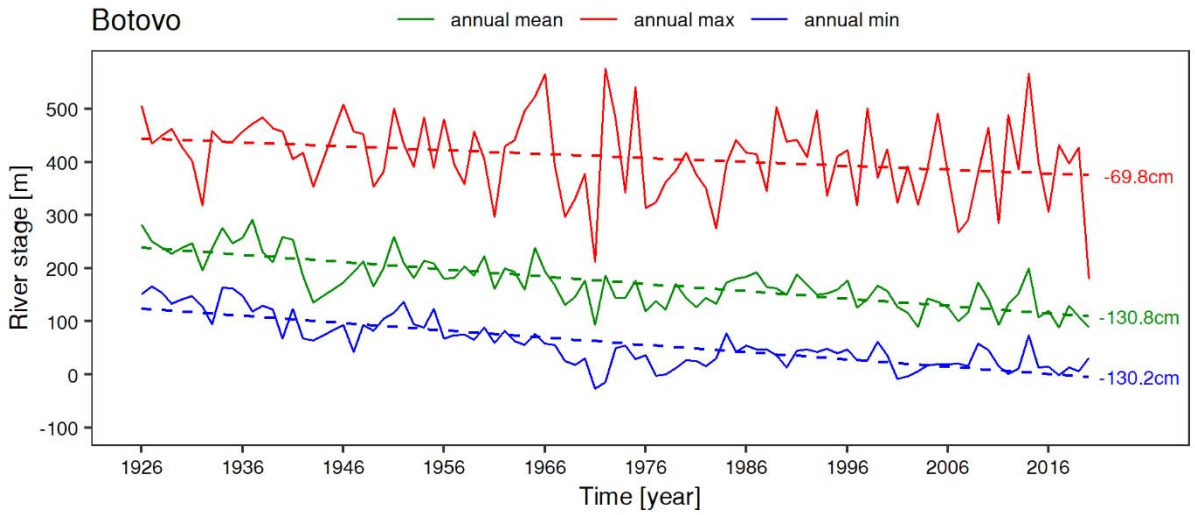

Figure 103. Annual minimum, maximum and mean river stage at Botovo.

Since 1926, the annual minimum river stage decreased by 1.3 m, or 1.4 cm per year on average.

At Terezino Polje, the situation is even more drastic. Here, over the last 96 years, the riverbed incised 2.7 m, which translates to a rate of 2.8 cm per year (Figure 104).

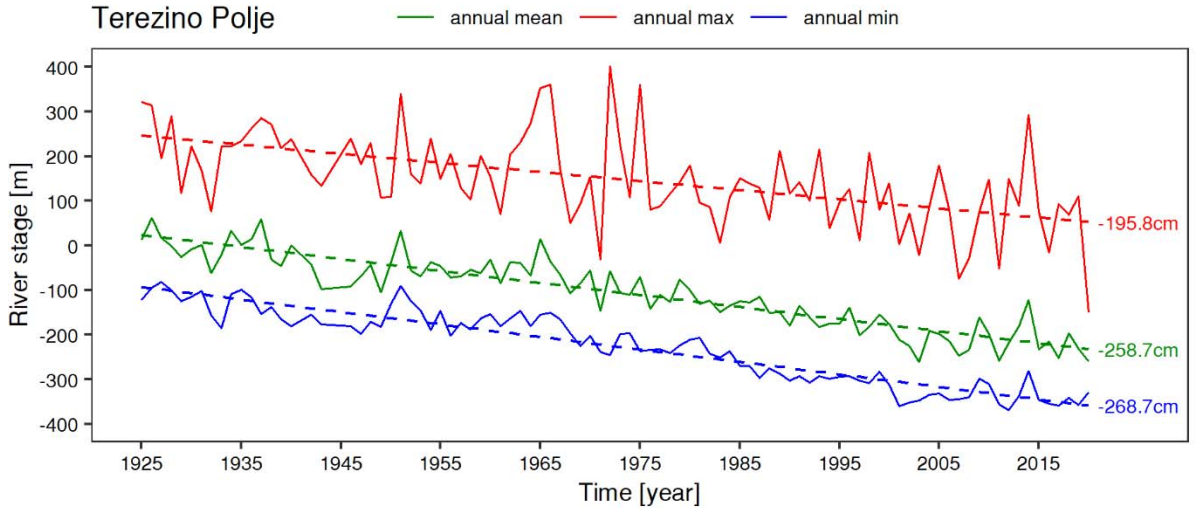

Figure 104. Annual minimum, maximum and mean river stage at Terezino Polje.

The Osijek gauge station is located at rkm 20. Here the records go back to 1900 (Figure 105).

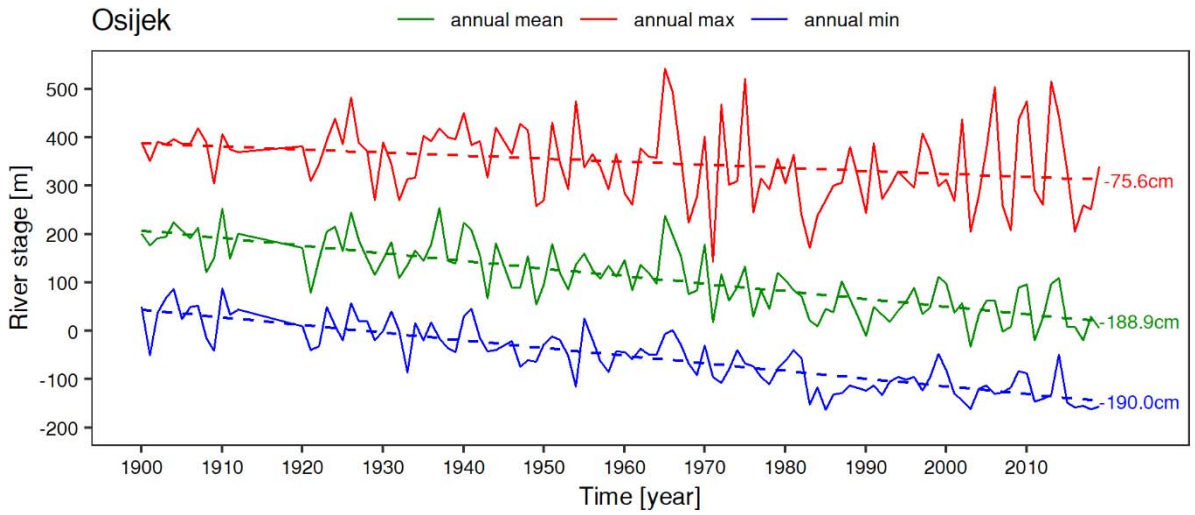

Figure 105. Annual mimimum, maximum and mean river stage at Osijek.

Since 1900, the annual miminum river stage decreased by 1.9 m in total, with a rate of 1.6 cm/year.

Just one km upstream of the Danube-Drava confluence is the gauging station Bijelo Brdo (Figure 106).

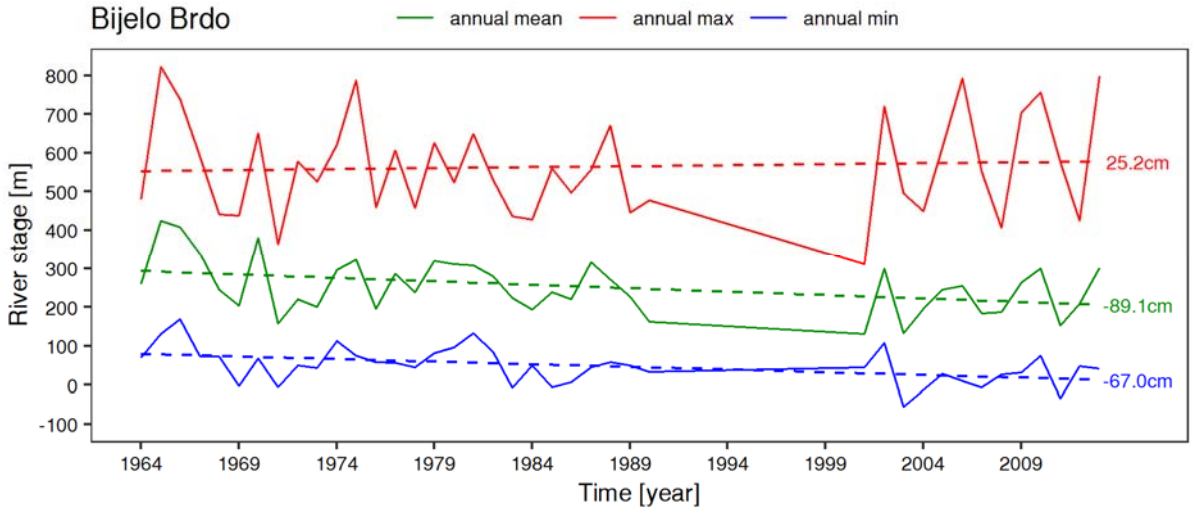

Figure 106. Annual minimum, maximum and mean river stage at Bijelo Brdo; here Data is only available until 2013.

Over the last 50 (1964-2013) years, the riverbed at Bijelo Brdo has deepened by 67 cm, which translates to a rate of approximately 1.3 cm/year.

In the following, the annual minimum, maximum and mean water levels of the available gauging stations along the Danube within the TBR are listed. Data at the stations Dombori, Baja and Mohács data pre 1950 was available. However, changes at the gauge datum were detected. which could not be corrected with the available information. Accordingly, the analysis at those gauging stations start with 1950.

The analyses of the section D1 above the confluence with the Drava River are based on the gauging stations Paks, Dombori, Baja, Mohács and Batina. Although Paks is not in the TBR, it was considered in this analysis, as it may to some extent be representative for the most upstream part of the Danube.

Table 18 shows the change of the annual minimum river stages along the Danube.

Table 18. Change in the annual minimum river stage at gauging stations along the Danube with derived incision rate and number of years recorded.

	total change	average change per year	years	Average change 1993-2019	Average change 2010-2019
	cm	cm/year		cm/year	cm/year
Paks	-154.9	-2.2	71	-3.2	-8.5
Dombori	-118.1	-1.7	71	-2.6	-8.9
Baja	88	-1.2	71	-2.7	-9.2
Mohács	-83.3	-1.2	71	-3.0	-9
Batina	-35.6	-1.8	20	-2.3	-8.7
Aljmaš	-88	-0.9	98	-2.6*	-8.7
Dalj	-29.1	-0.8	36	-3.1*	-9.1
Vukovar	-15.4	-0.1	121	-1.8*	-7
Ilok	5	0	121	-2.9*	-8.8

*entire 27 years not available, at those stations the time series includes only 22 years

At the gauging station Paks, upstream of the TBR MDD, the annual minimum river stage decreased by over 1,5m between 1950 and 2020 (Figure 107).

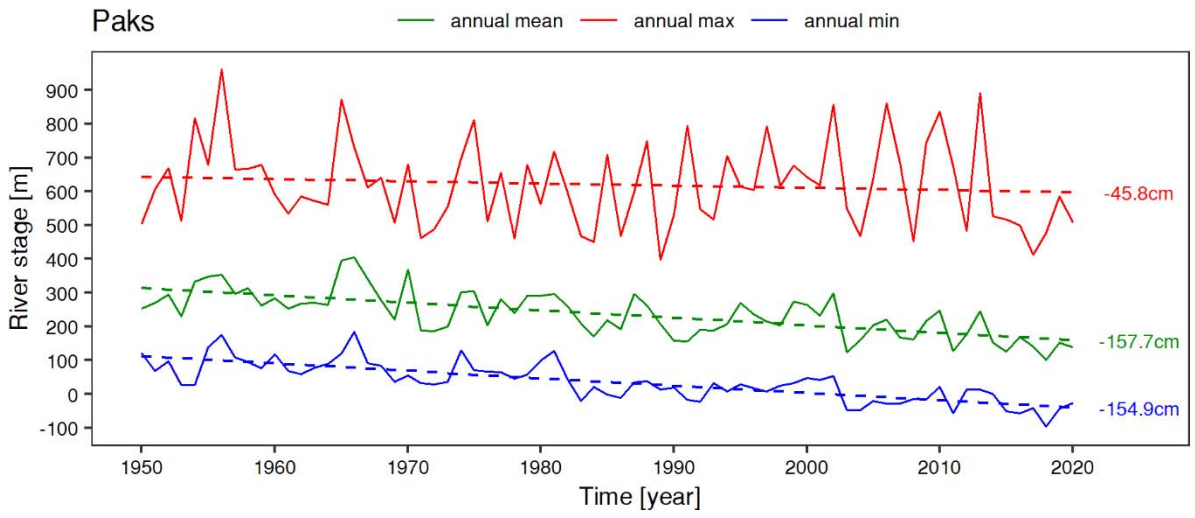

Figure 107 Change of the annual maximum, mean and minimum river stage at gauging station Paks upstream of the TBR MDD

The decrease in the water surface elevation becomes increasingly smaller with distance downstream. At gauging station Ilok, the minimum water level even increases since 1900 by 5 cm (Figure 108).

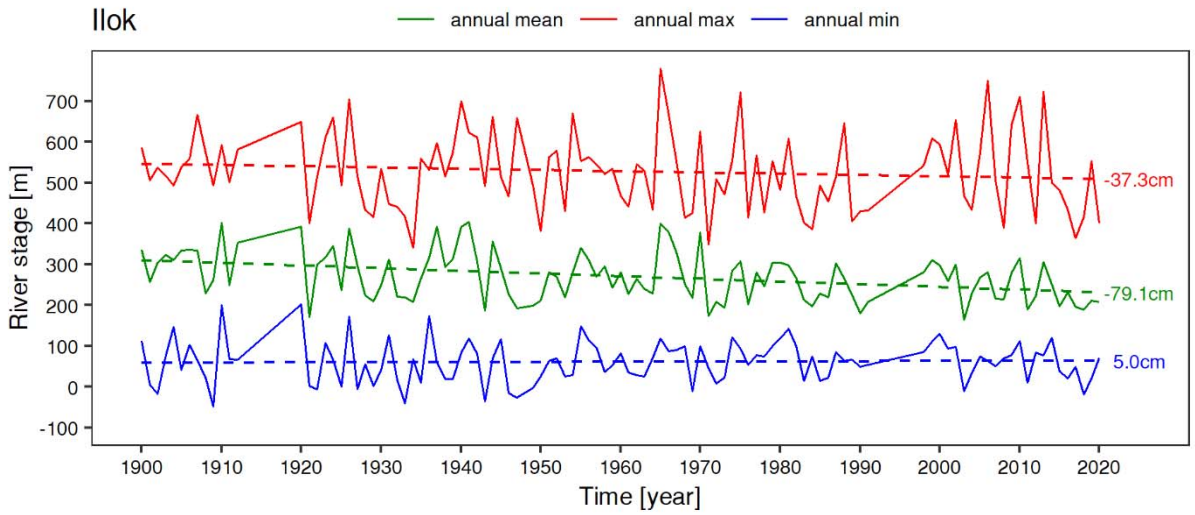

Figure 108 Change of the annual maximum, mean and minimum river stage at gauging station Ilok

Figure 109 shows the total incision since the respective start of recording (number of years in square brackets) based on the annual minimum river stage analysis.

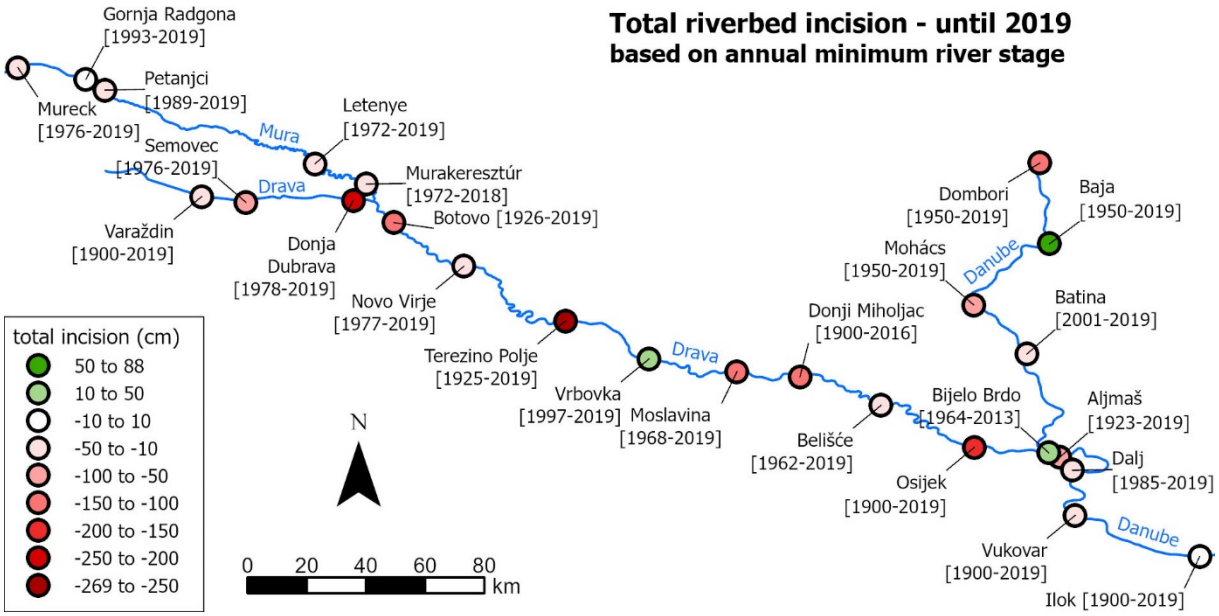

Figure 109. Total incision at gauging station cross sections based on minimum river stage analyses.

This translates to the average annual incision rates depicted in Figure 4.

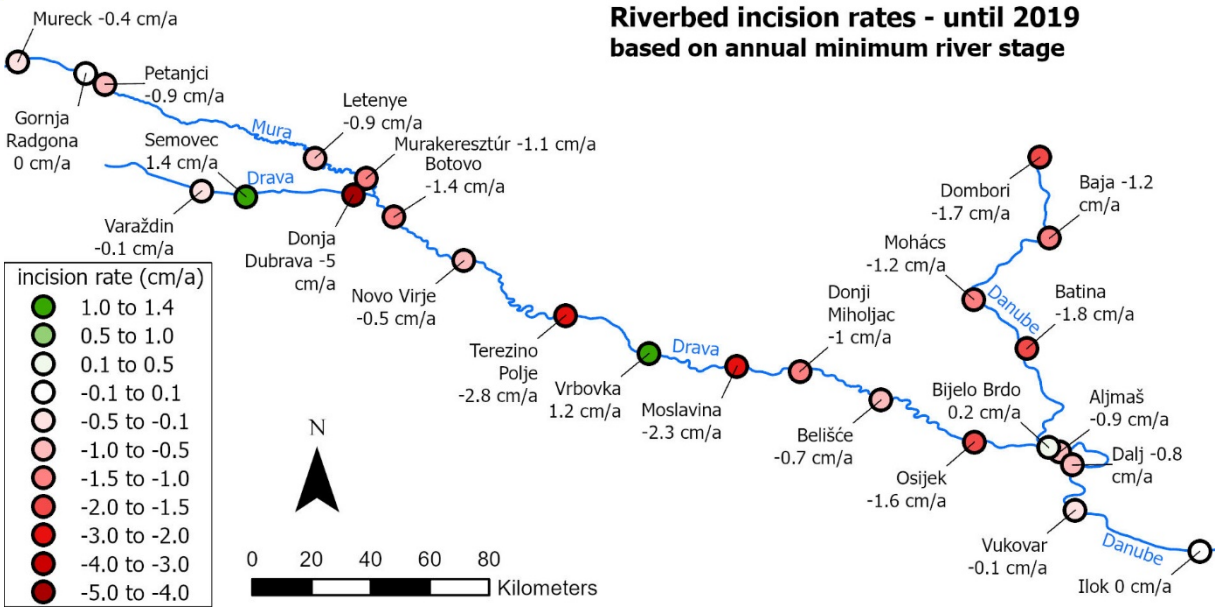

Figure 110. Mean annual riverbed incision rates at gauging stations along the TBR rivers. The incision rates are based on the annual minimum river stage analysis.

Furthermore, the incision rates between 1993 and 2019 are shown in Figure 111, representing the recent developments. At gauging stations Batina and Vrbovka, the longest available time series was taken in each case.

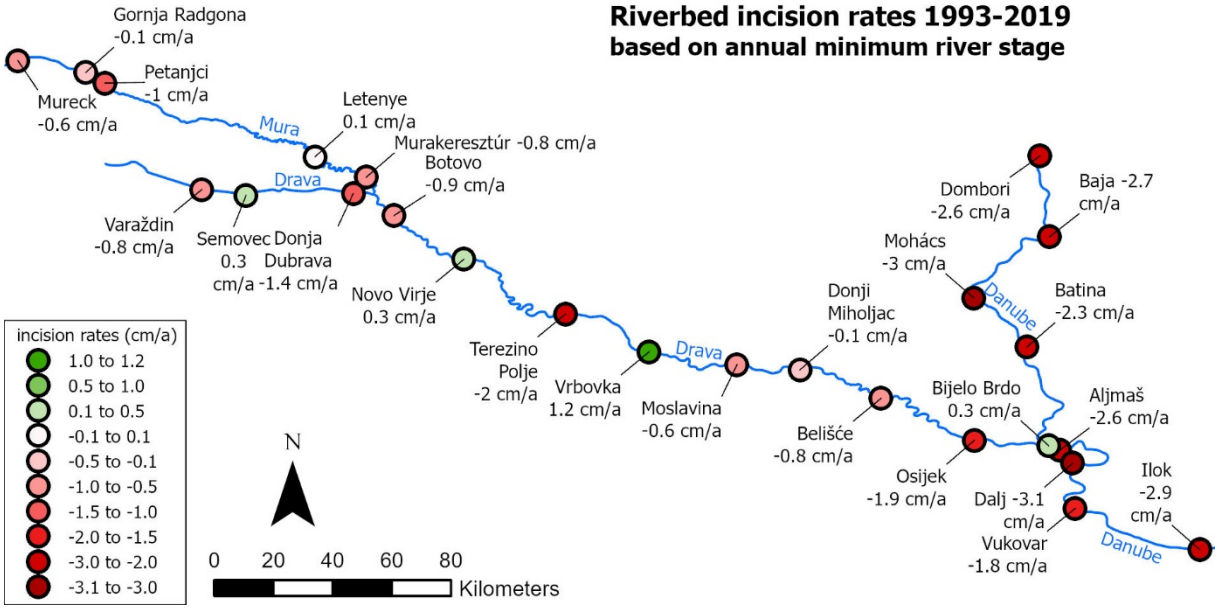

Figure 111. Mean annual riverbed incision rates between 1993 and 2019 based on annual minimum river stages.

3.6.2 Incision based on river stage-discharge relation

In the following, the riverbed incision is estimated based on the water level change at mean discharge.

The annual bed level changes in cross sections at gauging stations along the Mura river are listed below (Table 19). The results are derived from changes in the water level at the mean discharge during the periods between 2010-2019 and 1993-2019.

Table 19. Average annual bed incision rate at the Mura.

	1993-2019		2010-2019	
	cm	cm/year	cm	cm/year
Mureck	-15.6	-0.6	-7.0	-0.7
Gornja Radgona	-10.9	-0.4	-0.5	-0.1
Petanjci	-33.9	-1.3	-24.7	-2.5
Letenye	-8.6	-0.3	13.3	1.3

At Mureck, the rate of incision has remained relative constant over the last 27 years at 0.6 cm/year, resulting in deepening of 15.6 cm in total. Detailed analyses of bed levels of the Mura along the border between Austria and Slovenia verify this trend. At the gauging station at Gornja Radgona, the riverbed seems to be relative stable, while downstream at Petanjci, the incision rate over the 27-year period was 1.3 cm/year (Figure 112). Especially in the years between 2009 and 2017 the riverbed was rapidly incising.

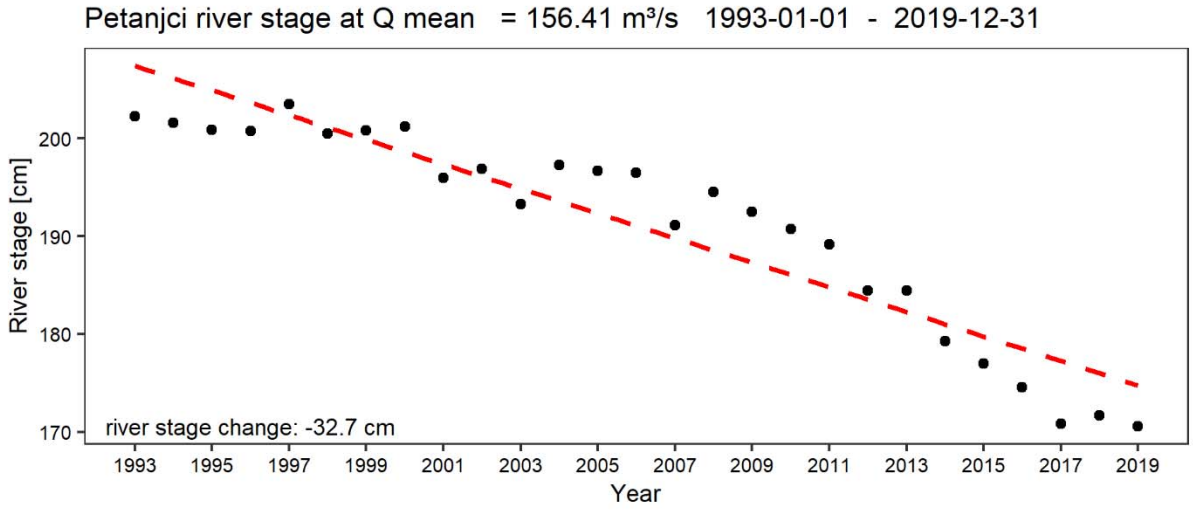

Figure 112. River stages at Qmean at Petanjci.

At Letenye, the analysis indicates ongoing aggradation of the riverbed since 2010, this however might be due to a change in the discharge-river stage rating curve (Figure 113).

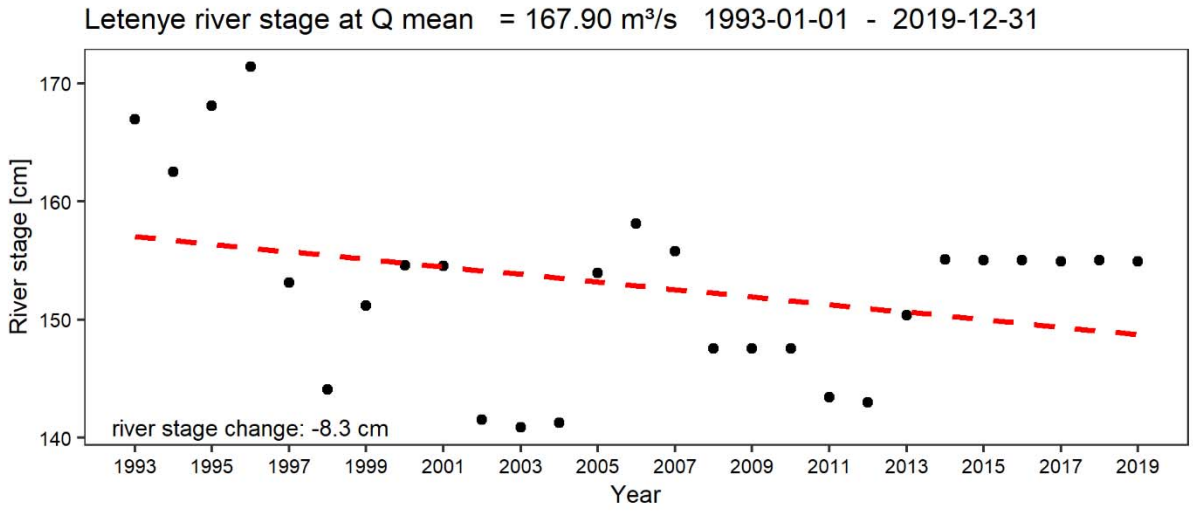

Figure 113. Abrupt changes in the riverstage within one year indicates a change to a diffrent rating curve.

Figure 113 shows the respective river stage at Q_{mean} (calculated in the period 1993-2019) between 1993 and 2019. Here "plateaus" indicate the use of the same discharge-rating curve, as between 2008 and 2010 or between 2014 and 2019. Sudden major shifts indicate the use of a different rating curve, which heavily affect incision analysis, especially when only a short time span is considered, as it is the case when analysing recent developments in the period between 2010 and 2019.

In Table 20, average annual changes in bed elevation are listed for the Drava River.

Table 20. Average annual bed incision rate at the Drava.

		1993-2019		2010-2019	
	alternative no. of years	cm	cm/year	cm	cm/year
Donja Dubrava		-90.5	-3.4	-16.8	-1.7
Botovo		-62.6	-2.3	-20.9	-2.1
Novo Virje		-15.0	-0.6	-3.5	-0.4
Terezino Polje		-68.5	-2.5	-2.7	-0.3
Donji Miholjac	24	-12.1	-0.5	-15.8	-2.3
Belišće		-47.7	-1.8	-30.2	-3.0

At Donja Dubrava, the annual incision rate over the long period was 3.4 cm; this value drops to 1.7 cm when considering only the years 2010-2019. At Botovo, Novo Virje and Terezino Polje, incision also seems to have slowed down in the years since 2010. Further downstream however, incision increased, with rates of 3.2 cm/year at Donji Miholjac and 3 cm/year at Belišće. At Donji Miholjac however, major shifts in the river stage – discharge rating curves again caused the calculated incision in the last 10 years to be larger than the incision over the 27-year period.

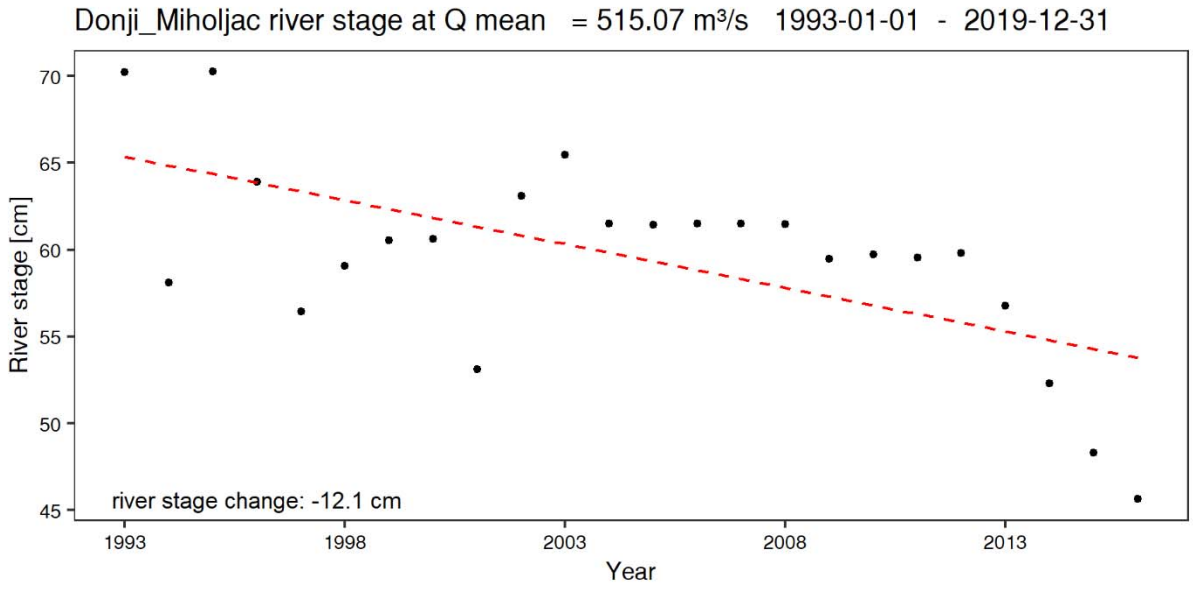

Figure 114. River stage at Q_{mean} at Donji Miholjac.

Industrial dredging also plays a major role in this data: As mentioned above, dredging of riverbed material above Barcs (opposite Terezino Polje) was stopped in 2011, which may explain the decreasing incision rates in the years since 2010. Figure 115 shows the river stage at Terezino Polje at Qmean in the period between 1993 and 2019. Here, with the year 2011 a change is apparent; the river seems to have reached a new equilibrium.

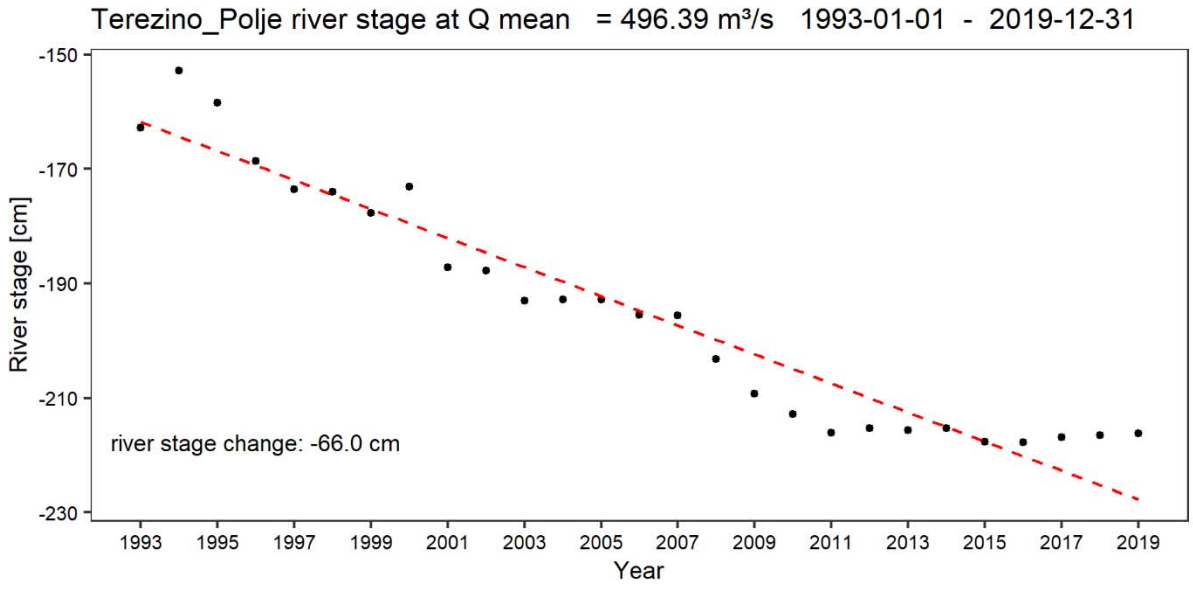

Figure 115. River stage at Q_{mean} at Terezino Polje. Since 2011 the riverbed seems to be relative stable.

The geometry of the gauging station cross section at Terezino Polje is depicted in Figure 116.

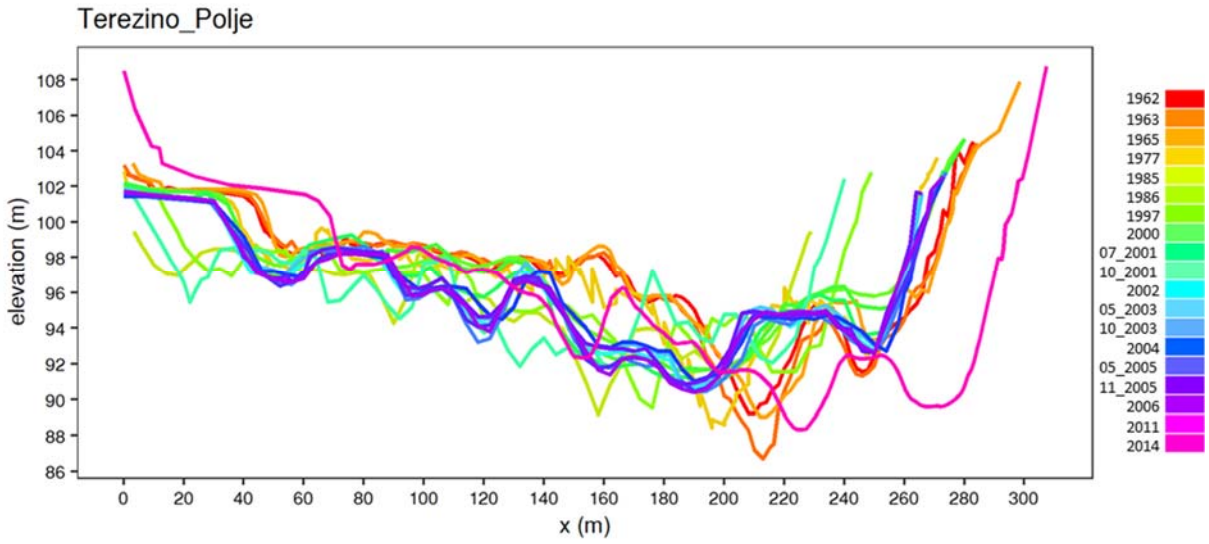

Figure 116. Gauging station cross section at Terezino Polje between 1962 and 2014.

The pattern in the lateral shift suggests that the shift is only due to a survey or data preparation error.

Due to lacking availability of long-term data along the Danube, only the recent 10-year period was considered, with the exception of the gauging station at Mohács, for which the 27-year period was also available. To consider more long-term data, at Dombori (2000-2019) and Baja (1999-2018) available data over a 20-year period was also analysed.

Table 21. Average annual bed incision rate at the Danube.

	1993-2019			2010-2019	
	alt. no. of years	cm	cm/year	cm	cm/year
Dombori	20	-20.6	-1.0	4.9	0.5
Baja	20	-42.6	-2.1	-33.0	-3.7
Mohács		-40.3	-1.5	-15.3	-1.5
Batina				-31.4	-3.1
Aljmas				-20.5	-2.1
Dalj				-27.6	-2.8
Vukovar				-22.5	-2.3
Ilok				-19.6	-2.0

In the long-term period, the riverbed incision ranges from 1 cm/a at Dombori to 2.1 cm/a at Baja. Incision rates in the 10-year period vary from +0.5 cm and therefore a slight aggradation to 3.7 cm/a in the reach upstream of the Drava confluence. Downstream, the rates range from 2 to 2.8 cm/a.

Figure 117 shows the riverbed incision at the gauging stations based on the abovementioned approach in the period between 2010 and 2019.

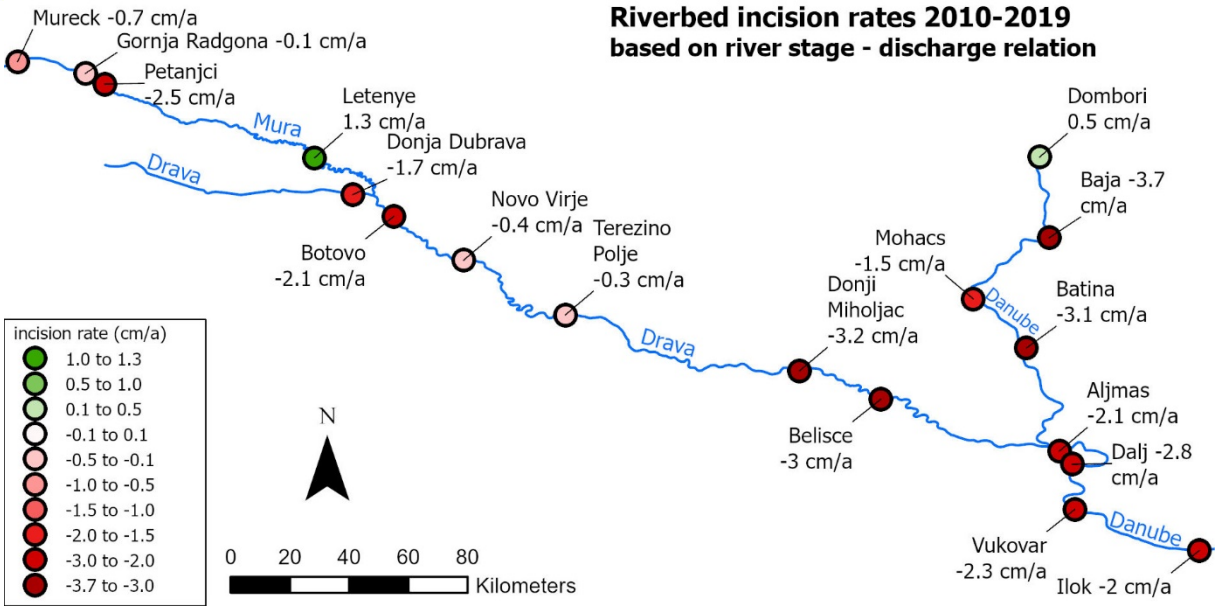

Figure 117. Riverbed incision at gauging stations from 2010-2019.

The incision rate when considering a longer time period (1993-2019) is depicted below:

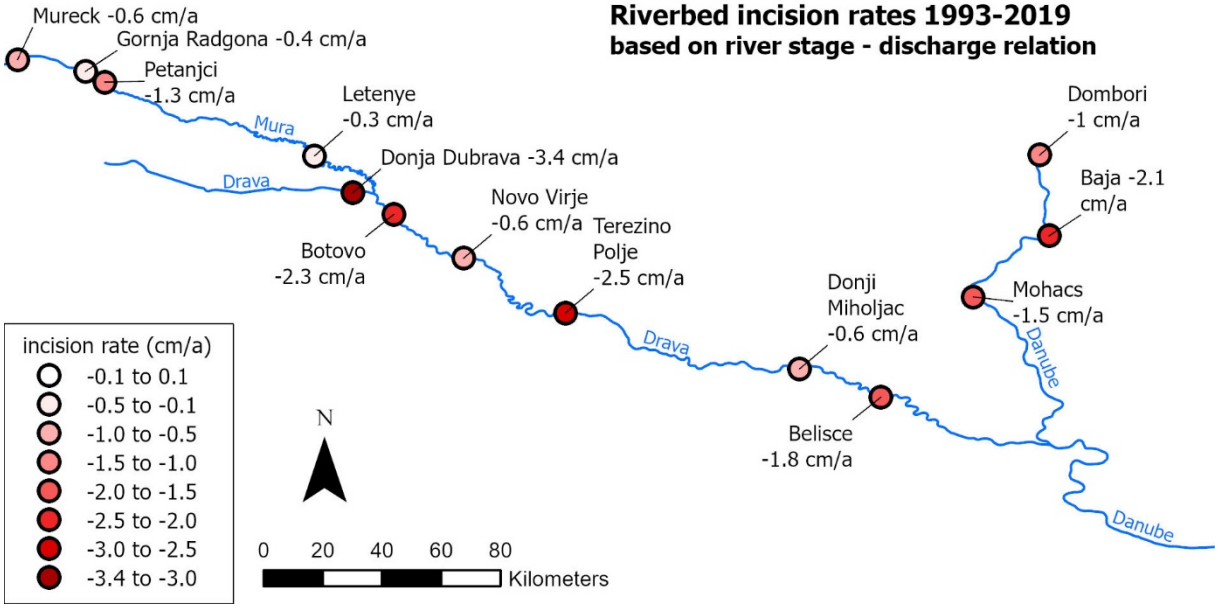

Figure 118. Riverbed incision at gauging stations from 1993-2019.

Differences may be due to different factors: Due to the morphological conditions in the channel, the same average incision might have different effects on the low water levels than on the water levels at mean discharge. The second main factor are changes in the hydrological conditions: While stage – discharge relation curves are adjusted accordingly, the analyses of just the low water levels do not account for changes in the hydrology, respectively extreme wet or dry years.

Regarding the discharge, it is to be considered, that, at all available gauging stations along the Drava, an increase in both, minimum and mean discharge, are apparent in the data, whereas the three Danube gauging stations Dombori, Baja and Mohacs show a distinct decrease of the annual minimum discharge (Figure 119).

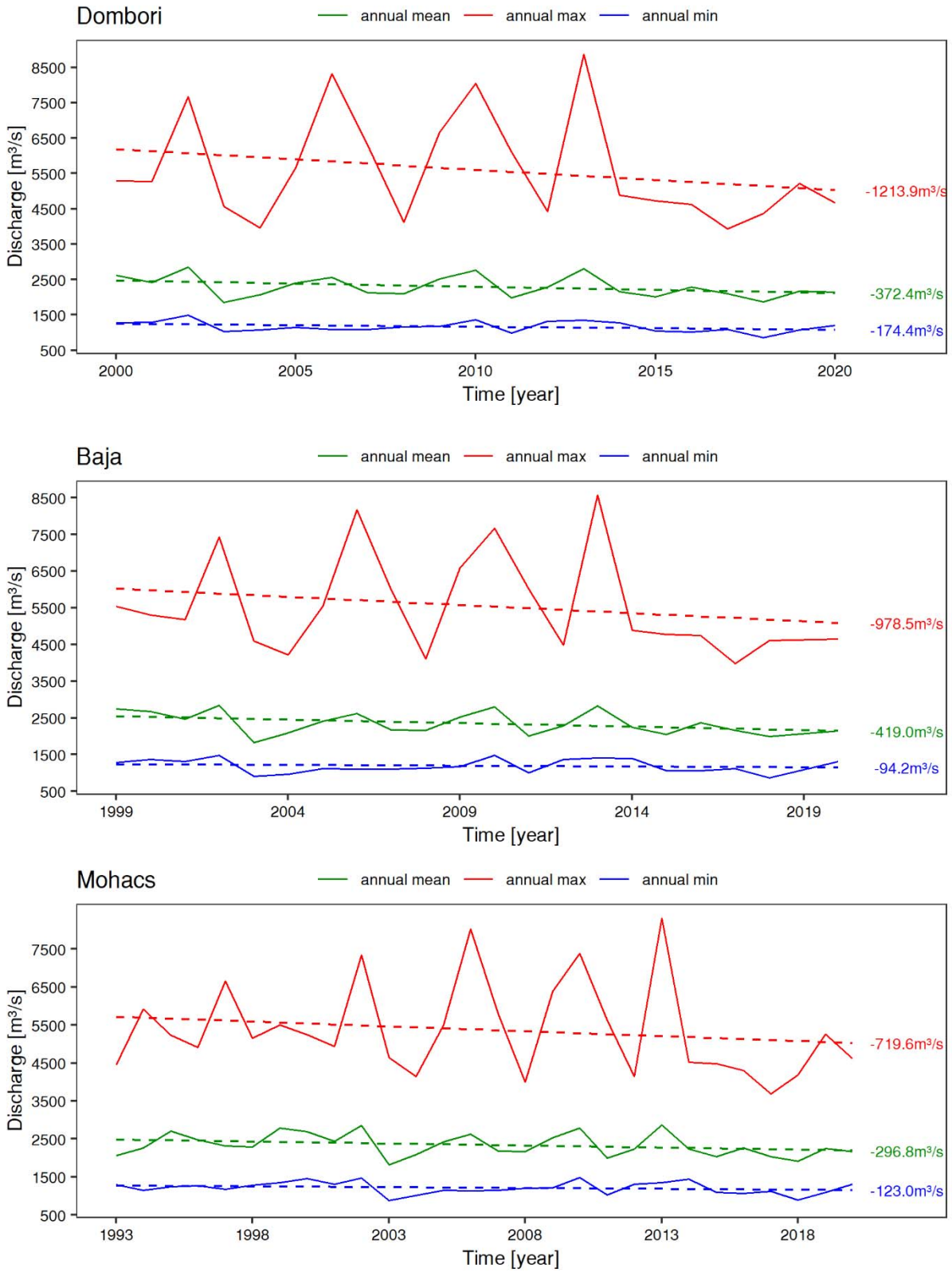

Figure 119. Annual miminum (blue), maximum (red) and mean (green) discharges at the Hungarian gauging stations along the Danube.

At the Mura, the minimum and mean discharges stayed relatively constant (Figure 120 and Figure 121).

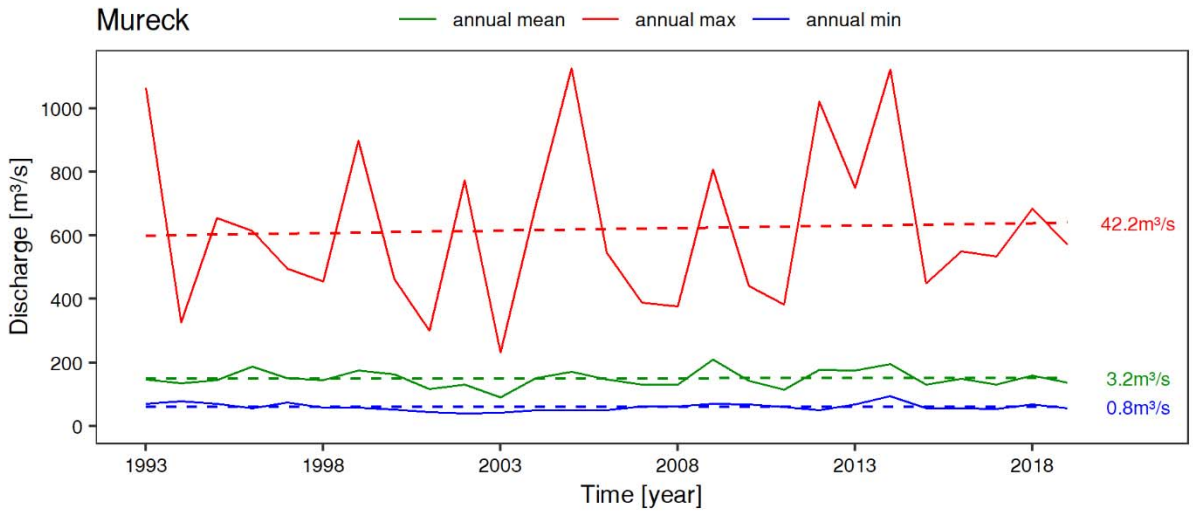

Figure 120. Annual minimum, maximum and mean discharge at Mureck.

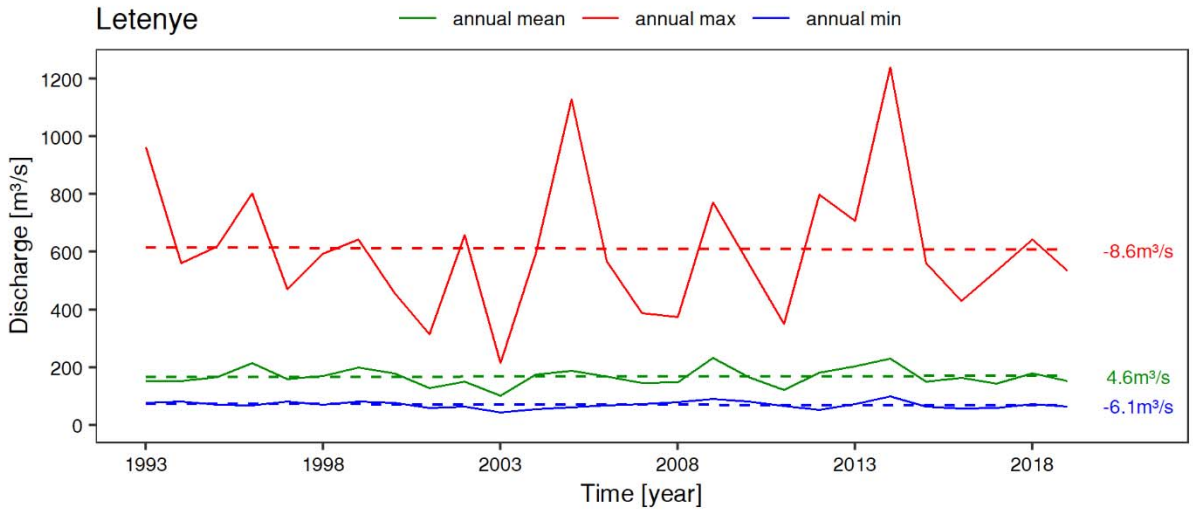

Figure 121. Annual minimum, maximum and mean discharge at Letenye.

These two factors together with the effect of shifts between periods of the same stage – discharge rating curves, mentioned in the above chapter, may be responsible for the occurring differences between the two analysis methods.

3.7 Relevance of lateral dynamics in habitat provision

In a section near Sicheldorf, located at the downstream end of the border section of the Mura between Austria and Slovenia, the bank protections were removed along the Austrian bank over a length of approx. 1.4 km in summer 2012 (Figure 21a). This section benefited from sediment input from upstream bed erosion and from input from upstream measure relocations, in that a gravel bank was deposited there on the inner bank of the section. More severe erosion took place on the outer bank of the river bend (Figure 21b).

a)

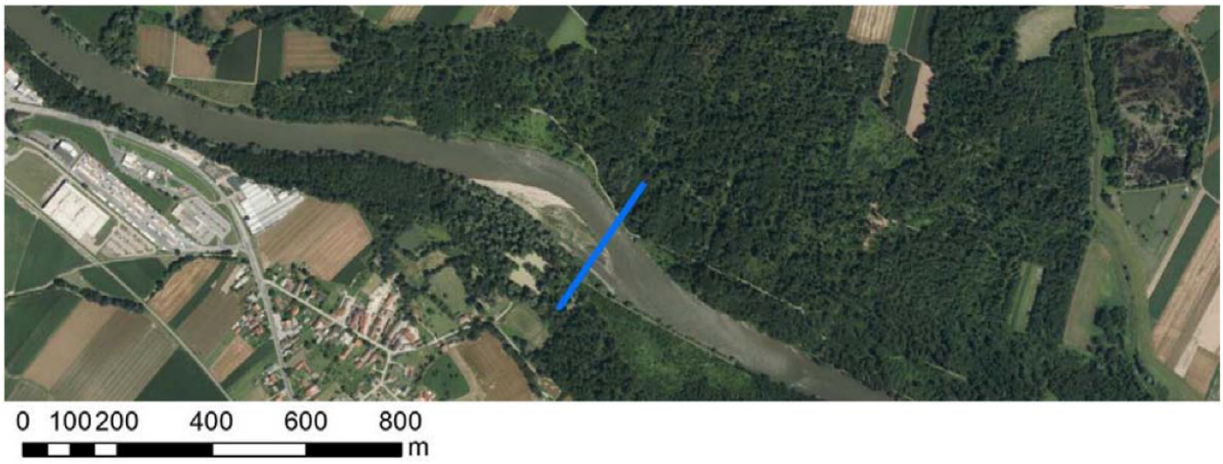

b)

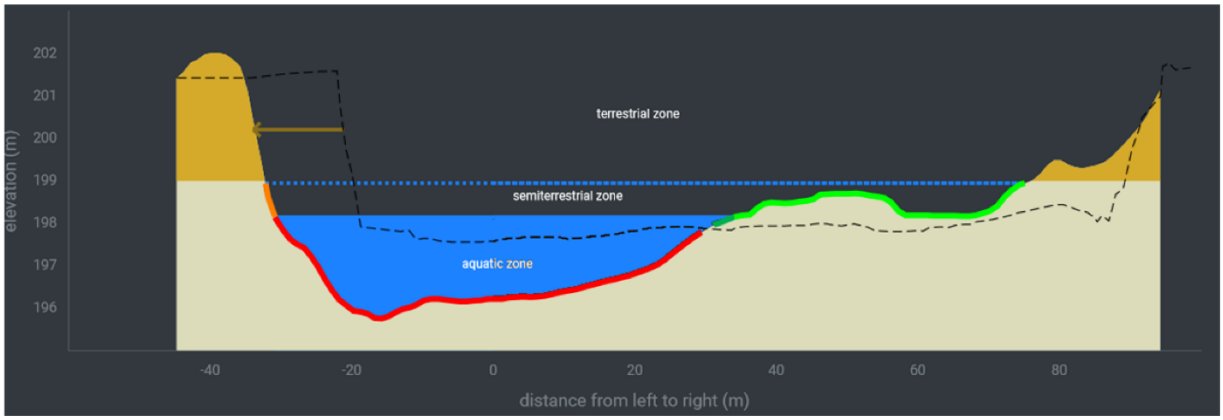

Figure 122. a) Restored site at Sicheldorf with the analysed cross section and b) cross-sectional change in the period between 2012 and 2018, analysed with the HyMoLink tool (Klösch et al., 2019b) for potential habitat provision.

Lateral shift of riverbanks increases width, which reduces sediment transport capacity and causes aggradation. Sediment erosion and deposition causes bare (unvegetated) sediment surfaces, which are important habitats for the rejuvenation of riverine species. Bank-nesting birds require steep banks for creating their burrows for breeding, loosely deposits favour gravel spawners, bare bars provide habitat to pioneer vegetation and bar-breeding birds. While here the curvature fostered erosion of the outer bank of the bend, bank erosion is also depending on the bedload supply and the deposition of bars deviating the flow towards the banks.

4 Conclusions

In the area of the Five-Country Biosphere Reserve, the Mura, Drava and Danube rivers shaped riverscapes in wide floodplains in the past, which corresponded to the natural morphologies that developed through the interaction of flow, sediment and vegetation. The river morphology ranged from a predominantly braided, anabranching river system upstream to a meandering, single-thread main channel with smaller side-channels and typical floodplain waters further downstream. Despite anthropogenic impacts on the river system, some of the river sections still retained part of their characteristic morphology and the associated dynamics.

However, anthropogenic impacts such as channelization and sediment retention in the upstream catchment have been affecting these rivers mainly since the 19th century, with consequences becoming increasingly evident and threatening the functionality of the biosphere reserve. The aim of the present study was to investigate the conditions of and for sediment transport along the river network of the TBR MDD in order to identify deficits, which – together with the results of parallel biotic and abiotic studies – form the basis for locating priority reaches for restoration and the recommendation of appropriate restoration measures. The analyses in this study were carried out using existing data collected in the partnership, from associated strategic partners and from externals, and using maps of historical and current condition prepared in the parallel river training structures study (Schwarz, 2022).

The comparison of the current condition with the more natural, historical condition showed the morphological consequences of the channelization, which systematically started in the 19th century, in combination with sediment retention in the upstream catchments. The formerly braided and anabranching upstream river sections of the TBR MDD, where the Drava and the Mura split into more than three channels on average, transformed into a mostly single-thread channel system. Furthermore, the discharging (wetted) width decreased, e.g. to 39 % in the uppermost section of the Mura. Downstream, the channelization showed itself more in the form of straightening. The straightening of the Drava and the Danube led to a reduction in length of 35 % and 23 %, respectively, which increased the channel gradient. The capacity for transporting sediment increased as a result of increased water depth in the narrowed channel, increased gradient, and concentration of flood flows between levees. Moreover, the protection of the riverbanks impeded lateral dynamics and the increased uniformity of channel width reduced bed morphodynamics.

While the bed levels and the lateral dynamics of a river are known to depend on the sediment supply, transversal structures upstream of the TBR MDD have been trapping sediment in their reservoirs for more than one century (The first hydropower plant in the Mura was constructed in 1899-1903 near Lebring in Austria, the first in the Drava in 1913-1918 near Fala in Slovenia, first in the Danube in 1924-1927 near Passau in Germany). Expanded to series of hydropower plants, nearly no bedload enters the TBR MDD.

As a result, the rivers in the TBR MDD transported more bedload due to the increased sediment transport capacity, while the supply from upstream strongly decreased, leading to a strong imbalance in the sediment budget. The rivers in the TBR MDD incised into their alluvium, while siltation increased the elevation a floodplain which became mostly inerodible behind the protected banks, both further increasing the water depths between the banks. Analyses of low water levels measured at gauging stations exhibited strong incision, at Terezino Polje amounting to ca. 2.7 m since 1925. Measurements of discharges, which were started later, allowed the investigations of water surface elevations at certain discharges, showing incising trends also since the 1990s for the riverbed carrying the mean discharge (2.5 cm incision per year at Terezino Polje). On the Mur between Austria and Slovenia, which is highly exposed to sediment deficit due to its proximity to a series of hydropower plants, it was found that the thickness of the gravel layer of the riverbed is very low (Austrian-Slovenian Standing Committee for the Mur River, 2001) and that the riverbed is rapidly approaching the underlying tertiary fine material, threatening a breakthrough of the riverbed. The lower reaches of the TBR MDD are still supplied with bedload originating from eroding river beds upstream, but this supply is not sustainable and will not last long. After the construction of the hydropower plants on the Drava in the area of today's TBR MDD, the suspended sediment transport on the Drava at Botovo decreased by 72 %, while the reservoirs show massive sedimentation, thus strongly affecting the sediment balance.

These developments urge for restoration measures to preserve and improve the abiotic conditions in the TBR MDD. Sediment connectivity needs to be improved and sediment needs to be supplied in appropriate quantity and composition from upstream to compensate for sediment deficits. Restored river sections with greater curvature and/or width (see measure types A, B and C in Klösch et al., 2019) would require less sediment supply to maintain and restore the bed elevations than the current condition, while also resulting in better morphodynamics. Bank protections should be removed and levees set back to allow lateral dynamics through bank erosion and bar/bank accretion, thus making use of the space available for morphodynamics. Measures should aim to stop channel incision and to establish a dynamic equilibrium (based on a mobile river bed) that is neither maintained by self-armouring (a coarsening of the bed, which may develop at an apparent equilibrium due to sediment deficit), nor by natural rocks or artificially constructed transverse structures.

Currently, about 29,000 m^3 of gravel is eroded annually from the riverbed of the Mur between Austria and Slovenia along a 30 km stretch. The amount of gravel to hold the channelized Mura there in a dynamic equilibrium was modelled to be about 45,000 m^3 per year (Klösch et al., 2021). In a widened and more sinuous channel, the required bedload supply for the border section between Austria and Slovenia would be reduced to 20,000 m^3 per year. In the larger Drava at Botovo, bedload transport was measured to be about 50,000 m^3 per year (Rákóczi and Szekeres, 2004); the bedload transport capacity and hence the demand may be even higher considering armouring effects of incising beds. Again, the amount of required bedload supply would be reduced in a widened and more curved channel.

When implementing restoration measures, sediment gained during construction should be supplied to the river for self-dynamically shaping the more natural morphology and for a sediment transport ensuring continued morphodynamics. A stabilizing effect also on upstream sections may be expected, while downstream the sediment supply may be temporarily reduced and require specific attention. With increasing size of the measure, transport capacity decreases while sediment volumes gained from construction increases, both increasing the bedload efficiency of the supply. Depending on the original morphology, which has adapted to the natural boundary conditions, restoration should focus either on increasing the wetted width (widening/self-dynamic erosion and/or reconnection/creation of side channels) or on increasing the sinuosity (enabling bank erosion, reconnection of meanders), but both parameters should be taken into account and artificial constraints removed to allow lateral dynamics.

5 Annex

The annex shows the hydrologic analyses for all gauging stations. The annual minimum water level was used for concluding on bed elevation changes in chapter 3.6.1. Chapter 3.6.2 reports results of the method using the stage-discharge relationships.

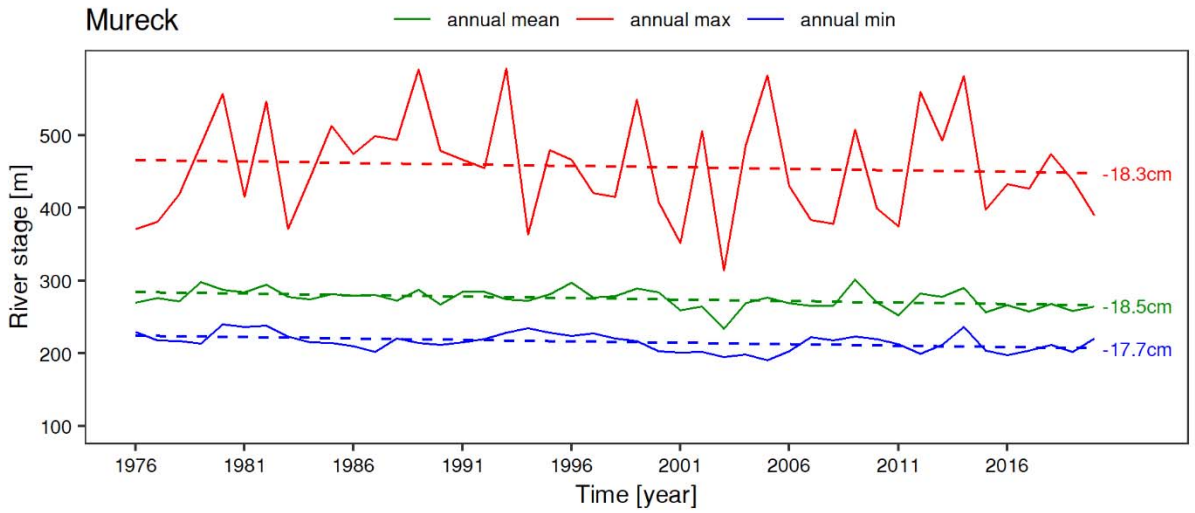

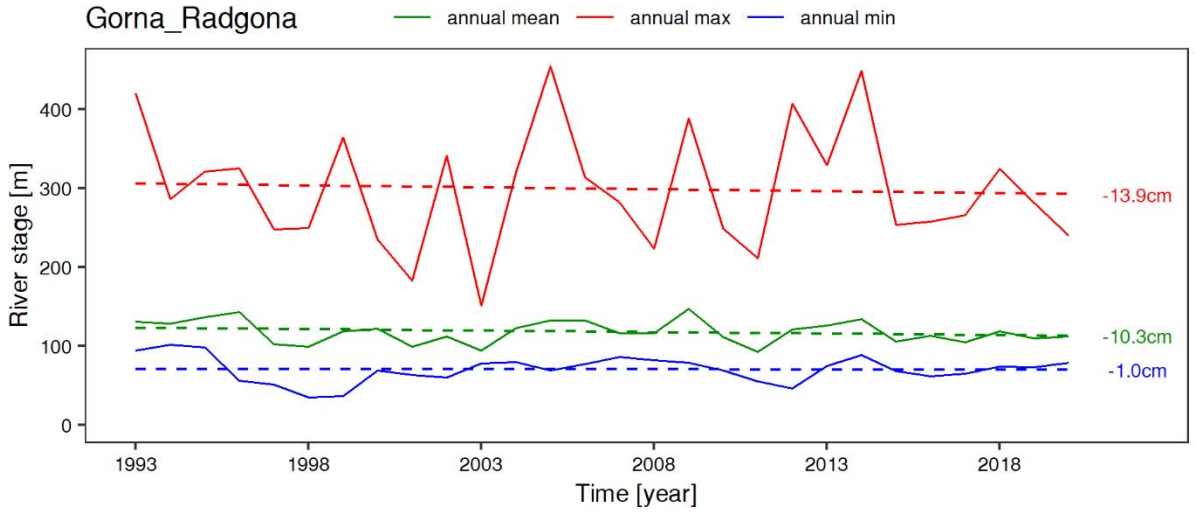

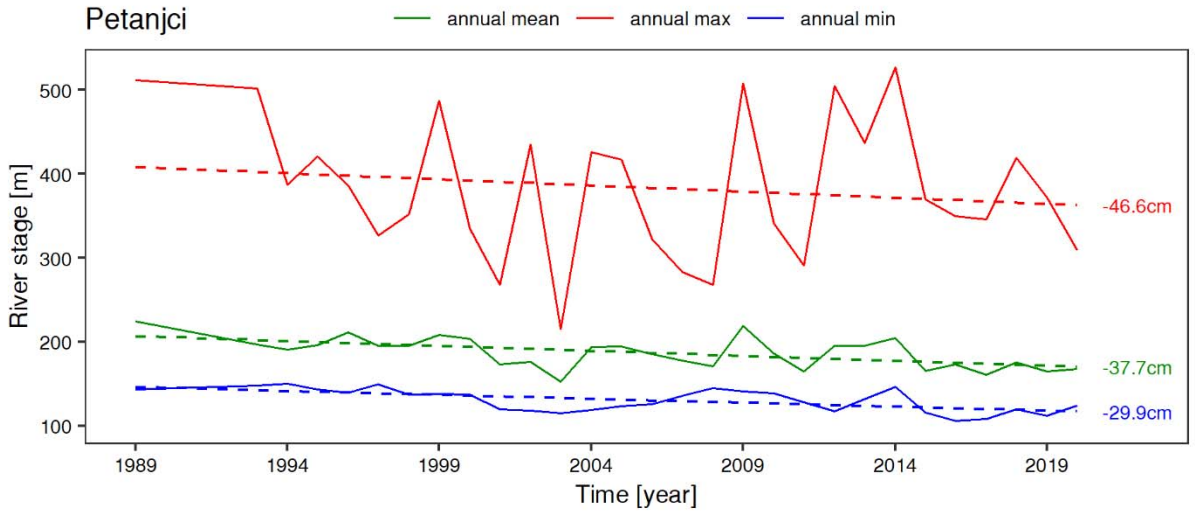

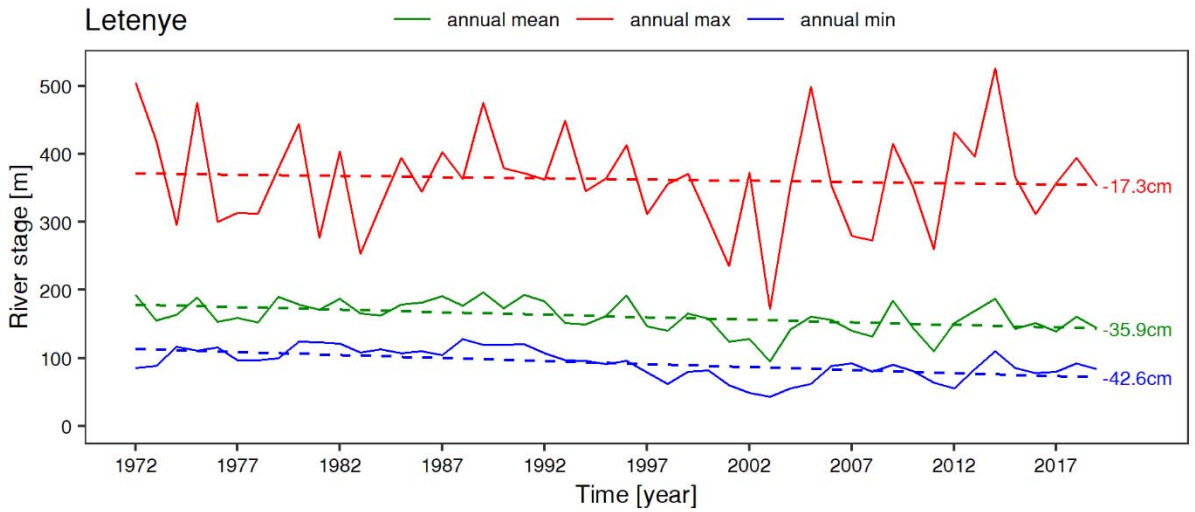
Letenye
annual mean
annual max
annual min
River stage [m]
500
400
300
200
100
0
1972
1977
1982
1987
1992
1997
2002
2007
2012
2017
Time [year]
-17.3cm
-35.9cm
-42.6cm

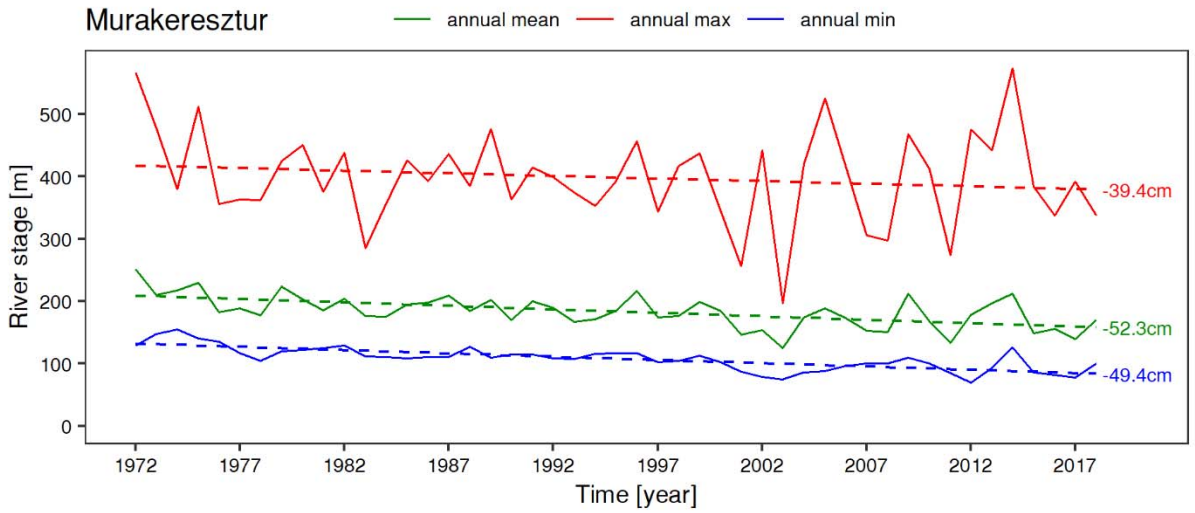
Murakeresztur
annual mean
annual max
annual min
River stage [m]
500
400
300
200
100
0
1972
1977
1982
1987
1992
1997
2002
2007
2012
2017
Time [year]
-39.4cm
-52.3cm
-49.4cm

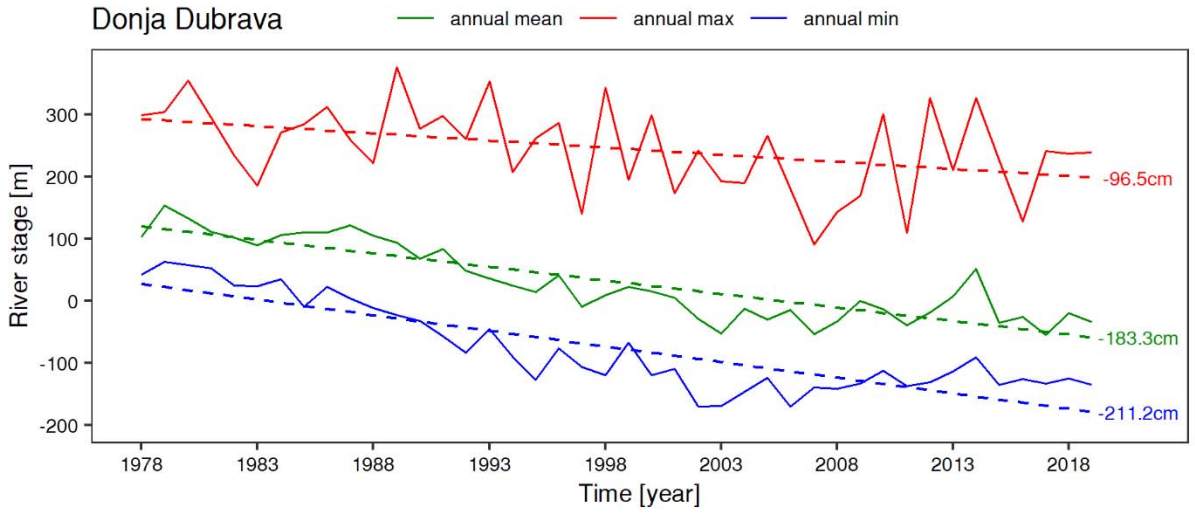
Donja Dubrava
annual mean
annual max
annual min
River stage [m]
300
200
100
0
-100
-200
1978
1983
1988
1993
1998
2003
2008
2013
2018
Time [year]
-96.5cm
-183.3cm
-211.2cm

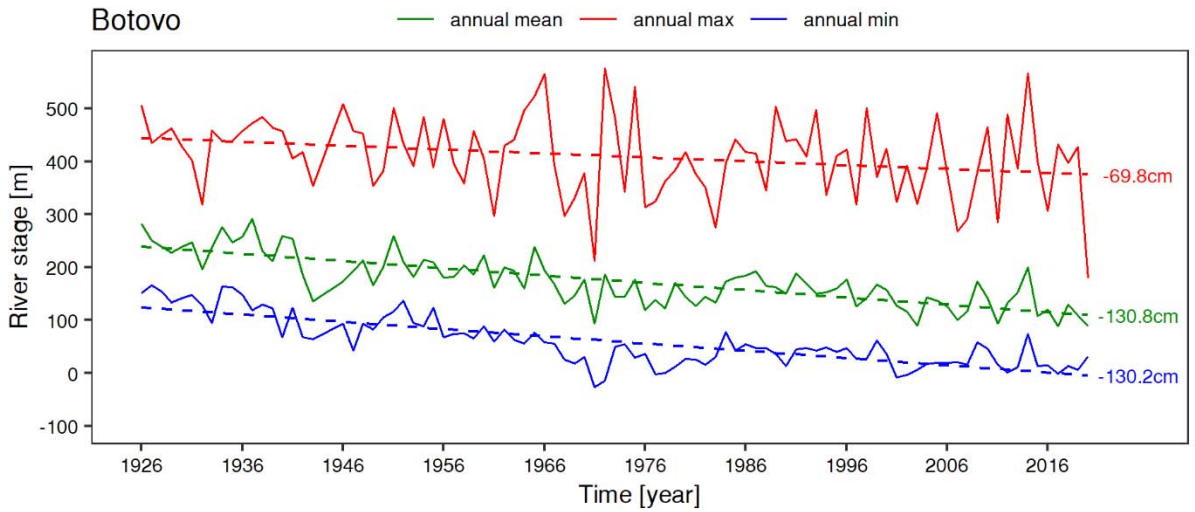
Botovo
annual mean
annual max
annual min
River stage [m]
500
400
300
200
100
0
-100
1926
1936
1946
1956
1966
1976
1986
1996
2006
2016
Time [year]
-69.8cm
-130.8cm
-130.2cm

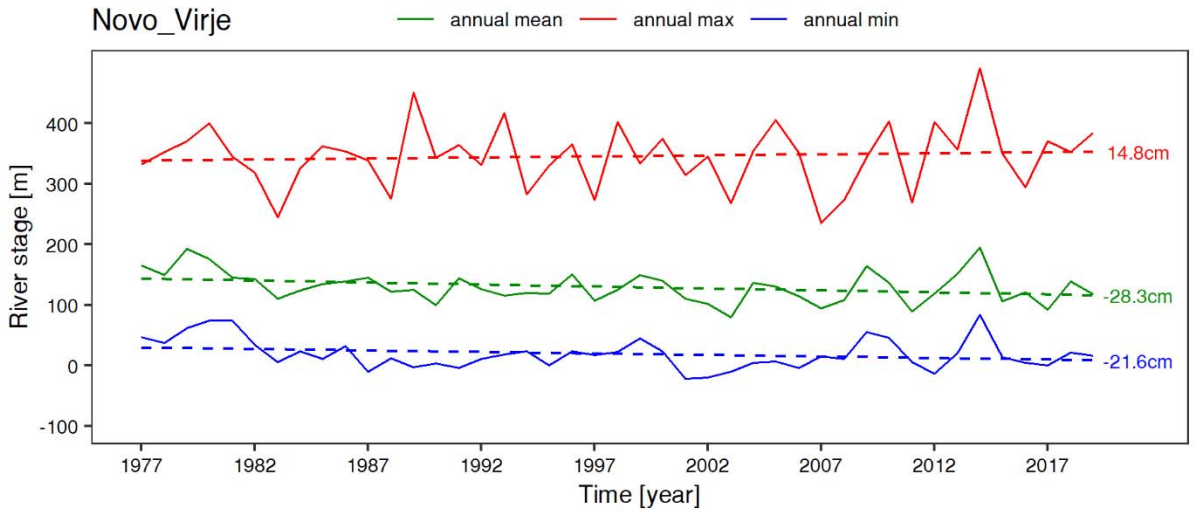
Novo_Virje
annual mean
annual max
annual min
River stage [m]
400
300
200
100
0
-100
1977
1982
1987
1992
1997
2002
2007
2012
2017
Time [year]
14.8cm
-28.3cm
-21.6cm

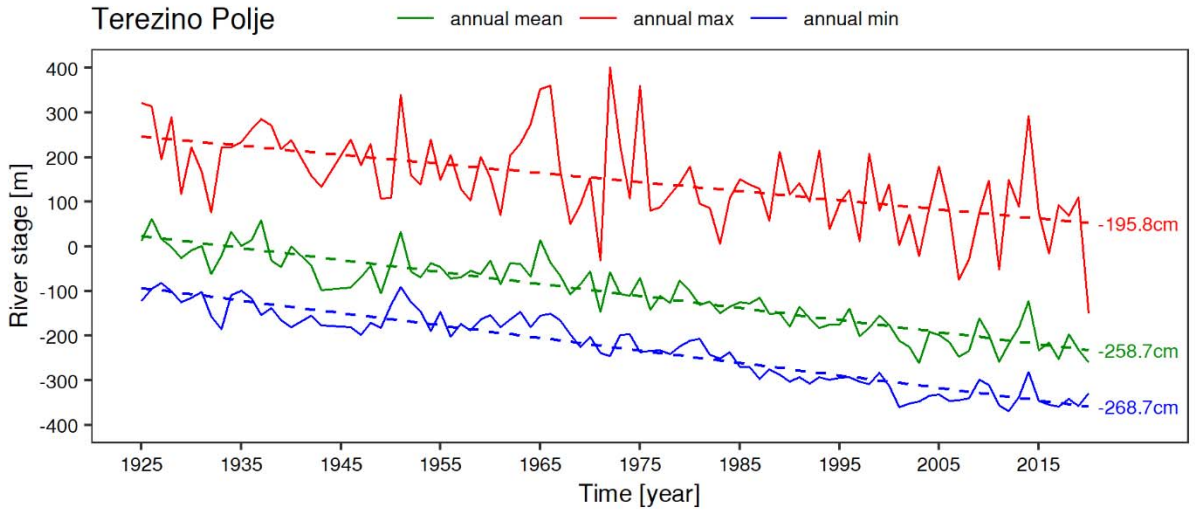
Terezino Polje
annual mean
annual max
annual min
River stage [m]
400
300
200
100
0
-100
-200
-300
-400
1925
1935
1945
1955
1965
1975
1985
1995
2005
2015
Time [year]
-195.8cm
-258.7cm
-268.7cm

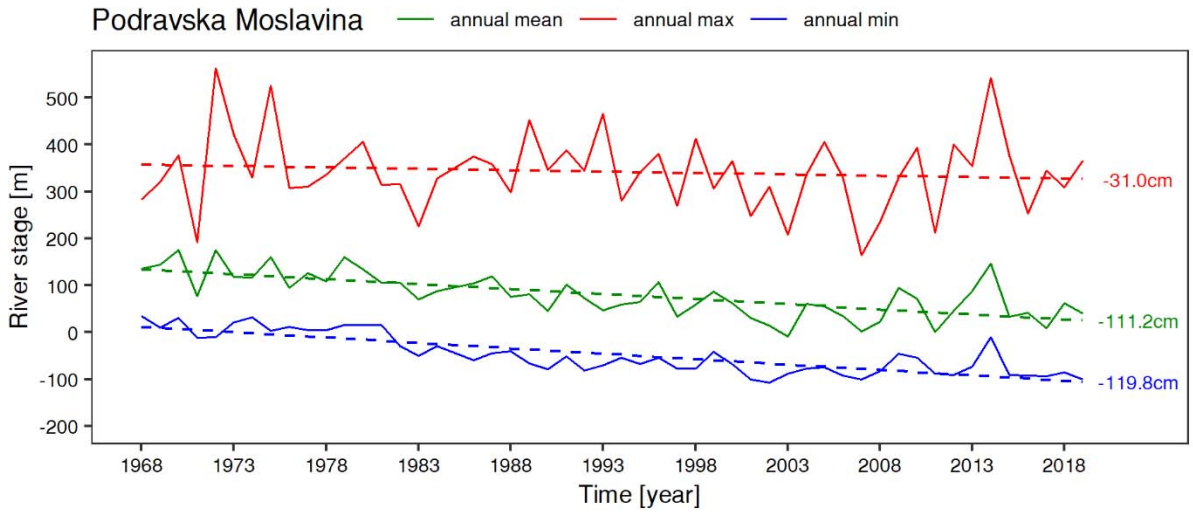
Podravska Moslavina
annual mean
annual max
annual min
River stage [m]
Time [year]
-31.0cm
-111.2cm
-119.8cm

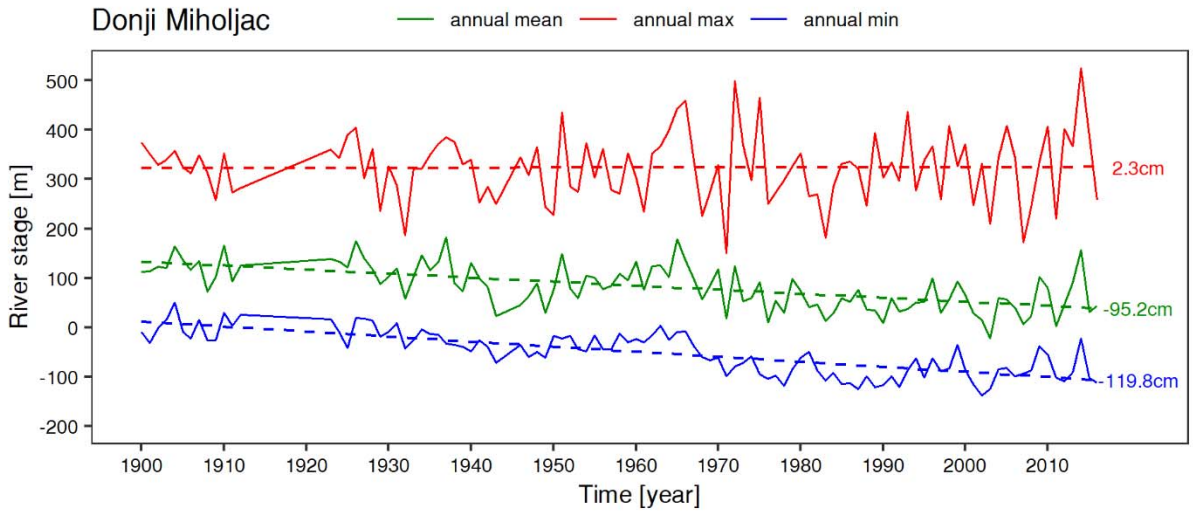
Donji Miholjac
annual mean
annual max
annual min
River stage [m]
Time [year]
2.3cm
-95.2cm
-119.8cm

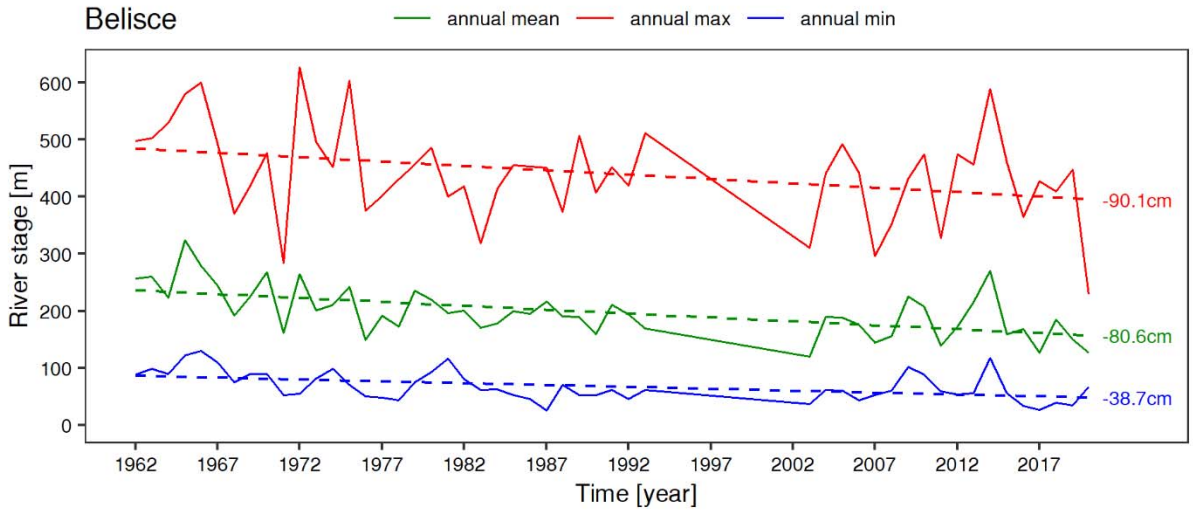
Belisce
annual mean
annual max
annual min
River stage [m]
Time [year]
-90.1cm
-80.6cm
-38.7cm

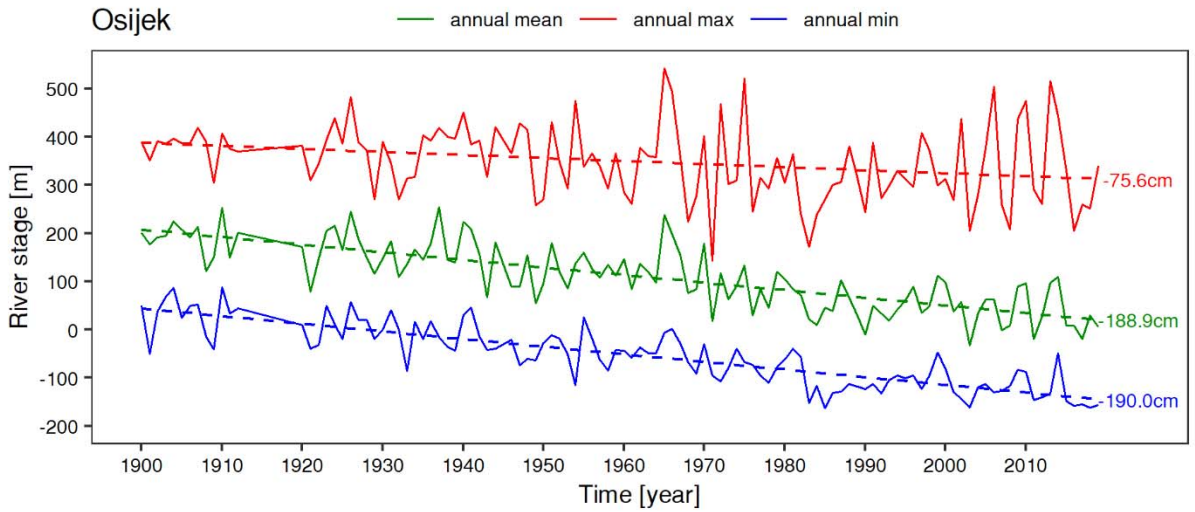
Osijek
annual mean
annual max
annual min
River stage [m]
Time [year]
-75.6cm
-188.9cm
-190.0cm

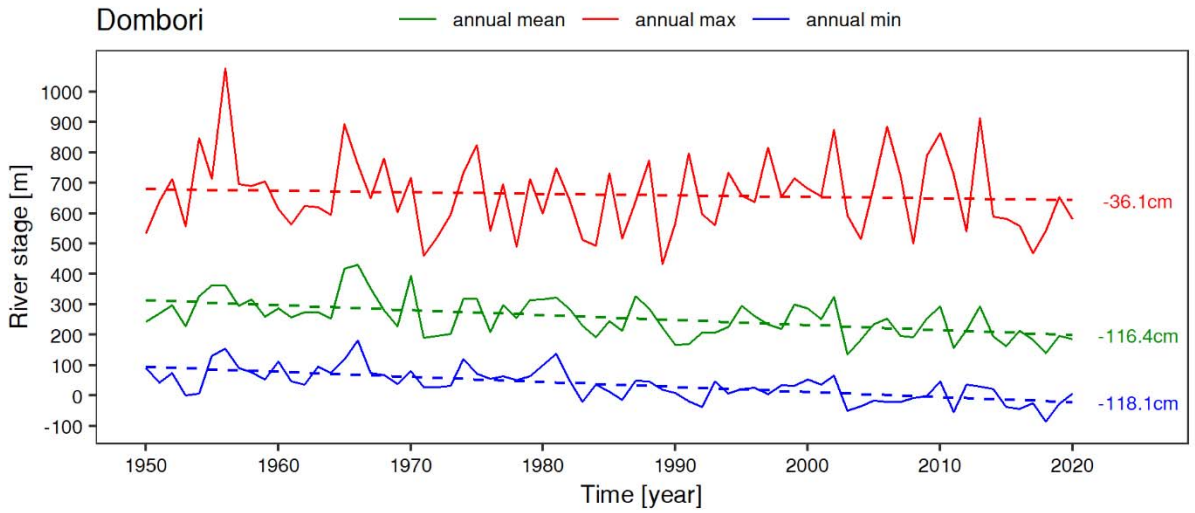
Dombori
annual mean
annual max
annual min
River stage [m]
Time [year]
-36.1cm
-116.4cm
-118.1cm

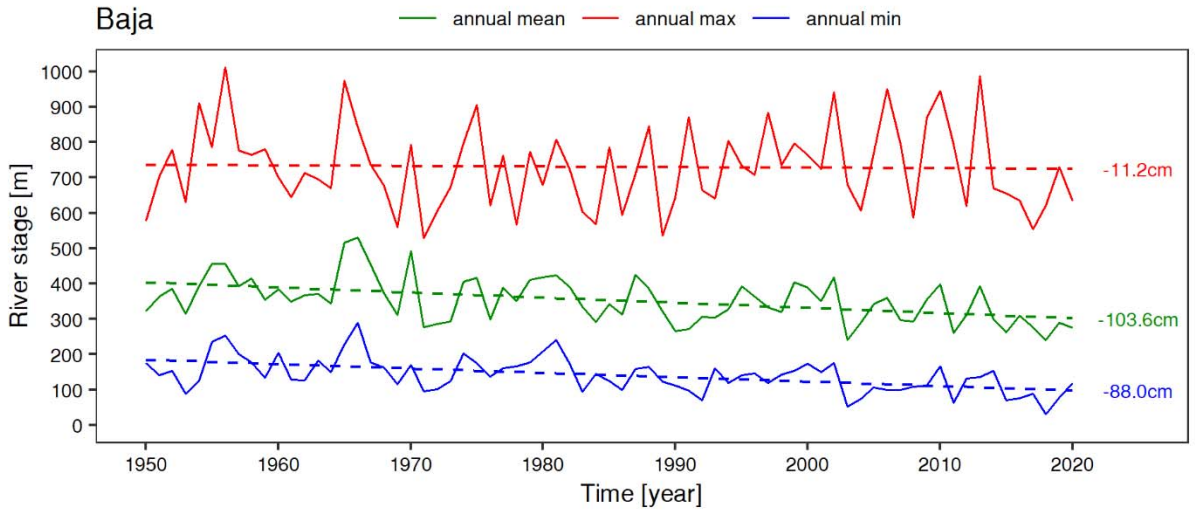
Baja
annual mean
annual max
annual min
River stage [m]
Time [year]
-11.2cm
-103.6cm
-88.0cm

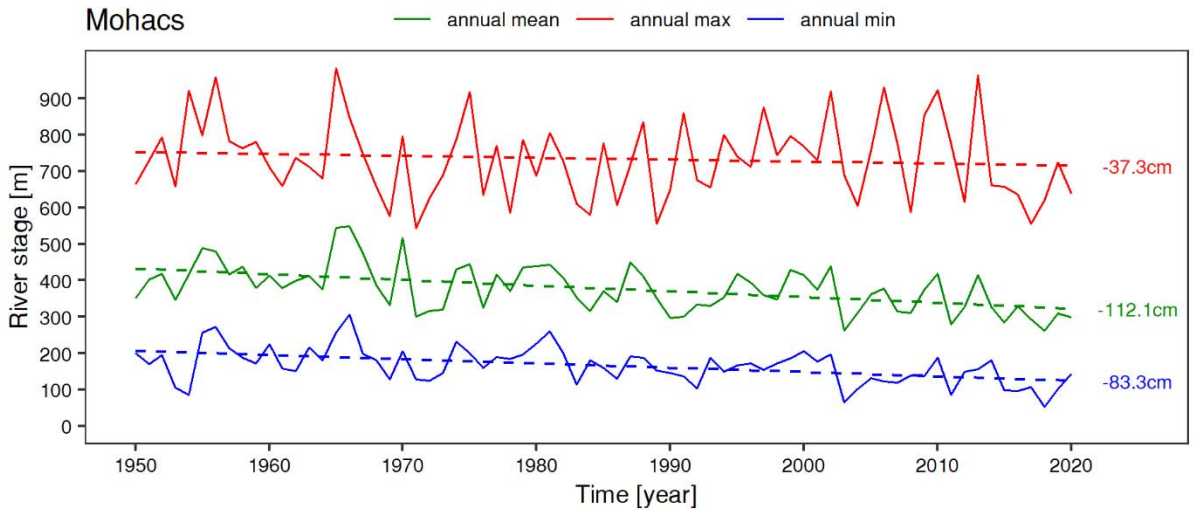
Mohacs
annual mean
annual max
annual min
River stage [m]
Time [year]
-37.3cm
-112.1cm
-83.3cm

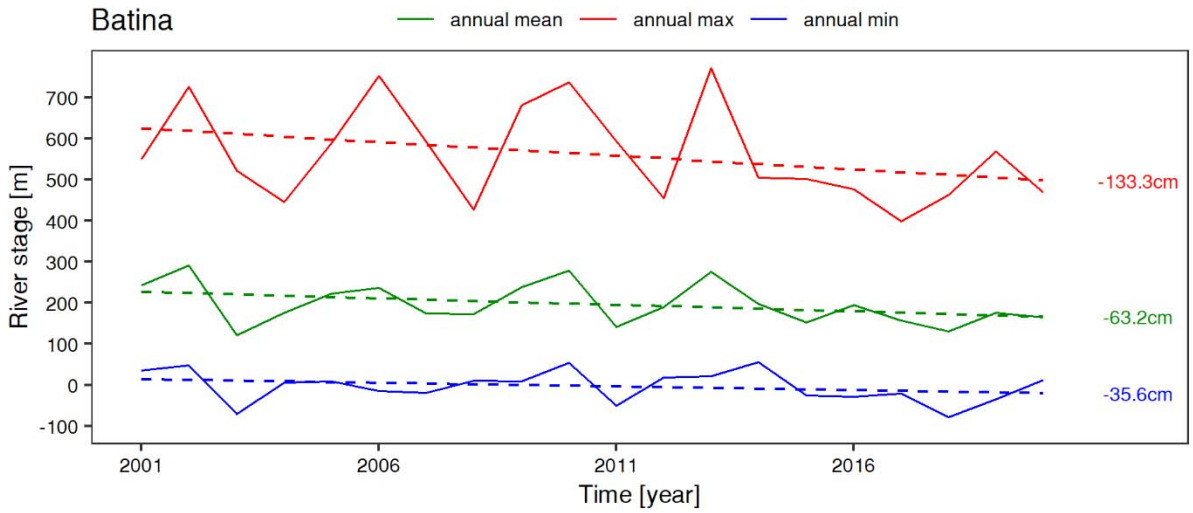
Batina
annual mean
annual max
annual min
River stage [m]
Time [year]
-133.3cm
-63.2cm
-35.6cm

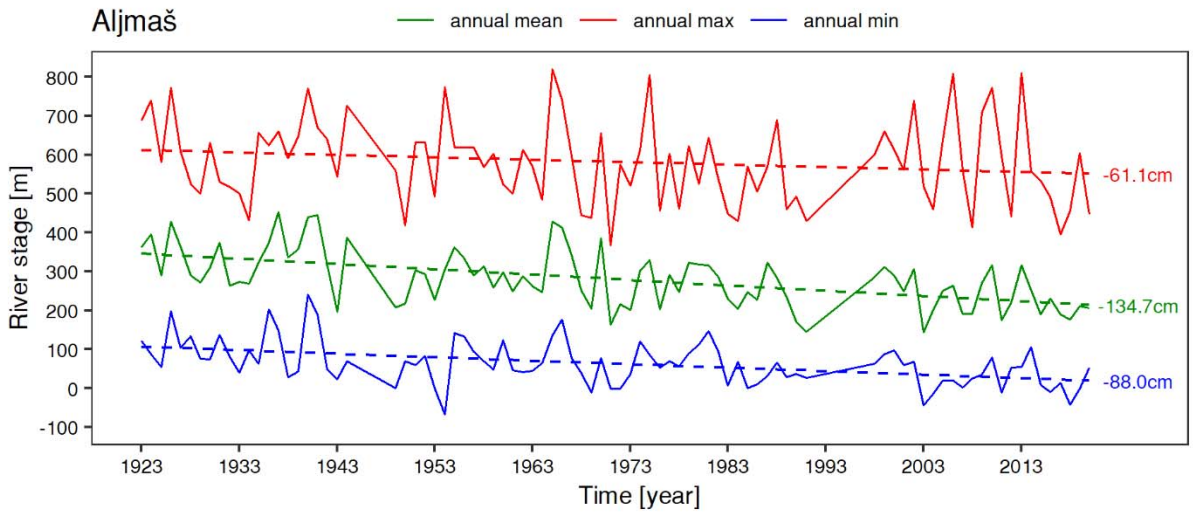
Aljmaš
annual mean
annual max
annual min
River stage [m]
Time [year]
-61.1cm
-134.7cm
-88.0cm

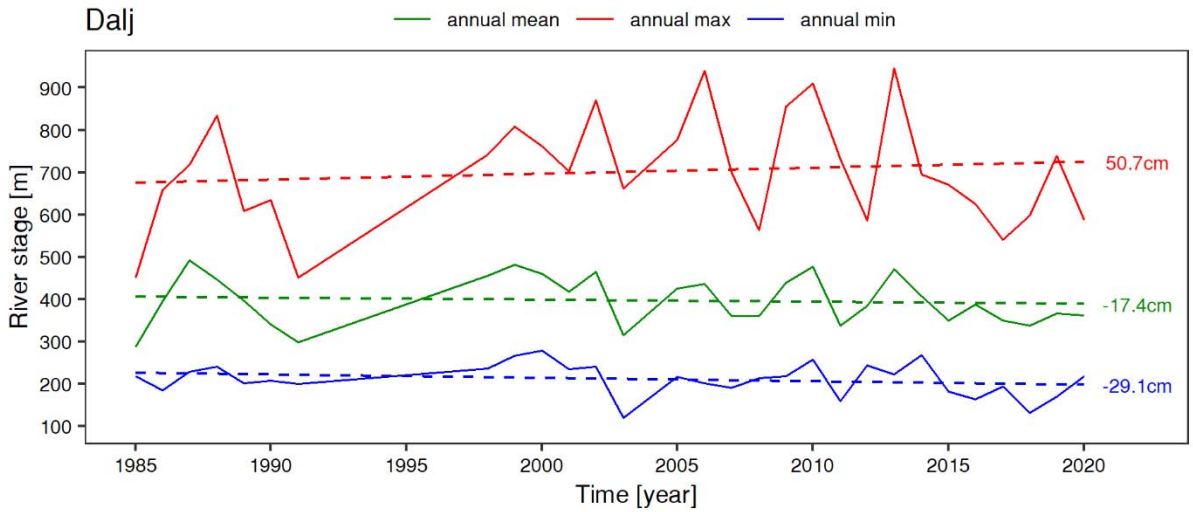
Dalj
annual mean
annual max
annual min
River stage [m]
Time [year]
50.7cm
-17.4cm
-29.1cm

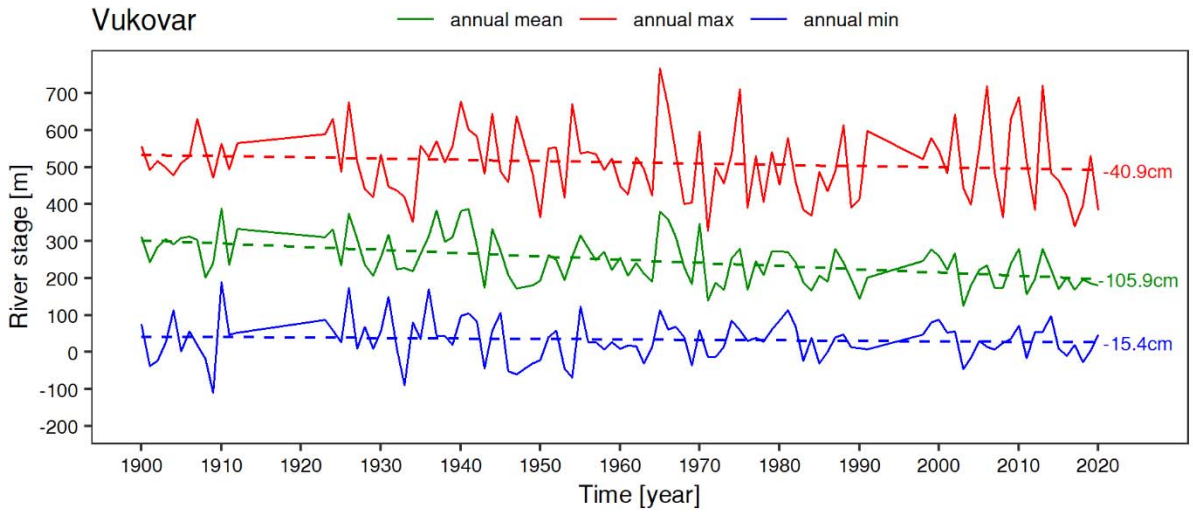
Vukovar
annual mean
annual max
annual min
River stage [m]
Time [year]
-40.9cm
-105.9cm
-15.4cm

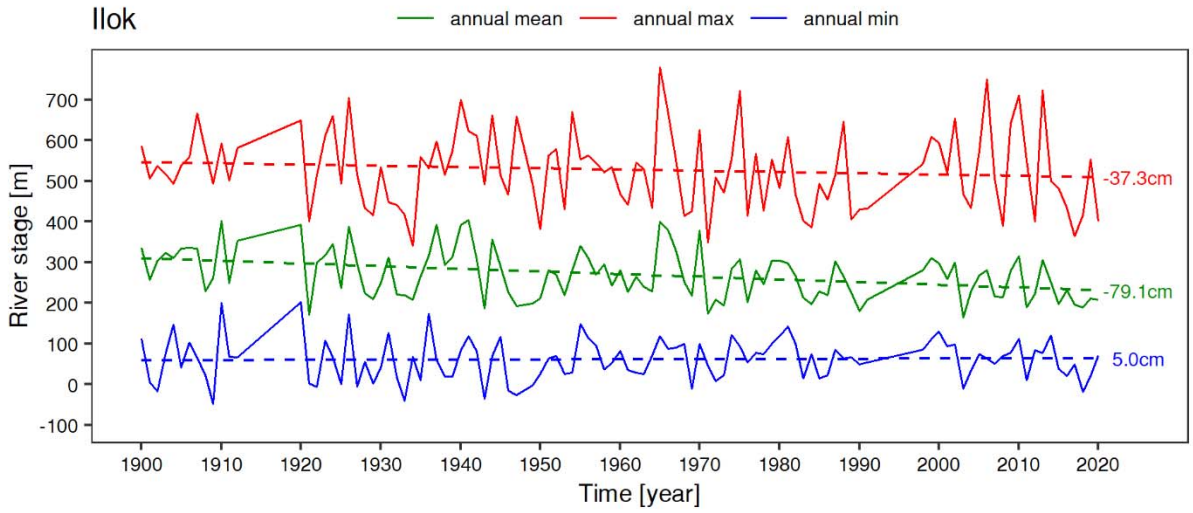
Ilok
annual mean
annual max
annual min
River stage [m]
Time [year]
-37.3cm
-79.1cm
5.0cm

6 References

Ahmari H., Da Silva A. M. (2011): Regions of bars, meandering and braiding in da Silva and Yalin's plan, Journal of Hydraulic Research, 49:6, 718-727.

ASCE Task Committee to Expand and Update Manual 54, 2008, Chapter 2: Sediment transport and morphodynamics, Marcelo García, Reston, Va. : American Society of Civil Engineers.

Austrian-Slovenian Standing Committee for the Mur River (2001), Basic Water Management Concept—Phase I, report, Vienna.

Baranya, S., Pomázi, F., Fleit, G., Németh, D., Sütheő, M., (2020). Assessing causes and controls of bed erosion for the Drava River (between 0-236 rkm sections)

Bonacci, O., Oskoruš, D. (2010). The changes in the lower Drava River water level, discharge and suspended sediment regime. Environ Earth Sci 59, 1661–1670. https://doi.org/10.1007/s12665-009-0148-8

Cantin, A. and Post, J.R. (2018), Habitat availability and ontogenetic shifts alter bottlenecks in sizestructured fish populations. Ecology, 99: 1644-1659. https://doi.org/10.1002/ecy.2371

Da Silva, A M (1991): Alternate bars and related alluvial processes. Thesis of master science, Queens University Kingston, Ontario, Canada.

DHMZ (Državni hidrometeorološki zavod) (2021). Godišnje Izvješće o mjerenju nanosa na slivu Drave i Mure za 2020. godinu

Einstein HA. 1936. Bedload transport as a probability problem. PhD Thesis. Eidgenössische Technische Hochschule: Zürich.

Ferguson, R., Hoey, T., Wathen, S., and Werritty, A., 1996, Field evidence for rapid downstream fining of river gravels through selective trans port: Geology, v. 24, p. 179–182, https://doi.org/10.1130/0091-7613(1996)024<0179:FEFRDF>2.3.CO;2.

Frings, R.M., Gehres, N., Promny, M., Middelkoop, H., Schüttrumpf, H., Vollmer, S., 2014. Today's sediment budget of the Rhine River channel, focusing on the Upper Rhine Graben and Rhenish massif. Geomorphology 204, 573–587.

Habersack H., Baranya S., Holubova K., Vartolomei F., Skiba H., Babic-Mladenovic M., Cibilic A., Schwarz U., Krapesch M., Gmeiner Ph., Haimann M. (2019). Danube Sediment Management Guidance. Output 6.1 of the Interreg Danube Transnational Project DanubeSediment co-funded by the European Commission, Vienna.

Habersack H., Baranya S., Holubova K., Vartolomei F., Skiba H., Schwarz U., Krapesch M., Gmeiner Ph., Haimann M. (2019). Sediment Manual for Stakeholders. Output 6.2 of the Interreg Danube Transnational Project DanubeSediment co-funded by the European Commission, Vienna.

Hengl H, Habersack H, Nachtnebel HP, Schneider J, Hunziker R, Mikos M (2001). Geschiebetransportmodell. Endbericht des Themenbereichs 1.6 des Wasserwirtschaftlichen

Grundsatzkonzepts für die Grenzmur – Phase I, im Auftrag der Ständigen österreichisch-slowenischen Kommission für die Mur.

Klösch, M., Blamauer, B., and Habersack, H. (2015), Intra-event scale bar–bank interactions and their role in channel widening. Earth Surf. Process. Landforms, 40, 1506–1523. doi: 10.1002/esp.3732.

Klösch M, Habersack H. 2017. The hydromorphological evaluation tool (HYMET). Geomorphology 291 : 143– 158. https://doi.org/10.1016/j.geomorph.2016.06

Klösch M, Pessenlehner S, Dunst R, Langendoen EJ, Liébault F, Goltara A, Aigner J, Reebs F, Bertrand M, Habersack H (2019a). D.T2.2.1. Technical note on a multi-scale framework for assessing the hydromorphological conditions of rivers.

Klösch M, Bertrand M, Boz B, Carolli M, Chouquet I, Dunst R, Egger G, Fragola G, Gaucher R, Gmeiner Ph, Goltara A, Hauer C, Holzapfel P, Humar N, Langendoen EJ, Javornik L, Liébault F, Maldonaldo E, Marangoni N, Molnar P, Pessenlehner S, Pusch M, Recking A, Rossi D, Rozman D, Šantl S, Stephan U, Habersack H (2019b). D.T2.3.1. Technical notes in tools to support planning and design of hydromorphological management and restoration measures, Delovni sklop 2, EU-Interreg Alpski prostor, projekt HyMoCARES.

Klösch, M., Tritthart, M., Beikircher, U., Dunst, R., Eder, M., Habersack, H. (2021) Grenzüberschreitender Managementplan zur innovativen nachhaltigen Bewirtschaftung der Grenzmur und zur Verbesserung des Hochwasserschutzes - D.T1.3.2 Sedimenttransportstudie. EU Interreg V-A SI-AT goMURra.Knighton D (1998). Fluvial form and processes - a new perspective. John Wiley and Sons, New York.

Kovačićek, N. Mešin, J., Rubić, D., Đurkan, F. (2021). Annual report on sediment measurement on the Drava and Mura basin for the year 2020. DHMZ – Croatian State Hydrometeorological Institute

Kresser, W. (1964): Gedanken zur Geschiebe- und Schwebstoffführung der Gewässer. ÖWW, 16. Jg., H. 1/2, S. 6–11.

Lane, E. W. 1955. `Design of stable channels', Transactions of the American Society of Civil Engineers, 120, 1±34.

Leopold, L.B. and Wolman, M.G. (1957) River Channel Patterns, Braided, Meandering and Straight. U.S. Geol. Surv. Paper. 282-B.

Meyer-Peter E, Müller R (1948). Formulas for bed-load transport. Proc. 2nd IAHR Congress, Stockholm, 39–64.

Mollard, J. D. 1973. Air photo interpretation of fluvial features. In Fluvial Processes and Sedimentation, Proc. Hydrol. Symp., Univ. Alberta, pp. 341-80. Ottawa : Natl. Res. Counc. Can.

Parker, G., P. R. Wilcock, C. Paola, W. E. Dietrich, and J. Pitlick (2007), Physical basis for quasi-universal relations describing bankfull hydraulic geometry of single-thread gravel bed rivers, J. Geophys. Res., 112, F04005, doi:10.1029/2006JF000549.

Partheniades, E., 1965. Erosion and depostion of cohesive soils. J. Hydraul. Div. ASCE 91, 105–139.

Pirkhoffer, E, Halmai, Á, Ficsor, J, et al. Bedload entrainment dynamics in a partially channelized river with mixed bedload: A case study of the Drava River, Hungary. River Res Applic. 2021; 37: 699– 711.

Rákóczi L & Szekeres J (2004) Environmental effects of industrial dredging on alluvial riverbeds,

Rinaldi, M., & Darby, S. E. (2008). Modelling river-bank-erosion processes and mass failure mechanisms: Progress towards fully coupled simulations. In H. Habersack, H. Piégay, & M. Rinaldi (Eds.), Gravel-Bed Rivers 6 - From Process Understanding to River Restoration, (pp. 213-239). Netherlands: Elsevier.

Schumm, S. A. 1981. Evolution and response of the fluvial system, sedimentologic implications. Soc. Econ. Paleontol. Mineral. Spec. Publ. 3 1 : 19-29

Schumm, S.A., 1985. "Patterns of alluvial rivers", Annual Review of Earth and Planetary Sciences 13, 5-27.

Schwarz, U. (2022). D.T1.2.1 „River Training Structures" Draft March 17, 2022

Schwarz, U. (2007). Pilot Study: hydromorphological survey and mapping of the Drava and Mura Rivers. IAD Report prepared by FLUVIUS, Floodplain Ecology and River Basin Management, Vienna pp. 140.

Shaw, J., and Kellerhals, R., 1982, The Composition of Recent Alluvial Gravels in Alberta River Beds:Alberta, Canada, Alberta Research Council, 151 p.

Shields, A. (1936). Application of similarity principles and turbulence research to bed-load movement (translated version). Mitteilungen der Preußischen Versuchsanstalt für Wasserbau. Vol. 26. Berlin: Preußische Versuchsanstalt für Wasserbau.

Tamas, E. A. (2019). Sediment Transport of the Drava River. In D. Lóczy (Ed.), The Drava river, Springer geography. Berlin: Springer International Publishing AG. https://doi.org/10.1007/978-3-319-92816-6_13

Terra-Graph Kft. (2020). A középvízi meder modellvizsgálata a Dráván, WISEDRAVALIFE report.

Thorne, C. R. (1982). Processes and mechanisms of riverbank erosion. In R. D. Hey, J. C. Bathurst, & C. R. Thorne (Eds.), Gravel-bed rivers (pp. 227-271). New York: Wiley.

Verbund (2015). Anpassung der Betriebsweise bei Hochwasser – Murkraftwerke Mellach bis Spielfeld. Technischer Bericht.

Water Research Institute & project partners (BME, BOKU, OVF, NARW, NIHWM, LfU, NIMH, EAEMDR, HRVODE, IzVRS, TUM, JCI, Plovput) (2019). Data Analyses for the Sediment Balance and Long-term Morphological Development of the Danube. EU Interreg project DanubeSediment in the Danube Transnational Programme, co-funded by European Union funds (ERDF, IPA).